PROGRESS IN RESEARCH

APRIL 1, 2003 - MARCH 31, 2004

Prepared By

The Cyclotron Institute Staff

Texas A&M University

College Station, TX 77843-3366

Phone: (979) 845-1411
Fax: (979) 845-1899

Web: http://cyclotron.tamu.edu

June 2004

TABLE OF CONTENTS

SECTION II: HEAVY ION REACTIONS

SECTION III: NUCLEAR THEORY

Introduction
April 1, 2003 - March 31, 2004

This document summarizes the progress in research and operations at the Texas A&M Cyclotron Institute for the period April, 1, 2003 through March 31, 2004. Sections I through IV contain reports from individual research projects. Operation and technical developments are given in Section V. Section VI lists the publications with Cyclotron Institute authors and the Appendix gives additional information including talks presented by members of the Institute during the past year. *Since most of the contributions presented here are truly reports on progress in research, results and conclusions should not be quoted from the report without the consent of the authors.*

This volume of Progress in Research is the second one that will be available solely from our web site (http://cyclotron.tamu.edu). Over the past year, a number of impressive projects have been carried out by Institute researchers. Some recent achievements are noted here.

(1) Extensive comparisons of experimental data for the reaction systems, ^{64}Zn + ^{58}Ni, ^{64}Zn + ^{92}Mo, ^{64}Zn + ^{197}Au, at 26, 35 and 47 MeV/A, with results of Anti-symmetrized Molecular Dynamics transport model calculations have suggested a new scenario for multi-fragmentation reactions.

(2) Secondary fragment beams produced in MARS have been used to measure the evolution toward N/Z equilibration in Deep Inelastic Collisions.

(3) The new "precision decay facility" has been used on-line to measure the half-life and branching ratio for the superallowed beta-decay of ^{34}Ar as part of our program to sharpen the test of CKM unitarity; it has also been used off-line for one of the most precise measurements ever made of an internal conversion coefficient (ICC) – the K-shell ICC for the M4 decay of ^{193m}Ir – which demonstrates that the most recent table of ICCs is based on an invalid approximation.

(4) Experiments on $^{112\text{-}124}$Sn and $^{110\text{-}116}$Cd have shown that the isotopic dependence of the giant monopole resonance energy can be reproduced with Skyrme interactions having their density dependence modified to improve extrapolations to neutron rich systems (and with K_{NM}~220-240MeV) but not with standard Skyrme interactions.

(5) An updated rate for the hot CNO cycle reaction ^{13}N(p,γ)^{14}O has been determined based on new ANC results.

(6) Resonance scattering has been used with several radioactive beams to determine information about nuclear structure in systems of importance to astrophysics.

(7) A comprehensive analysis of the spectra of Ho L x rays excited by 6 MeV/u C, Ne, Ar, and Kr ion impact revealed the scaling properties of the M-shell ionization probability in near-central collisions.

(8) The recently observed enhancement of baryons relative to mesons at intermediate transverse momentum at RHIC and the scaling of hadron elliptic flows according to their quark content can be explained by quark coalescence during hadronization.

(9) Measurements of high-p_T particle production in 200 GeV d+Au collisions by the STAR Collaboration demonstrated that the strong suppression of high-p_T particle yields and back-to-back di-hadron correlations in central Au+Au collisions are due to final-state interactions in the dense medium produced in the Au+Au collisions.

(10) BRAHMS has discovered a marked high-p_T suppression in d+Au collisions that may be related to the existence of the Color Glass Condensate (CGC).

(11) Hadronic many-body calculations of the $\Delta(1232)$ (and nucleon) spectral function in hot and dense matter, consistent with photo-absorption spectra on nuclei, are in qualitative agreement with preliminary RHIC data from STAR for pion-proton invariant mass spectra.

As in the past, Institute scientists remain active in a number of collaborative research efforts around the world. Major programs include: experiments at TRIUMF laboratory to measure heavy (A > 60) superallowed β decays and a measurement of Michel parameters in normal μ^+ decay; new mass measurements using the Canadian Penning Trap (CPT) at Argonne National Laboratory; and continued work with both the BRAHMS and STAR collaborations at RHIC.

The K500 cyclotron continues to serve the broader community through testing of radiation effects on electronics components. Again this past year a bit over 20% of the scheduled accelerator time was devoted to single-event-upset testing. Both U.S. and foreign companies continue to utilize our facility.

I am pleased to acknowledge the effort made by Y.-W. Lui in putting together this report. He managed it in a very prompt and efficient manner.

R.E. Tribble
June 21, 2004

SECTION I

NUCLEAR STRUCTURE, FUNDAMENTAL INTERACTIONS, AND ASTROPHYSICS

Isoscalar Giant Resonance for Nuclei with A ≅ 60

Y. -W. Lui, X. Chen, H. L. Clark, B. John,* Y. Tokimoto, and D. H. Youngblood

The locations of the isoscalar giant monopole resonace (GMR) and giant dipole resonance (ISGDR) are important because their energies can be directly related to the nuclear compressibility and from this the compressibility of nuclear matter (K_{NM}) can be obtained [1,2]. In the past few years, experiments with much improved peak to continuum ratio have been performed mostly in heavy nuclei A ≥ 90 [3,4] as well as in light nuclei A ≤ 40 [5-8]. Together with development of the multipole analysis program, high precision strength distributions of isoscalar multipoles in these nuclei have been obtained. The results of GMR strength distributions in heavy nuclei concluded the nuclear matter compressibility is 231±5 MeV [3]. With the available of large amount of data in wide range of A (12 ≤ A ≤208), we have also studied the mass dependence of GMR and the characteristic of GMR [3,8]. In heavy nuclei (A ≥ 110), the shape of GMR strength distribution is typically symmetric (Gaussian like) [3], in ^{90}Zr, the shape changes to mostly sysmmetric with a tail at high excitation side of the GMR [3]. This changes to asymmetric with a slower slope on the high excitation side of the peak in ^{58}Ni and ^{40}Ca and becomes fragmented in A ≤ 28. The origin of this is not clear, it may be due to nuclear structure or some other effects. From our data, the transition from mostly symmetric to asymmetric shape occurs between ^{90}Zr and ^{58}Ni [10], however, between 40 ≤ A ≤90, only one nucleus ^{58}Ni has been thoroughly studied. Therefore, it is important to have more information in this region to study this interesting effect and the mass dependence of GMR. We have studied ^{46,48}Ti, ^{56}Fe, ^{60}Ni, ^{64}Ni and ^{64}Zn recently, the preliminary result for the Ti isotopes has been reported [11] in a previous progress report. We will present preliminary results for ^{56}Fe, ^{60}Ni and ^{64}Zn in this report.

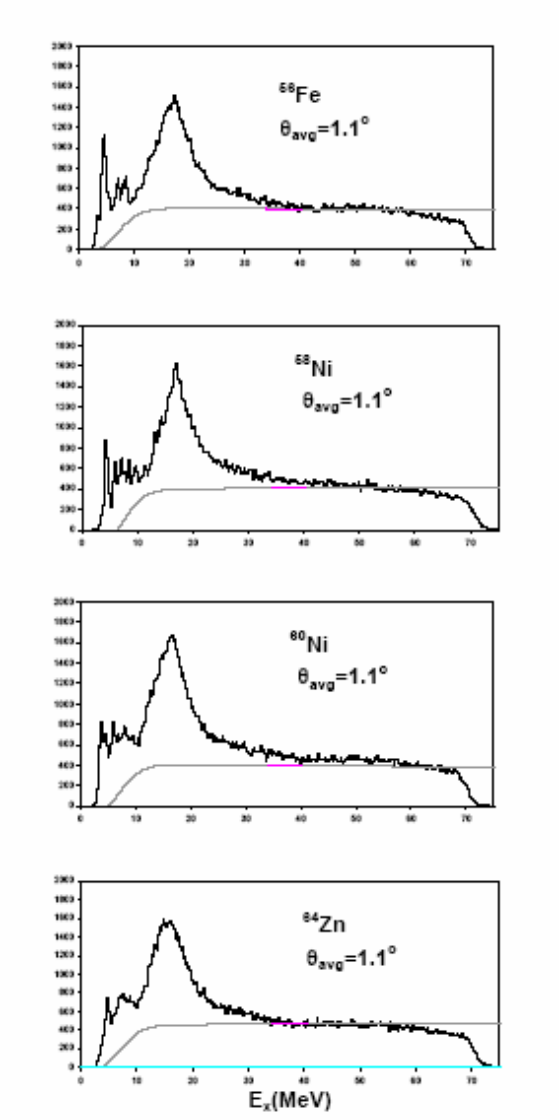

Figure 1.Inelastic α spectra for ^{56}Fe, ^{58,60}Ni and ^{64}Zn at θ_{avg} = 1.1°. The solid lines show the continuum chosen for the analysis.

The experimental technique has been described thoroughly in Ref. [6] and is summarized briefly below. Beams of 240 MeV α particles from the Texas A&M K500 superconducting cyclotron bombarded self-supporting foils located in the target chamber of the multipole-dipole-multipole spectrometer. the horizontal acceptance of the spectrometer was 4 deg. and raytracing was used to reconstruct the scattering angle. The vertical acceptance was set at ± 2°. The focal plane detector measured position and angle in the scattering plane and covered from 47 to 55 MeV of excitation, depending on scattering angle. The out-of-plane scattering angle was not measured. Position resolution of approximately 0.9 mm and scattering angle resolution of about 0.09° were obtained. Cross sections were obtained from the charge collected, target thickness, dead time and known solid angle. The cumulative uncertainties in target thickness, solid angle, etc., result in about ±10% uncertainty in absolute cross sections. ^{24}Mg spectra were taken before and after each run with each target and the 13.85±0.02 MeV L=0 state was used as a check on the calibration in the giant resonance region.

Sample spectra obtained for ^{56}Fe,^{58,60}Ni and ^{64}Zn are shown in Fig. 1. The spectrum was divided into a peak and a continuum, where the continuum was assumed to have the shape of a straight lines at high excitation joining onto a Fermi shape at low excitation to model particle threshold effects. The

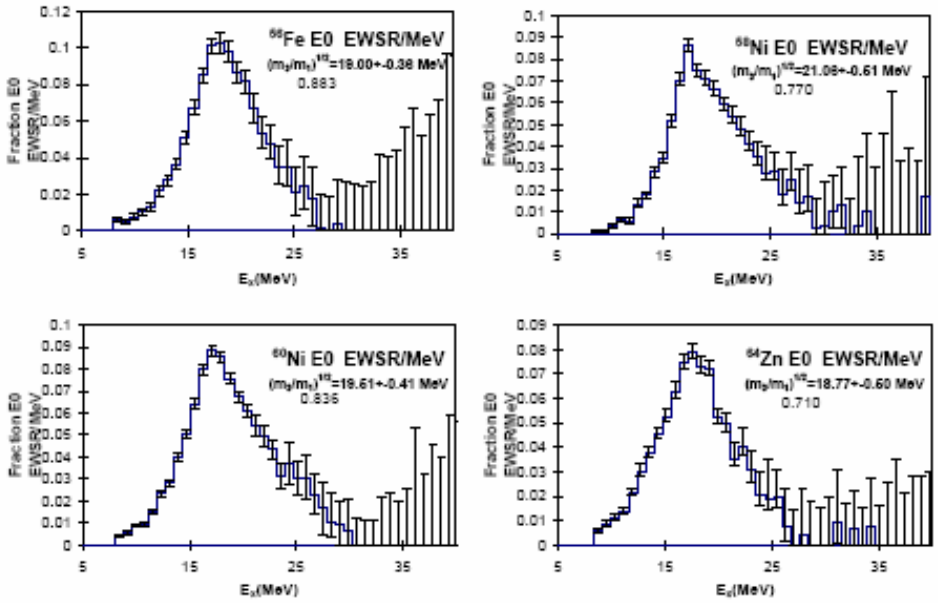

Figure 2. GMR strength distributions for ^{56}Fe, ^{58,60}Ni and ^{64}Zn are shown by histrogram. Error bars represent the uncertainty due to the fitting for angular distributions.

multipole components of the giant resonance peak were obtained by dividing the peak into multipole regions (bins) by excitation energy and then comparing the angular distributions obtained for each of these bins to distorted wave born approximation (DWBA) calculations. Optical model parameters obtained for ^{58}Ni were used for ^{56}Fe, ^{60}Ni and ^{64}Zn calculations. The transition densities, sum rules, and DWBA calculation were discussed in Ref. [6]. Preliminary GMR strength distributions for ^{56}Fe, ^{58}Ni, ^{60}Ni

and ^{64}Zn are shown in Fig. 2. More than 70% of GMR strength have been located in these nuclei and the experimental energies $(m_3/m_1)^{1/2}$ are labeled in Fig. 2.

*Present address: Nuclear Physics Division, BhaBha Atomic Research Center, Mumbai-400085, India.

[1] J.P. Blaizot, Phys. Rep. **64**, 171 (1980).

[2] S. Stringari, Phys. Lett. **108B**, 232 (1982).

[3] D.H. Youngblood, H.L. Clark, Y.-W. Lui, Phys. Rev. Lett. **82**, 691 (1998).

[4] D.H. Youngblood, Y.-W. Lui, H.L. Clark,B. John, Y. Tokimoto, and X. Chen, Phys. Rev. C **69**, 034315 (2004).

[5] B.John,Y. Tolimoto, Y.-W. Lui, H.L. Clark, X. Chen, and D.H. Youngblood, Phys. Rev. C **68**, 014305 (2003).

[6] D.H. Youngblood, Y.-W. Lui, and H.L. Clark, Phys. Rev. C **65**, 034302 (2002).

[7] Y.-W. Lui, H.L. Clark, and D.H. Youngblood, Phys. Rev. C **64**, 064308 (2001).

[8] D.H. Youngblood, Y.-W. Lui, and H.L. Clark, Phys. Rev. C ***63***, 067301 (2001).

[9] Y.-W. Lui, D.H. Youngblood, Y. Tokimoto, H.L. Clark, and B. John, Phys. Rev. C **69**, 034611 (2004).

[10] Y.-W. Lui, H.L. Clark, and D.H. Youngblood, Phys. Rev. C **61**, 067307 (2000).

[11] Y. Tokimoto, B. John, X. Chen, H.L. Clark, Y.-W. Lui, and D.H. Youngblood, *Progress in Research*, Cyclotron Institute, Texas A&M University (2002-2003), p.I-4.

Giant Resonance Study by ^{6}Li Scattering

X. Chen, Y. -W. Lui, H. L. Clark, Y. Tokimoto, and D. H. Youngblood

The compressibility of nuclear matter (K_{nm}) is important in the description of the properties of the nuclei, supernova explosions, neutron stars, and heavy ion collisions. The value of K_{nm} can be obtained directly from the energies of the isoscalar giant monopole resonance (ISGMR) in nuclei.

Alpha inelastic scattering including 0^{o} measurements has been successfully used to identify the ISGMR in heavy and medium nuclei. In order to determine K_{nm} precisely, measurements over a wide mass range are necessary. For light nuclei (A<40), however, E0 (GMR) strength is more elusive than that in the higher mass region. In medium and heavy nuclei, the monopole resonance is concentrated in a broad peak. But for lighter (A<40) nuclei, the resonance is fragmented and extends to excitation energies above 35 MeV. The continuum in the high excitation energy range for α inelastic scattering, which is due in part to the multi-step reactions, makes it difficult to extract strength in this range.

For ^{6}Li scattering, the low-lying particle emitting threshold will give a large breakup probability into dominant channel ^{6}Li→α + d. Therefore the contribution of multi-step processes is low especially at higher excitation energy and a better ratio between the resonance peak and the continuum is expected. ISGMR studies in ^{12}C and ^{24}Mg with 156 MeV ^{6}Li inelastic scattering have been reported respectively by W. Eyrich *et al.* [1] and H. Dennert *et al.* [2] with some success, however, the low bombarding energy limited the useful excitation range to $E_x \leq 30$ MeV.

Another important motivation for ^{6}Li scattering is to explore the possibility to expand current research from stable nuclei to radioactive nuclei by inverse reactions. The inverse reactions have to be used because it is impossible to make targets of unstable nuclei. The unstable nuclei will be used as projectiles. As it is difficult to make a helium target, ^{6}Li may be a better candidate for inverse reactions.

We have initiated a study of giant resonance with 40 MeV/nucleon ^{6}Li ions both to identify ISGMR strength at higher excitation in lighter nuclei and to study the feasibility of using inverse reactions on a ^{6}Li target. In addition to taking inelastic scattering data to study the giant resonance over a large excitation range, we have studied ^{6}Li elastic and inelastic scattering to low lying states to obtain optical parameters for distorted-wave Born approximation (DWBA) and optical-model calculations.

Beam of 240 MeV ^{6}Li ions from Texas A&M K500 superconducting cyclotron, which went through the beam analysis system, bombarded self-supporting target foils in the target chamber of the multipole-dipole-multipole (MDM) spectrometer. The horizontal acceptance of the spectrometer was 4^{o} and ray tracing was used to reconstruct the scattering angle. The vertical acceptance was set at $\pm 2^{o}$ for giant resonance and large angle elastic scattering measurements, $\pm 1^{o}$ for small angle elastic scattering measurements. The focal plane detector consisted of four 60 cm long proportional counters (separated by 13.55 cm) to measure horizontal positions and also horizontal angle θ, an ionization chamber to measure ΔE, and a scintillator to measure E and to provide a trigger signal. The principals of the operation are

similar to the detector described in Ref. [3]. The angle calibration was done using a collimator with five slit openings spaced 1^o apart. The known excited states in certain nuclei were used to obtain energy calibrations for each of the angle bins. The details of the energy calibration are described in Ref. [4].

Two runs have been done during last year. Inelastic scattering over the excitation energy range from 6 MeV to 60 MeV was measured at the spectrometer angles of 0^o, 4^o and 6^o on targets of ^{12}C, ^{24}Mg, ^{28}Si, ^{64}Zn, ^{116}Sn, with thicknesses 2.0, 3.74, 7.9, 3.7, and 11.44 mg/cm^2, respectively. Elastic scattering as well as inelastic scattering to low-lying states was measured at spectrometer angles of 5^o, 7^o, 9^o, 11^o, 13^o, 15^o, 17^o, 19^o, 21^o, 23^o, 26^o, 29^o, 32^o, and 35^o. The targets were ^{24}Mg, ^{28}Si, ^{58}Ni, ^{90}Zr, ^{116}Sn, with thicknesses 4.51, 7.99, 3.79, 5.18, and 11.44 mg/cm^2, respectively. In the analysis, data taken at one spectrometer angle were divided into ten angle bins, each angle bin corresponding to $\Delta\theta \approx 0.4^0$. The average angle for each angle bin was determined by integrating over the height of the solid angle and the width of the angle bin. The absolute cross-sections for elastic and inelastic scattering peaks were obtained by the combination of charge integration, target thickness, solid angle, and dead time correction. The angular distribution of elastic and inelastic scattering to low-lying states for ^{116}Sn are plotted versus average center of mass angle in Fig.1. Optical-model calculations were carried out with code PTOLEMY [5] and optical parameters were obtained by fitting the angular distribution of the elastic scattering

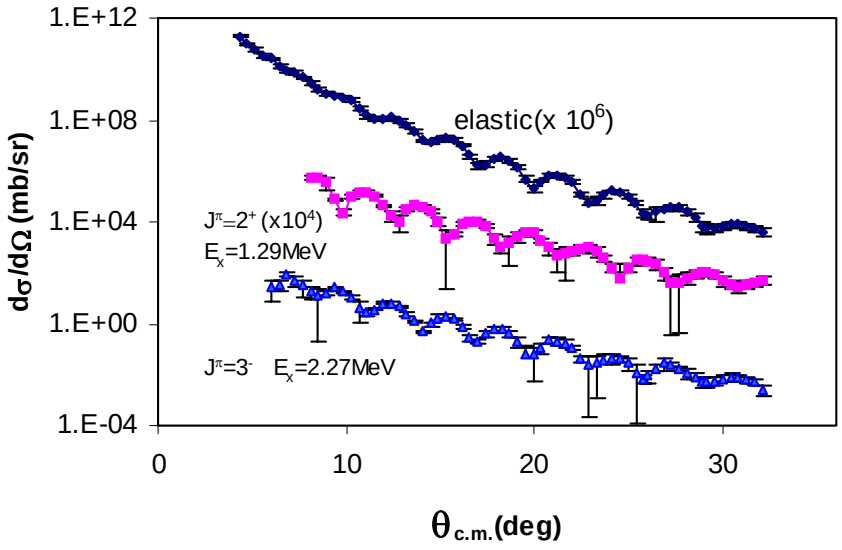

Figure 1. The differential cross-section for elastic scattering and inelastic scattering to low-lying states of ^{116}Sn is plotted versus average center of mass angle. The differential cross-section data for elastic scattering are multiplied by 10^6, while those for inelastic scattering to the 2^+ state are multiplied by 10^4.

differential cross section. The parameters obtained are shown in Table 1 and the calculation along with the data are shown in Fig. 2. Fig. 3 shows a comparison between α inelastic scattering and ^{6}Li inelastic scattering to ^{28}Si low-lying states and GR region taken at $\theta_{c.m.} = 1.2^{o}$. As expected, the continuum in the ^{6}Li scattering is lower than that of α inelastic scattering for $E_x > 35$ MeV. Analysis of the data is in progress.

Table 1. Optical potential parameters obtained from fit to elastic scattering data.

	V (MeV)	r_0 (fm)	a (fm)	V_i (MeV)	r_{i0} (fm)	a_i (fm)
^{116}Sn	188	0.837	0.905	28.4	1.17	0.816

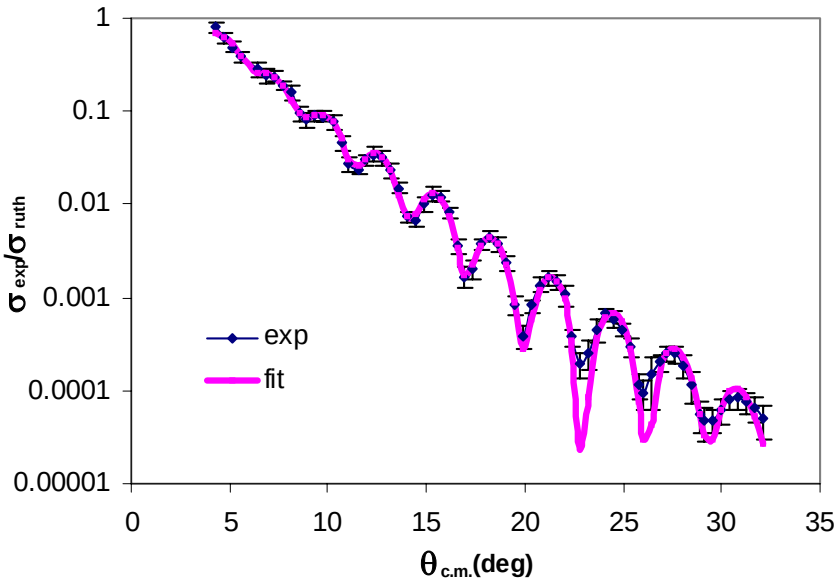

Figure 2. Angular distribution of the ratio of elastic scattering differential cross-section to Rutherford scattering for 240 MeV ^{6}Li particles on ^{116}Sn is plotted versus average center-of-mass angle. The optical model fit is shown by the gray line.

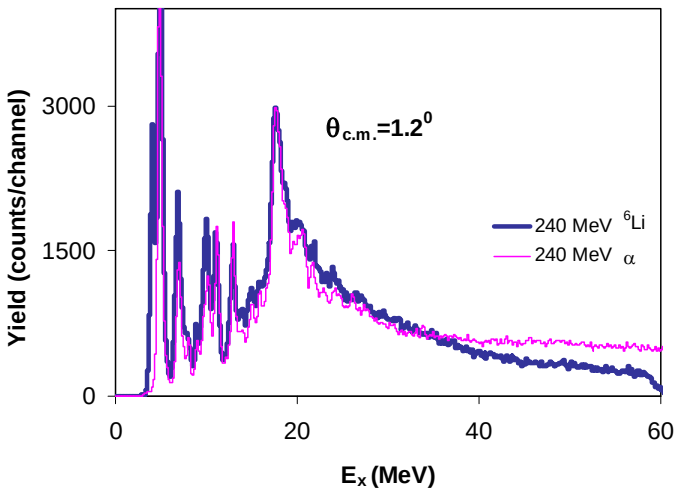

Figure 3. Comparison between α inelastic scattering and ^{6}Li inelastic scattering from ^{28}Si.

[1] W. Eyrich, A. Hofmann, A. Lehmann, B. Muhldorfer, H. Schlosser, H. Wirth, H. J. Gils, H. Rebel, and S. Zagromski, Phys. Rev. C **36**, 416 (1987).

[2] H. Dennert, E. Aschenauer, W. Eyrich, A. Lehmann, M. Moosburger, N. Scholz, H. Wirth, H. J. Gils, H. Rebel, and S. Zagromski, Phys. Rev. C **52**, 3195 (1995).

[3] D.H. Youngblood, Y.-W. Lui, H.L. Clark, P. Oliver, and G. Simler, Nucl. Instrum. Methods Phys. Res. A **361**, 539 (1995).

[4] D.H. Youngblood, Y.-W. Lui, and H.L. Clark, Phys. Rev. C **55**, 2811 (1997).

[5] M. Rhoades-Brown, M.H. Macfarlane, and S.C. Pieper, Phys. Rev. C **21**, 2417 (1980); M.H. Macfarlane, and S.C. Pieper, Argonne National Laboratory Report No. ANL-76-11, Rev. 1, 1978, unpublished.

Elastic Scattering of RNB ^{17}F on Light Targets

J. C. Blackmon,[1] D. W. Bardayan,[1] C.R. Brune,[2] F. Carstoiu,[3] A. E. Champagne,[4] R. Crespo,[5] T. Davinson,[6] J. C. Fernandes,[5] C. A. Gagliardi, U. Greife,[7] C. J. Gross,[1] P. A. Hausladen,[1] C. Iliadis,[4] C. C. Jewett,[7] R. L. Kozub,[8] T. A. Lewis,[1] F. Liang,[1] B. H. Moazen,[8] A. M. Mukhamedzhanov, C. D. Nesarja,[8] F. M. Nunes,[9] P. D. Parker,[10] D. C. Radford,[1] L. Sahin,[1,4] J. P. Scott,[8] D. Shapira,[1] M. S. Smith,[1] J. S. Thomas,[11] L. Trache, R. E. Tribble, P. J. Woods,[6] and C. -H. Yu[1]

[1]*Physics Division, Oak Ridge National Laboratory, Oak Ridge, TN 37831*

[2]*Department of Physics and Astronomy, Ohio University, Athens, OH 45701*

[3]*Institute of Atomic Physics, Bucharest, Romania*

[4]*Department of Physics and Atronomy, University of North Carolina, Chapel Hill, NC 27599*

[5]*Dept. de Fisica, Instituto Superior Tecnico, Av. Rovisco Pais, 1049-001 Lisboa, Portugal*

[6]*Dept. of Physics and Astronomy, University of Edinburgh, Edinburgh EH9 3JZ,United Kingdom*

[7]*Department of Physics, Colorado School of Mines, Golden, CO 80401*

[8]*Physics Department, Tennessee Technological University, Cookeville, TN 38505*

[9]*NSCL, Michigan State University, East Lansing, MI 48824*

[10]*A. W. Wright Nuclear Structure Laboratory, yale University, New Haven, CT 06511*

[11]*Department of Physics and Astronomy, Rutgers University, New Brunswick, NJ 08903*

The ^{17}F(p,γ)^{18}Ne reaction is important for the understanding of nucleosynthesis in explosive hydrogen burning in novae, but its reaction rate is difficult to determine from direct measurements. Therefore, a measurement was done to determine the capture S-factor using the ANCs determined from the proton-transfer reaction ^{14}N(^{17}F,^{18}Ne)^{13}C. Some results were presented already [1]. For a precise DWBA analysis of the proton transfer reaction we need to determine reliable optical model potentials (OMP). For this purpose, elastic scattering cross sections for ^{14}N(^{17}F,^{17}F)^{14}N and ^{12}C(^{17}F,^{17}F)^{12}C were measured over an extended angular range. A 10 MeV/u beam of isotopically-pure ^{17}F from the Holifield Radioactive Ion Beam Facility bombarded melamine and carbon targets. The elastic scattering cross sections were measured over an angular range θ_{cm}=8° - 40°. At small angles the scattered and transfer particles were detected with two telescopes made of 5x5 cm^2 position-sensitive silicon-strip detectors backed by thick detectors, positioned symmetrically around the beam, and at larger angles an annular array of strip detectors was used. These data were analyzed both in terms of phenomenological Woods-Saxon potentials and with potentials resulting from a double-folding procedure established before [3] and tested on several cases of RNB elastic scattering (^{7}Be, ^{8}B, ^{11}C, ^{13}N on melamine and C). However the present data represent the best set of experimental elastic data so far, both in terms of resolution of the beam and of the detectors, and in terms of angular coverage.

We found that the OMP parameters extracted from the phenomenological fit have significant ambiguities. The double-folding procedure using the JLM effective interaction and renormalization works better. A fit to the data give renormalizations of the real and imaginary parts close to the averages extracted in Ref. [2] for p-shell nuclei. For ^{14}N(^{17}F,^{17}F)^{14}N we find the renormalizations N_V=0.61 and

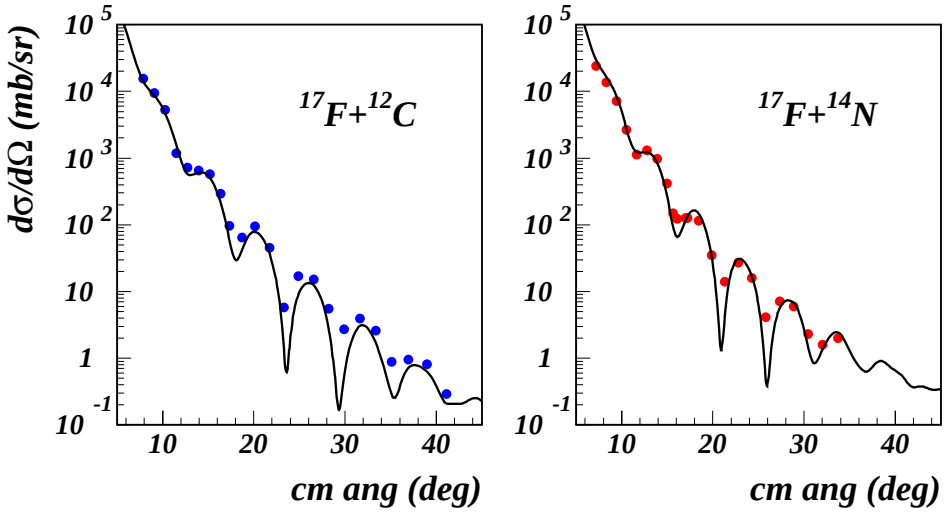

Figure 1. The measured $^{12}C(^{17}F,^{17}F)^{12}C$ and $^{14}N(^{17}F,^{17}F)^{14}N$ elastic scattering cross sections compared with those calculated using the optical model potentials described in the text.

N_W=0.91 for the real and imaginary parts of the potential, and for $^{12}C(^{17}F,^{17}F)^{12}C$ we find N_V=0.53 and N_W=1.03. The renormalization needed for the real part is less than that found earlier for loosely bound p-shell nuclei (N_V(ave)=0.37) and closer to what we found for a better bound system $^{13}C(^{14}N,^{14}N)^{13}C$ (N_V=0.46), a sign that the importance of the dynamical polarization potential diminishes for this heavier sd-shell nucleus. Again, we find that the imaginary part needs practically no renormalization.

[1] J. Blackmon *et al.*, RNB6 Conference, Argonne, Sept. 2003, and Nucl. Phys. A, in press.
[2] L. Trache *et al.*, Phys. Rev. C **61**, 024612 (2000).

Study of Resonance Scattering of ^{18}O, ^{18}Ne, and ^{14}O on Helium

V. Z. Goldberg, G. G. Chubarian, C. Fu, G. Tabacaru, L. Trache, R. E. Tribble, G. V. Rogachev,[1]
B. B. Skorodumov,[1] and P. Boutachkov[1]
[1]*Department of Physics, University of Notre Dame, South Bend, IN 46556*

Results of experimental studies of resonance interaction of ^{18}O and ^{18}Ne with helium has been published in [1]. This work reports the first investigation of elastic resonance scattering of mirror nuclei with T=1 on ^{4}He by the thick target inverse kinematics method (TTIK) [2]. The detailed comparison of the available results obtained by the conventional approach with these obtained by the TTIK method is presented. The spin-parity assignments are given for over 40 states, and it is shown that some of these states can have very exotic nuclear structure. Then we tested the possibilities to extend this study to an ^{14}O beam. The main goals of the study of resonance interactions of ^{14}O with helium were to get information on possibilities to study the following processes: (1) the reaction $\alpha+^{14}O \rightarrow p+^{17}F$, (2) two proton decay of excited states in ^{18}Ne, (3) α cluster structure in ^{18}Ne.

The ^{14}O experiment was performed at the Texas A&M University. The K500 superconducting cyclotron primary beam of ^{14}N with energy 10 MeV/A was used to produce ^{14}O with energy ~6 MeV/A in gas cell filled with hydrogen. The recoil spectrometer MARS [3] was used to filter reaction products into the secondary 5 MeV/A ^{14}O beam of 99.9% purity and intensity of 30000/s. The TTIK method was used. The identification of the $\alpha+^{14}O$ reaction products was made by the energy vs. time-of-flight analysis. The time signals from a PPAC, positioned at the front of the scattering chamber, and the signals from Si detectors, positioned in the chamber filled with helium, were used.

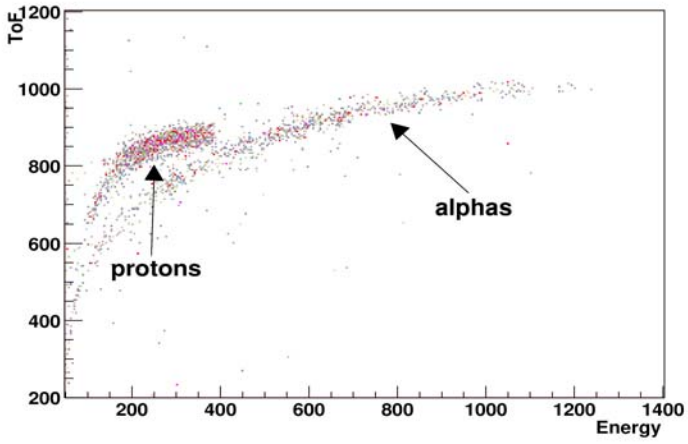

Figure 1. The two dimensional spectrum ToF-E for light particle products of the $^{14}O+\alpha$ interaction.

As can be seen in Fig. 1, protons and α particles can be easily identified in ToF-E two dimensional spectra, and several groups are evident at the high energy part of the α particle locus. The 3 day run showed that the experiments in question are promising after some increasing of the intensity of the ^{14}O beam. The estimation shows that an intensity of ^{14}O beam up to 10^5 is feasible at the Texas A&M University cyclotron.

[1] V.Z. Goldberg *et al.*, Phys. Rev. C **69**, 024602 (2004).
[2] V.Z. Goldberg and A.E. Pachomov, Phys. At. Nucl. **56**, 1167 (1993).
[3] R.E. Tribble *et al.*, Nucl. Phys. **A701**, 278c (2002).

Resonance Scattering of Radioactive ^{11}C and ^{14}O on Hydrogen

V. Z. Goldberg, G. G. Chubarian, G. Tabacaru, L.Trache, R. E. Tribble, G. V. Rogachev,[1]
B. B. Skorodumov,[1] A. Aprahamian,[1] and X. D. Tang*
[1]*Department of Physics, University of Notre Dame, South Bend, IN 46556*

The experiments were performed at the Texas A&M University K500 superconducting cyclotron. Primary beams of ^{11}B and ^{14}N with energy of 12 MeV/A were used to produce ^{11}C and ^{14}O correspondingly. The recoil spectrometer MARS was used to filter reaction products into the secondary beams [1] of 99.9% purity. In both experiments we used the thick target inverse kinematics method [2] to study resonance scattering in the chamber filled by methane gas.

In the experiment with ^{14}O two resonances were observed, and unique assignments was made for the quantum characteristics of the lowest states in ^{15}F, $1/2^+$ and $5/2^+$ correspondingly. The widths and the levels positions were also determined. The data obtained were used to define shell model potential for the ^{15}C and ^{15}F nuclei. A more general analysis brought evidence for unusually large diffuseness of the nuclear potential for nuclei at the borders of nuclear stability. The results were published in [3]. The main goal of the ^{11}C experiment was a search for states in ^{12}N near the threshold for the decay into $^{8}B+\alpha$, which could play an important role in nuclear synthesis in stars through the $^{8}B+\alpha \rightarrow {}^{11}C+p$ process.

The measurements included a short (about one hour) run to observe elastic scattering and a 12 hours run to study elastic and inelastic resonance scattering near the $^{8}B+\alpha$ threshold. The intensity of the ^{11}C beam was~10^6/s. A 20 μ Pt foil was positioned in the gas filled scattering chamber to eliminate elastic scattering on hydrogen in the region, where it could interfere with inelastic scattering peaks of excitation of states near the $^{8}B+\alpha$ threshold in ^{12}N.

As can be seen in Fig. 1, we have observed a state (or states) near the $^{8}B+\alpha$ threshold in ^{12}N in

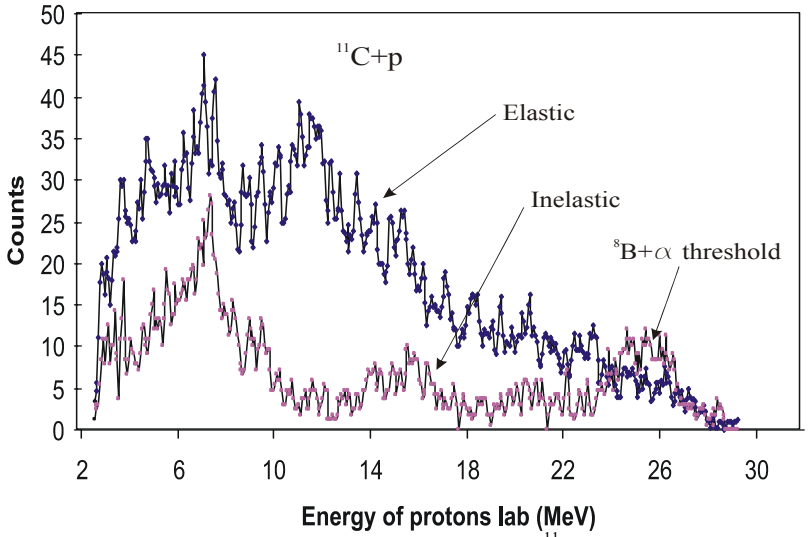

Figure 1. Excitation functions (Laboratory system) for $^{11}C+p$ interaction. The upper curve is the yield of protons from CH_4 target (mainly the elastic scattering). The bottom curve is the proton yield with a Pt foil in the CH_4 gas. The proton in the energy region 11-22 MeV are mainly results of resonant inelastic scattering of ^{11}C on

elastic as well in the inelastic scattering. The data are analyzed in the frame of R-matrix approach, which is complicated due to unusual experimental conditions and the presence of many broad resonances.

*Present address: Physics Division, Argonne National Laboratory, Argonne, IL 60439

[1] R.E. Tribble *et al.*, Nucl. Phys. **A701**, 278c (2002).
[2] V.Z. Goldberg and A.E. Pachomov, Phys. Atomic. Nucl. **56**, 1167 (1993).
[3] V.Z. Goldberg *et al.*, Phys. Rev. C **69**, 031302 (R) (2004).

Remeasurement of ^{7}Be +^{14}N (87 MeV) for the Astrophysical $S_{17}(0)$ Factor

G. Tabacaru, A. Azhari,* J. Brinkley, V. Burjan,[1] C. Fu, C. A. Gagliardi, X. Tang,**
L. Trache, and R. E. Tribble
[1] *Institute of Nuclear Physics, Czech Academy of Sciences, Prague-Rez, Czech Republic*

Last year we announced [1] that we have repeated the measurement to determine the asymptotic normalization coefficient (ANC) for the ^{7}Be+p→ ^{8}B using the transfer reaction ^{14}N(^{7}Be,^{8}B)^{13}C. Two improvements were made to our earlier experiment [2]: a new way to monitor the secondary beam intensity and the extension of the angular range for the detection of elastic scattering. Since, we have analyzed the new data obtained and we have the first results. In the earlier experiment, monitoring of the beam intensity was done by measuring the primary beam intensities with a Faraday cup (FC) placed in MARS's coffin, but later we suspected that a "tunneling" effect in the gas target was causing a drop of isotope production rate per nA of primary beam current. Such an effect was observed in other measurements, when the intensity of the beam was increased, due to an increased local heating in the gas. We presumed that when we increased our ability to produce more intensity of the primary ^{7}Li beam we affected our precision to measure the secondary beam rate, and suspected that this problem had an influence on the results obtained in [2].

The primary beam used was ^{7}Li at 18.6 MeV/A from the K500 cyclotron. The final energy of the radioactive ^{7}Be beam at the end of MARS was 87 MeV with intensities ≈150 - 200 kHz. The new beam monitoring system measured directly the secondary beam using a screen to reduce the ^{7}Be beam intensity by 88% and a scintillator coupled with a photo-multiplier tube. This could be run at a rate acceptable for our acquisition system. In parallel, we run the old monitoring system with a FC for the primary beam, and compared the results. In the inset of the figure we plot the ratio between the two normalization factors, one corresponding to the Faraday cup primary beam intensity measurements and the other to the scintillator secondary beam intensity measurements. An average difference of about 5.5% was noted with the scintillator normalization. The extracted ANC value increases by 5.5% which translates into a corrected value $S_{17}(0)$= 18.0±1.7 eVb.

The angular distribution for ^{7}Be elastic scattering on melamine measured over an extended range is shown in Figure 1. The experimental points are compared with the theoretical prediction using double-folded JLM1 potentials, renormalized as determined before [3]. As in previous analyses, a Monte Carlo simulation was used to smooth the calculations with the experimental resolutions. We observe a good fit at small angles, with some deviations at larger angles, out of the range of the previous measurement. The fit at small angles reflects a good absolute normalization of the cross sections. The difference at larger angles suggests less absorption in the OMP than previously considered. We are currently working on an improved overall fit of the data and on the consequences it may have on the final value of the ANC.

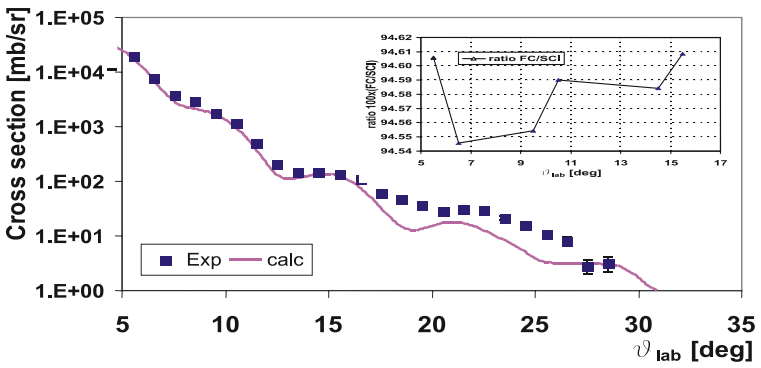

Figure 1. The angular distribution for ^{7}Be 87 MeV elastic scattering on melamine. Full curve is calculation.

*Present address: Alix Partners, Dallas, Texas.

**Present address: Physics Division, Argonne National Laboratory, Argonne, IL 60439.

[1] G. Tabacaru *et al.*, *Progress in Research*, Cyclotron Institute, Texas A&M University (2002-2003), p. I-12

[2] A. Azhari *et al.*, Phys. Rev. C **63,** 055803 (2001).

[3] L. Trache *et al.*, Phys. Rev. C **61,** 024612 (2000).

Consequences of a Possible $1d_{5/2}$ and $2s_{1/2}$ Level Inversion in ^{23}Al on the ^{22}Mg(p,γ)^{23}Al Stellar Reaction Rate

L. Trache, R. E. Tribble, F. Carstoiu,[1] and N. Orr[1]
[1]*Laboratoire de Physique Corpusculaire, Universitè de Caen, France*

Space-based gamma-ray telescopes now provide the ability to detect γ rays of cosmic origin. Among the expected γ-ray emitters is ^{22}Na ($T_{1/2}$=2.6 y) produced in the thermonuclear runaway and the high-temperature phase in novae through the reaction chain ^{20}Ne(p,γ)^{21}Na(p,γ)^{22}Mg(β,ν)^{22}Na. However, ^{22}Mg can be depleted by the radiative proton capture reaction ^{22}Mg(p,γ)^{23}Al. The reaction is dominated by direct capture and resonant capture to the first excited state in ^{23}Al. Currently the rate of this reaction is estimated based on the mass and resonance energy determined experimentally [1] and assuming the spins and parities as in the mirror nucleus. ^{23}Al is a weakly bound proton rich nucleus (S_p=0.123(19) MeV), close to the drip line. Recent measurements [2] of its reaction cross section lead to the conclusion that it is one of the rare proton halo nuclei, due to a presumed level inversion between the $2s_{1/2}$ and $1d_{5/2}$ orbitals. This inversion is further supported by several microscopic nuclear structure calculations [3] that find $J^{\pi}=1/2^{+}$ for ^{23}Al ground state. Assuming such an inversion, we recalculate the astrophysical S-factor (Fig. 1a) and the stellar reaction rate (Fig. 1b) for the ^{22}Mg(p,γ)^{23}Al capture and find an increase of 30 to 50 times over the current estimate for the temperature range T_9=0.1-0.3. This results in a significant

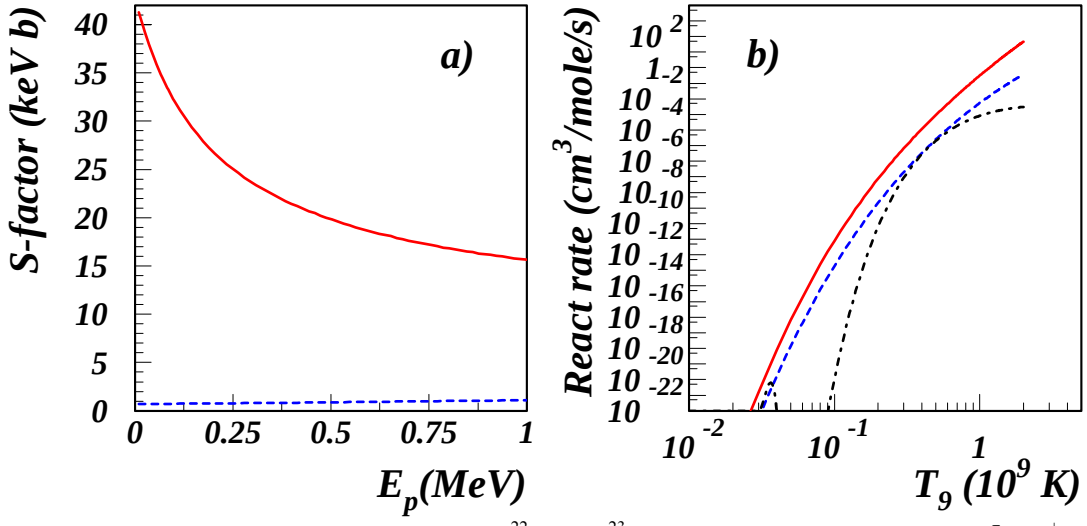

Figure 1. a) The astrophysical S-factor for the ^{22}Mg(pγ)^{23}Al reaction, calculated assuming $J^{\pi}=5/2^{+}$ (dashed line), or $J^{\pi}=1/2^{+}$ (orbital inversion, full line) for the g.s. of ^{23}Al. b) The corresponding reaction rate calculated for the case of non-inversion (dashed), or inversion (full line). The dash-dot line shows the resonant contribution of the 1st excited state in ^{23}Al.

depletion of ^{22}Mg before it beta-decays into ^{22}Na and, if confirmed, could explain the non-observation of the 1.25 MeV γ-ray from ^{22}Na by COMPTEL. Clearly it is important to determine the spin and parity of the low-lying levels in ^{23}Al. We propose the use of one-proton-removal reaction on a light target as a way

to determine the ground state properties. We calculate that for a $^{12}C(^{23}Al,^{22}Mg)$ experiment at 50 MeV/nucleon the parallel momentum distribution is about 2 times narrower for a $2s_{1/2}$ orbital than for a $1d_{5/2}$ orbital and the breakup cross section is about a factor two larger, which is enough to distinguish between them. Careful measurements of the momentum distributions in coincidence with gamma-rays from the core will allow us to disentangle a more complex structure of the wave function. Other complementary spectroscopic studies of ^{23}Al will be sought.

[1] J. Caggiano *et al.*, Phys. Rev. C **64**, 025802 (2001).
[2] X.Z. Cai *et al.*, Phys. Rev. C **65**, 024610 (2002).
[3] H.-Y. Zhang *et al.*, Chin. Phys. Lett. **19**, 1599 (2002); ibidem **20**, 46 (2003).

Refractive Effects in the Scattering of Loosely Bound Nuclei

F. Carstoiu,[1] L. Trache, R. E. Tribble, and C. A. Gagliardi
[1]*Institute for Physics and Nuclear Engineering Bucharest, Romania*

This year we finalized a new theoretical analysis of the experimental elastic scattering studies we conducted in the past years with loosely bound, but stable projectiles on light targets. The study is a complement of our previous detailed study of elastic scattering [1] between light p-shell nuclei around 10 MeV/u, and has as primary purpose to find reliable ways to predict/determine the optical model potentials needed for use in our transfer reactions with rare isotope beams. These proton or neutron transfer reactions employ DWBA techniques to extract nuclear structure information used consequently in indirect methods in nuclear astrophysics [2]. Experimental studies using RNBs have, heretofore, not been suitable for detailed elastic scattering analyses. The best information comes from studying the elastic scattering of stable loosely bound nuclei with similar masses. In this study our focus was on the interaction of ^{6,7}Li at 9 and 19 MeV/nucleon with light ^{9}Be, ^{12}C, ^{13}C targets. With the determination of unambiguous optical potentials in mind, elastic data for four projectile-target combinations and one neutron transfer reaction ^{13}C(^{7}Li,^{8}Li)^{12}C [3] have been measured over a large angular range in past years. The present analysis shows that the kinematical regime encompasses a region where the mean field (optical potential) has a marked variation with mass and energy, but turns out to be sufficiently surface transparent to allow strong refractive effects to be manifested in elastic scattering data at intermediate angles. This transparency is somewhat unexpected, given the fragile, cluster-like, structure of ^{6,7}Li projectiles. The identified exotic feature, a "plateau" in the angular distributions at intermediate angles, is fully confirmed in four reaction channels and is interpreted as a pre-rainbow oscillation resulting from the interference of the barrier and internal barrier far-side scattering subamplitudes.

The analysis involves both phenomenological Woods-Saxon volume potentials and semi-microscopic double-folding potentials. The same JLM nucleon-nucleon effective interaction is used for folding, allowing this time the renormalization coefficients and the range parameters of the real and imaginary parts to vary. This allows a unitary and better description of the large angle part of the measured angular distributions, with the minimal price of two extra parameters. With the extra condition to fulfill the dispersion relation, we arrive at unique optical potentials with volume integrals around 300 MeV fm^3/nucleon pair. We show, however, that the previously determined recipe to predict OMP [1] describes very well the Fraunhoffer diffraction region of the elastic scattering angular distributions and the transfer reactions, testimony that the surface of the potential is well determined. The results were submitted for publication [4].

[1] L. Trache *et al.*, Phys. Rev. C **61**, 024612 (2000).
[2] A.M. Mukhamedzhanov, C.A. Gagliardi, and R.E. Tribble, Phys. Rev. C **63**, 024612 (2001).
[3] L. Trache *et al.*, Phys Rev. C **67**, 062801(R) (2003).
[4] F. Carstoiu *et al.*, submitted to Phys. Rev. C.

Observation of Resonance Yield of Neutrons and γ Rays in the Interaction of Radioactive ^{6}He with Hydrogen

V. Z. Goldberg, G. Chubarian, G. V.Rogachev,[1] P. Boutachkov,[1] and A. Aprahamian[1]
[1]*Department of Physics, University of Notre Dame, South Bend, IN 46556*

Several years ago it was suggested [1] that studies of analog states of neutron rich drip line nuclei by means of resonance reactions could become a powerful instrument of nuclear spectroscopy of neutron rich drip line nuclei. Simultaneously it was shown that excitation of the states in question could manifest itself by the resonance yield of neutrons and γ rays.

Two first experiments were carried out using a low energy ^{6}He beam of the University of Notre Dame. In both cases a thick target inverse kinematics method, using a solid, CH_2, target, was used. There are two main and general problems, which should be cleared by these experiments. (1) The levels of high isobaric spin in neutron rich nuclei are in the excitation region, which has been scarcely investigated (if investigated at all). Therefore the level scheme of states with a lower isobaric spin is unknown and their interference with higher isobaric spin levels is unclear. (2) The feasibility of these experiments, using the modern technique should be tested.

The coincidence between neutrons ejected in the forward direction in the reaction ^{6}He+p→ ^{7}Li(T=3/2)→^{6}Li(T=1)+n and γ rays of the transition ^{6}Li(T=1)→^{6}Li$_{g.s.}$, were measured in the first experiment. The neutrons were detected in a position sensitive plastic-scintillator neutron wall, and the γ rays were detected by four large BaF_2 detectors at angles near 90 degrees. Fig.1 presents the excitation function for the ^{6}He(p,n)^{6}Li reaction measured under the conditions above. No normalization factor is

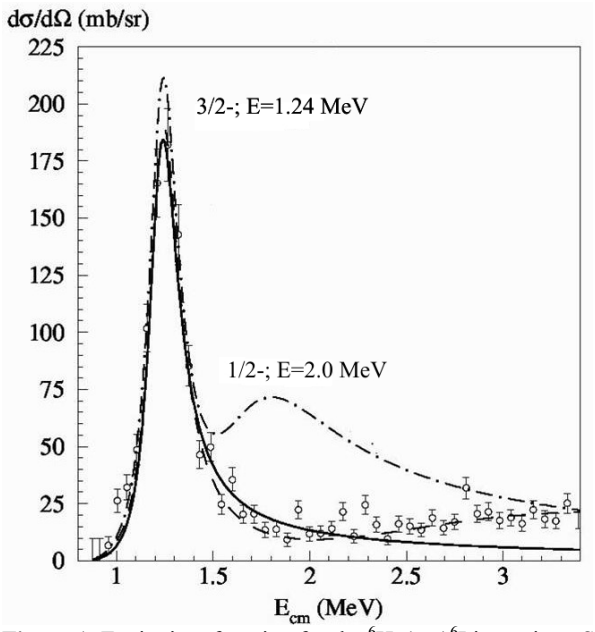

Figure 1. Excitation function for the ^{6}He(p,n)^{6}Li reaction. See text for the explanation

introduced in the calculations. The solid line in Fig.1 corresponds to a single $3/2^-$ (T=3/2) resonance. The dash-dotted line corresponds to the addition of $1/2^-$ (T=3/2) resonance, as was claimed in [2,3] and the dashed line corresponds to the presence of the $1/2^-$ resonance at a higher excitation energy (~3.6 MeV). Fig. 1 clearly demonstrates the dominant population of T=3/2 state in ^{7}Li (isobar analog of the ^{7}He ground state) and absence of the $1/2^-$ state, claimed in [2,3]. Our data present some evidence for this state at much higher excitation energy. The work will be published in [4].

The second experiment was an attempt to measure the excitation function for the ^{6}He+p→ ^{7}Li(T=3/2)→^{6}Li(T=1)+n process by the observation of the Doppler shifted γ rays from the decay of 3.56 MeV T=1 level in ^{6}Li. The data are still under analysis due to difficulties of the exact simulation of the shape of the γ lines in the presence of neutrons from the reaction in question. However we can state that the results look very promising.

[1] V.Z. Goldberg, ENAM98, Exotic nuclei and Atomic Masses, ed., by B.M. Sherrill, D.J. Morrissey and C.N. Davids (AIP, 1998) p. 319.
[2] K. Markenroth *et al.*, Nucl. Phys. **A679**, 462 (2001).
[3] M. Meister *et al.*, Phys. Rev. Lett. **88**, 102501 (2002).
[4] G.V. Rogachev *et al.*, Phys. Rev. Lett., (in press).

The Updated Reaction Rate for $^{13}N(p,\gamma)^{14}O$

X. Tang,[1] A. Azhari,[*] C. Fu, C. A. Gagliardi, A. M. Mukhamedzhanov, F. Pirlepesov,
L. Trache, R. E. Tribble, V. Burjan,[2] V. Kroha,[2] F. Carstoiu,[3] and B. F. Irgaziev[4]
[1]*Physics Division, Argonne National Laboratory, Argonne, IL 60439*
[2]*Insitute of Nuclear Physics, Czech Academy of Sciences, Prague-Rez, Czech Republic*
[3]*Institute of Physics and Nuclear Engineering, H. Hulubei, Bucharest, Romania*
[4]*Department of Physics, National University, Tashkent, Uzbekistan*

The $^{13}N(p,\gamma)^{14}O$ is one of the key reactions which trigger the onset of the hot CNO cycle [1]. This transition occurs when the β-decays of ^{14}O and ^{15}O are slower than the proton capture reactions on ^{13}N and ^{14}N. The rate of the $^{13}N(p, \gamma)^{14}O$ reaction is dominated by resonant capture through the first excited state of ^{14}O (E_r=0.528 MeV). However, through constructive interference direct capture below the resonance makes a non-negligible contribution to the reaction rate.

In the past year, we finished the data analysis for $^{14}N(^{13}N,^{14}O)^{13}C$. Details of the experiment can be found in previous annual reports. The final value of the ANC for $^{14}O \rightarrow {}^{13}N+p$ was found to be $C^2_{1/2} = 29 \pm 4.3\ fm^{-1}$. The uncertainties include statistics (3%), absolute normalization of the cross section (7%), the error from setting the Q-value windows (5%), Monte Carlo simulation (2%), DWBA (8%) and knowledge of the $^{14}N \rightarrow {}^{13}C+p$ ANCs.

The cross section for direct and resonant captures through the broad first excited state are calculated from the measured ANC and the experimental resonance parameters using the R-matrix approach. The S factor calculated in this approach is shown together with the result from Decrock et al. [2] in Fig. 1. The relatively flat lower solid line, which is our result for direct capture alone, is about 30% larger than the result obtained by Decrock et al., which is shown as the lowest dash-dotted line. The two results barely agree within the quoted uncertainties. At E_{cm}=140 keV, where the Gamow peak is located for $T_9 = 0.2$, our updated result using constructive interference, shown as

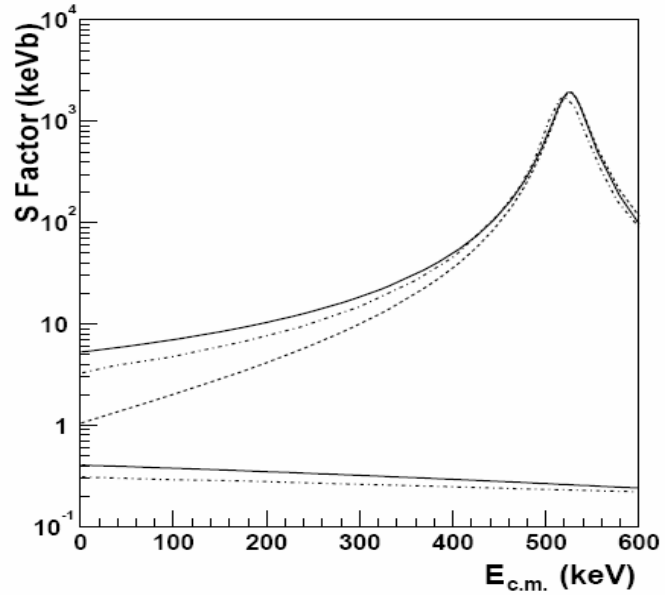

Figure 1. The astrophysical *S* factor for ^{13}N $(p,\gamma)^{14}O$. The flat solid line is the direct capture contribution determined from the present experiment. It is higher than that obtained by Decrock *et al.* [2] (lowest dash-dotted line). The total *S* factor (the top solid line), obtained from direct-resonant constructive interference, is about 38% higher than the previous result (upper dash-dotted line). For completeness, we show the result that would be obtained with destructive interference as the dashed line.

the upper solid line, is about 38% higher than the previous result, which is shown as the upper dash-dotted line in Fig. 1. This is due to the larger direct capture contribution from the ANC measurement. We found through microscopic calculation that in the R-matrix calculations the interference between direct capture and first resonance should be constructive. For completeness only, we also show the result that would be obtained with destructive interference as the dashed line. The sign of the interference could be easily checked with a direct measurement at higher energies (E_p=200-400 keV).

The new reaction rates are about 2 times NACRE's compilation [3] at low temperature and are almost identical at higher temperature. The uncertainties, dominated by the error of the γ width of the first resonance, drop from 30% to 20% by varying the temperature from T_9=0.01 to T_9=0.97.

With the updated rates, we found that the reaction rate for $^{14}N(p,\gamma)^{15}O$ is slower than $^{13}N(p, \gamma)^{14}O$ when $T_9<0.16$ and $T_9>0.73$. Therefore, for the typical novae temperature and density conditions, the transition from the cold to hot CNO cycle is still governed by the competition between $^{14}N(p,\gamma)^{15}O$ and the β-decay of ^{14}O and ^{15}O. The results are currently being published [4].

*Present address: Alix Partners, Dallas, Texas.

[1] M. Wiescher, J. Gorres and H. Schatz, J. Phys. G **25**, R133 (1999).
[2] P. Deckrock *et al.*, Nucl. Phys. **A646**, 261 (1999).
[3] C. Angulo, NACRE (Nuclear Astrophysics Compilation of REaction Rates), http://pntpm.ulb.acbe /Nacre/
[4] X.Tang *et al.*, Phys. Rev. C **69**, (in press).

Determination of the S_{34} Astrophysical Factor from the $^7Be \rightarrow {}^3He+\alpha$ Breakup

C. Fu, L. Trache, G. Tabacaru, Y. Zhai, and R. E. Tribble

The reaction $^3He(\alpha,\gamma)^7Be$ is very important for the solar neutrino problem and for primordial nucleosynthesis in the Big Bang. Because of the difficulties in direct measurements of the S factor at very low energies (corresponding to temperatures ~10^6-10^9K), indirect reactions are sought as alternatives. In ^7Be nuclei, the $\alpha+^3He$ configuration is the dominant cluster configuration, and their binding energy is small (~1.58MeV). We are exploring the possibility to study the nuclear + Coulomb breakup $^7Be \rightarrow {}^3He+{}^4He$ around and above the Fermi energy, in order to extract nuclear astrophysical information.

In order to take advantage of this method, a radioactive beam ^7Be was developed. We had a test experiment in last September to obtain ^7Be at 25 MeV/ nucleon (in the past we only got 12 MeV/nucleon ^7Be). The ^7Li beam at 27A MeV was delivered from the K500 superconducting cyclotron and impinged on a liquid-nitrogen-cooled hydrogen gas target. The secondary ^7Be beam at 25A MeV was purified and transported by MARS. The production found was about 1000 ^7Be nuclei per pnA of incoming ^7Li. Its purity was over 99%, and it was well collimated. With the current ^7Li intensities from the cyclotron, the expected ^7Be beam intensity is about $3\text{-}7\times10^5$ pps at 25 MeV/nucleon. We also are modifying the way we operate the silicon strip position sensitive detectors (PSD) to give them multi-hit capability. We do this by using the signals from both ends of each strip to determine the energy loss and position, rather than using that from a single end and the common back signal for the energy deposit. Using two PSDs in a telescope, with the strips perpendicular to each other, 1-3 mm position resolution can be achieved in each direction. This solution implies more electronics than we had in the previous arrangements. Another problem that we need to overcome is that our current detector telescopes are not thick enough to stop high energy light ions of this reaction. With the data from theoretical calculations[1], a simulation for the whole experiment is carried out, which helps to determine the optimum setup. We intend to study the breakup on a light target (carbon) in order to maximize the contribution of the nuclear part of the nucleus-nucleus interaction and minimize that of the Coulomb interaction. We also intend to measure the breakup at two energies, one in our laboratory (25A MeV) and another at GANIL (75A MeV).

[1] N.C. Summers and F.M. Nunes, to be published.

Extracting the ANCs for $^{23}Al \rightarrow {}^{22}Mg + p$ from Its Mirror System $^{23}Ne \rightarrow {}^{22}Ne + n$

T. Al-Abdullah, X. Chen, H. L. Clark, C. A. Gagliardi, Y. -W. Lui, G. Tabacaru, Y. Tokimoto, L. Trache, and R. E. Tribble

The 1275 keV gamma-ray from the decay of the long-lived ($T_{1/2}$ = 2.61 yr) ^{22}Na nucleus, supposedly synthesized during nova explosions via the rp-process in the Ne-Na cycle as in Fig. 1, was not observed in satellite gamma-ray telescopes such as COMPTEL. One suggested explanation is that the precursor ^{22}Mg can be depleted by the radiative proton capture reaction ^{22}Mg (p, γ) ^{23}Al [1]. The rate of this reaction is not precisely known. We plan to determine this rate with an indirect method using transfer reactions [2]. The normal candidate is a proton transfer reaction, but since the radioactive ^{22}Mg beam is not easily available, the (^{22}Mg,^{23}Al) reaction is replaced by the neutron transfer reaction (^{22}Ne,^{23}Ne). The structure of the ground state and first exited state in ^{23}Ne is studied and then transposed to the corresponding states of the mirror nucleus ^{23}Al. The analysis will be done by extracting the asymptotic normalization coefficients (ANCs) using the charge symmetry and following the same procedure as in (^{7}Li, ^{8}Li) reaction [3].

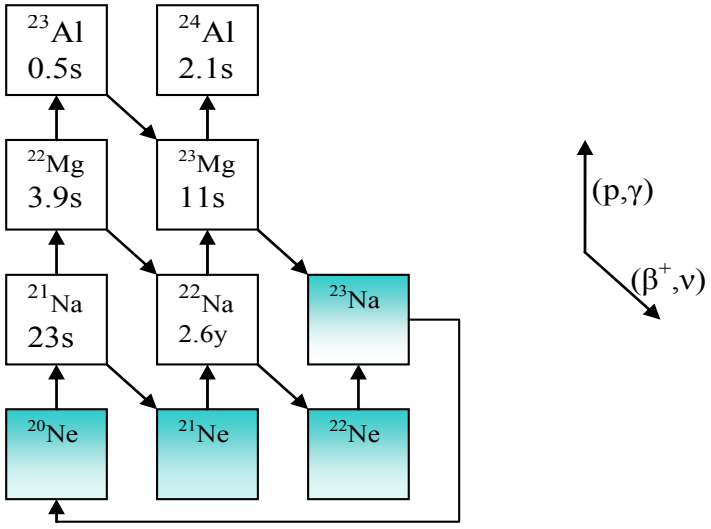

Figure 1. Section of the chart of nuclides representing nuclear reactions and β-decays included the rp-process (NeNa cycle). The stable nuclei in the cold cycle have been shaded.

Two experiments using a 264 MeV ^{22}Ne beam from the K500 superconducting cyclotron were carried out so far. The MDM spectrometer was used to study detailed angular distributions for the elastic scattering and for the neutron transfer reaction $^{13}C(^{22}Ne,^{23}Ne)^{12}C$. The bombarding $^{22}Ne^{+4}$ beam impinged on a 100 μg/cm^2 ^{13}C target located in the target chamber. The Oxford detector was filled with pure isobutane gas at 50 torr. The detector consists of an ionization chamber to measure the energy loss inside

the ionization chamber, four resistive wires to determine position at various depths in the chamber, and a plastic scintillator sitting 42 mm behind it to determine the residual energy. An angle mask consisting of five opening slits 0.77° apart and 0.1° wide was used to perform the position and angle calibration by comparing the elastic scattering of ^{22}Ne beam on a 300 μg/cm^2 ^{197}Au target with Raytrace calculations. During measurements a 4° x 1° window was used to accept the reaction products in the spectrometer, and the position in the focal plane and target angle are reconstructed using raytracing. A new acquisition ROOT code was written and checked to replace the code Goosy (used before on the VAX-VMS acquisition system which was retired recently).

In the first experiment, in September 2003, we tested our ability to measure the elastic scattering of ^{22}Ne on ^{13}C and the neutron transfer reaction. The results showed that we can clearly separate ^{22}Ne from ^{23}Ne, but that special care is needed at larger angles due to their close Bρ. We determined that we need to enlarge the entrance window of the Oxford detector to ensure full efficiency of the detector at large angles. Another experiment was performed in May 2004. We succeeded to make elastic scattering on ^{12}C and ^{13}C targets and transfer reaction measurements on ^{13}C target at four MDM positions, equivalent to the angular range $\theta_{C.M.}$ = 3°-32°. The preliminary angular distribution for neutron transfer to the ground state in ^{23}Ne is shown in Fig. 2. More measurements need to be done for full elastic scattering angular distribution, which will determine the optical potential parameters that will be used in DWBA calculations.

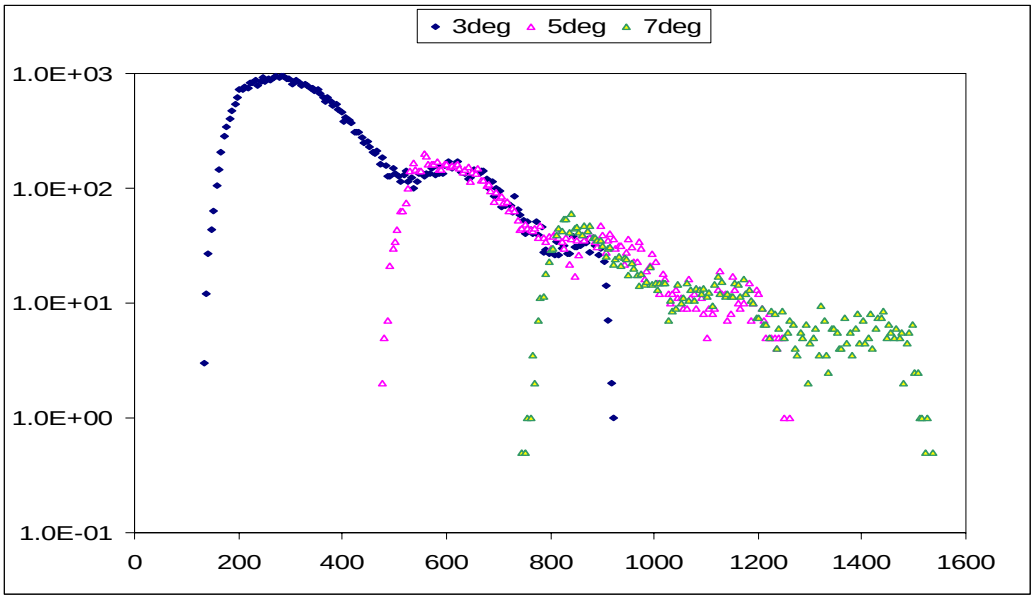

Figure 2. The yield of the reaction ^{13}C(^{22}Ne,^{23}Ne)^{12}C measured at 3, 5 and 7 deg. The x-axis represents the angle in channels. Preliminary.

[1] J.A. Caggiano *et al.*, Phys. Rev. C **64**, 025802 (2001).

[2] A. Azhari *et al.*, Phys. Rev. Lett. **82**, 3690 (1999).

[3] L. Trache *et al.*, Phys. Rev. C **67**, 062801 (2003).

The Superallowed β-Decay of ^{14}O and Its Ground-State Transition

I.S. Towner[1] and J.C. Hardy
[1]*Queen's University, Kingston, Ontario, Canada and Cyclotron Institute, Texas A&M University, College Station, Texas*

The nucleus ^{14}O decays predominantly by a superallowed $0^+ \rightarrow 0^+$ (Fermi) transition to the 2.314-MeV first-excited state in ^{14}N. Weak Gamow-Teller branches have also been observed to the 1^+ ground state, with a branching ratio, BR = 0.61(1)%, and to an excited 1^+ state at 3.94 MeV, with BR = 0.055(2)%. These results, when subtracted from 100%, yield a branching ratio of 99.33(1)% for the superallowed transition. Taken at face value, this result is more than precise enough to be used in our systematic studies of superallowed β-decay [1]; however, it depends critically on the branching ratio to the ground state, which was measured with sufficient precision only once, 48 years ago [2], and never repeated since. We have now reexamined that original experiment and reanalyzed its results.

The Gamow-Teller transition from ^{14}O to the ground-state of ^{14}N is strongly hindered. Its *ft*-value is roughly 10^4 times larger than is typical for favored $0^+ \rightarrow 1^+$ transitions. The inhibition is attributed to accidental cancellation in the allowed Gamow-Teller matrix element for this transition [3]. Because the allowed matrix elements are so small, the induced terms – particularly "weak magnetism" – as well as the relativistic and second-forbidden terms are expected to contribute appreciably to the decay probability. One important consequence is that the spectrum shape can be expected to deviate markedly from the allowed (or "statistical") shape.

In their original experiment, Sidhu and Gerhart measured the shape factor for the ground-state Gamow-Teller transition above 2.3 MeV, the energy at which the effects of the much stronger Fermi transition disappear. However, in order to extract the transition's branching ratio they had to make assumptions, in effect, about its shape factor over the full energy range. Their techniques were rather primitive compared to what is possible today, but a more modern investigation [4] was unable to fit the original spectrum at all, and suggested that there may have been systematic problems with the data.

We have reanalyzed the data presented in Sidhu's thesis [2]. In calculating the shape factor we have used two well-based sets of *0p*-shell wave functions [5,6], and adopted a procedure suggested by Garcia and Brown to treat the small amount of mixing between the two 1+ states as an adjustable parameter to obtain the best fit with the experimental shape factor. This small mixing has a large effect on the weak ground-state transition rate and could easily arise from non-*0p*-shell parts of the wave functions as well as from effective three-body forces not present in the calculation. With very small adjustments of this mixing parameter and with either set of wave functions, we can produce very good agreement with the measured β^+ spectrum shape in both slope and magnitude. From this analysis, we can deduce a ground-state β-branching ratio of 0.567(15)%, which differs somewhat from the 0.61(1)% value published by Sidhu and Gerhart [2], but not by enough to affect the superallowed *ft*-value significantly.

One serious problem remains, however. According to the Conserved Vector Current (CVC) hypothesis, the slope of the β shape factor should relate the Gamow-Teller matrix element for the β-

transition with the equivalent matrix element for the γ-decay of the analog state in the daughter nucleus. The lifetime of the 2.314-MeV analog state in ^{14}N is well known but is inconsistent with the observed slope of the shape factor. We are still examining this problem.

[1] J.C. Hardy and I.S. Towner, *Progress in Research*, Cyclotron Institute, Texas A&M University (2003-2004), p. I-28.

[2] G.S. Sidhu and J.B. Gerhart, Phys. Rev. **148**, 1024 (1966); G.S. Sidhu, *An experimental study of the spectrum shape for the Gamow-Teller transition 14O → ^{14}N*,.Ph.D. thesis, University of Washington (1966)

[3] H.J. Rose, O. Häusser and E.K. Warburton, Rev. Mod. Phys. **40**, 591 (1968).

[4] A. Garcia and B.A. Brown, Phys. Rev. C **52**, 3416 (1995).

[5] S. Cohen and D. Kurath, Nucl. Phys. **73**, 1 (1965).

[6] E.K. Warburton and B.A. Brown, Phys. Rev. C **46**, 923 (1992).

A New Critical Survey of Superallowed $0^+ \rightarrow 0^+$ Nuclear β-Decay

J. C. Hardy and I. S. Towner[1]

[1]*Queen's University, Kingston, Ontario, Canada and Cyclotron Institute, Texas A&M University, College Station, TX*

The measured *ft*-values for superallowed $0^+ \rightarrow 0^+$ nuclear β-transitions provide a direct determination of the weak vector coupling constant, G_V, which, in turn, yields the value of V_{ud}, the up-down mixing element of the Cabibbo-Kobayashi-Maskawa (CKM) matrix. The unitarity of the CKM matrix is a fundamental pillar of the Electroweak Standard Model, and V_{ud} is a key element in the most demanding test available of CKM unitarity: the sum of the top row elements, $V_{ud}^2 + V_{us}^2 + V_{ub}^2$. Currently, that sum deviates from unity by more than 2 standard deviations [1], although there is growing evidence that the value of V_{us} may be incorrect [2]. Whatever the outcome for V_{us}, it is crucial to establish V_{ud} with the highest possible precision, either to define better the violation of CKM unitarity or to establish the unitarity of the matrix more firmly and, by doing so, to set tight limits on any possible new physics beyond the Standard Model. This goal has attracted considerable interest the last few years from nuclear physicists seeking to improve and extend measurements of superallowed beta decay.

The last critical survey of all lifetime, decay-energy and branching-ratio measurements relating to superallowed $0^+ \rightarrow 0^+$ nuclear β-decay was completed 15 years ago [3]. The input data incorporated in that survey had first been comprehensively reviewed by us and, where necessary and possible, we had used information given in the original references to correct the results quoted there to take account of the most up-to-date values of atomic masses and of α- and γ-ray energies used in calibration. At that time, there were only 8 superallowed emitters – ^{14}O, ^{26m}Al, ^{34}Cl, ^{38m}K, ^{42}Sc, ^{46}V, ^{50}Mn and ^{54}Co – whose properties were known with sufficient precision (~0.1%) to warrant inclusion in the survey. Since that time, the survey has been updated periodically, most recently in 1998 [4], by the addition of the ^{10}C superallowed decay and other new measurements for the original 8 transitions, but there has been no comprehensive reexamination of the whole body of input data to reflect masses and calibration energies that have evolved since 1989.

We have now finished a completely new comprehensive survey, with input data corrected to modern calibration standards, and with many more superallowed transitions considered. In the past five years, with interest growing in a possible violation of CKM unitarity, attention has focused on measurements that could test the validity of the small nuclear-structure-dependent corrections that must be applied to the measured *ft*-values in order to extract G_V. The strategy has been to select superallowed emitters exhibiting a relatively large range of calculated correction terms and see if the experimentally observed variations among them confirm the theoretical calculations [5]. Such measurements involve a different set of nuclei, ones that previously have not been amenable to the required high experimental precision. A combination of factors has made this possible: the increased availability of radioactive beams [6], the development at Texas A&M of techniques to permit precise branching-ratio measurements [7], and the appearance of a number of on-line Penning traps that make it possible to measure precise atomic masses for very short-lived species [8]. Accordingly, the new survey comprises 20 nuclei: the

original eight, with ^{10}C, plus seven new even-even T_z = -1 nuclei from ^{18}Ne to ^{42}Ti, and four new odd-odd T_z = 0 cases from ^{62}Ga to ^{74}Rb. Not many yet contribute meaningfully to the unitarity question but all are within reach and will likely contribute in the near future.

The results of this survey will be combined with new calculations of the statistical rate function *f* [9] and a complete set of calculated corrections [5] into a complete review of the current status of superallowed $0^+ \rightarrow 0^+$ β-decay. We expect to submit it for publication later this year. In addition to providing a best value for V_{ud}, it is expected that the data will yield new constraints on the presence of scalar currents (*via* the Fierz interference term) and of right-hand currents.

[1] I.S. Towner and J.C. Hardy, J. Phys. G: Nucl. Part. Phys. **29**, 197 (2003).

[2] A. Sher *et al.* Phys. Rev. Lett. **26**, 261802 (2003) and presentations to *Zero to Z^0: A workshop on precision electroweak physics*, Fermilab, May 2004.

[3] J.C. Hardy, I.S. Towner, V.T. Koslowsky, E. Hagberg and H. Schmeing, Nucl. Phys. **A509**, 429 (1990).

[4] I.S. Towner and J.C. Hardy, *Proc. 5th Int. WEIN Symp. Physics Beyond the Standard Model (Santa Fe, NM, June 1998)* ed. P Herczeg, C.M. Hoffman and H.V. Klapdor-Kleingrothaus (World Scientific, Singapore, 1999) p. 338.

[5] I.S. Towner and J.C. Hardy, Phys. Rev. C **66**, 035501 (2002).

[6] G.C. Ball *et al*., Phys. Rev. Lett. **86**, 1454 (2001).

[7] J.C. Hardy *et al*., Phys. Rev. Lett. **91**, 082501 (2003).

[8] A. Kellerbauer *et al*., submitted to Phys. Rev. Lett.

[9] I.S. Towner and J.C. Hardy, *Progress in Research,*Cyclotron Institute, Texas A&M University (2002-2003), p. III-1, and (2003-2004).*Progress in Research*, Cyclotron Institute, Texas A&M University (2003-2004), p. III-25.

Precise Measurement of α_K for the M4 Transition from ^{193m}Ir: A Test of Calculated Internal-Conversion Coefficients

N. Nica, J. C. Hardy, V. E. Iacob, S. Raman,[1] C. W. Nestor, Jr.,[1] and M. B. Trzhaskovskaya[2]
[1] *Oak Ridge National Laboratory, Oak Ridge, Tennessee 37830*
[2] *Petersburg Nuclear Physics Institute, Gatchina, Russia 188300*

Internal conversion coefficients (ICCs) play an essential role in the analysis of nuclear decay schemes. They are used both in assigning spins and parities, and in determining transition rates and branching ratios. Even so, tables of ICCs produced over the last five decades differ in detail from one another by a few percent or more, and a recent survey of world data [1] demonstrates similar systematic disagreements of all but the most recent table [2] with measured results. A particularly intriguing outcome of the survey was the apparent experimental preference for a "non-physical" approximation made in this recent table in dealing with the atomic sub-shell vacancy that occurs as a result of the conversion process. In producing their table, Band *et al* [2] actually chose to disregard the hole entirely, based on an earlier comparison with experimental data [3], which indicated that better agreement with experimental ICCs would result. The Raman *et al* survey [1] confirmed this surprising conclusion. Unfortunately, though, the body of world ICC data includes very few measurements of high precision, say <1%. Thus, it is only in the average over many different transitions that a few-percent discrepancy between experiment and theory can be discerned at all, and it could be argued that the difference in experimental agreement between the two types of calculations – one with the hole, the other without – is hardly a definitive reason to choose an unacceptable physical model. Perhaps, too, there are other deficiencies in the calculation that are playing a role at the 1% level.

In any case, precision γ-ray intensity calibration standards [4] demand reliable ICCs and, in particular, our program to measure precise superallowed β-decay branching ratios relies on such standards (see, for example [5]). Consequently, we have undertaken several key precision tests of calculated ICCs. The first, currently being readied for publication, is a measurement of the K-shell ICC, α_K, for the 80.2-keV M4 isomeric decay of the second excited state in ^{193}Ir. The transition energy is very close to the K-shell binding energy in iridium, which is at 76.112 keV, so the calculated value for α_K differs by more than 10% depending on whether the hole is incorporated in the calculation or not. The isomer is well suited to precise measurement since its half-life is 10.5 days, its single-branch decay directly feeds the ground state, and the energy of its γ-ray is very close to that of the K X-rays that follow its internal conversion.

The K-shell ICC, α_K, for a particular transition is defined to be the ratio of the probability for internal conversion onto a K-shell electron relative to the probability for emitting a γ-ray. Each electron vacancy created in the K shell produces K X-rays with a probability equal to the fluorescent yield, ω_K. Thus, if only a single transition is involved and a spectrum of X-rays and γ-rays is recorded for its decay, the ratio of the total number of K X-rays observed, N_K, to the total number of γ-rays, N_γ, relates to α_K by the simple relationship $\alpha_K\omega_K = (N_K/ N_\gamma)(\varepsilon_\gamma/\varepsilon_K)$, where ε_γ and ε_K are the detector efficiencies for the γ-rays and X-rays, respectively. Since fluorescent yields have been reviewed

recently [6] and are known rather precisely – typically to better than 0.5% – we can thus expect to extract α_K to <1% precision from the ratio of peak areas measured with our uniquely well-calibrated HPGe detector, whose relative efficiencies in this energy region are known [7] to 0.15%.

The ^{193m}Ir source was prepared from ~70 mg of highly enriched ^{192}Os (99.935%) metal powder irradiated in the Hydraulic Tube Facility at the Oak Ridge High Flux Isotope Reactor. It was chemically separated at Oak Ridge and deposited on a tantalum disc. In all, five source spectra and three background spectra were then recorded at Texas A&M over a total period of 98 days, nearly ten half-lives of ^{193m}Ir. A complete inventory of impurities with activities down to 1 ppm of the initial ^{193m}Ir activity was made based on observed γ-ray energies and half-lives. Twenty-one impurities were detected in all, but their *total* activity was less than 0.6% of that of ^{193m}Ir in the first spectrum. Only 74-day ^{192}Ir, which was responsible for weak platinum and osmium X-rays, had to be accounted for in the peak-ratio analysis, and the total contribution was a mere 0.8% of the iridium K X-ray peaks.

Figure 1 shows the spectrum obtained in the energy region of interest. The iridium K X-rays are seen to dominate, with the weak 80.2-keV γ-ray peak cleanly separated at the right. The tantalum X-rays that also appear in the spectrum are the result of fluorescence in the source backing, an unfortunate choice as it turned out, but the tantalum K_β contribution to the iridium K_α peak is only 2.2% and it was easily calculated from the observed area of the tantalum K_α peak.

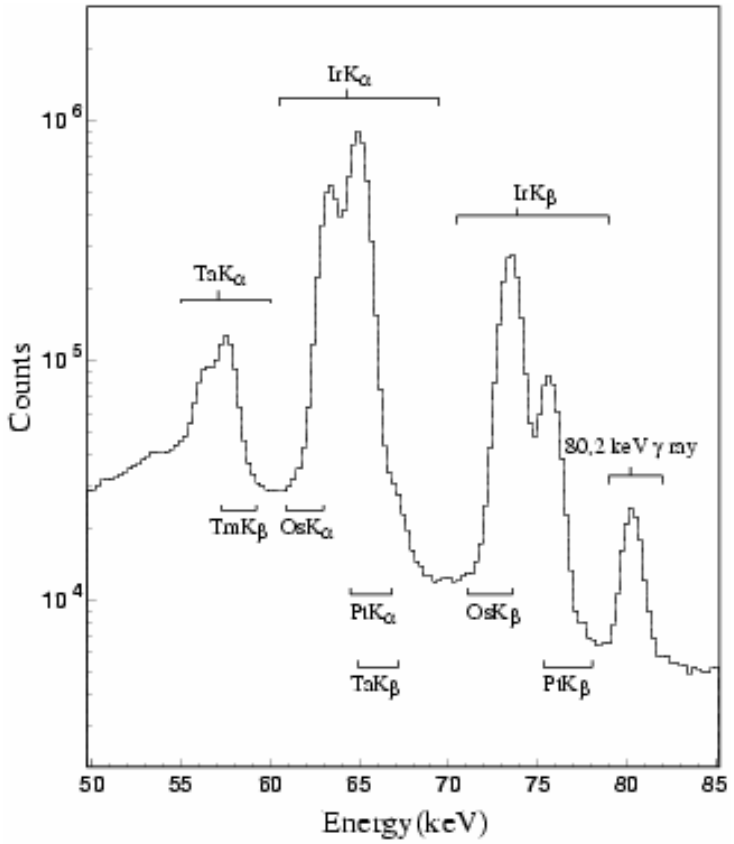

Figure 1. Spectrum of γ- and X-rays measured from the decay of ^{193m}Ir. The fluorescent X-rays from the tantalum backing are identified as are the X-rays from very weak contaminant

Our final result for the ^{193m}Ir 80.2-keV M4 transition is α_K = 103.0 (8). This number should be compared with 92.0, the value taken from the most recent ICC tables [2], in which the atomic hole has been ignored. This 10% disagreement is completely removed if the same calculations are repeated with the hole included, the calculated result becoming 99.6 or 103.3 depending on the approximation used to incorporate the hole. Our measurement clearly favors inclusion of the hole.

We plan to measure several other sensitive cases in order to ensure that our conclusion is universally valid.

[1] S. Raman, C.W. Nestor, Jr., A Ichhara, and M.B. Trzhaskovskaya, Phys. Rev. **C66**, 044312 (2002).

[2] I.M. Band, M.B. Trzhaskovskaya, C.W. Nestor, Jr., P. Tikkanen, and S. Raman, At. Data Nucl. Data Tables **81,** 1 (2002).

[3] I.M. Band and M.B. Trzhaskovskaya, At. Data Nucl. Data Tables **55,** 43 (1993).

[4] IAEA-TECDOC-619, X-ray and gamma-ray standards for detector calibration, International Atomic Energy Agency, 1991; and an updated version to be published soon.

[5] J.C. Hardy , V.E. Iacob, M. Sanchez-Vega, R.G. Neilson, A. Azhari, C.A. Gagliardi, V.E. Mayes, X. Tang, L. Trache, and R.E. Tribble, Phys. Rev. Lett. **91**, 082501 (2003).

[6] E. Schoenfeld and H. Janssen, Nucl. Instrum. Methods Phys. Res. A **369**, 527 (1996).

[7] R.G. Helmer, J.C. Hardy, V.E. Iacob, M. Sanchez-Vega, R.G. Neilson, and J. Nelson, Nucl. Instrum. Methods Phys. Res. A **511**, 360 (2003).

Precision Absolute Branching-Ratio Measurements: the Superallowed β-Decay of ^{34}Ar

V. E. Iacob, J. C. Hardy, N. Nica, C. A. Gagliardi, G. Tabacaru, L. Trache, and R. E. Tribble

For some years now, we have been embarked on an experimental and theoretical research program to test CKM (Cabibbo-Kobayashi-Maskawa) unitarity *via* precision measurements of *ft*-values for superallowed β-transitions. The thrust of this program is to determine and validate the nuclear-structure-dependent correction terms that must be applied to the experimental *ft*-values for $0^+ \rightarrow 0^+$ transitions in order to extract a value for the vector coupling constant, G_V. From G_V, the up-down mixing element of the CKM matrix can be determined and the unitarity of that matrix tested. We intend to study a number of superallowed transitions that have not previously been precisely characterized. The cases are being chosen to cover a relatively wide range of calculated correction terms in order to test if the experimentally observed variations among them confirm the theoretical calculations [1]. Aspects of this work have been described in previous progress reports and also appear elsewhere in this report [2].

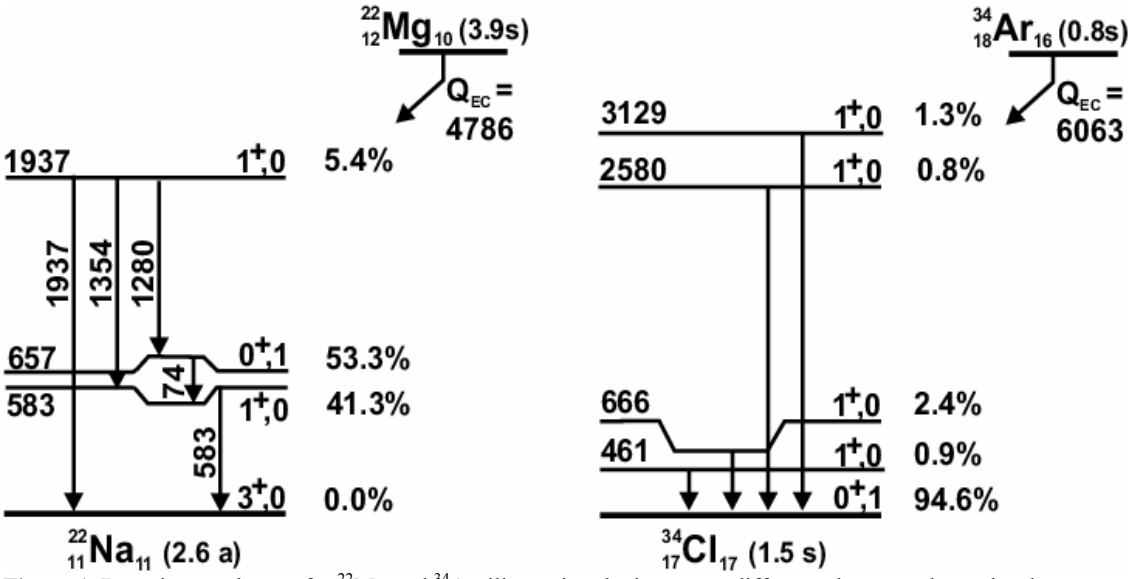

Figure 1. Beta-decay schemes for ^{22}Mg and ^{34}Ar, illustrating the important difference between them: the absence or presence of a ground-state β-transition. Note the different energy scale in the two schemes.

The experimental component of this program reached its first milestone with the completion and publication a year ago of our study of ^{22}Mg decay [3]. After several years of work, we had completed the calibration of the relative efficiency response of our HPGe detector to an unprecedented 0.15% precision between 50 and 1500 keV. With this detector, we then successfully determined the superallowed branching ratio for ^{22}Mg with comparable precision. However, we chose ^{22}Mg decay to be our first case for a good reason: all its decay branches feed excited states in its daughter, ^{22}Na, and are thus followed by at least one γ-ray transition (see Fig 1). The β-branching ratios for ^{22}Mg can all be determined from the *relative* γ-ray intensities as observed in our detector. This is the only one of our targeted superallowed decays where that simplification exists. In all other cases of interest, the ground state in the daughter

nucleus is also populated by β-decay so any determination of the β-branching ratios requires *absolute* γ-ray intensities to be determined. In anticipation of this requirement, we have already established the absolute efficiency of our detector [4] to 0.2% precision, only slightly less stringent a limit than the one we assign to its relative efficiency.

The most favorable case with which to begin our absolute branching-ratio measurements is the decay of ^{34}Ar. As illustrated in Fig. 1, unlike ^{22}Mg, ^{34}Ar does have a branch to the ground state of its daughter. In fact, that branch is the superallowed transition, and it alone accounts for 94.6% of the total β-decay of ^{34}Ar. Although, in this case, the absolute branching ratios must be determined for the allowed branches to excited states, their total can then be subtracted from 100% to yield the value for the superallowed branch. To obtain 0.1% precision on the latter, one need only determine the former to a combined uncertainty of ±0.1%. Since these other branches total to a mere 5.4%, an uncertainty of ±0.1% actually constitutes a precision of ~2%, a rather modest goal for our equipment. Even though this goal is very easy for us to achieve, we have chosen to use the decays of both ^{22}Mg and ^{34}Ar as a means to investigate the limits to our precision for absolute measurements in general. Much higher precision than 2% will be required in subsequent measurements.

Two methods for determining absolute branching ratios are open to us: 1) we can relate the number of γ-rays observed from a sample at our counting location to the number of source atoms observed exiting the MARS spectrometer on their way to being collected in that sample; and 2) we can relate the number of γ-rays observed in coincidence with β-particles at the counting location, $N_{\beta-\gamma}$, to the β-singles rate, N_β. Since

$$N_\beta = N_{decays} \mathbf{x} \varepsilon_\beta \quad \text{and} \quad N_{\beta-\gamma} = N_{decays} \mathbf{x} \varepsilon_\beta \mathbf{x} \varepsilon_\gamma \mathbf{x} BR_\gamma,$$

then

$$N_{\beta-\gamma}/N_\beta = \varepsilon_\gamma \mathbf{x} BR_\gamma,$$

where ε_β and ε_γ are the detector efficiencies for detecting β's and a particular γ-ray, respectively, and BR_γ is the branching ratio for producing that γ-ray – the quantity to be measured. The first of these two methods is, in principle, independent of the absolute HPGe detector efficiency if the relationship between detected atoms and observed γ-rays is determined first from a measurement on ^{22}Mg, where the absolute branching ratios are now known; this, of course assumes that there is no change in conditions between the ^{22}Mg calibration and the subsequent measurement of an unknown decay. The second method relies on knowledge of the absolute detector efficiency, but is independent of uncertainties associated with atom counting and collection on a tape.

We are currently testing both these methods on the known decay of ^{22}Mg, and on the "unknown" decay of ^{34}Ar. A spectrum of γ-rays observed in coincidence with β-particles for the latter decay is shown in Fig. 2. The ^{34}Ar was produced by a 30*A* MeV ^{35}Cl beam on a cooled hydrogen target, initiating the ^{1}H(^{35}Cl, p2n)^{34}Ar reaction. Fully stripped reaction products were separated in the MARS spectrometer. The experimental method was the same asd that described in reference [3]. So far, the results are promising but we require further study of the energy-dependence of our beta-detection efficiency, which influences the relative intensities of γ-rays in the coincidence spectrum. This was not an issue in the ^{22}Mg-decay study, where the key γ-rays to be compared followed β-transitions of nearly

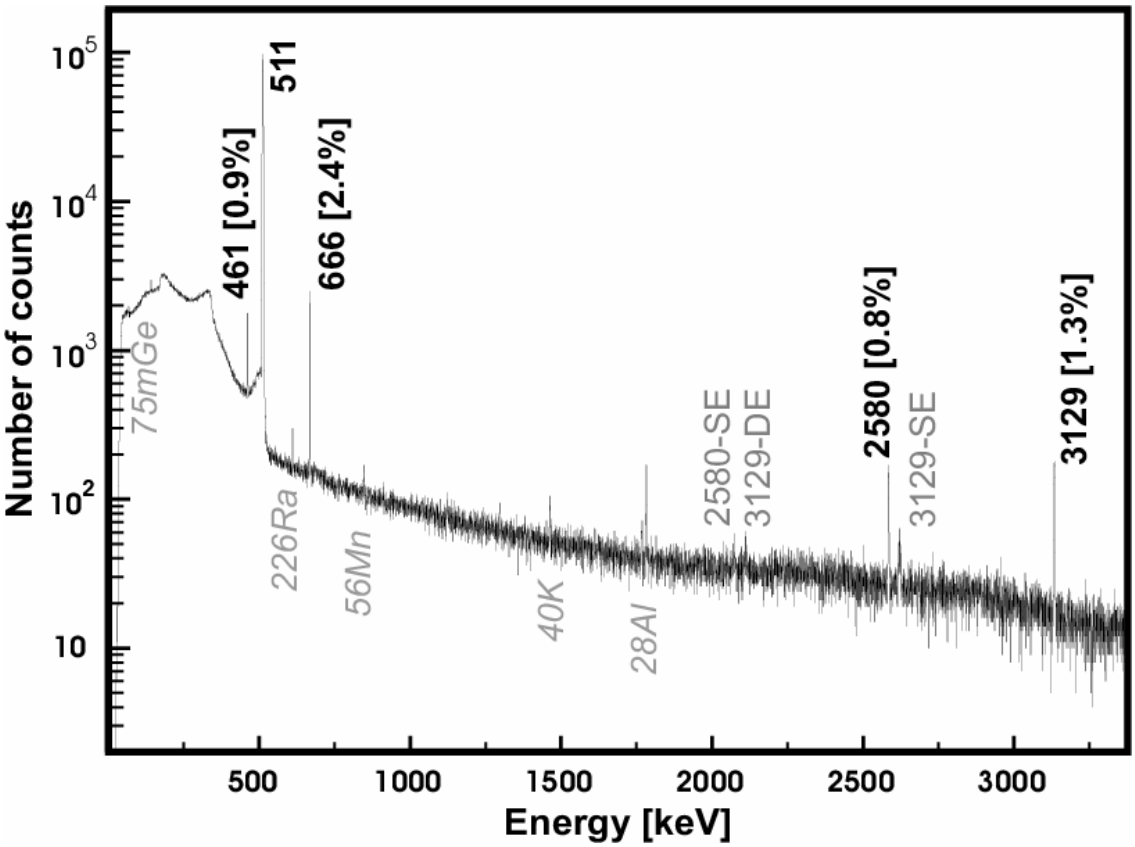

Figure 2. Spectrum of γ-rays observed in coincidence with β-particles following the decay of a sequence of pure collected samples of ^{34}Ar

identical end-point energies. We are using Monte Carlo simulations to help understand and ultimately control this aspect of our measurement technique.

[1] I.S. Towner and J.C. Hardy, Phys. Rev. C **66**, 035501 (2002).

[2] J.C. Hardy and I.S. Towner, *Progress in Research*, Cyclotron Institute, Texas A&M University (2003-2004); I.S. Towner and J.C. Hardy, *ibid*.

[3] J.C. Hardy , V.E. Iacob, M. Sanchez-Vega, R.G. Neilson, A. Azhari, C.A. Gagliardi, V.E. Mayes, X. Tang, L. Trache and R.E. Tribble, Phys. Rev. Lett. **91**, 082501 (2003).

[4] R.G. Helmer, J.C. Hardy, V.E. Iacob, M. Sanchez-Vega, R.G. Neilson and J. Nelson, Nucl. Instrum. Methods Phys. Res. A **511**, 360 (2003); R.G. Helmer, N. Nica, J.C. Hardy and V.E. Iacob, Appl. Radiat. Isot. **60**, 173 (2004).

The Physics of STAR at RHIC

C. A. Gagliardi, T. W. Henry, R. E. Tribble, and the STAR Collaboration

The past year was an eventful one within the STAR High-p_T Physics Working Group. Early in the year, STAR reported results [1] on the yield of high-p_T charged hadrons in Au+Au and p+p collisions at 200 GeV/nucleon-nucleon pair. The data showed that the charged-hadron yield in central Au+Au collisions for $5 < p_T < 12$ GeV/c is a factor of 4-5 lower than would be expected, based on the yield observed in peripheral Au+Au collisions or p+p collisions. The p_T dependence of the effect was found to be different from that expected in hadronic reinteraction models, pointing toward partonic energy loss, often referred to as "jet quenching", as a possible explanation. However, an alternative explanation – that fewer high-p_T particles are produced due to gluon saturation in the initial-state Au nuclei – could not be ruled out. Subsequent measurements of d+Au collisions [2] found that high-p_T particle production is enhanced in this case, as shown in Fig. 1, and that high-p_T di-hadron correlations are very similar to those in p+p collisions, as shown in Fig. 2. The d+Au results demonstrated that the suppression of high-p_T particle production [1] and back-to-back di-hadron correlations [3] seen in central Au+Au collisions is due to final-state interactions in the dense medium created in those collisions. The d+Au results were featured on the cover of the August 15, 2003 issue of *Physical Review Letters*. One of us (CAG) was among the principal authors for Refs. [1] and [2].

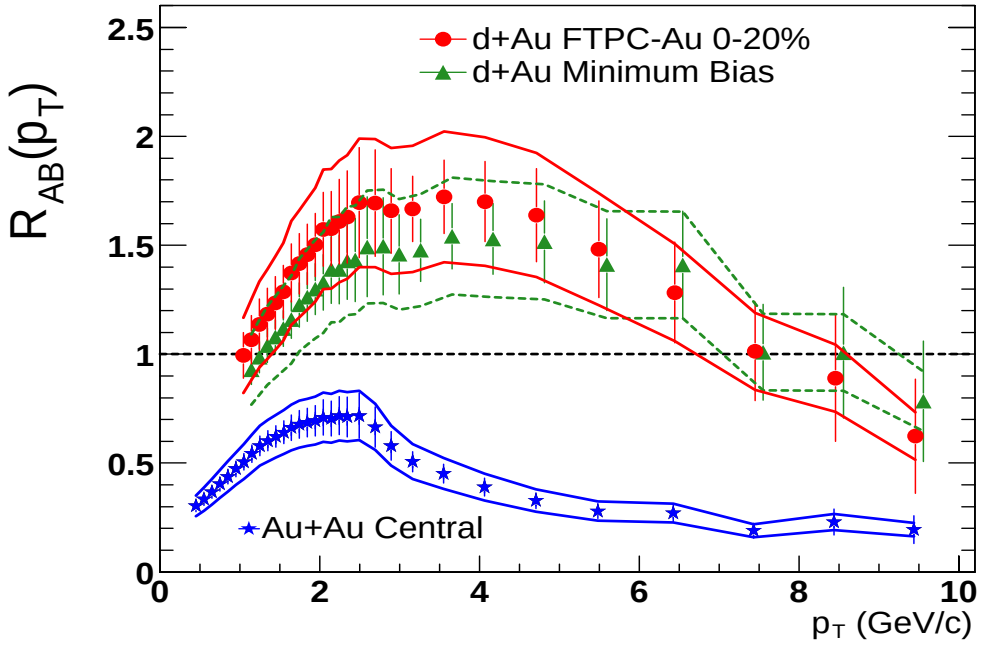

Figure 1. The ratio of charged-hadron production in d+Au and central Au+Au collisions at 200 GeV/nucleon-nucleon pair, relative to that expected based on measurements of p+p collisions at the same energy. From Ref. [2].

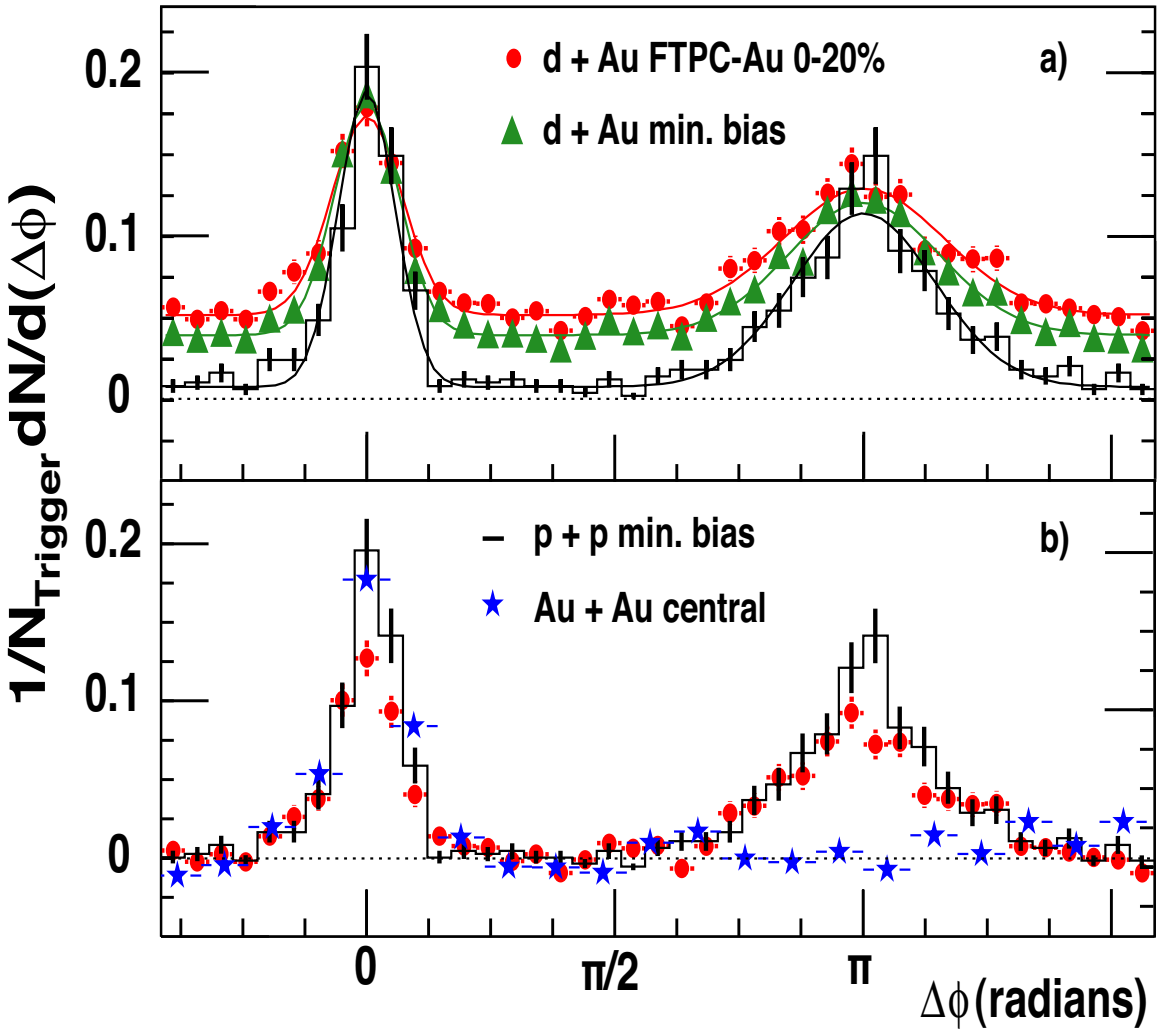

Figure 2. Upper panel: The high-p_T di-hadron angular correlation functions measured in p+p and d+Au collisions at 200 GeV. Lower panel: A comparison of di-hadron angular correlations in p+p, central d+Au, and central Au+Au collisions, after pedestal and flow subtraction. From Ref. [2].

Our group has also made significant contributions during the past year to the development of jet reconstruction algorithms for STAR. The charged-jet codes that were described in last year's progress report have been extended to include neutral energy measured in the STAR electromagnetic calorimeters. We are now utilizing these jet reconstruction codes to explore the properties of the jets that are produced in p+p and d+Au collisions at RHIC, including the fragmentation function and j_T for single jets and intrinsic k_T and nuclear k_T from di-jets. The same codes are being used by collaborators at UCLA to

measure A_{LL} for inclusive jet production in polarized p+p collisions. The results will represent the first STAR determination of the gluon polarization within the proton. One of us (TWH) gave a talk about jet reconstruction in p+p and d+Au collisions at the Quark Matter '04 conference [4].

We have continued our activities within the STAR Endcap Electromagnetic Calorimeter (EEMC) group. Early last year, we completed the magnetic shielding boxes to house the PMTs that read out the EEMC towers. Later in the summer, we completed the magnetic shielding boxes for one-third of the multi-anode PMTs that read out the pre-shower, post-shower, and shower-maximum detectors for the EEMC. The complete mechanical structure for the EEMC was installed at BNL during the 2003 shut-down period. All the available read-out was also installed. The EEMC was commissioned during the first part of the recent 200 GeV Au+Au run, then took data during both the remainder of the 200 GeV Au+Au run and the brief 62 GeV Au+Au run. It is also taking data during the p+p run that is underway at present. The EEMC seems to be working quite well. In parallel, we completed the mechanical construction for all of the remaining magnetic shielding boxes needed for the EEMC, including spares. The remaining multi-anode PMTs will be installed on the back of the STAR pole-tip during the 2004 shut-down. That will complete the construction of the EEMC.

Finally, we continue to carry administrative responsibilities within STAR outside of the spin and high-p_T areas. This past year, members of the group chaired two god-parent committees for papers from the event structure physics working group and participated on other god-parent committees for papers from the event-by-event, spectra, and strangeness physics working groups.

[1] J. Adams *et al*. (STAR Collaboration), Phys. Rev. Lett. **91**, 172302 (2003).
[2] J. Adams *et al*. (STAR Collaboration), Phys. Rev. Lett. **91**, 072304 (2003).
[3] C. Adler *et al*. (STAR Collaboration), Phys. Rev. Lett. **90**, 082302 (2003).
[4] T.W. Henry for the STAR Collaboration, nucl-ex/0403031.

TWIST: Measuring the Space-Time Structure of Muon Decay

C. A. Gagliardi, J. R. Musser, R. E. Tribble, M. A. Vasiliev, and the TWIST Collaboration

The primary focus of the TWIST Collaboration during the past year has been analysis of the data taken during the first physics run in Fall, 2002. The goal of that run was to determine the muon decay parameters ρ and δ to $\sim 10^{-3}$, a factor of 3-4 improvement on the best previous measurements. This will be an important milestone on the path toward ultimate determinations of the muon decay parameters ρ, δ, and $P_\mu \xi$ to a few parts in 10^4. TWIST is a systematics-dominated experiment. Most of the beam time during Fall, '02, was devoted to measurements designed to amplify various systematic effects, and most of the analysis effort since then has been devoted to validating our GEANT simulation of the experiment and minimizing the sensitivity of our pattern recognition and event reconstruction codes to those systematic effects. The basic analysis scheme involves comparison of the measured positron energy-angle spectrum from normal muon decay to the sum of a "standard" spectrum obtained by analyzing Monte Carlo events and derivative spectra that measure deviations of the muon decay parameters from the values assumed by the standard. The muon decay parameters used to generate the Monte Carlo standard spectrum are hidden. This provides a way for TWIST to perform a blind analysis without hiding essentially the entire data set. Initially, progress was constrained by the computing available to TWIST at TRIUMF. In November, TWIST gained access to the Westgrid computer farm at the University of British Columbia for beta-testing. Westgrid, with over 1000 3.0 GHz Xeon processors, represented a dramatic increase in cpu resources. Since then, we've performed a broad range of data vs. data, data vs. Monte Carlo, and Monte Carlo vs. Monte Carlo comparisons in order to quantify the systematic uncertainties in the experiment and identify those parts of the Monte Carlo and analysis codes that need improvement.

Our group has continued to contribute to the pattern recognition effort. One of the data sets taken during Fall, '02, explored the impact of additional material mounted downstream of the detector in order to quantify the importance of the material that is located upstream of the detector during routine running. Early analyses indicated that interactions of the decay positrons with the extra material reduces the event reconstruction efficiency by several percent when $0.25 < \cos(\theta) < 0.4$. This is outside the fiducial region of the experiment. However, similar analyses of Monte Carlo events only reproduced approximately half of the observed efficiency loss. A number of significant improvements have been made to the pattern recognition codes while investigating this problem. The analysis codes now identify and remove many of the hits that arise from low-energy delta-ray tracks. They are also far better at identifying tracks that involve hard-scattered positrons. Finally, we are now able to track several different particles within the spectrometer simultaneously. Overall, these changes allow us to analyze events that are far more complex than was practical previously. Recent results with the revised analysis codes show much reduced sensitivity to the presence or absence of the extra material.

The current schedule anticipates the TWIST first physics results will be available in Summer to Fall, 2004.

SECTION II

HEAVY ION REACTIONS

$\langle N \rangle / Z$ Ratio in Heavy Ion Reaction at Intermediate Energies

S. Kowalski, R. Wada, K. Hagel, T. Materna, J. B. Natowitz, J. S. Wang, Y. Ma, T. Keutgen, L. Qin, M. Murray, A. Makeev, P. Smith, J. Cibor, C. Hamilton, A. S. Botvina, E. Bell, S. Liddick, D. Rowland, A. Ruangma, M. Veselsky, E. Winchester, G. Souliotis, S. J. Yennello, A. Samant,[1] M. Cinausero,[1] D. Fabris,[1] E. Fioretto,[1] M. Lunardon,[1] G. Nebbia,[1] G. Prete,[1] G. Viesti,[1] Z. Majka,[2] P. Staszel,[2] W. Zipper,[3] M. E. Brandan,[4] A. Martinez-Rocha,[4] A. Menchaca-Rocha,[4] and Y.El Masri[5]

[1]*INFN-Legnaro, Padova, Italy,*

[2]*Jagiellonian University, Krakow, Poland,*

[3]*Institute of Physics Silesia University, Katowice, Poland,*

[4]*IFUNAM, Mexico,*

[5]*UCL, Louvain-la-Neuve, Belgium*

One of the primary interests in the study of excited nuclear matter is possible separation into two phases: gas and liquid. The nuclear gas is predicted to be neutron rich and consist of light elements, whereas the liquid phase is predicted to include more symmetric heavy fragments [1,2]. This phenomenon is manifested in the $\langle N \rangle / Z$ values of the nuclear reaction products.

Fig. 1 shows $\langle N \rangle / Z$ as a function of the fragment atomic number Z for the ^{64}Zn+^{197}Au, ^{64}Zn+^{92}Mo and ^{64}Zn+^{58}Ni reactions at 47A MeV. The presented data represent ‘‘violent’’ to “semi-violent” collisions based upon the neutron and light charged particle multiplicities and the total transverse energy of the light charged particles [3]. The $\langle N \rangle / Z$ value decreases with increasing Z and is near constant for the heavier fragments. Moreover, a decrease in $\langle N \rangle / Z$ of the fragments with decreasing $\langle N \rangle / Z$ of the system is clearly evidenced.

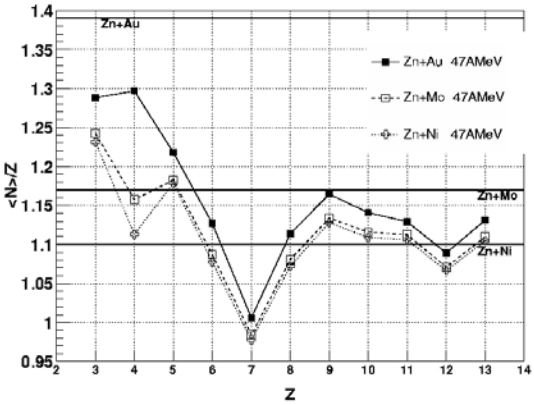

Figure 1. $\langle N \rangle / Z$ as a function of the fragment charge Z. For `violent" and `semi-violent" ^{64}Zn+^{197}Au, ^{64}Zn+^{92}Mo and ^{64}Zn+^{58}Ni reactions at 47A MeV. The Solid straight lines represent the $\langle N \rangle / Z$ ratio for entrance channel. Data are integrated over all angles.

We are presently analyzing data for 26A and 35A MeV reactions for the same projectile target

combinations. These data will be introduced to an isoscaling analysis and also will be compared with predictions SMM, QMD and AMD in an attempt to probe the role of symmetry energy on determinations the $\langle N \rangle / Z$ ratios.

[1] H. Müller and B. D. Serot, Phys. Rev. C **52**, 2072 (1995).
[2] E. Martin *et al.*, Phys. Rev. C **62**, 027601 (2000).
[3] R. Wada *et al.*, Phys. Rev. C **69**, 044610 (2004).

Isotope Identification with NIMROD Super Telescopes

S. Kowalski, R. Wada, K. Hagel, T. Materna, J. B. Natowitz, J. S. Wang, Y. Ma, T. Keutgen, L. Qin, M. Murray, A. Makeev, P. Smith, J. Cibor, C. Hamilton, A. S. Botvina, E. Bell, S. Liddick, D. Rowland, A. Ruangma, M. Veselsky, E. Winchester, G. A. Souliotis, S. J. Yennello, A. Samant,[1] M. Cinausero,[1] D. Fabris,[1] E. Fioretto,[1] M. Lunardon,[1] G. Nebbia,[1] G. Prete,[1] G. Viesti,[1] Z. Majka,[2] P. Staszel,[2] W. Zipper,[3] M. E. Brandan,[4] A. Martinez-Rocha,[4] A. Menchaca-Rocha,[4] and Y.El Masri[5]

[1]*INFN-Legnaro, Padova, Italy*, [2]*Jagiellonian University, Krakow, Poland,*

[3]*Institute of Physics Silesia University, Katowice, Poland,* [4]*IFUNAM, Mexico,*

[5]*UCL, Louvain-la-Neuve, Belgium*

Analysis of isotopic characteristics of products for the inclusive data measured in heavy ion reactions is one of the primary jobs in the study, of the isospin degree of freedom of nuclear matter [1, 2]. A good isotope identification can be obtained by using a combination of Si and CsI(Tl) detectors. The isotope resolution obtained in ^{64}Zn+^{197}Au, ^{64}Zn+^{92}Mo, ^{64}Zn+^{58}Ni reactions at 47A, 35A, and 26A MeV energies by using the Si-Si-CsI(Tl) telescopes in the 4π detector array NIMROD are presented. NIMROD consists of 12 separate rings coaxial about the beam. In each of the 8 forward rings two Si-Si-CsI(Tl) super telescopes are mounted. The first Si is 150μm thick and second Si is 500μm thick, The thickness of the CsI(Tl) varies with the ring number [3].

The isotope identification for the particles stopped in the second silicon detector is made in two steps. In the first step each Z is assigned on the two-dimensional Si-Si energy loss spectrum as a line fitted to the experimental points. Then a linearization in the Z is made. In the second step, individual isotopes are separated. The experimental Si-Si spectra for the considered reactions allows us to clearly identify isotopes up to atomic number Z=13. Fig. 1 presents the experimental Si-Si spectra with very good isotope resolution. The particle identified spectrum is shown in Fig. 2.

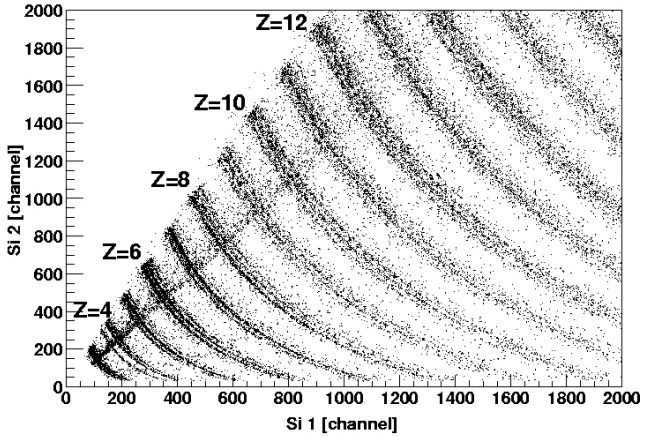

Figure 1. Si-Si spectrum from ring number 3 (Θ=6.41°)

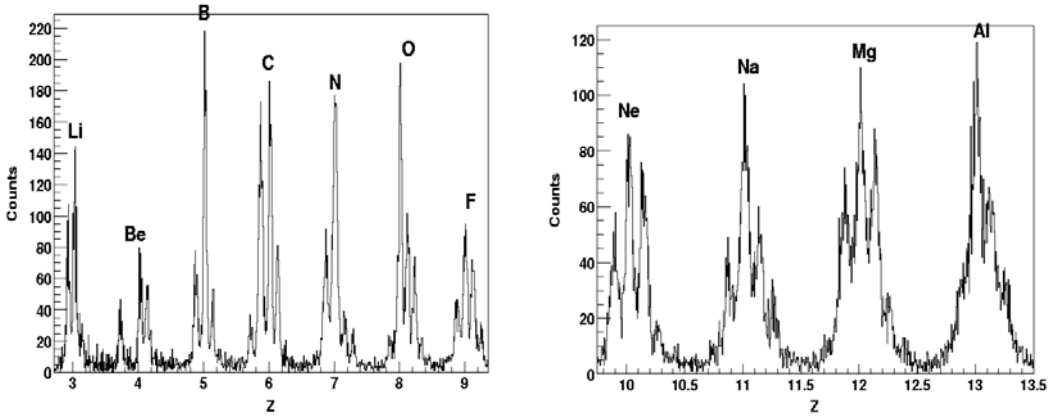

Figure 2. The projection of the experimental points on the Z line (ring number 3 Θ=6.41^o)

The identification procedure for particles stopped in CsI(Tl) is similar, but is based on the two-dimensional spectra for the second Si and the fast CsI(Tl) signals. The maximum atomic number, with isotope separation, for Si-CsI(Tl) is equal to 16. Si-CsI(Tl) spectrum and the resultant particle identified spectrum is presented in Fig. 3 and Fig. 4.

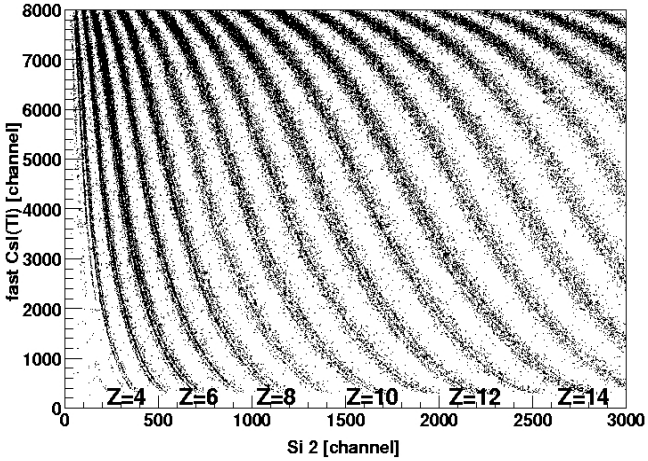

Figure 3. Si-fast CsI(Tl) spectrum from ring number 2 (Θ=4.31^o)

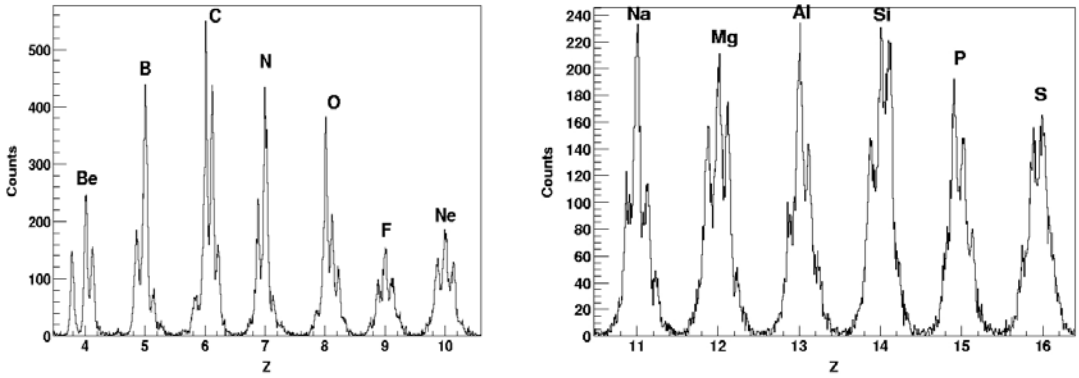

Figure 4. Projection of the experimental points on the Z line (ring number 2 $\Theta = 4.31^{o}$)

[1] D.V. Shetty *et al.*, Phys. Rev. C **68**, 054605 (2003).
[2] M.B. Tsang *et al.*, Phys. Rev. C **64**, 054615 (2001).
[3] R. Wada *et al*., Phys. Rev. C **69**, 044610 (2004).

Reaction Dynamics and Multifragmentation in Fermi Energy Heavy Ion Reactions

R. Wada, T. Keutgen, K. Hagel, Y. G. Ma, J. Wang, M. Murray, L. Qin, J. B. Natowitz, T. Materna, S. Kowalski, and NIMROD collaboration

The analysis of the reaction systems, ^{64}Zn + ^{58}Ni, ^{92}Mo, ^{197}Au, at 26A, 35A and 47A MeV, has been completed and published [1]. The experiment has been performed using a 4π detector array, NIMROD and the results have been compared in detail with those of Antisymmetrized Molecular Dynamics model calculations employing different effective interactions, corresponding to soft and stiff equations of state(EOS), and different in-medium nucleon-nucleon(NN) cross sections. All calculations have been done in Riken super computer facility in Japan. Direct experimental observables, such as multiplicity distributions, charge distributions, energy spectra and velocity spectra, have been reproduced reasonably well by all calculations. No conclusive preference for either EOS or in-medium NN cross sections has been observed.

Reaction dynamics has been further investigated using the calculated central collision events and the following scenario has been drawn for the multifragmentation in the Fermi energy domain:

(1) The projectile enters into the target nucleus and creates a hot overlap zone at a time of about 40-60 fm/c after contact.
(2) The overlap zone decays quickly by emitting fast nucleons before thermal equilibrium with the surrounding target nucleons is established.
(3) During the preequilibrium emission, the remaining system starts to equilibrate. Nucleons close to each other in the phase space start to form cold fragments which coexist with a hotter nucleon gas. In this stage, cold fragments share almost an equal internal energy per nucleon with each other. This shared internal energy is around -4A MeV, almost independent on the incident energy. The thermal equilibration time is evaluated around 120 fm/c for 47A MeV and 160fm/c at 26A MeV.
(4) The system continues to expand and undergoes multifragmentation with cold fragment emission. This multifragmentation process is accelerated by additional dynamical processes, suchas the semi-transparency for ^{58}Ni and ^{92}Mo targets at 47A MeV and the radial expansion for ^{197}Au at 47A MeV. These additional dynamical processes drastically change the kinetic properties of the emitted fragments.

[1] R. Wada *et al.*, Phys. Rev. C **62**, 044610 (2004).

A Ghoshal-like Test of Equilibration in Near Fermi Energy Heavy Ion Collisions

J. Wang, T. Keutgen, R. Wada, K. Hagel, S. Kowalski, Z. Majka, T Materna, L. Qin,
J. B. Natowitz, and the NIMROD Collaboration

Determining the extent to which the properties and subsequent de-excitation of an excited nucleus depend upon the entrance channel characteristics of the collision used to prepare that nucleus is a time honored way of exploring equilibration in such systems [1]. In the early, low energy, experiments of Ghoshal indications that the decay of identical compound nuclei produced at the same excitation energy in reactions with different entrance channel asymmetries was independent of the entrance channel provided very strong evidence for the utility of the independence hypothesis in statistical decay theories. In higher energy collisions at near Fermi energies, in which faster emission processes remove energy and mass and the subsequent composite nucleus undergoes some dynamic evolution prior to a possible equilibration, the establishment of equilibration and entrance channel independence is more difficult. Nevertheless, it is precisely in this domain that nuclei are being investigated to determine whether or not their disassembly modes are dynamically or thermodynamically driven and, in the latter case, whether they provide evidence of liquid-gas phase changes and critical behavior common to other liquids. Tests of the degree of equilibration achieved in these Fermi energy collisions are clearly of interest.

We have made a Ghoshal-like test of the evolution of density and temperature and of the subsequent equilibration of medium mass composite nuclei produced in central collisions of 35 MeV/u ^{64}Zn + ^{92}Mo, 40 MeV/u ^{40}Ar + ^{112}Sn and 55 MeV/u ^{27}Al + ^{124}Sn and in mid-central collisions of 47 MeV/u ^{64}Zn + ^{92}Mo. The average masses and excitation energies remaining at the end of the pre-equilibrium stage were determined using calorimetric techniques. The derived masses range from 85 to 114 amu and the excitation energies range from 4.88 to 5.31 MeV/u. Figure 1 presents a comparison of the hot nucleus masses, excitation energies and temperatures for the four different systems (in row 1 of the Figure) together with a comparison of a variety of parameters characterizing the ejectile emission during the TLF de-excitation, i.e., the neutron, proton and alpha multiplicities and spectral temperatures (rows 2 and 3) and the total Z,N and A removed during the de-excitation cascade (row 4). For each of the quantities represented, a dashed line representing the average values obtained for the 35 MeV/u ^{64}Zn+ ^{92}Mo, 40 MeV/u ^{40}Ar + ^{112}Sn and 47 MeV/u ^{64}Zn + ^{92}Mo reactions (which lead to nuclei with similar N/Z ratios) is also shown. For each individual system, deviations from those averages are seen to be relatively small and within the experimental uncertainties except for the enhanced neutron de-excitation component observed in both the neutron multiplicity and total neutron removal for the 55 MeV/u ^{27}Al + ^{124}Sn reaction, expected given the very different N/Z of the hot nucleus produced~\cite{Lou}, The very similar de-excitation patterns for the four hot nuclei produced in somewhat different dynamical conditions , except for that additional favoring of neutron emission over charged particle emission for the significantly neutron richer system, is most easily understood as a reflection of statistical emission from very similar equilibrated hot nuclei.

We have also employed correlations between ejectile energy and emission time predicted by AMD-V transport model calculations [2-4] to follow the evolution of the temperatures from the time of first particle emission to equilibration. The early temperature evolution for the four different systems shows a close correspondence although the time range for the observed evolution varies somewhat with reaction system. A very similar double isotope ratio temperature, T_{HHe} ~ 6 MeV, is reached at the end of the pre-equilibrium stage of each reaction.

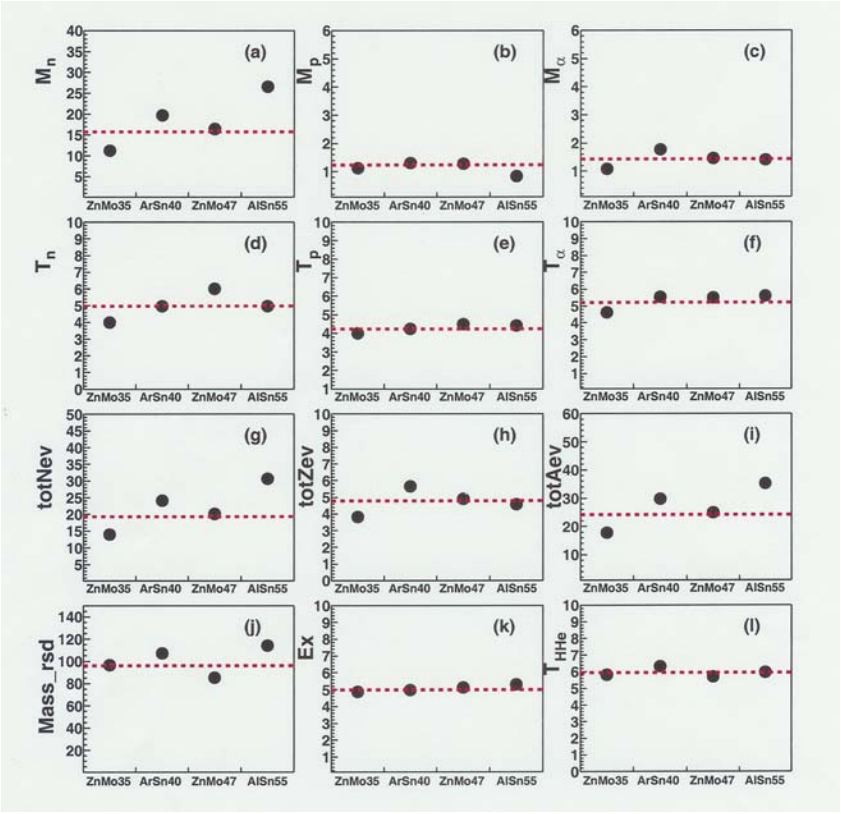

Figure 1. A comparison of various properties for the four systems studied (see text).

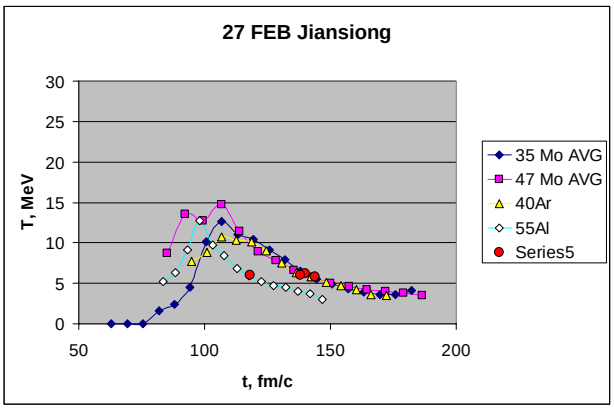

Figure 2. Time Evolution of the Temperature.

We present, in Figure 2, the double isotope ratio temperatures as a function of emission time. As time increases, each of the temperature evolution curves rises, peaks and then decreases. Maximum temperatures of 10-15 MeV are observed at times in the range of 95 to 110 fm/c. After that the temperatures drop monotonically. The transport model calculations indicate that contributions from the late stage evaporation become dominant below Vsurf = 3.5 cm/ns.

[1]. S.N. Ghoshal, Phys. Rev. **80**, 939 (1950)

[2]. A. Ono, Phys. Rev. C **59**, 853 (1999)

[3]. R. Wada, T. Keutgen, K. Hagel, Y.G. Ma, J. Wang, M. Murray, L. Qin, P. Smith, J.B. Natowitz, R. Alfarro, J. Cibor, M. Cinausero, Y. El Masri, D. Fabris, E. Fioretto, A. Keksis, M. Lunardon, A. Makeev, N. Marie, E. Martin, A. Martinez-Davalos, A. Menchaca-Rocha, G. Nebbia, G. Prete, V. Rizzi, A. Ruangma, D.V. Shetty, G. Souliotis, P. Staszel, M. Veselsky, G. Viesti, E.M. Winchester, S.J. Yennello, Z. Majka and A. Ono, Phys. Rev. C **69**, 044610 (2004)

[4]. J. Wang, Submitted to Phys. Rev. C.

Temperature Evolution in Near Fermi Energy Heavy Ion Collisions

J. Wang, T. Keutgen, R. Wada, K. Hagel, S. Kowalski, Z. Majka, T Materna, L. Qin,
J. B. Natowitz, and the NIMROD Collaboration

In several previous works we have employed coalescence model analyses to probe the early dynamic evolution of the reacting system [1,2] We have now employed similar techniques to explore the temperature evolution of hot nuclei produced in a series of reactions of 26A, 35A and 47A MeV ^{64}Zn projectiles with ^{58}Ni, ^{92}Mo and ^{197}Au target nuclei using the NIMROD combined 4π Charged –particle 4π Neutron Ball detection system. The data provide experimental evidence for an initial rapid thermalization of the incident energy, into a participant matter subsystem.

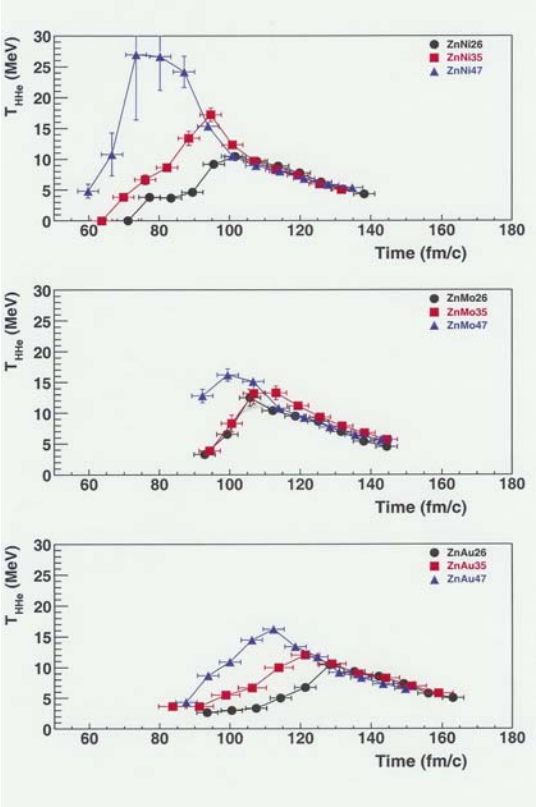

Figure 1. T_{HHe} vs surface velocity. See text. Horizontal bars are at 3-3.5 cm/ns, taken to be limit for time derivations.

Figure 1 presents the derived T_{HHe} temperatures as a function of time. The double isotope temperature first rises to a maximum, then decreases as further particle emission, expansion and diffusion of the excitation energy into the remainder of the composite system occurs. Temperatures comparable to those of limiting temperature systematics [3] are reached about 30 to 40 fm/c after the peak temperatures are observed. While all nine reactions show a qualitatively similar evolution with time, we see that the time at which the maximum in the temperature curve is reached increases with increasing target mass and decreases with increasing projectile energy. The former observation suggests a longer period required for establishment of a thermal and/or chemical equilibrium as the total system size increases and the latter observation suggests a more rapid thermalization of the initial projectile energy for the initially faster projectiles. The dynamic transport calculations indicate that the condition of thermal equilibrium of the whole system is not yet established as the earliest ejectiles are emitted. Non equilibrium effects may be most evident in the particularly high apparent peak

temperature for the 47A MeV ^{64}Zn +^{58}Ni case. The AMD-V calculations for the different systems predict the least stopping in that reaction [4].

The data indicate that a local thermal and chemical equilibrium is established at early times. This is further supported by observation of a close correlation between the peak temperatures and spectral slope temperatures for early emitted particles. After peaking the temperatures decrease rapidly apparently reflecting particle emission, diffusion of the excitation energy into the remaining system and expansion. For each individual target nucleus the later portions of the cooling curves for all three projectile energies are very similar, indicating that hot nuclei with similar properties are produced.

[1]. J. Cibor, R. Wada, K. Hagel, M. Lunardon, N. Marie, R. Alfaro, W.Q. Shen, B. Xiao Y. Zhao, J. Li, B.A. Li, M. Murray, J.B. Natowitz, Z. Majka and P. Staszel, Phys. Lett. B **473**, 29 (2000).

[2]. K. Hagel, R. Wada, J. Cibor, M. Lunardon, N. Marie, R. Alfaro, W. Shen, B. Xiao, Y. Zhao, Z. Majka, J. Li, P. Staszel, B.-A. Li, M. Murray, T. Keutgen, A. Bonasera, and J. B. Natowitz, Phys. Rev. C **62**, 034607 (2000).

[3]. J.B. Natowitz, R. Wada, K. Hagel, T Keutgen, M. Murray,Y. G. Ma , A. Makeev, L. Qin, , P. Smith and C.Hamilton, Phys. Rev. C **65**, 034618 (2002).

[4]. R. Wada, T. Keutgen, K. Hagel, Y.G. Ma, J. Wang, M. Murray, L. Qin, P. Smith, J.B. Natowitz, R. Alfarro, J. Cibor, M. Cinausero, Y. El Masri, D. Fabris, E. Fioretto, A. Keksis, M. Lunardon, A. Makeev, N. Marie, E. Martin, A. Martinez-Davalos, A. Menchaca-Rocha, G. Nebbia, G. Prete, V. Rizzi, A. Ruangma, D. V. Shetty, G. Souliotis, P. Staszel, M. Veselsky, G. Viesti, E. M. Winchester, S. J. Yennello, Z. Majka, and A. Ono, Phys. Rev. C **69**, 044610 (2004).

Mass Dependence of Critical Behavior

J. Wang, R. Wada, K. Hagel, Y. Ma, T. Keutgen, L. Qin, M. Murry, A. Makeev, P. Smith, J. B. Natowitz, A. S. Botvina, J. Cibor, C. Hamilton, E. Bell, S. Liddick, D. Rowland, A. Ruangma, M. Veselsky, E. Winchester, G. A. Souliotis, S. J.Yennello, A. Samant,[1] M.Cinausero,[1]D.Fabris,[1] E. Fioretto,[1] M. Lunardon,[1] G. Nebbia,[1] G. Prete,[1] G. Viesti,[1] Z. Majka,[2] P. Staszel,[2] S. Kowalski,[3] W.Zipper,[3] M. E. Brandan,[4] A. Martinez-Rocha,[4] A. Menchaca-Rocha,[4] and Y. El Masri[5]

[1]*INFN-Legnaro, Padova, Italy*

[2]*Jagiellonian University, Krakov, Poland*

[3]*Silesian University, Katowice, Poland*

[4]*IFUNAM, Mexico*

[5]*UCL, Louvain-la-Neuve, Belgium*

The critical behavior of nuclear matter has been an important topic in the nuclear field for many years. There are many observables and techniques to explore this feature of nuclear matter, such as maximal fluctuations, Fisher Droplet analysis and construction of a coexistence curve. Larger nuclear masses might evidence the critical point closer to that of infinite nuclear matter. But the Coulomb effects may cause a big distortion with increasing nuclear mass[1]. It is interesting, therefore, to study the mass dependence of the indicators of critical behavior. We have previously investigated the critical behavior for light nuclei with mass around 36[2]. In this contribution, we report on extensions of that work in the mass range of 30-60 and a comparison with Statistical Multifragmentation Model (SMM) calculations.

The same technique developed in Ref. [2] was used to reconstruct the projectile-like fragment (PLF) for the reactions of 47MeV ^{65}Zn + ^{58}Ni, which was studied using the NIMROD detector at TAMU. We are exploring the evolution of some observables, such as the effective Fisher-law parameter (τ_{eff}), the normalized second moment of fragment mass($<S_2>$), normalized variation of charge (NVZ), the mean charge number of the second largest fragment ($<Z_{2max}>$) and $<\gamma_2>$ (defined as M_2*M_0/M_1^2, where M_0, M_1, M_2 are the zeroth, first and second moment of the charge distribution) with excitation energy of the reconstructed PLF. Fig.1 shows the evolution of these observables with the excitation energy for the different mass regions. The Fisher-law parameter reaches a minimum (close to 2.0) at excitation energy about 5-6MeV/nucleon as shown in Fig1(a) and no significant mass dependence is observed. In Fig1(b)-(e), the maxima from observables, characterizing a region of maximum fluctuations, are also reached at excitation energy about 5-6 MeV/nucleon. The maximum increase with increasing of PLF mass. But the excitation energies at the point of maximum fluctuations are almost the same. The values for mass between 30-40 are similar to those in our previous paper with mass around 36 where PLFs are reconstructed from the reaction of 47MeV/nucleon ^{40}Ar + ^{58}Ni[2].

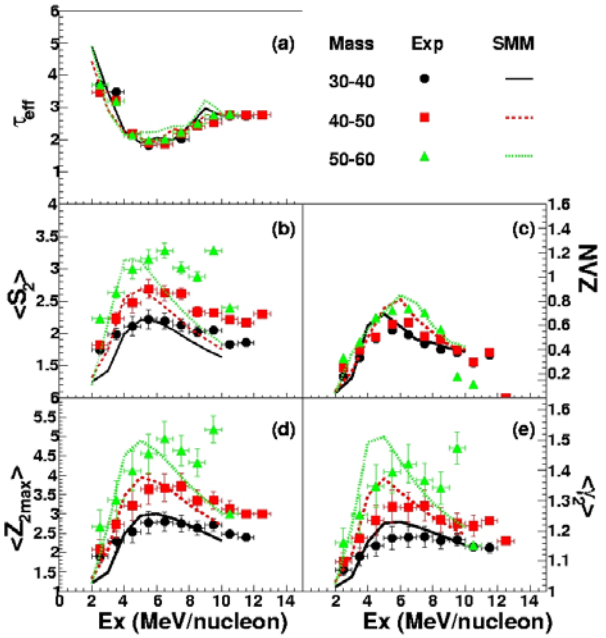

Figure 1. Evolution of τ_{eff}, $\langle S_2 \rangle$, NVZ, $\langle Z_{2max} \rangle$ and $\langle \gamma_2 \rangle$ with excitation energy for different mass regions from experimental data (symbols) and comparison with SMM calculations (lines)

The results of SMM calculations are compared with the experimental data in Fig.1. The agreement is quite reasonable for each mass region studied. This agreement indicates that the reconstructed PLFs are under equilibrated and undergoing statistical decay.

[1] J.B.Natowitz *et al.*, nucl-ex/020610.
[2] Y.G.Ma *et al.*, Phys.Rev. C **69**, 031604R (2004).

BRAHMS Results

K. Hagel, R. Wada, T. Materna, S. Kowalski, J. B. Natowitz, and the BRAHMS Collaboration

The BRAHMS experiment has published a variety of exciting results in 2003-2004. The data analysis of this year focused on BRAHMS' unique niche, namely the forward region, which is not substantially covered by the other RHIC experiments. Data on the Transverse Momentum Spectra in Au+Au and d+Au collisions at $\sqrt{s_{nn}} = 200GeV$ and the Pseudorapidity Dependence of High p_t Suppression[1] where published and several articles have been submitted for publication. These include papers on Nuclear Stopping in Au+Au Collisions at $\sqrt{s_{nn}} = 200GeV$, Centrality dependence of charged-particle pseudorapidity distributions from d+Au collisions at $\sqrt{s_{nn}} = 200GeV$, On the evolution of the nuclear modification factors with rapidity and centrality in d+Au collisions at $\sqrt{s_{nn}} = 200GeV$ and on Charged Meson Rapidity Distributions in central Au+Au Collisions $\sqrt{s_{nn}} = 200GeV$.

Perhaps the most exciting progress of the past year concerns the analysis of the d + Au data at forward rapidities which yields intriguing results on the possible existence of the Color Glass Condensate. Figure 1 shows the evolution of Rda as a function of pseudo-rapidity. At mid-rapidity, Cronin enhancement is observed (in contrast to the Au+Au results [1]). As pseudo-rapidity increases, the enhancement evolves into a suppression. The observed suppression of yield in d+Au collisions (as compared to p+p collisions) has been qualitatively predicted by several authors [2-4] within the framework of gluon saturation that includes the effect of the so called "quantum evolution" as particles are detected away from mid-rapidity, although no detailed numerical predictions are yet available. These approaches also predict the observed centrality dependence of the suppression at different pseudo-rapidities. While the theoretical framework for understanding the details of the observed phenomena needs further development, we note that the effects are in qualitative agreement with the prediction of the color glass condensate theory.

Our group here at Texas A & M has continued the ratio analysis of the Run II p + p data as described briefly in [5]. Several errors in calibrations and tracking were identified and redone. A number of

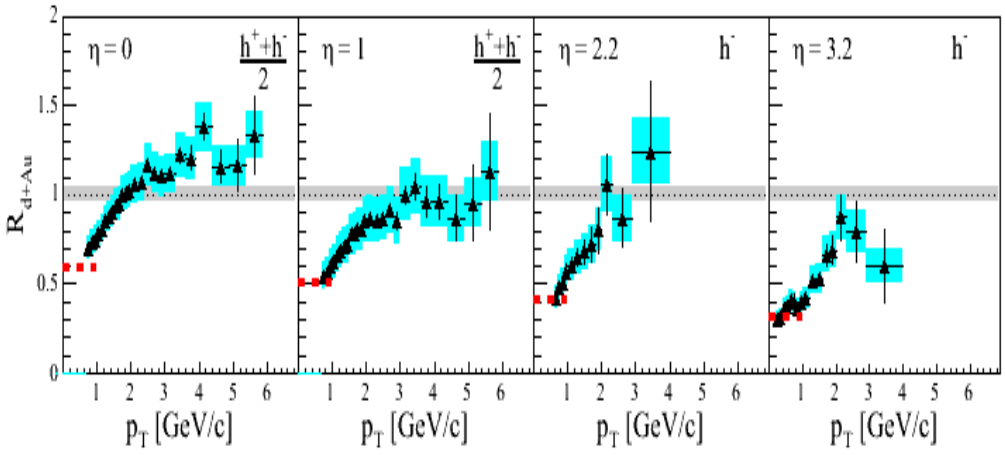

Figure 1. Pt dependence of Rda

refinements have been added to the ratio analysis since last year and we are approaching a final version of the results.

Figure 2 shows the pt dependence of the ratios for the different rapidity bins for the Mid-Rapidity Spectrometer (MRS) and figure 3 shows the same plot for the forward spectrometer (FS). In figure 2 the solid symbols represent the ratios extracted from the preferred MRS setting and the open symbols show the ratios for the ratios extracted from the non-preferred setting. We note that the pion ratios are near unity for all rapidity bins. The proton ratios in the MRS are fairly constant around .7 - .8. There is some oscillation structure as a function of pt. This is not yet understood and is under investigation. Statistics and binning are thought to be the cause, but investigations so far are inconclusive. In figure 3 the open symbols represent the data extracted from the front part of the FS (FFS) and the solid symbols represent the results extracted from the backward part of the FS (BFS). The proton ratios in the FS are near the MRS values at 20^{o} (y=1.5), but begin to plunge with increasing rapidity. There might be a hint of a pt dependence of the ratios at the most forward rapidites for the kaons and protons. It is under investigation to see whether this is an artifact of the analysis or if it is, in fact, real. The apparent increase of the proton ratio at the highest rapidity is puzzling although the data sample is very limited for the rapidity bin at that angle.

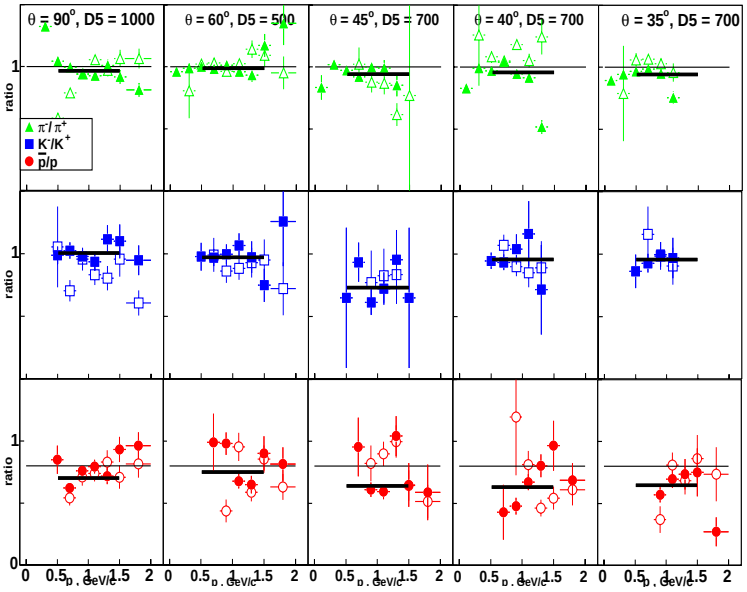

Figure 2 MRS ratios as a function of pt.

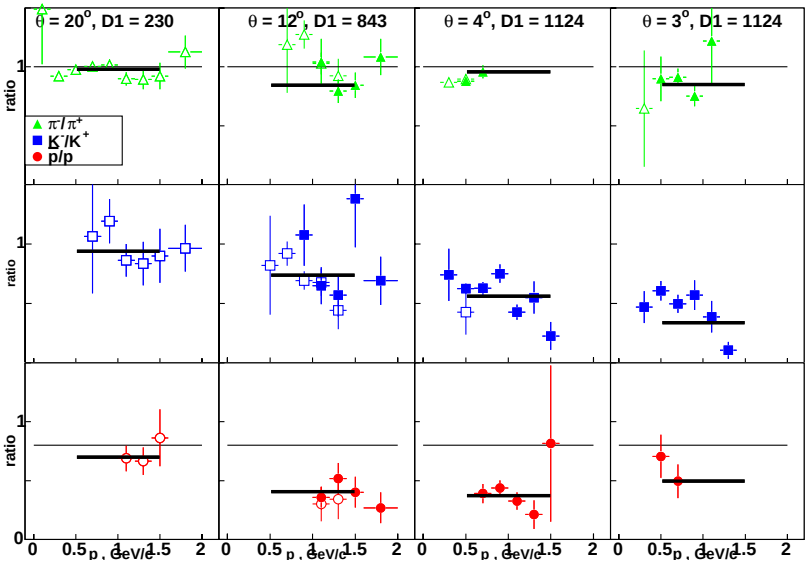

Figure 3. FS ratios as a function of pt

The bold horizontal lines in figures 2 and 3 represent a constant fit to the pt dependent ratios. The fit was done in the pt range of 0.5 – 1.5, that being the only range of pt that is covered by all of the angles. The summary of these ratios as a function of y are shown in figure 4.

In the figure we note that the kaon and proton data are fairly constant near mid rapidity and then begin to drop off. There is some structure in the ratios as a function of y and this continues to be investigated. It goes back to the straight line fits used in figures 2 and 3.

We plan in the near future to extract spectra from these angles all the way from mid-rapidity to the forward rapidities. Some preliminary spectra have already been generated, but they suffer from the same uncertainities that plague the ratios. Once these problems have been resolved and spectra generated, there will be a wealth of information on the spectra for rapidity values of $0 < y < 3.2$

In addition to continuing the data analysis, our group has covered a significant number of shifts while the experiment was running. We also contribute to the software infrastructure effort, both for online data acquisition and offline analysis.

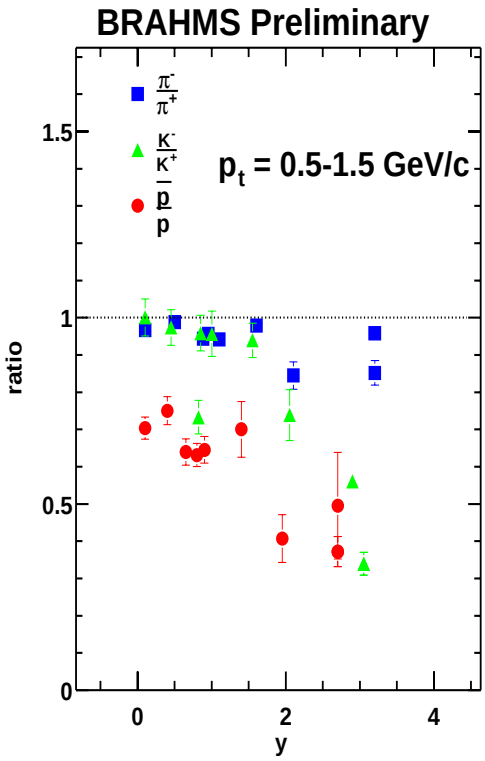

Figure 4. Ratios as a function of rapidy for p+p

[1]. I. Arsene *et. al.*, Phys. Rev. Lett. **91**, 072305 (2003).

[2]. D. Kharzeev, Y.V. Kovchegov and K. Tuchin Phys. Rev. D **68**, 094013 (2003); D. Kharzeev, E. Levin, and L. McLerran, Phys. Lett. B **561**, 93 (2003).

[3]. R. Baier *et al.*, Phys. Rev. D **68**, 054009 (2003); J. Albacete *et. al.*, hep-ph/0307179.

[4]. J. Jalilian-Marian, Y. Nara and R. Venugopalan, Phys. Lett. B **577**, 54 (2003); A. Dumitru and J. Jalilian-Marian, Phys. Rev. Lett. **89** 022301 (2002).

[5]. K. Hagel *et al.*, *Progress in Research*, Cyclotron Institute, Texas A&M University (2002-2003), p. II-21.

Exploring New Ways to Produce Heavy and Superheavy Nuclei with BigSol

T. Materna, S. Kowalski, K. Hagel, J. B. Natowitz, G. A. Souliotis, R. Wada, J. Wang, A. S. Botvina, S. Moretto,[1] D. Fabris,[1] M. Lunardon,[1] S. Pesente,[1] V. Rizzi,[1] G. Viesti,[1] M. Barbui,[2] M.Cinausero,[2] G. Prete,[2] F. Becchetti,[3] H. Griffin,[3] H. Jiang,[3] T. O'Donnel,[3] and Z. Majka[4]

[1]*Dipartimento di Fisica dell'Universitá and INFN Sezione di Padova, I-35131 Padova, Italy*

[2]*INFN Laboratori Nazionali di Legnaro, I-35020 Legnaro, Italy*

[3]*Department of Physics,University of Michigan, Ann Arbor, MI*

[4]*Smoluchkowski Institute of Physics, Jagiellonian University, Krakow, Poland*

The synthesis of super-heavy elements (SHE) has been an important field in both theoretical and experimental nuclear physics for many years. During the past 5 years, the elements with Z = 113-116 and 118 [1] have been synthesized after great efforts to improve the experimental methods used. The reaction used is fusion of the double-magic neutron-rich ^{48}Ca projectile with transuranium targets. The cross-sections involved are at the limit of sensitivity with the current technology. In this context, a new reaction to produce these elements with a higher (even if still very low) cross-section would open a new path to still heavier nuclei. Such a new path could be provided by a reaction where the fissile target nucleus (e.g. ^{238}U and ^{232}Th) would fission as the projectile approaches and where one of the fragments would be transferred to the projectile nucleus with subsequent fusion. The fission fragments can be relatively neutron-rich and close to shell closure, they should therefore enhance the fusion and survival probabilities of the formed superheavy nucleus [2].

An experiment involving a collaboration between the Cyclotron Institute and the Instituto Nazionale di Fisica Nucleare (INFN, Italy) has already been conducted in July 2003 using Uranium Fluoride (^{238}U) targets and ^{172}Yb, ^{198}Pt and ^{238}U beams with energies ranging from 10 to 15 A.MeV delivered by the K500 cyclotron. The isotopes produced are collected by the magnetic field of the superconducting solenoid BigSol and focused at ~4 meters from the magnet, where a multistage detector developed by the INFN group is set. This detector was composed of a position-sensitive detector of 7x7cm^2 followed by a Bragg Chamber at the end of which CsI scintillators were placed. A position-sensitive PPAC was also placed 1 meter before the focal position in order to obtain trajectory reconstruction and time-of-flight measurements. The data analysis is still in progress.

A new program, BigSolSim, has been developed in order to simulate the trajectories of the nuclei produced in the studied reactions. This program has been used extensively to test possible new improvements to the setup. This work led to a modified geometry where the target is now placed at the very entrance of BigSol, allowing us to collect ions at angles as large as ~16°, closer to the grazing angle, where super-heavy nuclei formed in peripheral collisions with little dissipated energy are more likely to appear.

A run with the new setup was conducted in March-April of this year with a thick target of ^{232}Th (5.9 mg/cm^2). For that run, the CsI crystals at the back of the Bragg Chamber were replaced by YAP scintillators [3]. Whenever a nucleus associated with a high Bragg peak signal was implanted, the beam was turned off and the signal coming from the scintillator was recorded by a flash ADC during 1.3 ms to look for a possible subsequent decay.

The data are being analyzed and a typical spectrum is displayed on figure 1. A lesson that this experiment already taught us is that it is difficult to get rid of the high cross-section reactions (e.g. elastics, deep-inelastics, …) only by making a selection on the magnetic rigidity Bρ. As a matter of fact, even if the products have different momenta p, the distribution of charge state q at the exit of the target implies that some fraction of these will have very similar Bρ=p/q to the one expected for superheavy nuclei. Since those reactions have cross-sections orders of magnitude higher than the ones we are looking for, even that small fraction is important when considering the signal to noise ratio.

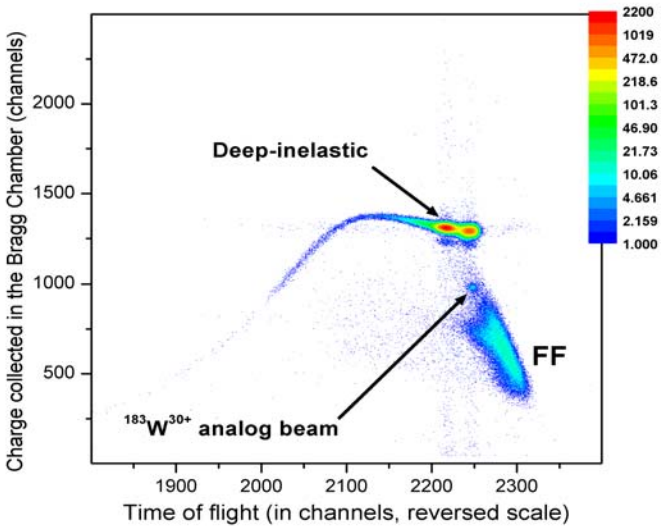

Figure 1. Charge collected in the Bragg chamber versus time of flight (inverted) for the reaction ^{238}U(12A MeV) + ^{232}Th, after rejection of the pile-up and demanding a coincidence with a YAP scintillator. The fission fragments of the ^{238}U are labeled FF. The double structure seen for the deep-inelastic products is due to the fact that the products at angles below 6° are stopped before BigSol and hence do not appear in the

BigSolSim has therefore been improved to test new ways of selecting interesting fragments in flight. The gas-filling of BigSol seems the most promising idea as the charge states of the ions would change often during their journey in the magnetic field. The trajectories are then close to the trajectory of an ion that would carry the mean charge. First simulations show a clear reduction of the dispersion of the trajectories, and hence a better separation between the different classes of products. However, the energy-loss induced by the gas-filling (particularly by the entrance and exit windows whose thickness must increase with the desired pressure) have the effect of defocusing all the products. A compromise is currently under study to achieve the best result.

The possibility of using, close to the target, a start detector that would work in the intense magnetic field and handle a high counting rate is also under study. This would allow us to increase the path length over which the time of flight is measured from 1 to about 5 meters providing us with a better tagging of the detected ion.

[1] Yu. Ts. Oganessian *et al.*, Phys. Rev. C**69** (2004) R021601; Yu. Ts. Oganessian *et al.*, Nature **400,** 242 (1999); Y. Ts. Oganessian *et al.*, Scientific American **282,** 45 **(**Jan 2000); Yu. Ts. Oganessian *et*

al., Phys. Rev. C **63,** R011301 (2001); Yu. Ts. Oganessian, "JINR Preprints and Communications", D7-2002-287, Dubna, 2002.

[2] Y. Aritomo, T. Wada, M. Ohta and Y. Abe, Phys. Rev. C **59**, 796 (1999).

[3] M. Moszynski *et al.*, Nucl. Instrum. Methods Phys. Res. A **404**, 159 (1998).

Relative Nucleon Density and the Secondary De-excitation Effect in the Isospin Fractionation of Asymmetric Nuclear Matter

D. V. Shetty, A. S. Botvina, A. L. Keksis, E. Bell, G.A. Souliotis, and S. J. Yennello

The Liquid-Gas phase transition in isospin asymmetric nuclear matter results in an inhomogeneous distribution of the neutrons and the protons within the system (isospin fractionation), where a dilute neutron-rich (N/Z > 1) gas (light clusters) and a dense and symmetric (N/Z ~ 1) liquid (heavy fragments) is formed [1]. In this work, the composition of the gas phase in ^{58}Fe + ^{58}Ni and ^{58}Fe + ^{58}Fe reactions with respect to ^{58}Ni + ^{58}Ni reaction was studied at 30, 40 and 47 MeV/nucleon. Figure 1 (left) shows the relative neutron and proton densities in the gas phase obtained from the measured isotope and isotone yield ratios as a function of N/Z of the composite system. It is observed that the neutron content of the gas phase is sensitive to both, the isospin (N/Z) of the initial colliding nuclei and the excitation energy. The asymmetry (difference in the neutron and the proton density) in the gas phase increases with the isospin (N/Z), of the composite nuclei and decreases with increasing beam energy. A comparison of the relative neutron and proton density with the statistical multifragmentation model (right) shows that the initial asymmetry in the gas phase, composing of light clusters, is strongly affected by the secondary de-excitations. While the effect is less pronounced for the symmetric systems and lower excitation energies, it becomes significant for neutron-rich systems and higher excitation energies.

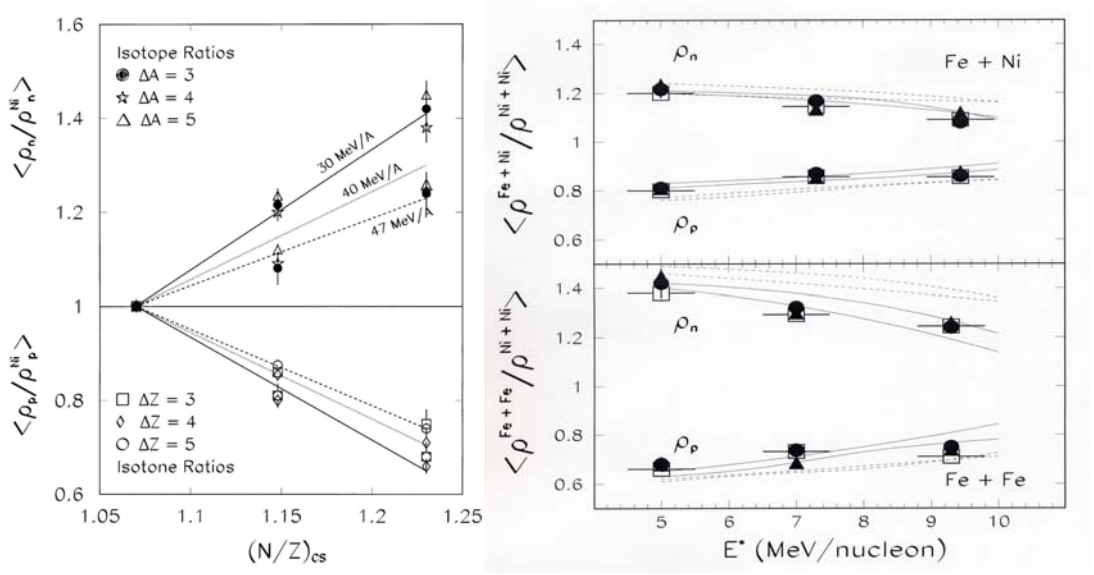

Figure 1. (Left) Relative neutron (top) and proton (bottom) densities as a function of N/Z of the composite system for various beam energies. (Right) Relative neutron and proton densities as a function of excitation energy. The region enclosing the dotted (primary fragments) and the solid lines (secondary fragments) are comparisons to the statistical model calculations

[1] H. Muller and B. Serot, Phys. Lett. B **371**, 175 (1996).
[2] D.V. Shetty *et al.*, Phys. Rev. C **68**, 021602 (2003).
[3] S.J. Yennello *et al.*, Phys. Lett. B **321**, 15 (1995).
[4] E. Ramakrishnan et al., Phys. Rev. C **57**, 1803 (1998).

Symmetry Energy and the Isospin Dependent Equation of State

D. V. Shetty, A. S. Botvina, G. A. Souliotis, M. Jandel, E. Bell, A. L. Keksis, S. N. Soisson, B. Stein, J. Iglio, and S. J. Yennello

The isotopic composition of fragments produced in multifragmentation reactions is known to have significant sensitivity to the density dependence of the asymmetry term in the nuclear equation of state of strongly interacting matter. Recently [1], a linear relationship between the isoscaling parameter α, and the isospin asymmetry (Z/A) of the fragments, with appreciably different slopes for two different choices of the effective nucleon-nucleon interaction force, was reported within the framework of antisymmetrized molecular dynamics (AMD) calculation. In this work we report the isoscaling parameter α, from the fragments produced in the multifragmentation of ^{58}Ni + ^{58}Ni, ^{58}Fe + ^{58}Ni, ^{58}Ni + ^{58}Fe and ^{58}Fe + ^{58}Fe reactions at 30, 40 and 47 MeV/nucleon. The observed value of this parameter is compared with that predicted by the antisymmetrized molecular dynamic (AMD) calculation based on two different nucleon-nucleon effective forces, namely the Gogny and Gogny-AS interactions. It is observed that the present data, along with other data from the literature, agrees better with the choice of Gogny-AS effective interaction, resulting in a symmetry energy of ~ 18 – 20 MeV. The observed results indicates that the fragments are formed at a reduced density of ~ 0.08 fm^{-3}.

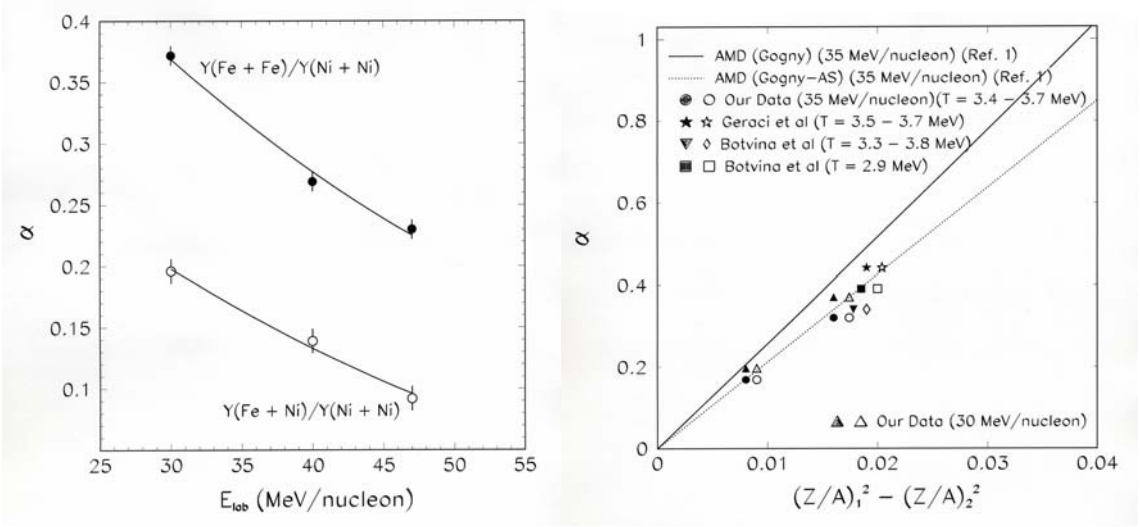

Figure 1. (Left) Experimentally determined isoscaling parameter α, as a function of the bombarding energy. The solid lines are exponential fit to the data. (Right) AMD model prediction [1] of the α as a function of the asymmetry of the fragments at 35 MeV/nucleon for the Gogny (solid line) and Gogny-AS (dotted line) interactions. The solid and hollow circles are the interpolated values for the 35 MeV/nucleon from the present work. Other symbols are taken from Refs. [2] and [3] as described in the top left corner of the figure.

[1] A. Ono *et al.*, Phys. Rev. C **68**, 051601 (2003).
[2] E. Geraci *et al.*, Nucl. Phys. **A732**, 173 (2004).
[3] A.S. Botvina *et al.*, Phys. Rev. C **65**, 044610 (2002).
[4] W.P. Tan *et al.,* Phy. Rev. C **64**, 051901 (2001).
[5] M. Tsang *et al.,* Phys. Rev. Lett. **86**, 5023 (2001).

(N/Z) Equilibration

E. Bell, J. Garey, K. Hagel, D. V. Shetty, S. N. Soisson, R. Wada, S. J. Yennello,
and the NIMROD Collaboration

NIMROD, or the Neutron Ion Multi-detector for Reaction Oriented Dynamics [1], was used to examine the reactions of 35 and 45 MeV/nucleon ^{54,58}Fe and ^{58,64}Ni on ^{54,58}Fe and ^{58,64}Ni in order to study (N/Z) equilibration. The beams were produced by the K500 Superconducting Cyclotron at the Cyclotron Institute of Texas A&M.

The (N/Z) tracer method [2], can be used to gauge the amount of (N/Z) mixing that was occurred in the system prior to fragment emission. Shown in Figure 1 are the cuts in centrality made on NIMROD data. Cuts are made on the ratio of neutrons to charged particles given by the slope of the line drawn through the ridge on Figure 1. Cut 5 selects for the 10% most central events. Cut 4 selects 10 to 20% most cenral, cut 3 for 20 to 30% most central, cut 2 for 30 to 40% most central and cut 1 for 40 to 50% most central events.

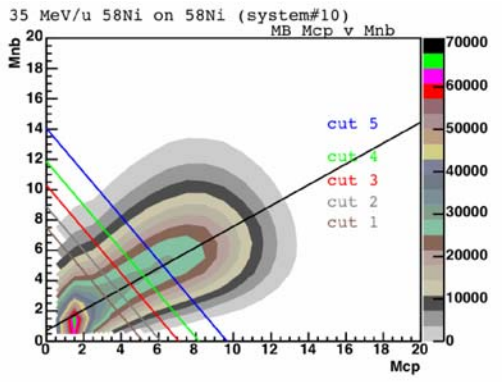

Figure 1. Multiplicity of charged particles plotted versus multiplicity of neutrons for 35 MeV/u ^{58}Ni on ^{58}Ni with centrality cut lines overlaid.

Shown in Figure 2 are the p/d ratio (N/Z) tracer terms for each centrality cut for both 35 and 45 MeV/u projectile systems at lab angle of 18 degree. The dotted lines are polynomial fits to the data of second order. The (N/Z) tracer term shows increased (N/Z) mixing as centrality increases and the effect is more pronounced at the higher energy.

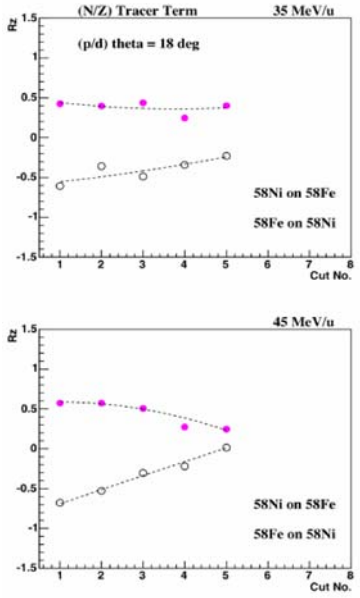

Figure 2. (N/Z) tracer term plotted as a function of centrality cut for 35 (top) and 45 (bottom) MeV/u projectile systems. (Cut 1=40-50%, 2=30-40%, 3=20-30%, 4=10-20%, 5=10% most central)

Isotope and isobar ratios are also being used to investigate (N/Z) equilibration [3].

[1] N. Marie *et al.*, *Progress in Research*, Cyclotron Institute, Texas A&M University (1997-1998), p. V-19; R. Wada *et al.*, *Progress in Research*, Cyclotron Institute, Texas A&M University (1998-1999), p. V-15; T. Keutgen *et al.*, *Progress in Research*, Cyclotron Institute, Texas A&M University (1999-2000), p. V-11.

[2] F. Rami, *et al.*, Phys. Rev. Lett. **84**, 1120 (2000).

[3] H. Johnston *et al.*, Phys. Lett. B **371**, 186 (1996); H. Johnston *et al.*, Phys. Rev. C **56**, 1972 (1996).

Quasiprojectile Fragmentation Around Mass 40

A. L. Keksis, M. Veselsky, G. A. Souliotis, E. Bell, M. Jandel, A. Ruangma, D. V. Shetty, E. M. Winchester, and S. J. Yennello

The effect of isospin, or N/Z, on the breakup of excited systems has been an area of much research [1]. Quasiprojectiles with a wide range in isospin can be generated in peripheral collisions [2-3]. Here, FAUST, the Forward Array Using Silicon Technology [4], was used to collect fragments from the quasiprojectile fragmentation reactions of ^{40}Ar, ^{40}Ca and ^{48}Ca on ^{112}Sn and ^{124}Sn at 32 and 45 MeV/nucleon.

The calibrations, analysis and simulations have previously been described and are in progress [5-6]. Gating has been completed with an example of the gates drawn on detector number 67 in Fig. 1. Extensive gating routines have been developed to assist in drawing and plotting the gates in ROOT. Most detectors have elemental resolution up to Oxygen, with some up to Magnesium, and isotopic resolution up to Boron, with some up to Carbon.

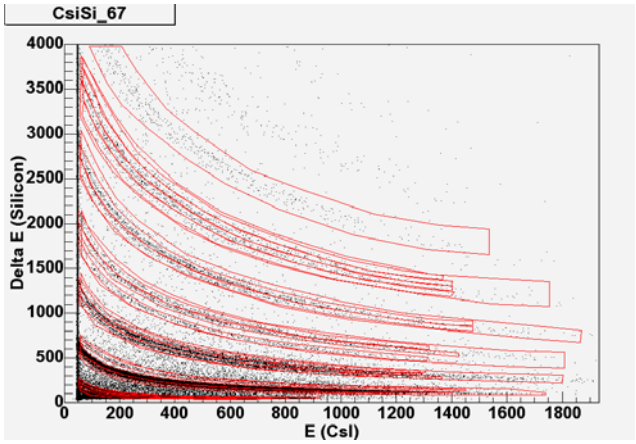

Figure 1. Uncalibrated 2D spectra of ΔE (300 μm Si) vs E (3 cm CsI) with gates as shown.

This data will be used to investigate N/Z effects on fragmentation including the distribution of neutrons and protons between light charged particles (LCPs) and intermediate mass fragments (IMFs), the timescale for fragmentation using the proximity effect and the Coulomb re-acceleration technique, and the scaling of the fragment yields, called isoscaling, which can be related to the symmetry energy coefficient in the nuclear equation of state (nEOS).

[1] *Isospin Physics in heavy-Ion Collisions at Intermediate Energies*, edited by. B.A. Li and W.U. Schroeder, (NOVA Science Publishers, New York, 2001).

[2] D.J. Rowland, Ph.D. Thesis, Texas A&M University (2000).

[3] D.J. Rowland *et al*. Phys. Rev. C **67**, 064602 (2003).

[4] F. Gimeno-Nogues *et al*.,Nucl. Instrum. Methods. Phys. Res. A **399**, 94 (1997).

[5] A.L. Keksis *et al*., *Progress in Research*, Cyclotron Institute, Texas A&M University (2001-2002), p. II-38.

[6] A.L. Keksis *et al*., *Progress in Research*, Cyclotron Institute, Texas A&M University (2002-2003), p. II-11.

Angular Anisotropy of LCP as a Tool for the Determination of Short Emission Times in the Region 50-500 fm/c

M. Jandel, A. S. Botvina, G. A. Souliotis, D. V. Shetty, E. Bell, A. L. Keksis, and S. J. Yennello

Data from the reaction of ^{28}Si+^{112}Sn at 50 MeV/nucleon [1] has been reanalyzed in order to investigate the possibility of extracting new results [2]. A novel method was developed for the extraction of short emission times of light particles from projectile-like fragments in peripheral deep-inelastic collisions in the Fermi energy domain. We were able to determine the emission times in the interval 50-

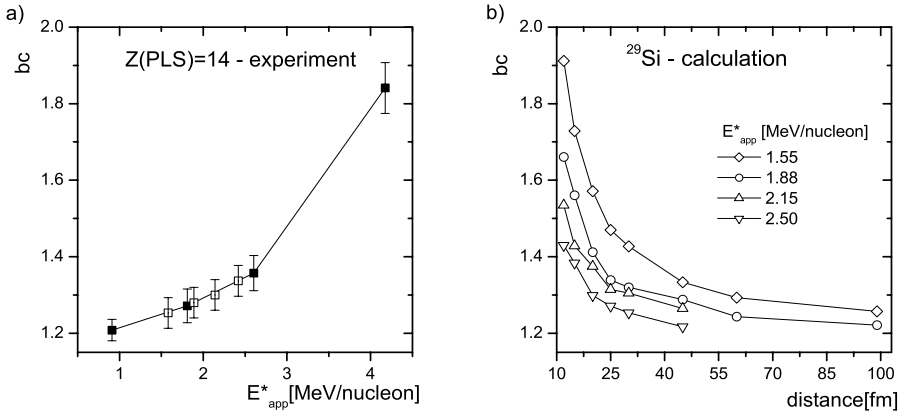

Figure 1. Anisotropy parameter bc as a function of the apparent excitation energy E^*_{app} obtained from experimental data - (a), and calculated values of anisotropy parameter bc as a function of the distance for different E^*_{app} - (b). Empty squares in (a) show estimated values of bc parameter for E^*_{app} involved in the calculation shown in (b).

500 fm/c using asymmetrical emission of light particles observed in reaction ^{28}Si+^{112}Sn at 50 MeV/nucleon. The backward emission anisotropy of α-particles relative to largest residue was compared to the values calculated from a statistical evaporation model taking into account the Coulomb interaction with the target (see Fig. 1). To our knowledge, these are the smallest decay times which can be identified in a sequential framework (see Fig.2). At higher excitation energies, we expect a multi-fragment breakup into many small fragments.

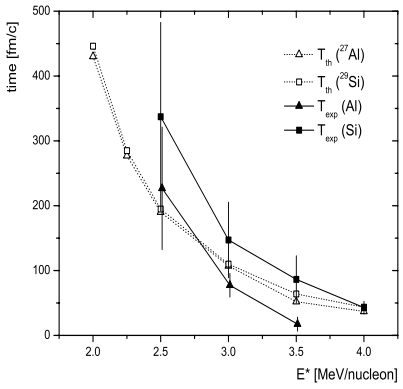

Figure 2. Time of the first emission T_{exp} obtained by comparison of angular anisotropy parameter bc observed in experiment (full symbols). Time of the emission T_{th} calculated from total decay width is shown for comparison (empty symbols). Square and triangle symbols correspond to results for Z(PLS)=13 (Si) and Z(PLS)=13 (Al), respectively.

[1] A. Laforest *et al.*, Phys. Rev. C **59**, 2567 (1999).
[2] M. Jandel *et al.*, nucl-ex/0405002.

Heavy-Residue Isoscaling as a Probe of Isospin Transport and Equilibration

G. A. Souliotis, M. Veselsky, D. V. Shetty, E. Bell, M. Jandel, A. L. Keksis, and S. J. Yennello

The isotopic and isobaric scaling behavior of the yield ratios of heavy projectile residues from the collisions of 25 MeV/nucleon ^{86}Kr projectiles on ^{124}Sn and ^{112}Sn targets was investigated and shown to provide information on the process of N/Z transport and equilibration occurring between the projectile and the target [1]. The residue data were obtained with the MARS recoil separator [2].

The logarithmic slopes α and β' of the residue yield ratios with respect to residue neutron number N and neutron excess N–Z are obtained as a function of the atomic number Z and mass number A, respectively, whereas excitation energies are deduced from velocities. The relation of the isoscaling parameters α and β' with the N/Z of the primary (excited) projectile fragments is employed to gain access to the degree of N/Z equilibration prior to fragmentation as a function of excitation energy. A monotonic relation between the N/Z difference of fragmenting quasiprojectiles and their excitation energy is obtained indicating that N/Z equilibrium is approached at the highest observed excitation energies of E*/A ~2.2 MeV/nucleon (Fig. 1). Simulations with a deep-inelastic transfer (DIT) model [3] are in overall agreement with the isoscaling conclusions. Calculations with microscopic models are currently underway. We have obtained additional data on residue isoscaling from recent experiments with the BigSol line with beams of ^{64}Ni(25MeV/u) and ^{136}Xe(20MeV/nucleon) on ^{64,58}Ni, ^{124,112}Sn, ^{197}Au, ^{208}Pb and ^{232}Th targets whose data are currently being analysed. We expect systematic information on isoscaling and isospin transport to be obtained from the new data. In general, the present residue isoscaling approach seems to offers an attractive tool of isospin and reaction dynamics studies in collisions involving beams of stable or rare isotopes.

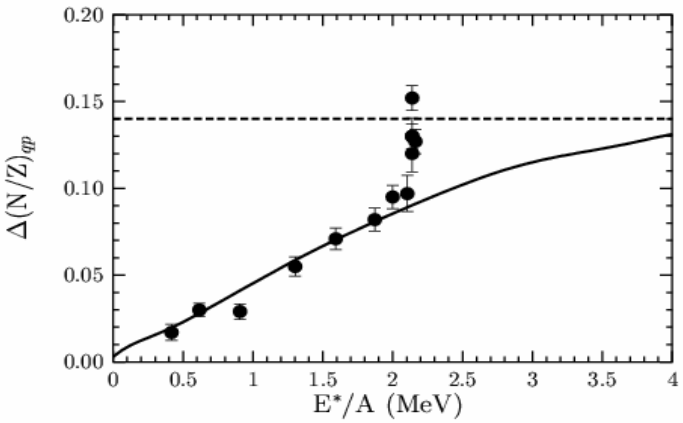

Figure 1. Difference in N/Z of fragmenting quasiprojectiles [1] as a function of excitation energy per nucleon for projectile residues from ^{86}Kr (25MeV/nucleon)+ ^{124,112}Sn (full circles). Dashed line: N/Z difference of isospin-equilibrated quasiprojectiles. Solid line: DIT code prediction [3].

[1] G.A. Souliotis *et al.*, Phys. Lett. B **588**, 35 (2004).

[2] G.A. Souliotis *et al.*, Phys. Rev. C **68**, 024605 (2003).

[3] L. Tassan-Got and C. Stefan, Nucl. Phys. **A524**, 121 (1991).

Neutron-Rich Isotope production with the Superconducting Solenoid (BigSol) Line

G. A. Souliotis, A. L. Keksis, D. V. Shetty, E. Bell, S. N. Soisson, B. Stein, and S. J. Yennello

The complete (two-stage) Superconducting Solenoid (BigSol) Line was commissioned in August 2003. The line (see also [1]), consisiting of the BigSol 7-Tesla superconducting solenoid (first stage) and a large-bore quadrupole triplet (second stage) was successfully used to produce neutron-rich nuclei in deep-inelastic collisions. The prospects of using DIC for very n-rich isotope production were investigated in our earlier work with MARS ([2] and references therein). In the present measurements, the reactions of ^{64}Ni (25MeV/nucleon) and ^{136}Xe (20MeV/nucleon) beams with a series of targets (^{64,58}Ni, ^{124,112}Sn, ^{197}Au, ^{208}Pb and ^{232}Th) were studied. The experimental setup used in the measurements is shown in Fig. 1. The primary beam, after hitting the target, is collected on an on-axis blocker. Fragments are focused at the intermediate-image location, where, with the use of a circular aperture, certain groups of them can be selected (based on magnetic rigidity). These fragments are then transported through a 7.5 meter line and focused with the aid of the quadrupole triplet at the end of the separator. Time-of-flight is provided between two PPACs (Fig. 1). A Si detector stack provides ΔE,E information, which, combined with TOF, gives Z and A identification (0.5 and 0.6 units respectively for ^{64}Ni fragments).

We plan to proceed with RIB production efforts with lighter beams (A=20-30). We expect that we will be able to obtain in-flight identification of RIBs (based on ΔE and TOF) with the subsequent goal of using these tagged beams to study multifragmentation with the FAUST multidetector array.

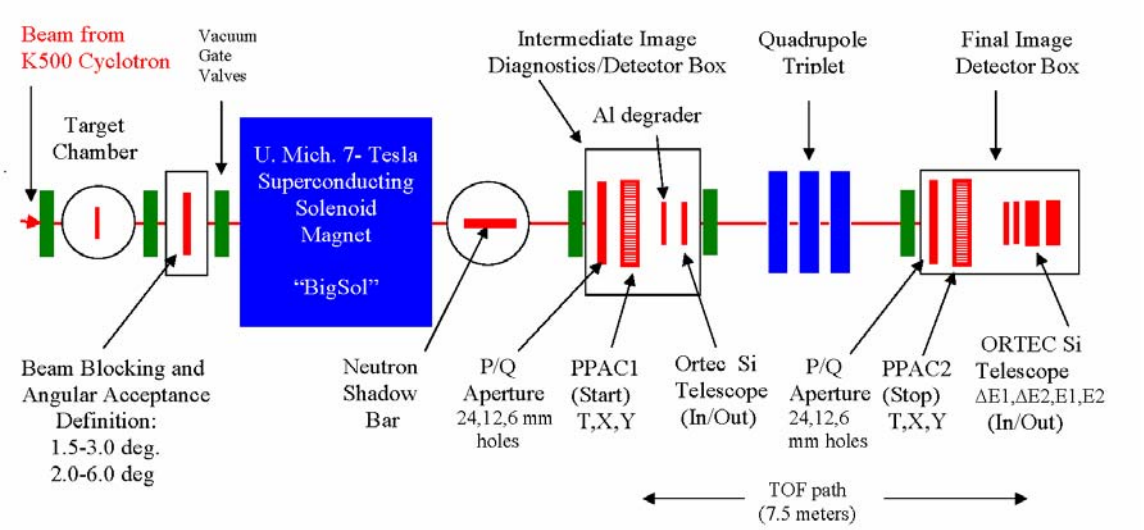

Figure 1. Schematic diagram of the experimental setup for RIB production with BigSol.

[1] G.A. Souliotis *et al.*, *Progress in Research*, Cyclotron Institute, Texas A&M University (2002-2003), p.V-5.

[2] G.A. Souliotis *et al.*, Phys. Rev. Lett. 91, 022701 (2003).

Influence of Nuclear and Coulomb Proximity Effect in the Projectile-like Decay of ^{64}Zn at 45 MeV/nucleon

B. Davin,[1] R. T. deSouza,[1] S. Hudan,[1] T. Paduszynski,[1] J. Gauthier,[2] F. Grenier,[2] R. Roy,[2]
D. Theriault,[2] E. Bell, J. Garey, J. Iglio, A. L. Keksis, S. Parketon, C. Richers,
D. V. Shetty, S. N. Soisson, G. A. Souliotis, B. Stein, and S. J. Yennello
[1]*Department of Physics, Indiana University, Bloomington, IN 47401*
[2]*Department of Physics, Universite Laval, St. Foy, Cana*da

To investigate projectile-like decay, in particular the influence of both nuclear and Coulomb proximity effects, a collaboration from Indiana University, Universite Laval, and Texas A&M bombarded ^{209}Bi,^{64}Zn, and ^{27}Al targets with a beam of ^{64}Zn at E/A=45 MeV from the TAMU K500 cyclotron. In addition to examining the angular and velocity correlations between the decay products of the projectile-like fragment, we also focused on their N/Z to probe the degree of N/Z equilibration attained in the collision.

Charged particles produced in the reaction were detected by a new detector array FIRST (Forward Indiana Ring Silicon Telescopes) coupled to the silicon strip array LASSA. Both arrays are based on a Si(IP)-CsI(Tl)/PD design and are highly segmented to provide adequate angular resolution of the kinematically forward focused reaction products. This segmentation requires ~750 channels of peak sensing silicon electronics. FIRST consists of three annular detectors designated T1,T2, and T3 which cover successively larger angles in the range $2°\leq\theta_{lab}\leq28°$. Eight LASSA telescopes placed in an azimuthally symmetric geometry provided detection for charged particles emitted at larger angles $28°\leq\theta_{lab}\leq48°$. Neutrons produced in the reaction were measured by seven neutron TOF detectors placed at selected angles.

Data analysis to date has focused on the calibration of FIRST and the neutron TOF detectors. The excellent isotopic resolution achieved in T1 is evident in Fig. 1. This ΔE-E plot for the T1 telescope, which is a matched 2D of all segments in the telescope and is integrated over all projectile-target combinations, clearly shows that the isotopes of Aluminum are resolved. The T2 and T3 telescopes exhibit comparable resolution. At this time, neutron identification was done by analyzing the 2D "fast-slow" spectra and TOF energy calibration is completed. Work is underway to correct energy spectra for background emission, using shadow bar measurements, and for detector efficiency with the help of GEANT4 simulations.

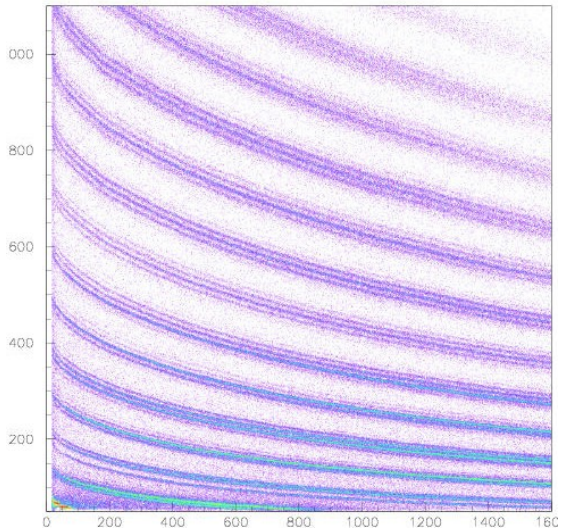

Figure 1. ΔE-E plot for the T1 telescope.

Using Light Cluster Production to Determine the Density Dependence of Nuclear Symmetry Energy

S. N. Soisson, E. Bell, L. W. Chen, S. J. Yennello, and the NIMROD Collaboration

Using a coalescence model for treating cluster production from an isospin dependent transport model, it has been shown that the multiplicities and the energy spectra of light clusters produced is sensitive to the density dependence of the nuclear symmetry energy but not to the isospin-independent part of the nuclear equation of state or the in-medium nucleon-nucleon cross sections [1,2]. Experimental data was taken with NIMROD for ^{58}Ni + ^{58}Ni, ^{58}Fe + ^{58}Fe, ^{58}Ni + ^{58}Fe, and ^{58}Fe + ^{58}Ni systems at 45 MeV/A.

During this period, gating and calibration of the CsI detectors in NIMROD was accomplished. From this, both the multiplicities and energy spectra for tritons and ^{3}He was extracted. To minimize effects such as heavy fragment evaporation and decay from excited states of the triton and ^{3}He, an isobaric yield ratio has been determined as well. Coalescence calculations are being performed on the above aforementioned systems using MDI interactions with x = -2 (stiff) and x = 1 (soft) [3]. Comparisons are underway between model calculations and experimental data to determine the extent of the effects of density dependence on light cluster production

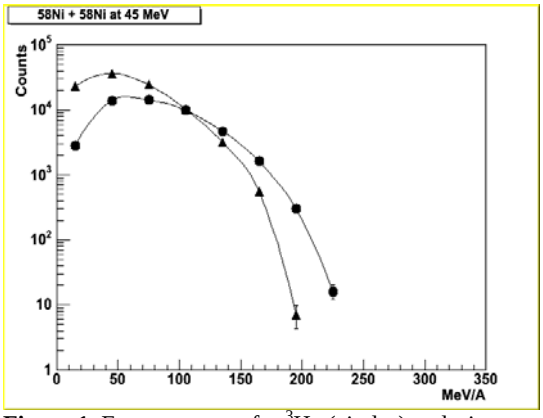

Figure 1. Energy spectra for ^{3}He (circles) and triton (triangles) for the system ^{58}Ni + ^{58}Ni at 45 MeV/A.

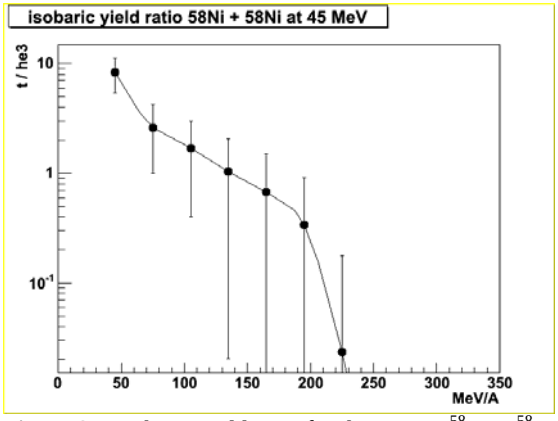

Figure 2. . Isobaric yield ratio for the system ^{58}Ni + ^{58}Ni at 45 MeV/A.

[1] Lie-Wen Chen, C.M. Ko, Bao-An Li, Phys. Rev. C **68**, 01601 (2003).

[2] Lie-Wen Chen, C.M. Ko, Bao-An Li, Nucl. Phys. **A739** 809 (2003).

[3] Lie-Wen Chen, C.M. Ko, Bao-An Li, Phys. Rev. C **69**, 054606 (2004).

Isotope Temperatures from Heavy Residues Produced by Multifragmentation of Neutron-Rich Systems

J. A. Iglio, G.A. Souliotis, D. V. Shetty, E. Bell, M. Jandel, A. L. Keksis, S. N. Soisson, B. Stein, M. Veselsky, and S. J. Yennello

A great deal of research has been focused on measuring light charged particle and intermediate mass fragment (IMF) yields to extract the temperature of fragmenting nuclei using the double isotope formalism of Albergo [1]. Much of this data has been interpreted in the framework of statistical multifragmentation models. It is our intention to investigate if similar information can be obtained from the yields of isotopically resolved heavier fragments (heavy IMFs and heavy residues).

From the reactions of 25 MeV/nucleon ^{86}Kr with ^{64}Ni, ^{58}Ni, ^{124}Sn, and ^{112}Sn, as well as 20 MeV/u ^{124}Sn with ^{124}Sn [2,3,4], heavy fragments were collected with the MARS recoil separator at the Cyclotron Institute of Texas A&M University and characterized event-by-event by their Z, A and velocity. Details of the data collected and analysis procedures can be found in the references.

Using the yields of specific sets of intermediate-mass fragments or heavy residues, the isotopic temperature can be extracted, using the double isotope ratio method [1]. The combinations of different isotopes are chosen to maximize the difference in the binding energy as much as possible. The extracted temperatures will be compared with the statistical multifragmentation model (SMM) [5], which gives an estimate of microcanonical temperatures. The intent of the analysis is to investigate the relationship between the N/Z of neutron-rich heavy fragments and their temperature. The hypothesis is that the temperature of the neutron rich fragments may be lower than those of more N/Z symmetric fragments.

[1] S. Albergo *et al.*, Nuovo Cimento A **89,** 1 (1985).
[2] G.A. Souliotis, *et al.*, Phys. Rev. C **68**, 024605 (2003).
[3] G.A. Souliotis *et al.*, Nucl. Instrum. Methods Phys. Res. B **204**, 166 (2003).
[4] M. Veselsky *et. al.*, Nucl. Phys. **A724**, 431 (2003).
[5] A.S. Botvina, O.V. Lozhkin, and W. Trautmann, Phys. Rev. C **65**, 044610 (2002).

Investigations of A=20 Systems for Evidence of Critical Behavior
Elastic Scattering of ^{8}B on ^{12}C and ^{14}N

B. C. Stein, E. Bell, M. Jandel, D. V. Shetty, G. A. Souliotis, and S. J. Yennello

Search for evidence of a liquid-gas phase transition in nuclear matter has been an important area of research during the last several years. It was suggested by Y.G. Ma in a recent paper that lower mass systems would be preferred for further investigation of critical behavior [1]. This is due to the tendency of coulomb instability to set in before the critical point is reached in larger systems. With this in mind, a system with an A = 20 projectile is being investigated. The data includes the systems ^{20}F, ^{20}Ne, and ^{20}Na on ^{197}Au and ^{20}F on ^{nat}Ag taken on the FAUST detector in April of 1998 [2, 3].

Figure 1 shows the Z distribution for nine excitation energy cuts. There is a noticeable evolution from a binary breakup at low energies to a multi-body breakup at higher energies. This suggests a change in the reaction mechanism with increasing excitation energy. The data is currently being analyzed for several indicators of critical behavior such as caloric curves, Campi plots, Fisher-law parameters, and exponential law parameters.

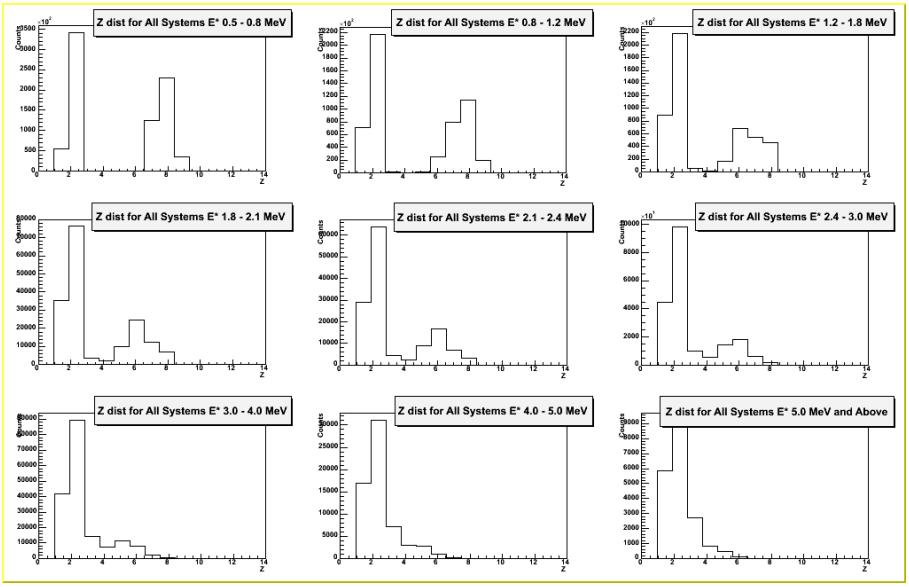

Figure 1. Combined fragment Z distributions for all systems being investigated.

[1] Y.G. Ma *et al.*, Phys. Rev. C **69**, 031604 (2004).

[2] D.J. Rowland, *A Study of the Projectile Fragmentation of Isobaric Nuclei*, Ph.D. diss., (Texas A&M University, December 2000).

[3] D.J. Rowland *et al.*, Phys. Rev. C **67**, 064602 (2003).

Pulse Shape Discrimination Using an nTD Silicon Detector

M. C. Sarahan, J. Garey, C. Richers, R. Burch, G. A. Souliotis, D. Shetty, M. Jandel, E. Bell, A. L. Keksis, J. Iglio, B. Stein, S. N. Soisson, and S. J. Yennello

Pulse shape discrimination is an important technique for identifying products of nuclear fragmentation reactions. Historically, this has been the domain of scintillation detectors. Recently, work has been done demonstrating the possibility of extracting pulse-shape information from silicon detectors [1,2]. Using a doped nTD silicon detector, one can obtain rise time information. When the rise time is correlated with the amplitude of the pulse, good separation of isotopes can be seen.

This research was performed at Texas A&M University's Cyclotron Institute using a two-detector telescope, which held a FAUST silicon detector (#40), and an nTD detector. Measurements thus far have been with stable beams of ^{40}Ar on gold, aluminum, and zinc targets.

Using conventional electronics, we have achieved moderate separation on-line. In this mode, we extracted a relative rise time from the difference in time between two CFDs with different delay times. In an attempt to further refine our approach, we have recorded the waveforms using a digital scope. We are now developing a complete simulation of the module-driven method using National Instruments' Labview software. This should make troubleshooting far easier, since runs can be simulated with settings much more easily changed. Thus far, a constant fraction discriminator has been created and can process the data transmitted from the ethernet-equipped oscilloscope.

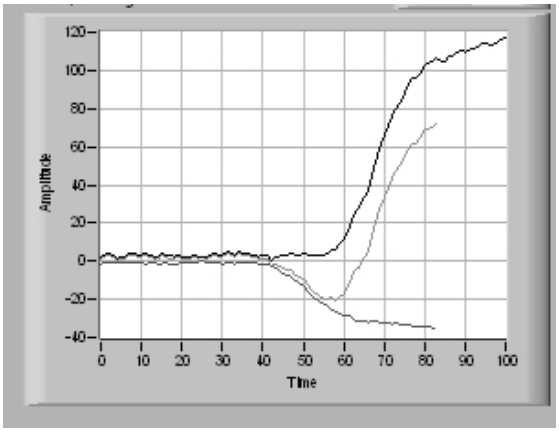

Figure 1. CFD program in action. Showing original pulse, delayed inverted pulse and the sum.

A screen shot of the mock CFD in action is shown in Figure 1. Using the Labview "modules" to process the experimental waveforms, we will determine the optimal settings of the electronics. We will then apply this information to an on-line test.

[1] M. Mutterer *et al.*, IEEE Trans. Nucl. Sci. **47**, 256 (2000).
[2] J. Lu *et al.*, Nucl. Instrum. Methods Phys. Res. A **471**, 374 (2001), and references therein.

SECTION III

NUCLEAR THEORY

Charm Production from Proton-Proton Collisions

W. Liu, C. M. Ko, and S. H. Lee[1]
[1]*Department of Physics, Yonsie University, Seoul 120-749, Korea*

Using a hadronic model based on the SU(4) flavor-invariant Lagrangian with empirical masses and coupling constants, we have studied charmed hadron production from proton-proton reactions through the reactions pp → p $\overline{D}^{0}\Lambda_c^{+}$ and pp → p $\overline{D}^{*0}\Lambda_c^{+}$ [1]. These reactions involve exchange of pion, rho meson, D and D*, and their cross sections can be expressed in terms of the cross sections for the off-shell processes Mp → $\overline{D}^{*0}\Lambda_c^{+}$ and Mp → $\overline{D}^{0}\Lambda_c^{+}$, where M denotes one of the above exchanged off-shell mesons. With cutoff parameters in form factors adjusted to fit the cross section for strange hadron production in proton-proton reactions, the resulting cross section for charmed hadron production from proton-proton reactions at center-of-mass energy of 11.5 GeV is about 0.1 μb, comparable to the measured inclusive cross section [2] as shown in Fig. 1. The predicted cross section decreases to about 1 nb at 40 MeV above threshold. Our results will be useful for the experiments to be carried out at future accelerator at the German Heavy Ion Research Center [3].

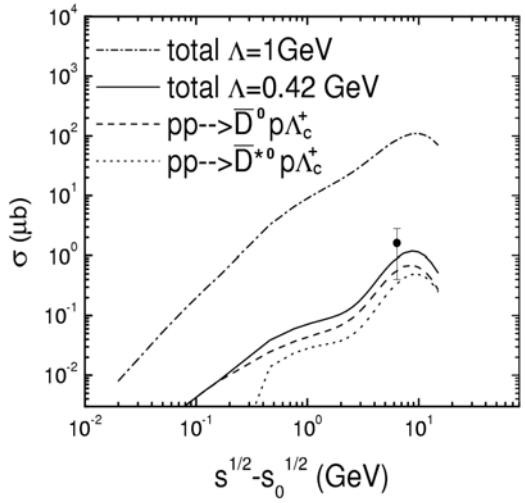

Figure 1. Cross sections for charmed hadron production in proton-proton reactions. Dashed and dotted lines are results obtained with empirical cutoff parameter Λ=0.42 GeV for pp → p $\overline{D}^{0}\Lambda_c^{+}$ and pp → p $\overline{D}^{*0}\Lambda_c^{+}$, respectively, while the total cross section is shown by the solid line. The threshold energy refers to that of the reaction pp → p$D^{0}\Lambda_c^{+}$. Experimental data [2] are shown by the filled circle. The dash-dotted line is the total cross section obtained with Λ=1.0 GeV.

[1] W. Liu, C.M. Ko, and S.H. Lee, Nucl. Phys. **A728**, 457 (2003).
[2] N.S. Amaglobei *et al.*, SVD Collaboration, Phys. At. Nucl. **64**, 891 (2001).
[3] See http://www.gsi.de/GSI-future.

Momentum Anisotropies in the Quark Coalescence Model

P. Kolb,[1] L. W. Chen, V. Greco, and C. M. Ko
[1]*Physik Department, Technische Universitat Munchen, D-85747 Garching, Germany*

Using a naive quark coalescence model for hadron production from the quark-gluon plasma formed in relativistic heavy ion collisions, which only allows partons of equal momenta to recombine, we have expressed the Fourier coefficients of the azimuthal distribution of meson and baryon momentum spectra in terms of those of partons. Neglecting higher-order terms, simple relations are found between the ratio of the hadrons 4th order term to the square of their 2nd order to the corresponding ratio for the partons. Furthermore, a simple relation is obtained between such ratios for baryons and mesons. For hadrons at finite rapidities or spectra from collisions of non-identical nuclei, odd-order terms are nonzero. We have shown that the ratio of their third-order term to the product of their 1st-order and 2nd-order terms is also simply related to the corresponding ratio for the partons. To account for the observed large ratio ~ 1.2 of hadron 4th-order to the square of 2nd-order anisotropy, a larger value (~ 2) for the corresponding ratio for the partonic anisotropy is needed. The present analysis based on the schematic quark coalescence model thus allows one to have a simple understanding of the effect of higher-order partonic anisotropies on those of the observed hadrons.

[1] P. Kolb, L.W. Chen, V. Greco, and C.M. Ko, Phys. Rev. C (in press); nucl-th/0402049.

Pentaquark Baryon Production in Hadronic Reactions

W. Liu and C. M. Ko

The cross sections for the production of Θ^+ baryon consisting of $uudd\bar{s}$ quarks from meson-nuleon and proton-proton reactions are evaluated in a hadronic model that includes the KNΘ interaction with coupling constant determined by a Θ^+ width of 20 MeV, largely given by experimental resolutions. Form factors of monopole type are introduced at interaction vertices with values of the cutoff parameters taken from fitting known cross sections for other reactions based on similar hadronic models. It is found that for meson-nucleon reactions, shown in Fig.1, the one induced by kaon has the largest cross section of about 1.5 mb and is almost order of magnitude larger than those for reactions induced by pion and rho meson. For proton-proton reactions, the total cross sections is about 20 μb and is dominated by the final state $pK^0\Theta^+$ with only about 25% for final states of $\Sigma^+\Theta^+$ and $\pi^+\Lambda\Theta^+$. Knowledge on these cross sections is useful for studying Θ^+ production not only in elementary reactions involving hadrons but also in relativistic heavy ion collisions, where final hadronic effects need to be understood in order to infer its production from the initial quark-gluon plasma.

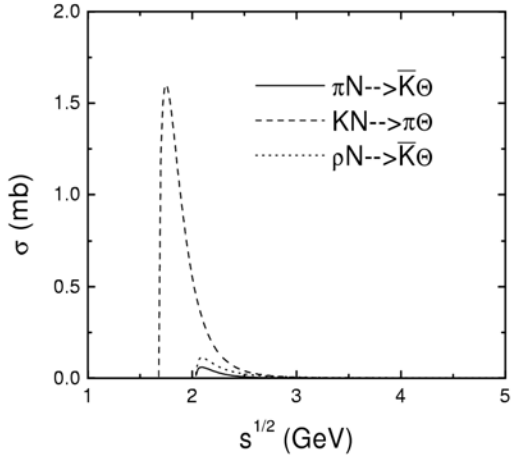

Figure 1. Spin and isospin averaged cross sections for Θ^+ production from meson-nucleon reactions as functions of center-of-mass energy.

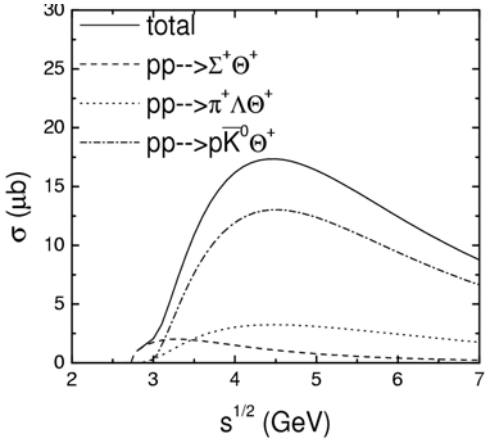

Figure 2. Cross sections for Θ^+ production from proton-proton reactions as functions of center-of-mass energy.

[1] W. Liu and C.M. Ko, Phys. Rev. C **68**, 045203 (2003).

Exotic Cascade Baryon Production in Photon-Nucleon Reactions

W. Liu and C. M. Ko

Using a hadronic model that includes the coupling of pentaquark Ξ_5 to usual Σ and K or K*, we have evaluated the cross sections for their production in the reactions $\gamma p \to K^0 K^0 \Xi_5^+$ and $\gamma n \to K^+ K^+ \Xi_5^{--}$ by assuming that Ξ_5 has spin 1/2 and positive parity [1]. Using coupling constants related to those for pentaquark Θ^+ couplings to NK and NK*, and also including form factors at the strong interaction vertices with empirical cutoff parameters, these cross sections are found in the range of 0.03-0.6 nb for $\gamma p \to K^0 K^0 \Xi_5^+$ (Fig.1) and 0.1-0.6 nb for $\gamma n \to K^+ K^+ \Xi_5^{--}$ (Fig.2) at photon energy of 4.5 GeV. These cross sections are significantly smaller than those for Θ^+ production in photo-nucleon reactions [2]. Also shown are the cross sections obtained without form factors, and they are about two orders of magnitude larger.

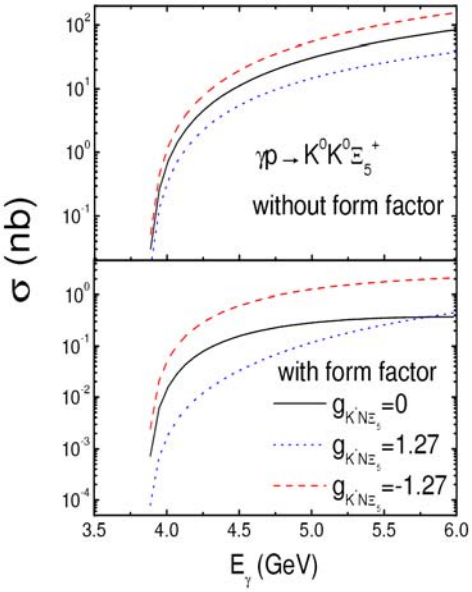

Figure 1. Cross sections for the production of positive parity Ξ_5^+ from photon-proton reactions as functions of center-of-mass energy for different values of the coupling constant $g_{K^*N\Xi}$.

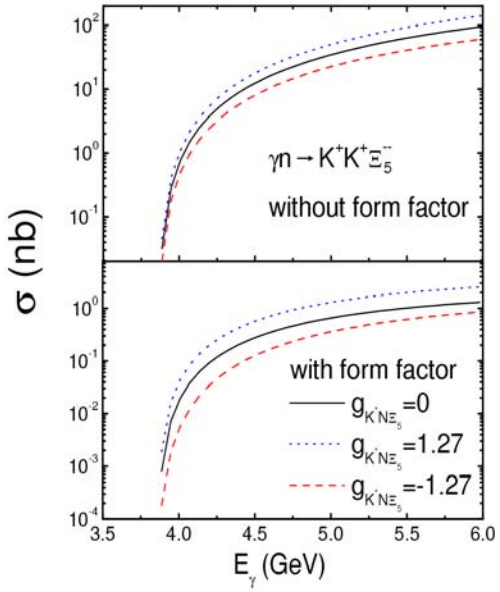

Figure 2. Same as Fig. 1 for the production of positive parity Ξ_5^- from photon-neutron reactions as functions of center-of-mass energy.

[1] W. Liu and C.M. Ko, Phys. Rev. C **69**, 045204 (2004).

[2] W. Liu and C.M. Ko, Nucl. Phys. A. (in press); nucl-th/0309023.

Pentaquark Baryon Production in Photon-Nucleon Reactions

W. Liu and C. M. Ko

Using interaction Lagrangians that involve couplings of pentaquark baryon Θ^+ to both KN and K*N, we have studied its production in the reaction $\gamma p \to \pi^+ K^- \Theta^+$. For the coupling constant $g_{KN\Theta}=3$, corresponding to a width of 9 MeV for a positive parity Θ^+, the cross section has been evaluated using covariant form factors with empirical cutoff parameters and for different values of $g_{K^*N\Theta}$. As shown in Fig.1, the cross section with $g_{K^*N\Theta}=0$, involving only the t-channel kaon-exchange diagram, has values between those with positive or negative nonzero $g_{K^*N\Theta}$, involving both s-channel nucleon and u-channel Θ pole diagrams. Depending on the value of $g_{K^*N\Theta}$, the cross section has a peaked value of 50-110 nb at photon energy around 3.2 GeV. The cross section is reduced by an order of magnitude if Θ^+ has a negative parity as the $KN\Theta$ coupling becomes smaller, i.e., $g_{KN\Theta}=0.42$, and if we assume that the ratio $g_{K^*N\Theta}/ g_{KN\Theta}$ remains the same as in the case of positive parity Θ^+. We have also evaluated the differential cross section of produced Θ^+. For both positive and negative parity Θ^+, it peaks at small four momentum transfer or forward angles.

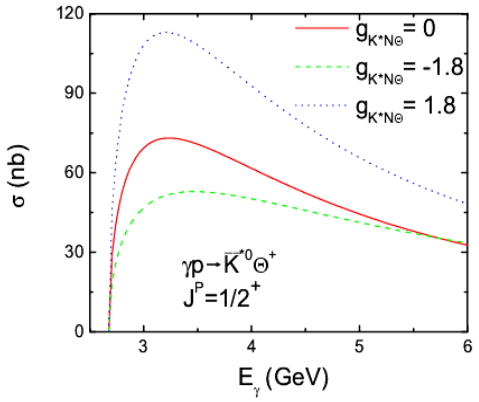

Figure 1. Cross section for the production of positive parity Θ^+ from photon-proton reactions as functions of center-of-mass energy for different values of the coupling constant $g_{K^*N\Theta}$.

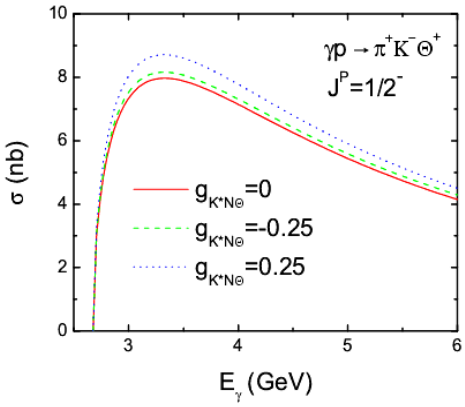

Figure 2. Same as Fig. 1 for the production of negative parity Θ^+.

[1] W. Liu, C.M. Ko, and V. Kubarovsky, Phys. Rev. C **69**, 025202 (2004).

Effect of Resonance Decays on Hadron Elliptic Flows

V. Greco and C. M. Ko

The elliptic flow of pions at RHIC deviates from the quark number scaling observed for other identified hadrons [1], i.e., the dependence of their elliptic flows on their transverse momentum becomes similar if both are divided by the number of constituent quarks in hadrons. This can be understood by the effect of resonance decays and finite quark momentum spread in hadrons [2]. As shown in Fig.1, the elliptic flow of pions from the decays of most resonances, except the rho meson, can be quite different from that of pions produced directly from quark coalescence (upper panel) , while those of K and protons are not affected much by decays of K* and delta (middle panel). However, the resonance decay effect can only account for about half of the observed pion elliptic flow (lower panel). Taking into account also the effect of quark momentum distribution in hadrons [3], which allows quarks with different momenta to coalescence into hadrons, leads to a good flows of both pions and own in Fig. 2.

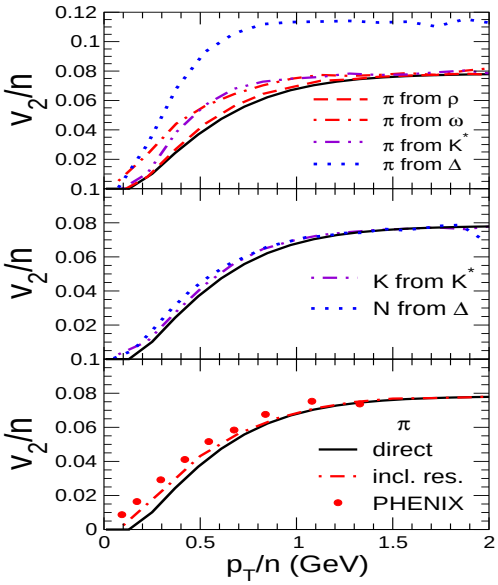

Figure 1. Scaled hadron elliptic flows as functions of scaled momentum from the decay of resonances: pions (upper panel); kaons and protons (middle panel); pions including all resonance decays and from experimental data (lower panel). The solid line in all panels is a fit to the experimental elliptic flows of hadrons other than pions.

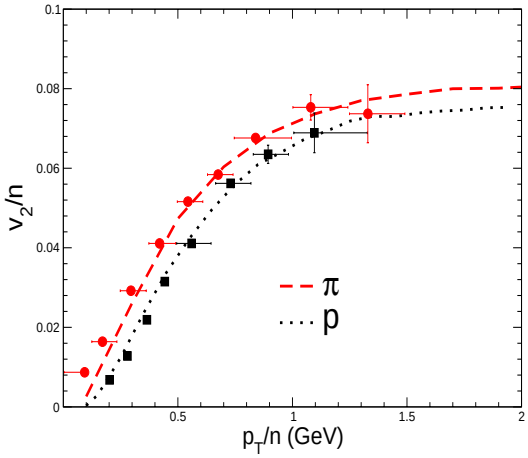

Figure 2. Scaled pion and proton elliptic flows in the coalescence model that includes effects due to both resonance decays and the quark momentum distribution in hadrons. Data are shown by circles for pions and squares for protons [1].

[1] S.S. Adler *et al.*, (PHENIX Collaboration), Phys. Rev. Lett. **91**, 182301 (2003).

[2] V. Greco, and C.M. Ko, nucl-th/0402020.

[3] V. Greco, C.M. Ko, and P. Levai, Phys. Rev. C **68**, 034904 (2003).

Quark Coalescence for Charmed Mesons in Ultrarelativistic Heavy-Ion Collisions

V. Greco, C. M. Ko, and R. Rapp

Within a coalescence approach, which has been successfully applied in the light-quark sector [1], we have studied charm meson production at RHIC. Two limiting scenarios for the charm quark momentum distributions are considered: (i) pQCD spectra from PYTHIA, representing no rescattering, and (ii) complete thermalization including radial and elliptic expansion. We find that both pQCD-based (circles) and thermal charm quark spectra with flow (triangles) are approximately exponential with inverse slopes of 720 MeV and 350 MeV, respectively, as shown in Fig.1 by solid lines. The total number of charmonium obtained by employing the charm quark spectrum from pQCD is smaller than that from the thermal model by about a factor of 3 due to its much flatter spectrum. In Fig. 2, the charm meson elliptic flows are shown for two limiting cases: (i) the charm quark elliptic flow is zero (D w/o), and (ii) the charm quark has the same elliptic flow as that of light quarks (D w). The single electrons from charmed meson decays are found to essentially preserve the elliptic flow of their parent particles, which makes it a highly interesting observable.

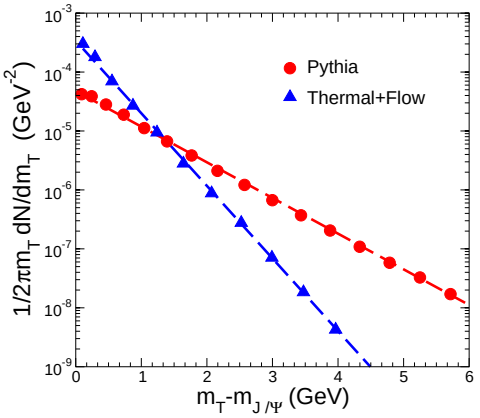

Figure 1. Transverse mass distribution of charmed mesons in central Au+Au collisions at $\sqrt{s_{NN}}$ =200 AGeV from charm-quark coalescence: circles are results with PYTHIA distribution, while triangles with thermal spectrum.

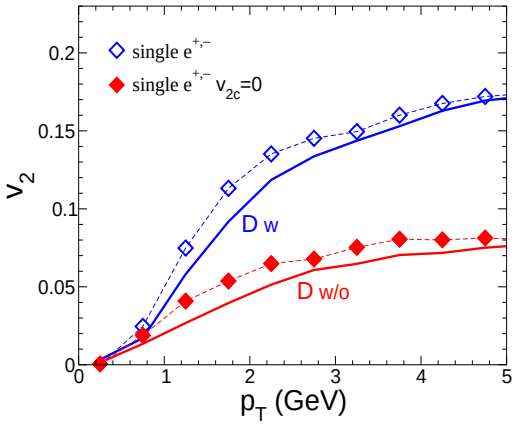

Figure 2. Elliptic flow of charmed mesons (solid lines) and decay electrons (diamonds) in minimum bias Au+Au collisions at $\sqrt{s_{NN}}$ =200 AGeV, using charm quark spectra from pQCD and based on thermal distribution with flow.

[1] V. Greco, C.M. Ko, and P. Levai, Phys. Rev. C **68**, 034904 (2003).
[2] V. Greco, C.M. Ko, and R. Rapp, nucl-th/0312100.

Effects of Momentum-Dependent Nuclear Potential on Two-Nucleon Correlation Functions and Light Cluster Production in Intermediate Energy Heavy-Ion Collisions

L. W. Chen, C. M. Ko, and B. A. Li[1]

[1]*Department of Chemistry and Physics, Arkansas State University, State University, AR 72467*

Using an isospin- and momentum-dependent transport model, we have studied the effects due to the momentum dependence of isoscalar nuclear potential as well as that of symmetry potential on two-nucleon correlation functions and light cluster production in intermediate energy heavy-ion collisions induced by neutron-rich nuclei [1]. For light cluster production, a nucleon coalescence model has been used. Based on the potentials shown in Fig. 1, our results show that both observables are affected significantly by the momentum dependence of nuclear potential, leading to a reduction of their sensitivity to the stiffness of nuclear symmetry energy. However, the t/^{3}He ratio shown in Fig. 2 remains to depend on the stiffness of nuclear symmetry energy even with the inclusion of its momentum dependence. Study of these observables in intermediate energy heavy-ion collisions thus offers the possibility to probe both the momentum dependence of nuclear symmetry potential and the density dependence of nuclear symmetry energy.

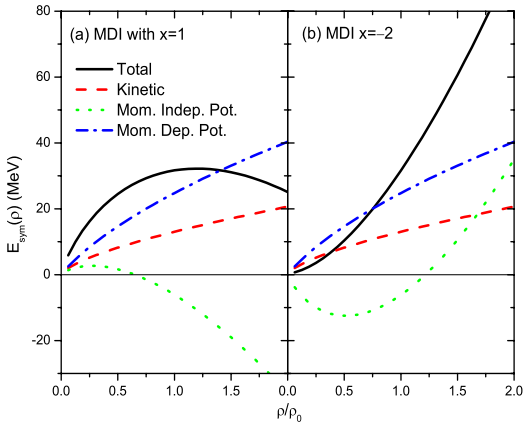

Figure 1. Density dependence of nuclear symmetry energy and contributions from the kinetic energy as well as the momentum-independent and momentum-dependent potential energies in the Gogny effective interaction (MDI) with (a) x=1 and (b) x=-2.

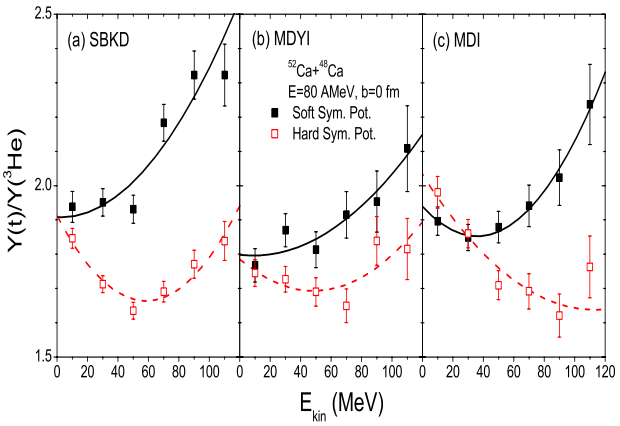

Figure 2. The t/^{3}He ratio as a function of cluster kinetic energy in the center-of-mass system for different interactions (a) SBKD, (b) MDYI, and (c) MDI with the soft (solid squares) and stiff (open squares) symmetry energies. Lines are drawn to guide the eyes.

[1] L.W. Chen, C.M. Ko, and B. A. Li, , Phys. Rev. C **69**, 054606 (2004).

Partonic Effects on Higher-Order Anisotropic Flows in Relativistic Heavy-Ion Collisions

L. W. Chen, C. M. Ko, and Z. W. Lin[1]
[1]*Physics Department, Ohio State University, Columbus, OH 43120*

Using a multiphase transport (AMPT) model that was previously used successfully for describing the elliptic flow v_2 of identified hadrons in heavy-ion collisions at the Relativistic Heavy Ion Collider, we have studied paronic effects on higher-order anisotropic flows v_4 and v_6 of charged hadrons [1]. We find that the same parton scattering cross section of about 10 mb used in explaining the measured v_2 of charged hadrons can also reproduce recent data on their v_4 and v_6 from Au + Au collisions at $\sqrt{s}$=200 AGeV as shown in Fig. 1 [2]. It is further found that v_4 is a more sensitive probe of the initial partonic dynamics in these collisions than v_2. Moreover, higher-order parton anisotropic flows are non-negligible and satisfy the scaling relation $v_{n,q}(p_T) = v_{2,q}^{n/2}(p_T)$, which leads naturally to the observed similar scaling relation among hadron anisotropic flows when the coalescence model is used to describe hadron production from the partonic matter.

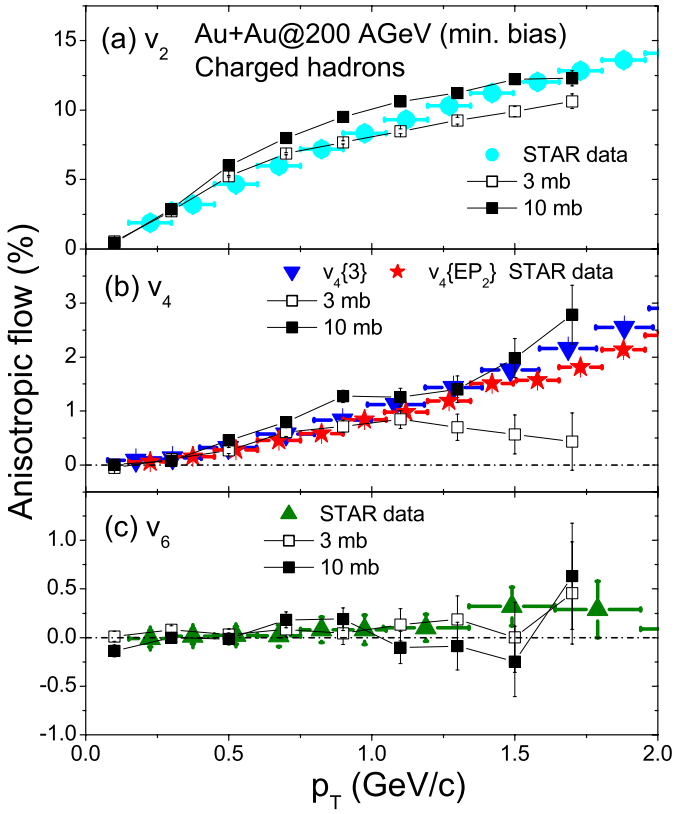

Figure 1. Anisotropic flows v_2 (a), v_4 (b), and v_6 (c) of charged hadrons in the pseudorapidity range $|\eta|<1.2$ from minimum bias Au + Au collisions at s=200 AGeV as functions of transverse momentum p_T for parton scattering cross sections σ_p=3 (open squares) and 10 (solid squares) mb. The experimental data are from STAR Collaboration [2].

[1] L.W. Chen, C.M. Ko, and Z. W. Lin, Phys. Rev. C **69**, 031901(R) (2004).
[2] J. Adams *et al.*, (STAR Collaboration), Phys. Rev. Lett. **92**, 062301 (2004).

Pentaquark Baryon Production at the Relativistic Heavy Ion Collider

L. W. Chen, V. Greco, C. M. Ko, S. H. Lee,[1] and W. Liu
[1]*Department of Physics, Yonsie University, Seoul 120-749, Korea*

Baryons consisting of five quarks ($uudd\bar{s}$) have recently been observed in various reactions. The extracted mass is around 1.54 GeV with a width in the range 9-25 MeV, mainly due to experimental resolutions. The observed properties of this pentaquark baryon are consistent with those of the Θ^+ baryon with spin J=1/2, isospin I=0, and strangeness S=+1predicted by the chiral soliton model [1]. To study its production probability at the Relativistic Heavy Ion Collider (RHIC), we have used a kinetic model [2]. Assuming that a quark-gluon plasma is produced in the collision, we first determine the number of Θ^+ produced from the quark-gluon plasma using a quark coalescence model, and then take into consideration its production and absorption in subsequent hadronic matter via the reactions $KN \leftrightarrow \Theta$, $KN \leftrightarrow \pi\Theta$, and $\pi N \leftrightarrow \bar{K}\Theta$. As shown in Fig. 1, we find that although the final Θ^+ number is affected by hadronic interactions, it remains sensitive to the initial number of Θ^+ produced from the quark-gluon plasma, particularly in the case of a small Θ^+ width as imposed by the KN and Kd scattering data. Because of the small baryon chemical potential in the hot dense matter produced in heavy ion collisions at RHIC, the number of anti-Θ produced is expected to be only slightly smaller than that of Θ^+.

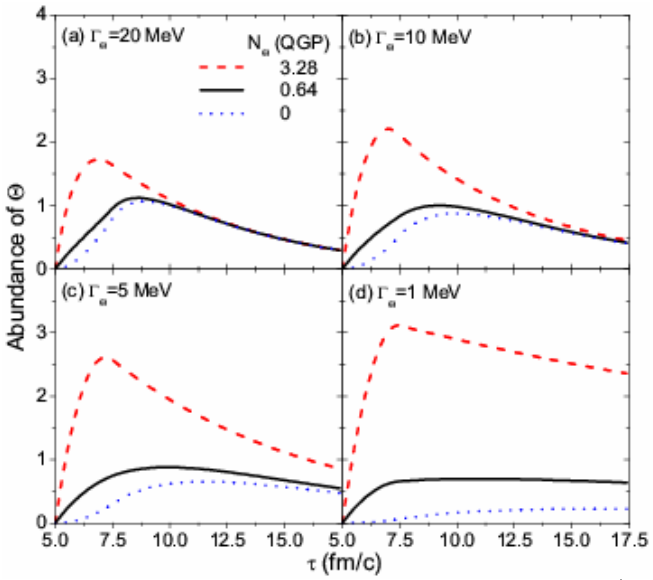

Figure 1. Time evolution of Θ^+ abundance in Au+Au collisions at $\sqrt{s}$= 200 GeV for different initial numbers of Θ^+ produced from the quark gluon plasma as well as different Θ^+ width.

[1] D. Diakonov, V. Petrov, and M. Polyakov, Z. Phys. A **359**, 305 (1997).
[2] L.W. Chen, V. Greco, C.M. Ko, S.H. Lee, W. Liu, nucl-th/0308006.

Subthreshold Cascade Production in Heavy-Ion Collisions at SIS Energies

L. W. Chen, C. M. Ko, and Y. Tzeng[1]
[1]*Institute of Phyiscs, Academia Sinica, Taipei 11529, Taiwan, ROC*

Using a relativistic transport model, we have studied the production of doubly strange Ξ baryon in heavy-ion collisions at SIS energies, which are below the threshold of about 3.7 GeV for its production from nucleon-nucleon collisions in free space [1]. Because of the small production probability, Ξ is treated perturbatively via the strangeness-exchange reactions $\bar{K}\Lambda\rightarrow\pi\Xi$ and $\bar{K}\Sigma\rightarrow\pi\Xi$. Taking their cross sections from the prediction of a coupled-channel approach based on a flavor SU(3)-invariant hadronic Lagrangian [2], we find that the Ξ yield is about 10^{-4} in central collisions of ^{58}Ni + ^{58}Ni at E/A=1.93 GeV as shown in Fig. 1. The Ξ yield is further found to be more sensitive to the magnitude of the cross sections for strangeness-exchange reactions than to the medium effects due to modified kaon properties, thus offering the possibility of testing the predicted cross sections from the hadronic model. We have also made predictions for Ξ production in Au+Au collisions at energies from 1 to 2 GeV/nucleon.

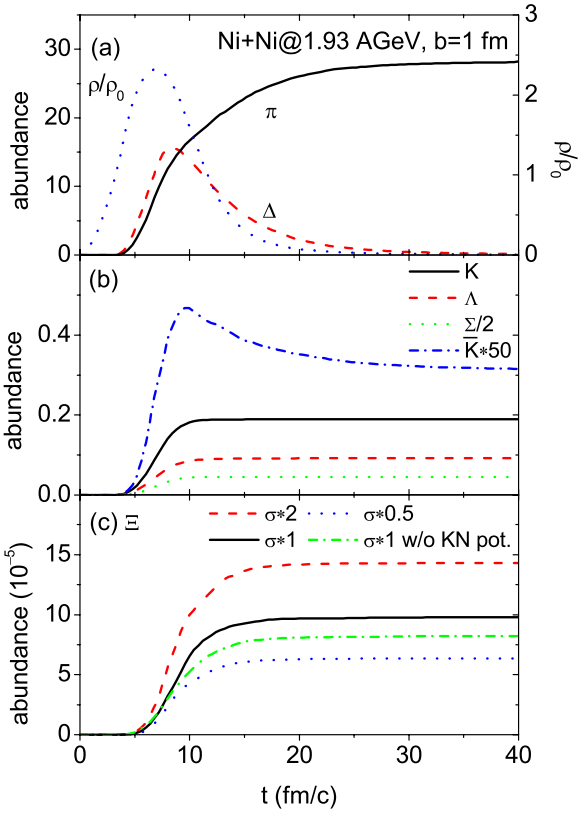

Figure 1. Time evolutions of (a) central baryon density (right scales) and abundance (left scales) of π and Δ; (b) abundance of *K*, Λ,Σ and $\bar{K}$; and (c) the Ξ abundance in cases with and without kaon medium effects and different cross sections in collisions of ^{58}Ni + ^{58}Ni at E/A=1.93 GeV at b=1 fm.

[1] L.W. Chen, C.M. Ko, and Y. Tzeng, Phys. Lett. B **584**, 269 (2004).
[2] C.H. Li, and C.M. Ko, Nucl. Phys. **A712**, 110 (2002).

Photon Emission from Dense Quark Matter

C. Vogt,[1] R. Rapp, and R. Ouyed[1,2]

[1] *NORDITA, Blegdamsvej 17, 2100 Copenhagen, Denmark*

[2] *Department of Physics and Astronomy, University of Calgary, Alberta, T2N 1N4 Canada*

At high baryon density and small temperature the ground state of QCD is believed to be color-superconducting quark matter (CSC) with ***qq***-paring gaps as large as ~100MeV [1]. In nature, such form of matter could exist in the interior of compact stellar objects (neutron stars). To detect signatures of CSC, it is thus essential to asses its electroweak (photon and neutrino) emissivities. In the present project [2], we have computed thermal emission rates and mean free paths of photons in the so-called color-flavor locked (CFL) phase [3] of superconducting quark matter at high densities and moderate temperatures. Since chiral symmetry is spontaneously broken in the CFL phase, our calculations are based on a low-energy effective theory involving Goldstone boson excitations and their electromagnetic as well as strong interactions. In-medium coupling strengths of vector mesons turn out to be smaller than in vacuum. In-medium modified pion dispersion relations have been found to induce novel processes such as $\boldsymbol{\pi^+ \pi^- \rightarrow \gamma}$ and $\boldsymbol{\gamma \rightarrow \pi^+ \pi^-}$. The photon production rates (Fig. 1) and total emissivities (Fig. 2) exceed the contributions from thermal $\mathbf{e^+e^-}$ annihilation above temperatures of ~5MeV. At the same time, the

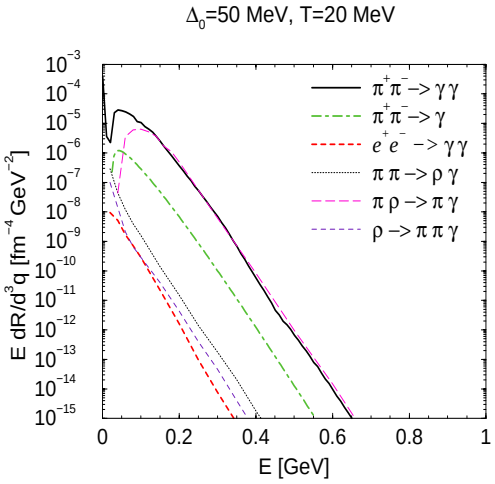

Figure 1. Photon production rates for various processes in CFL matter at a temperature of 20 MeV and a zero-temperature gap of 50 MeV.

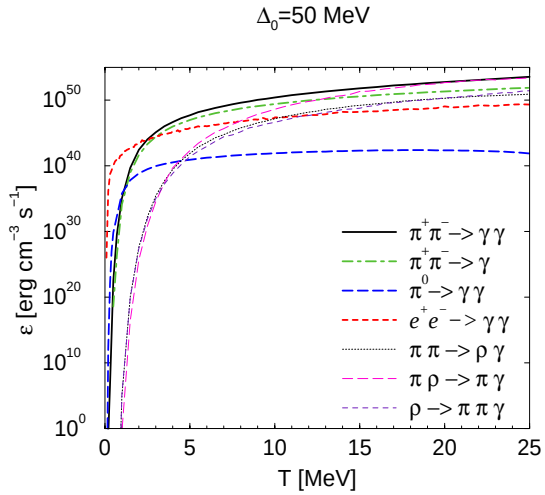

Figure 2. Integrated photon emission rates (=emissivities) for various processes in CFL quark matter as a function of temperature.

corresponding mean free paths become very small. Our results imply that the photon flux from the surface of a (hypothetical) CFL star in its early hot stages saturates the black-body limit.

[1] R. Rapp, T. Schaefer, E.V. Shuryak and M. Velkovsky, Phys. Rev. Lett. **81**, 53 (1998).

[2] C. Vogt, R. Rapp, and R. Ouyed, Nucl. Phys. **A735**, 543 (2004).

[3] M.G. Alford, K. Rajagopal, and F. Wilczek, Nucl. Phys. **B537**, 443 (1999).

In-Medium Effects on Charmonium Production in Heavy-Ion Collisions

L. Grandchamp,[1] R. Rapp, and G. E. Brown[2]
[1] *Lawrence Berkeley National Laboratory, Berkeley, CA 94720*
[2] *Department of Physics, State University of New York, Stony Brook, NY 11794-3800*

Heavy-quark bound states (charmonium and bottomonium) constitute valuable probes of the hot and dense matter created in high-energy collisions of heavy nuclei. A suppressed production of **J/Ψ**'s (relative to expectations from p-p collisions) has been suggested as a signature of the creation of a (deconfined) Quark-Gluon Plasma (QGP). However, it has been realized recently that QGP formation also facilitates the regeneration of charmonium states through recombination of charm and anticharm quarks, provided the latter are produced abundantly.

We have continued our analysis of the competition between charmonium dissociation and regeneration [1] by employing a kinetic theory framework [2] incorporating in-medium properties of open- and hidden-charm states in line with recent QCD lattice calculations. First, a continuously decreasing open-charm threshold across the phase boundary of hadronic and quark-gluon matter is found to (i) decrease (increase) the equilibrium abundance of charmonium states in the hadronic (QGP) phase, and (b) accelerate **Ψ'** dissociation in hadronic matter which turns out to be essential to explain the observed **Ψ'/Ψ** ratio at SPS energies, cf. Fig.1. Second, the survival of **J/Ψ** resonance states above the critical temperature enables their recreation also in the QGP, which is responsible for a substantial regeneration of their yield in central Au-Au collisions at RHIC energy, cf. Fig.2. Future evaluation of charmonium p_t-spectra, as well as bottomonium production systematics, will allow to scrutinize the proposed approach.

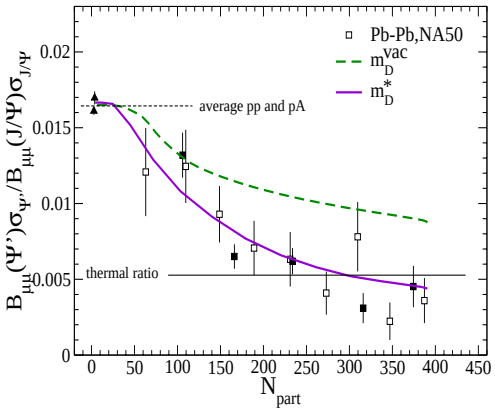

Figure 1. Centrality dependence of the **Ψ'/Ψ** ratio in √s=17.3GeV Pb-Pb collisions, with and without (full and dashed line) in-medium modified D-meson masses.

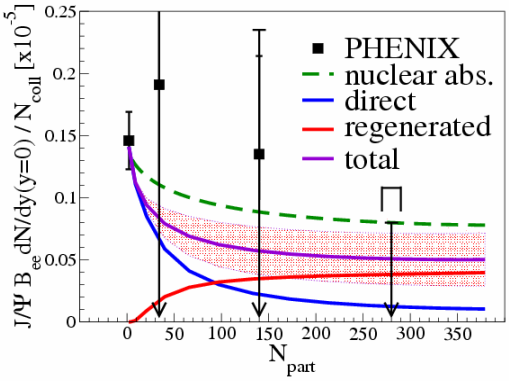

Figure 2. Centrality dependence of the **J/Ψ** yield in √s=200GeV Au-Au collisions, normalized to the number of primordial **N-N** collisions.

[1] L. Grandchamp and R. Rapp, Phys Lett. **523**, 60 (2001).
[2] L. Grandchamp, R. Rapp, and G.E Brown, arXiv:hep-ph/0306077, Phys. Rev. Lett. (in press).

Photoproduction of Rho-Mesons Off Nucleons and Nuclei

T. -S. H. Lee,[1] Y. Oh,[2] and R. Rapp
[1] *Physics Division, Argonne National Laboratory, Argonne, IL 60439*
[2]*Department. of Physics and Astronomy, University of Georgia, Athens, GA 30602*

Among the major objectives of electron-nucleon scattering experiments at Jefferson Laboratory is the investigation of nucleon resonance properties, in particular the changeover from hadronic to partonic degrees of freedom (dof) as a function of momentum transfer. Recently, an additional component has been implemented into this program by using nuclear targets, opening the possibility to simultaneously assess the impact of in-medium modifications of baryon and meson resonances (in particular vector mesons). This may be put into context with the RHIC program, where the transition from hadronic to partonic dof is studied in high-temperature matter. In the present project we attempt to establish closer connections between these two areas of nuclear research by evaluating in-medium effects in photo-induced **ρ** production off nuclei.

Our starting point is the meson-exchange model for the **γN→ρN** process developed in [1] for fixed mass **ρ**-mesons, based on *t*-channel exchanges of **π**, **η**, **σ**, f_2 and Pomeron. In a first step, we implement a free **ρ** spectral function as inferred from **ππ** scattering phase shifts, resulting in **ππ** mass distributions for production off the nucleon as shown by the dashed lines in Fig.1. The full lines are calculated using a medium-modified **ρ**-propagator (as employed before in the context of thermal dilepton production in ultrarelativistic heavy-ion collisions [2]) coupled with the free final-state decay into a **ππ** pair. The elementary production process has been averaged over nuclear Fermi motion assuming a uniform profile at half saturation density. We find a substantial suppression of the 2-pion yield per nucleon, caused by a strong broadening of the in-medium **ρ** spectral function, and a moderate peak shift towards lower invariant masses. The effects of pion absorption, as well as more realistic nuclear wave functions, remain to be accounted for.

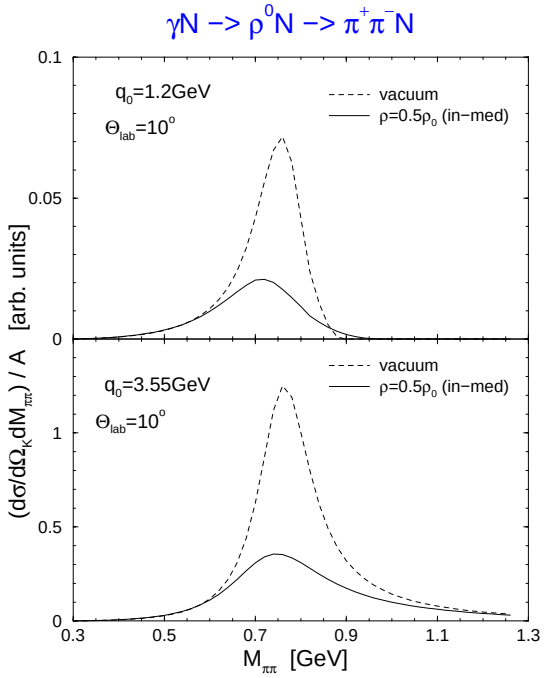

Figure 1. Differential cross section per nucleon for photo-produced **ππ** pairs via intermediate **ρ**-mesons using either the free (dashed lines) or in-medium (full line) **ρ** - propagator.

[1] Y. Oh and T.-S. H. Lee, Phys. Rev. C **69**, 025201 (2004).
[2] R. Rapp and J. Wambach, Adv. Nucl. Phys. **25**, 1 (2000).

In-Medium Modifications of the Nucleon and Δ(1232) at RHIC

H. van Hees and R. Rapp

One of the main goals of heavy-ion collision experiments is the investigation of the phase structure of strong-interaction matter. At sufficiently high temperature and/or density, QCD predicts the occurrence of a (pseudo-) phase transition from hadronic matter into a Quark-Gluon Plasma, associated with the restoration of the spontaneously broken chiral symmetry, and quarks and gluons as the relevant microscopic degrees of freedom. The approach towards chiral restoration should manifest itself in the modifications of hadron properties which one hopes to detect phenomenologically within the hot and dense fireball created in relativistic heavy-ion collisions (see e.g. Ref. [1] for a review of the intense theoretical efforts in recent years).

As a further step towards a more complete understanding of hadron properties in hot and dense matter, we employ a hadronic model, describing interacting pions, nucleons, and baryon resonances, to evaluate the modifications of the nucleon and **Δ**(1232)-resonance in a hot and dense hadronic medium. The interactions between nucleons, pions, and delta resonances are treated with a p-wave coupling including a monopole form factor with a 3-momentum cutoff of 290MeV, fitted to elastic pion-nucleon scattering phase shifts in the **Δ**(1232) channel [2]. For direct delta scattering off thermal pions, we calculated a selfenergy contribution, including the baryon resonances **N**(1440), **N**(1520) and **Δ**(1600), with coupling constants determined from the pertinent partial decay widths. **ππ** interactions are modeled as the temperature part of a sunset diagram in a $\boldsymbol{\varphi}^4$-model. **πN** interactions are consistently treated within the same **πNΔ** Lagrangian as above; in addition, short-range correlations (employing standard Migdal parameters) and vertex corrections in the **Δ**-selfenergy loop (suppressing an unphysical threshold enhancement due to the in-medium pion dispersion relation) are incorporated. The resulting model has been checked to agree with photo-absorption data on nuclei.

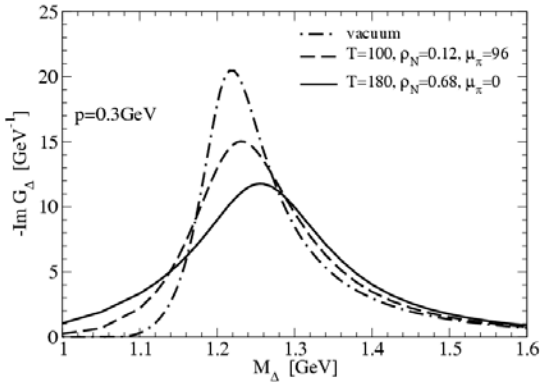

Figure 1. The Delta-spectral function at finite temperature and density in comparison to the vacuum.

Fig. 1 displays the **Δ**-spectral functions under conditions expected at the Relativistic Heavy-Ion Collider (RHIC). With increasing temperature and density, the peak position of the spectral function shifts to higher masses and the width increases as compared to the vacuum. The broadening is mainly caused by a Bose enhancement of the pion in the decay of the delta, as well as resonant **Δ–π** interactions.

We have also dressed the nucleon with **πN** and **πΔ** loops, requiring a renormalization of the nucleon selfenergy in the vacuum to ensure that the propagator has its pole at the physical nucleon mass with a residue of one. Pertinent in-medium nucleon spectral functions are shown in Fig.2, indicating a substantial broadening and a slight downward shift of its pole mass.

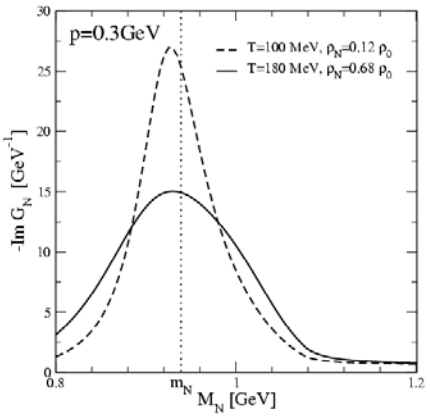

Figure 2. : The nucleon spectral function at RHIC.

The net impact of the in-medium nucleon propagator on the delta resonance consists of a small upward mass shift; for T=100 MeV and a nucleon density of $0.12\boldsymbol{\rho_0}$ ($\boldsymbol{\rho_0}$=0.16fm^{-3}), the calculated upward shift of the delta-peak position is about 11 MeV, and the increase of width amounts to 53 MeV, both of which are in qualitative agreement with preliminary data from the STAR collaboration at RHIC [3].

The next step in evaluating in-medium modifications of the delta resonance will be the inclusion of interactions with both vector and axialvector mesons, with particular emphasis on potential consequences and/or realizations of (partial) chiral symmetry restoration.

[1] R. Rapp, and J. Wambach, Adv. Nucl. Phys. **25**, 1 (2000).
[2] W. Weinhold, B. Friman, and W. Nörenberg, Phys. Lett. B **433**, 236 (1998).
[3] P. Fachini (STAR Collaboration), arXiv:nucl-ex/0403026.

A Relation Between Proton and Neutron Asymptotic Normalization Coefficients for Light Mirror Nuclei and Its Relevance to Nuclear Astrophysics

N. K. Timofeyuk,[1] R. C. Johnson,[1] and A. M. Mukhamedzhanov
[1]*Department of Physics, School of electronics and Physical Sciences, University of Surrey, Guildford, Surrey GU2 7XH, United Kingdom*

The astrophysical S-factor associated with the peripheral proton capture reaction at stellar energies is well known to be related to the Asymptotic Normalization Coefficient (ANC) of the virtual decay. The same ANCs play a crucial role in other peripheral processes such as transfer reactions whose cross sections are significantly higher and therefore more easily measurable than those of the direct capture processes at astrophysically relevant energies. The study of ANCs of astrophysical interest is a new and rapidly developing direction in modern experimental nuclear physics. However, in order to exploit these ideas to determine the ANCs for light proton-rich nuclei of importance to nuclear astrophysics the corresponding transfer reactions often require the use of weak radioactive beams, which generally involves more difficult and less accurate experiments than are possible with stable beams. The higher intensities of stable beams mean that they can be used at energies below the Coulomb barrier where the sensitivity to optical potentials, which is the main uncertainty of ANCs determined from transfer reactions, is minimised. We point out here that the ANC of the virtual neutron decay of the mirror nucleus, which may be susceptible to study with stable beams, is related in a model independent way by the charge symmetry of nuclear forces to the ANC of the corresponding proton decay of the mirror partner. We propose to exploit this new insight to predict peripheral reaction cross sections in stars. Near the edge of stability, where neutron separation energies become very small, the corresponding mirror proton states have positive energies and are observed manifest themselves as resonances. The width of a narrow proton resonance is related to the ANC of the Gamow wave function for this resonance. In this case, a link is obtained between the proton width and the squared ANC of the mirror neutron state. We indicate some examples of astrophysical interest when charge symmetry can help to determine the astrophysical S factors. For example, the direct capture reaction ^{14}N(p,γ)^{15}O(3/2$^+$, 6.79 MeV) controls the energy production in the CNO cycle. The ^{15}O(3/2$^+$, 6.79 MeV) state is separated from the neighboring ^{15}O($5/2^+_2$) state by only 70 keV, which influences the precision of measurements involving this state. The proton ANC of the ^{15}O(3/2$^+$, 6.79 MeV) state can be determined using the neutron ANC of the mirror ^{15}N($3/2^+_1$) state. Also, direct contributions to the cross sections of the ^{22}Mg(p,γ)^{23}Al and ^{26}Si(p,γ)^{27}P reactions, involving proton-rich radioactive nuclei, could be calculated through the mirror neutron ANC's using neutron transfer reactions with stable targets ^{22}Ne and ^{26}Mg

Insight into Continuum Couplings

F. M. Nunes,[1] A. M. Mukhamedzhanov, C. C. Roza,[2] and B. F. Irgaziev[3]
[1]*NSCL and Department of Physics and Astronomy, Michigan State University, East Lansing, MI 48824*
[2]*Faculdade de Ciencias, INESC-Porto, Porto, Portugal*
[3]*Physics Department, National University, Tashkent, 700174, Uzbekistan*

Due to the very weak binding of halo nuclei, breakup channels typically have a preponderant role in the reaction process. In the language introduced by the Continuum Discretization Coupled Channels (CDCC) method, one could say that the ground state (g.s.) of the loosely bound state systems couples strongly to the continuum, which essentially means that the projectile breaks up easily. One of the simplest process one can consider is the electromagnetic excitation $A+\gamma \rightarrow c+p$ (photo-absorption), which in turn is related to the inverse process, the radiative capture $c(p,\gamma)A$. The multipole electric couplings were previously studied in connection to astrophysics, specifically for proton capture reactions. It was found that the nearby pole does not solely determine the behavior of the couplings close to zero energy. It depends also on the interplay of various effects including bound state and scattering state centrifugal barriers, the Coulomb barrier, etc. Breakup reactions epitomize the radical effect that couplings to the continuum may have. Of particular importance was the finding that the continuum-continuum couplings could decrease the cross section by large factors. However, what makes continuum-continuum effects important in the reaction mechanism, what are decisive ingredients? The theoretical predictions taking into account CDCC rely on large-scale calculations where virtually all relevant energies and partial waves of the core + p system are included. The goal of our work is to shed light on the physical reasons determining the importance of the CDCC effect. As a typical case, we have calculated the CDCC couplings for the low energy breakup of ^{8}B on ^{58}Ni. We first analyze the couplings between the ground state and the continuum and find that regardless of the details of the continuum states, there is always a low-energy strength stretching slightly outside the range of the projectile-target interaction. As to the continuum-continuum couplings, they peak typically around the surface and tend to extend out farther, as there no bound state to truncate the integral. For the monopole and quadrupole case with $l_i = l_f$, continuum couplings are stronger amongst similar energy pairs. An offset in energy can be found for the cases where $l_i \neq l_f$, as in the dipole coupling. In all the cases, most of the nonzero contributions come when the initial and final energies are not far apart. For continuum-continuum couplings to have a large impact on the reaction observables with loosely bound systems, our main results suggest the following conditions. 1. The coupling strengths should be comparable to the energy of the beam or to the incident momentum. From this simple condition, one can conclude that the continuum-continuum couplings are important for the low energy experiments and may be neglected for the high-energy ones. 2. We find that the resonance-resonance does not dominate the continuum-continuum couplings, and, on the contrary, the nonresonant continuum dictates the rule of the game.

Completeness of the Coulomb Eigenfunctions of the Two-Body Hamiltonian

A. M. Mukhamedzhanov

The proof of the completeness of the system of the bound and scattering wave functions for the short-range potential has been proved by Newton [1]. The Newton's completeness relationship has been later used by Berggren [2] to extend the completeness relationship by including the resonance states. There is a price for such an extension: 1) the integral over continuum is deformed into the complex plane; 2) the dual basis for the resonance state should be added. The Berggren's extended completeness relationship has been used to take the contribution of the continuum in the shell-model [3].

The importance of the completeness relationship for the shell-model calculations dictates the necessity to prove the completeness relationship for two charged particles also. Although everybody believes that a system of the bound state and continuum wave functions for charged particles is complete, there is no formal proof of it in the literature. Such a proof will be followed by the extension of the Berggren relationship for particles interacting via the Coulomb and nuclear potentials. It will allow one to use the Berggren's relationship for the shell-model calculations of proton-rich nuclei. The purpose of my work is to present the first formal proof of the completeness relationship of the eigenfunctions of the Hamiltonian with the sum of the Coulomb and nuclear potentials. Consider, for simplicity, two particles in the s-wave interacting via the Coulomb potential only. The idea of the proof is in the consideration of the auxiliary integral

$$I(r)=\oint_{\gamma} dk k \int_0^{\infty} dr' h(r') G_k(r,r'),$$

where $G_k(r,r')$ is the Coulomb Green function, $h(r)$ is the square-integrable arbitrary function, γ is the closed contour running along the real k axis from $-\infty$ to ∞ and completed by a large semicircle of radius $R \to \infty$.The Green function is expressed in terms of the regular and singular (Iost) solutions The completeness relationship follows from the consideration of the integral $I(r)$ using the behavior of the Coulomb regular and Iost solutions in the complex plane. The most difficult part is the investigation of the integrand behavior in the vicinity of the point $k = 0$, which is an essential singularity point. The Coulomb Iost solution $f_k^{(c)}(r)$ has the Coulomb cut along the negative imaginary axis in the momentum plane, while the regular solution is analytical function in the entire k-plane. Hence, the Green function is analytical in the upper half of the k plane and the integration contour γ can be closed in the upper half plane. I have proved the completeness condition for the case of $l=0$ and pure Coulomb interaction. The proof should be extended for arbitrary l and the potential given by the sum of nuclear and Coulomb ones.

[1] R. G. Newton, Scattering theory of waves and particles, (McGraw-Hill Book Company, 1966).

[2] T. Berggren, Nucl. Phys. **A109**, 265 (1968).

[3] N. Michel *et al*., Phys. Rev. C **67**, 054311 (2003).

Triple Collisions in Solar Matter

F. Pirlepesov, A. M. Mukhamedzhanov, and A. S. Kadyrov[1]
[1]*Center for Atomic, Molecular and Surface Physics, School of Mathematical and Physical Sciences, Murdoch University, Perth 6150, Australia*

We consider the impact of solar matter on reaction rates under conditions existing in solar core. There are static impact which is also known as a screening and dynamic impact of matter on binary reaction in stellar core. We consider dynamic impact of matter on binary reactions. Our purpose is to investigate the reaction rates of triple collisions where a third particle is a spectator and to compare them with the reaction rates of the corresponding binary processes. In the case of radiative capture, two different triple collisions can occur: nonradiative capture, when the emitted photon is absorbed by a third particle-spectator and radiative capture, when a photon is emitted. In both cases the presence of the third particle changes the relative momentum of two colliding nuclei involved in the binary capture process. A quantum mechanical description of the triple collisions dictates a necessity to know the three-body Coulomb scattering wave function in the initial state. Such a wave function in the asymptotic region where two particles are close to each other and far away from the third particle is now available [1,2]. We use this three-body scattering wave function to estimate the reaction rates of the radiative and nonradiative triple collisions $p+^7Be+p \rightarrow {}^8B+p+\gamma$ and $p+^7Be+p \rightarrow p+^8B$, correspondingly, to estimate the impact of the solar matter on ^8B production rate and compare it with the reaction rate of the notorious $^7Be+p \rightarrow {}^8B+\gamma$. A proton from the solar matter is considered to be a spectator. The presence of the proton-spectator changes the relative momentum of ^7Be and p involved in the capture process. It is a genuine three-body effect and we estimate its impact on the triple collision reaction rates. Nonradiative triple collisions with electron-spectators have been considered in [3]. Note that in our approach the contribution of an electron-spectator is negligible due to the small electron mass. Our calculations show that, due to the Coulomb barrier, effect of the proton -spectator on binary reaction is negligible even in radiative capture case in the stellar core. We also calculated the triple reaction rates at higher temperatures and densities existing in supernovae and on later stages of the big bang even though we know at such conditions existence of ^7Be might not be possible but other reactions are important. But still these calculations give some insight on the conditions when triple collisions might be important. Triple collisions are comparable to binary reactions only at high temperatures because of the Coulomb barrier and high densities of spectator particles.

[1] E. O. Alt and A.M. Mukhamedzhanov, Phys. Rev. A **47**, 2004 (1993).
[2] A.M. Mukhamedzhanov and M. Lieber, Phys. Rev. A **54**, 3078 (1996).
[3] D.E. Monakhov *et al.*, Nucl. Phys. **A635**, 257 (1998).

Theory of Electron-Impact Ionization

A. S. Kadyrov,[1] A. M. Mukhamedzhanov, A. T. Stelbovics,[1] and I. Bray[1]
[1]*Center for Atomic, Molecular and Surface Physics, School of Mathematical and Physical Sciences, Murdoch University, Perth 6150, Australia.*

A new general formulation of the theory of electron-impact ionization is given. The existing formulation suffers from a number of problems. An ambiguous and divergent definition of the ionization problem is one of them. An integral representation for the ionization amplitude, which is free of ambiguity and divergence problems, is derived. In the new formulation, the ionization amplitude is shown to have four alternative forms ideally suited for practical calculations. This formulation is extended to amplitudes of all possible scattering processes taking place in an arbitrary three-body system. The new formulation is also shown to resolve another longstanding formal problem, the extension of the conventional post form of the breakup amplitude valid for short-range potentials to long-range potentials. A well-defined post-form of the breakup amplitude valid for arbitrary potentials including the long-range Coulomb interaction is given.

Furthermore, yet another fundamental problem, the partial-wave expansion of the asymptotic wave functions, where the existing formal theory fails is shown to be solvable. Partial-wave expansion of the asymptotic forms of the total scattering wave function, developed both from the initial and final state, necessary for calculation electron-impact ionization of hydrogen is given. An integral representation is then extended to partial ionization amplitudes. A proof on an important assumption about the relationship between the magnitudes of the ionization amplitude and a trial integral, which calculations of the cross sections for the full electron-hydrogen ionization problem are presently based on, is given. Utility of the present formulation of the formal theory of electron-impact ionization is demonstrated on some well-known model problems. On the whole, the new formulation of the theory of electron-impact ionization given in this work, resolves all formal problems known so far and displays a remarkable self-consistency.

Theory of the Trojan Horse

A.M. Mukhamedzhanov, L. D. Blokhintsev,[1] S. Cherubini,[2] M.G. Pellegriti,[3] C. Spitaleri,[3] and A. Tumino[3]

[1]*Nuclear Physics Insitute, Moscow State University, Moscow, Russia*

[2]*Ruhr-Universität Bochum, Bochum, Germany*

[3]*Laboratori Nazionale del Sud-INFN, Catania, Italy*

Nuclear astrophysical processes due to the presence of the Coulomb barrier have so small cross sections that it is very difficult or often impossible to measure in the lab conditions nuclear cross sections at stellar energies. That is why different indirect techniques are used to extract astrophysical information. There are three widely used indirect techniques: asymptotic normalization coefficient, Coulomb breakup reactions and Trojan Horse. The Trojan Horse method provides astrophysical information about nuclear reactions at stellar energies. In our work we consider the theory of the Trojan Horse. As any indirect technique, the Trojan Horse method has advantages and disadvantages. This method allows one to measure the astrophysical cross sections down to a few keV, however, the extracted astrophysical factor corresponds to a process where one of the entry particles is off-energy-shell. The question is how important are off-shell effects at astrophysically relevant energies. In standard calculations the off-shell effects are neglected. The purpose of this work is to provide an insight into the theory of the Trojan Horse, and specifically to develop a method allowing us to estimate the off-shell effects. Let us consider the breakup reaction $a + A \to b + c + C$, where $a = b + x$, and the subreaction of interest is $x + A \to b + B$. The reaction amplitude is given by

$$M = < \chi^{(-)}_{bB} \chi^{(-)}_{cC} \varphi_b \varphi_c \varphi_C \mid V_{bB} - U_{bB} + (V_{bB} - U_{bB}) G (V_{aA} - U_{aA}) \mid \varphi_a \varphi_A \chi^{(+)}_{aA} > \quad (1)$$

This is the post-form of the exact amplitude. Here, G is the total Green function, $\chi^{(\pm)}_{(ij)}$ is the distorted wave describing the relative motion of particles i and j, φ_i is the bound-state wave function of nucleus i, $V_{ij}(U_{ij})$ is the interaction potential (optical potential) between particles i and j. From this equation we need to single out the amplitude of the subreaction $x + A \to c + C$. The on-shell subreaction amplitude is given by

$$M_0 = < \chi^{(-)}_{cC} \varphi_c \varphi_C \mid V_{cC} - U_{cC} + (V_{cC} - U_{cC}) G_{xA} (V_{xA} - U_{xA}) \mid \varphi_x \varphi_A \chi^{(+)}_{xA} > \quad (2)$$

An important point is the presence of the scattering wave function $\chi^{(+)}_{xA}$ in the on-shell amplitude. This wave function is absent in Eq. (1) due to the off-shellity of the transferred particle x. We singled out the half-off-shell subreaction amplitude from (1) and compare it with the on-shell Eq. (2). The impact of the off-shell effects is estimated differently for resonance and direct $x + A \to c + C$ reactions. On the first stage we develop a model to estimate the off-shell effects for the direct subreaction assuming that it is described by the particle t transfer, where $A = C + t$ and $c = x + t$.

Off-Shell Effects in the ^{2}H(p,pp)n Reaction

A. M. Mukhamedzhanov, L. D. Blokhintsev,[1] C. Spitaleri,[2] M. G. Pellegriti,[2] P. Figuera,[2] A. Musumarra,[2] C. Cherubini,[3] A. Di Pietro,[2] A. Del Zoppo,[2] L. Pappalardo,[2] R.G. Pizzone,[2] S. Romano,[2] S. Tudisco,[2] A. Tumino,[2] Đ. Miljanić,[4] S. Blagus,[4] M. Milin,[4] M. Bogovać,[4] and D. Rendić[4]

[1]*Nuclear Physics Institute, Moscow State University, Moscow, Russia*

[2]*Laboratori Nazionale del Sud-INFN, Catania, Italy*

[3]*Ruhr-Universität Bochum, Bochum, Germany*

[4]*Institut-Rudjer Bošković, Zagreb, Croatia*

The present report investigates on the half-off-energy shell effects on the shape of ^{2}H(p,pp)n cross section. This reaction has been studied in the framework of the Trojan Horse method that is an indirect method for nuclear astrophysics, based on a three-body reaction quasi-free mechanism. It allows cross section measurements at energy far below the Coulomb barrier [1-4] because the provided two-body cross section is free from Coulomb suppression. This method has been applied to the quasi-free p-p scattering, the simplest case where the Coulomb suppression effects can be measured. The free p-p cross section is well-known, its energy trend has been observed to be very similar to that of n-n or p-n systems ($\approx$1/v) except for low proton energies where it shows a deep minimum (E_{lab}= 382.43 keV, θ_{cm}= 90°) due to the interference between the nuclear and the Coulomb scattering amplitudes [5]. The ^{2}H(p,pp)n reaction was studied by choosing angular position of detectors and beam energy in such a way that the investigated proton-proton relative energy is in the region sensitive to the interference. In particular it was studied at Laboratori Nazionali del Sud (LNS), INFN, Catania [6] and at Ruđer Bošcović Institute, Zagreb by using a proton beam energy of 6 MeV on a deuterated poliyethylen film. For the LNS set-up, proton-proton coincidences were measured by two Position Sensitive Detectors (PSD) placed at two different angular configurations with respect to the beam direction. The first configuration was: $16.2°<\theta_1<24°$ and $15.6°<\theta_2<23.4°$ and the final proton-proton relative energy, E_{12}, ranging from 0.3 to 0.8 MeV. The second one was: $26.2°<\theta_1<34°$ and $15.6°<\theta_2<23.4°$ and E_{12} ranging from 0.5 to 1 MeV. In the Zagreb set-up, detectors were placed at $8.7°<\theta_1<22.5°$ and $11.1°<\theta_2<24.6°$ and the investigated proton-proton relative energy, E_{12} ranged from 0.2 to 0.7 MeV. The absolute cross section was also measured by normalization to the p-d elastic scattering. The quasi-free mechanism for the ^{2}H(p,pp)n reaction was already studied in [7] at a beam energy ranging from 4.5 to 13 MeV and the Plane Wave Impulse Approximation (PWIA) was used to reproduce the data. In [7], if the off-energy shell effects were neglected and the 3-body cross section was written, in PWIA, as a product of the kinematical factor, the square modulus of the Fourier transform of the deuteron internal wave function and the free two-body cross section [7]. These calculations reproduced data by using a factor 0.2. In this case the relative energy is almost constant and the p-p cross section does not modify the shape of the total cross section. In order to analyse half-off energy shell effects, the free p-p cross section has been replaced by the p-p half-off-shell cross section and the propagator of the virtual proton $\sigma = E_p - p_p^2/2m_p$ (E_p is the energy of the transferred proton and p_p is its momentum) has been also included. The cross section is expressed in terms of the coherent sum of the total half-off-shell Coulomb and Coulomb modified

nuclear s-wave amplitude. Note that the half-off-shell Coulomb scattering amplitude is significantly suppressed compared to the on-shell. The calculations have been compared with the experimental data and the agreement is quite good. In the case of the Zagreb set-up, where the absolute cross section also has been measured, data are a factor of two larger than the calculation, what is expected to be. Note that our purpose is to reproduce the energy behavior of the cross section and not its absolute value.

[1] G. Baur, Phys. Lett. B **178**, 35 (1986).
[2] S. Cherubini, Ap.J. **457**, 855 (1996).
[3] C. Spitaleri, Phys. Rev. C **60**, 055802 (1999).
[4] C. Spitaleri, Phys. Rev. C **63**, 055801 (2001).
[5] J.E. Brolley, Phys. Rev. **135**, B1119 (1964).
[6] M.G. Pellegriti , Proceeding of Fusion 03, Matsushima, Japan
[7] V. Valković, Nucl. Phys. **A166**, 547 (1971)

Superallowed Fermi Beta Decay: New Calculations of the Statistical Rate Function

I. S. Towner[1] and J. C. Hardy

[1] *Queen's University, Kingston, Ontario, Canada and Cyclotron Institute, Texas A&M University, College Station, Texas*

Last year, we reported [1] on a new computer code we have written to evaluate the statistical rate function, *f*, based on the formalism given in the book by Behrens and Bűring [2]. Although nuclear structure only plays a small role in *f*, it does enter through the relativistic and induced-current matrix elements and, at that time, we had not yet linked the *f*-value code with a shell-model code so that spectroscopic amplitudes produced in the latter could be used in the former. We have now completed this link and have produced a set of *f*-values for the superallowed $0^+ \rightarrow 0^+$ transitions using exactly the same shell-model calculations we used recently [3] to compute the nuclear-structure dependent part of the radiative corrections for the same cases. As it turns out, the effect of our using improved wave functions in *f* is negligible for all but the heaviest cases considered, and even for 74Rb, the heaviest, the difference was only 0.05%. Nevertheless, the set of *ft*-values that we produce from our critical data survey [4] will boast fully consistent nuclear wave functions used throughout the analysis.

In the 1970s, we first wrote a computer code to evaluate as exactly as possible the statistical rate function [5]. The code was based on the formalism given in Konopinski's book [6]. It has been used in the analysis of superallowed Fermi β-decay ever since, but it has never been possible to check it with a code of comparable completeness. We have now extensively tested the two codes against each other and, to leading order in induced currents, find the two codes agree to an accuracy of 0.003% or better. At the next order, though, some discrepancies occurred, which we attribute to a coding error in our earlier treatment of the $1/M_N$-order corrections to the induced terms. When these terms are dropped, the two codes agree. We conclude that the effect of the coding error in the earlier code was substantially less than 0.1% and is essentially negligible when compared with the quoted uncertainties.

[1] I.S. Towner and J.C. Hardy, *Progress in Research*, Cyclotron Institute, Texas A&M University (2002-2003), p. III-1.

[2] H. Behrens and W. Bűring, *Electron Radial Wave Functions and Nuclear Beta-decay* (Clarendon Press, Oxford, 1982).

[3] I.S. Towner and J.C. Hardy, Phys. Rev. C **66**, 035501 (2002).

[4] J.C. Hardy and I.S. Towner, *Progress in Research*, Cyclotron Institute, Texas A&M University (2003-2004), p. I-???.

[5] I.S. Towner and J.C. Hardy, Nucl. Phys. **A205**, 33 (1973).

[6] E.J. Konopinski, *The Theory of Beta Radioactivity* (Clarendon Press, Oxford,1966).

Isoscalar Giant Monopole Resonance and its Overtone in Microscopic and Macroscopic Models

S. Shlomo, V. M. Kolomietz, and B. K. Agrawal

The properties of a giant resonance in nuclei are usually determined from the distorted wave Born approximation (DWBA) analysis of its excitation cross section by in elastic scattering of a certain projectile. The transition potential required to carry out the DWBA analysis is obtained by convoluting the projectile nucleus interaction with the transition density associated with the giant resonance. The relevant transition density can be obtained from a microscopic theory of the giant resonance, such as the Hartree-Fock (HF) based random phase approximation (RPA). However, the use of a macroscopic transition density ρ_{tr}^{macr} (r) greatly simplifies the application of the giant multipole resonance theory to the analysis of the experimental data. The simple form of the transition density

$$\rho_{tr}^{sc}(\mathrm{r}) = \alpha_0 (3 + r\frac{d}{dr})\rho_{eq}(r)\, y_{00}(\mathrm{r}), \qquad (1)$$

obtained by the scaling approximation, is a well known example of the macroscopic transition density ρ_{tr}^{macr} (r) commonly used in the case of the isoscalar giant monopole resonance (ISGMR) [1]. The transition density of Eq. (1) nicely agrees with the ISGMR transition density obtained in microscopic HF-RPA calculations. Unfortunately, the scaling consideration can not be extended to the overtone of the ISGMR. To obtain a macroscopic transition density ρ_{tr}^{macr} (r) in this more general case, one can use the well know method [2] of determining ρ_{tr}^{macr} (r) from the local sum rule which is exhausted by one collective state with the appropriate choice of the transition operator f_ξ(r). This fact enables us to obtain the transition operator f_ξ(r) simply by maximizing the fraction of energy- weighted sum rule (FEWSR) exhausted by the single overtone.

We have developed a procedure to derive the transition density for the ISGMR overtone using both the HF based RPA and the Fermi-liquid approaches (FLA) [3]. We have used the local strength function S(r,E) to extend the quantum expression for the transition density $\rho_{tr,n}$(r) to the case of a group of the thin-structure resonances which are localized in the GMR region and are excited due to the specifically chosen transition operator $F(\{\mathrm{r}_i\}) = \sum_{i=1}^{A} f(\mathrm{r}_i)$. Our approach was applied to study the transition density of the ISGMR overtone. In this case, an appropriate form of the transition operator f(r) is given by f(r) = f_ξ(r) = $(\mathrm{r}^4 - \xi \mathrm{r}^2)\, y_{00}(r)$. The mixing parameter ξ was determined from the condition that the transition operator f_ξ(r) provides for the single overtone the maximum fraction of energy-weighted sum rule. We find that the mixing parameter ξ depends on the nuclear mass number A. This dependence is well approximated by $\xi \approx 2A^{2/3}$ fm^2. We have also applied our smearing procedure to the evaluation of the smeared out transition density $\tilde{\rho}_{tr,R}$(r) within the HF-RPA. We have shown that the smearing procedure for the ISGMR

overtone region provides a simple two nodal structure of $\tilde{\rho}_{tr,R}(\mathrm{r})$, as expected for the $L=0$ overtone. Moreover, the transition density $\tilde{\rho}_{tr,R}(\mathrm{r})$ resembles its macroscopic counterpart. We have also applied a simple semiclassical FLA to the evaluation of the smeared out (in quantum mechanical sense) transition density $\rho_{tr}^{FLA}(\mathrm{r})$. We have used the same form of the transition operator $f_{\xi}(\mathrm{r})$ as in the case of the HF-RPA calculation to provide an additional check of the derivation of the mixing parameter ξ from the energy-weighted sum. We found good agreement between the values of the parameter ξ obtained in both the quantum and the semiclassical approaches. We have also pointed out that the ISGMR and its overtone can be clearly identified by considering the response to the electromagnetic external field $\sim j_0(qr)$.

[1] J. P. Blaizot, Phys. Rep. **64**, 171 (1980).
[2] A. Bohr and B. Mottelson, Nucl Structure (Benjamin, London, 1975), Vol. II, Chap. 6.
[3] S.Shlomo, V.M. Kolomietz Phy. Rev. C **68**, 064301 (2003).

Consequences of Self-Consistency Violations in HF-RPA Calculations of the Nuclear Breathing Mode Energy

B. K. Agrawal and S. Shlomo

The Hartree-Fock based random phase approximation (HF-RPA) provides a good microscopic description of the nuclear compressional modes. The most special of these compressional modes is the isoscalar giant monopole resonance (ISGMR) also referred to as the breathing mode. The centroid energy E_c of the ISGMR enables one to determine the value of nuclear matter incompressibility coefficient K_{nm} which plays an important role in understanding a wide variety of phenomena ranging from heavy-ion collision to supernova explosions. Recent experimental data for the E_c in heavy nuclei have rather small uncertainties (~0.1 – 0.3 MeV). Since, the uncertainty δE_c associated with E_c is approximately related to the uncertainty δK_{nm} by,

$$\frac{\delta K_{nm}}{K_{nm}} = 2\frac{\delta E_c}{E_c},$$

the value of δK_{nm} is only about 10 MeV, for K_{nm} = 250 MeV and $E_c = 14.17 \pm 0.28$ MeV for the ^{208}Pb nucleus. However, most of the HF-RPA calculations as employed for the determination of E_c are plagued by the lack of self-consistency [1]. Self-consistency is violated due to the neglect of the spin-orbit and Coulomb terms in the particle-hole (p-h) interaction used in the RPA calculations. Furthermore, some of the RPA calculations are performed in the TJ (isospin) scheme. So, it is of utmost importance that in order to determine an accurate value of K_{nm} one must have an accurate knowledge of the effects of violations of self-consistency on the centroid energy of the ISGMR. We may also point out that modifying the p-h interaction in an adhoc manner in such a way that the spurious state associated with the center of mass motion appears at zero energy [2] dose not restore the self-consistency .

We have investigated in detail the effects of the violations of the self-consistency in the HF-RPA calculation of ISGMR energy [3]. In particular, we consider the self-consistency violations caused by ignoring the spin-orbit and Coulomb terms in the p-h interaction and by carrying out the RPA calculations in the TJ scheme. We performed the HF-RPA calculations for the ISGMR energies for several nuclei with the SGII Skyrme interaction and demonstrated that ignoring the spin-orbit term in the p-h interaction gives rise to a spurious enhancement in the values of ISGMR energies for spin unsaturated nuclei. On contrary, neglect of the Coulomb term in the p-h interaction and performing the RPA calculations in the TJ scheme underestimates the ISGMR energies. Finally, we calculated the ISGMR energies for the ^{90}Zr and ^{208}Pb nuclei for the five different Skyrme interactions SGII, SkM*, SLy4, SK255 and SK272 and show that in these nuclei, widely used to extract the value of K_{nm}, the various elements contributing to the self-consistency violations tend to counterbalance their effects leading to an uncertainty of about 0.1 – 0.4 MeV in the values of the ISGMR energies. These uncertainties are quite acceptable in view of the accuracy of the experimental data for the ISGMR energies currently available.

[1] S. Shlomo and A.I. Sanzhur Phys. Rev. C **65**, 044310 (2002).
[2] S. Shlomo and G.F. Bertsch, Nucl. Phys. **A243**, 507 (1975).
[3] B.K Agrawal and S. Shlomo, Submitted to Phys. Rev. C.

Critical Densities for the Skyrme Type Effective Interactions

B. K. Agrawal, S. Shlomo, and V. Kim Au

There are many different parameterizations of the Skyrme type effective nucleon-nucleon interaction. Values of the Skyrme parameters are usually obtained by fitting the results of the Hartree-Fock calculations for the binding energies, charge radii and spin-orbit splittings of a few closed shell nuclei to the observed ones using a least square procedure. Further, the Skyrme parameters are also constrained to yield appropriate values for some properties of the infinite symmetric nuclear matter at the saturation density ρ_{nm}. Recently, it has been shown in Ref. [1] that a more realistic parameterization of the Skyrme interaction can be obtained by subjecting it to stability requirements of the equation of state defined by the inequality conditions for the Landau parameters for symmetric nuclear matter and pure neutron matter. In other words, few of the Skyrme parameters not well determined by the experimental data used in the least square procedure can be restricted by requiring that the inequality conditions be satisfied upto a certain maximum value for the nuclear matter density, also referred to as the critical density ρ_{cr}. On the other hand, a very systematic study carried out in Ref. [2] using several Skyrme interactions indicates that the density dependence of the symmetry energy coefficient J plays a crucial role in determining the properties of neutron star. Out of 87 different parameterization for the Skyrme interaction considered in Ref. [2] only 27 of them, having a positive slope for the symmetry energy coefficient at nuclear matter densities ρ up to $3\rho_o$ (ρ_o = 0.16 fm^{-3}), are found to be suitable for the neutron star model [3]. Thus, it appears that the parameters of the Skyrme interaction can be better constrained by adopting the criteria employed in Refs. [1] and [2].

We have calculated critical densities for most of the Skyrme interactions recently recommended [2] for the neutron star models [3]. We show that many of these interactions yield a very low value for the critical density ρ_{cr} as determined by imposing the stability criteria on the Landau parameters for the symmetric nuclear matter and the pure neutron matter. We find that the critical density can be maximized by appropriately adjusting the values of the enhancement factor κ, coefficient $L = 3\rho \frac{dJ}{d\rho}$ and the Landau parameter G_0' as these quantities are not well determined by the Skyrme parameters conventionally obtained by fitting the experimental data for the ground state properties of finite nuclei. We exploit the fact that (i) the value of κ should be in the range of 0.25 – 0.5, needed to describe the Thomas-Reiche-Kuhn (TRK) sum rule for the isovector giant dipole resonance, (ii) $L > 0$ for $0 \le \rho \le 3\rho_o$; a condition necessary for a Skyrme interaction to be suitable for studying the properties of neutron star and (iii) $G_0' > 0$ in order to reproduce the energies of the isovector $M1$ and Gamow-Teller states. The maximum value of critical density so obtained is lower by up to 25% compared to the ones obtained without any such restrictions [1]. We show [3] that the critical density obtained for realistic values of the surface energy coefficient (E_s =18 ± 1 MeV) and effective mass (m^*/m=0.7 ± 0.1) lie in the range of $2\rho_o$ to $3\rho_o$. In view of these results it appears that the Sly7 and Sly10 are the most realistic parameterization of the Skyrme interaction.

[1] J. Margueron *et al.*, Phys. Rev. C **66**, 014303 (2002).
[2] J. Rikovska Stone *et al.*, Phys. Rev. C **68**, 034324 (2003).
[3] B.K Agrawal and S. Shlomo, Submitted to Phys. Rev. C.

Simulated Annealing Approach to Determine the Parameters of Skyrme Type Effective Interaction

B. K. Agrawal, S. Shlomo, and V. Kim Au

Since the pioneering work of Brink and Vautherin [1], continuous efforts have been made to improve the parameters of the Skyrme type effective nucleon-nucleon interaction. Recently a set of Skyrme parameters SKX [2] was obtained by fitting the results of Hartree-Fock (HF) calculations to the experimental data on the binding energy, charge radii and single particle energies for nuclei ranging from the normal (β-stable) to the ones near the proton and neutron drip lines. In the SKX interaction, to account for the Nolen-Schiffer anomaly in the Coulomb displacement energy the contribution due to the so called Coulomb exchange term in the HF mean field was ignored. However, it has been shown in Ref. [3] that the SKX interaction is not suitable for studying the properties of neutron star. Since, for the SKX interaction, the quantity $L = 3\rho \frac{dJ}{d\rho}$, where J is the symmetry energy coefficient, becomes negative for the nuclear matter densities ρ well below $3\rho_o$ (ρ_o = 0.16 fm^{-3}). Further, we find that for the SKX interaction the value of the critical density ρ_{cr}, determined from the stability conditions for the Landau parameters for the symmetric nuclear matter and the pure neutron matter is $1.25\rho_o$. The low value for ρ_{cr} implies that the SKX interaction can not be employed to study the properties of matter at the densities beyond ρ_o. Another family of Skyrme interaction named SLy [4] was obtained by fitting the ground state properties of a few normal nuclei together with a realistic equation of state for the pure neutron matter. These interactions have $\rho_{cr} \sim 3\rho_o$. However, unlike the SKX interaction, the SLy interactions are not adequate, for proton rich nuclei. Thus, it is highly desirable to determine the parameters of the Skyrme interaction in such a way that it not only fits the ground state properties of the nuclei along the line of the β-stability as well as away from it, but also yield a reasonable value for the critical density and appropriate density dependence of the coefficient J as required by the neutron star models.

We have implemented, for the first time, the simulated annealing method to fit the values of Skyrme parameters by searching for the global minimum of the chi-square function. To demonstrate the applicability of this method we have fitted the values of Skyrme parameters to an extensive set of experimental data together with a few additional constraints. Our experimental data set consists of the binding energies for 15 nuclei ranging from the normal to the exotic (proton or neutron rich) ones, rms charge radii for 7 nuclei, spin-orbit splittings for the $2P$ proton and neutron orbits for ^{56}Ni nucleus and the rms neutron radii for $1d_{5/2}$ and $1f_{7/2}$ unoccupied orbits in the ^{16}O and ^{40}Ca nuclei, respectively. The additional constraints imposed on the Skyrme parameters are (i) the critical density ρ_{cr}, determined from the stability conditions for the Landau parameters should lie in the range of $2\rho_o$ to $3\rho_o$, (ii) the quantity $L = 3\rho \frac{dJ}{d\rho}$, must be positive for the densities up to $3\rho_o$; a condition imposed by the neutron star models [3], (iii) the enhancement factor κ, associated with the Thomas-Reiche-Kuhn (TRK) sum rule for the

isovector giant dipole resonance, should lie in the range of 0.25 – 0.5 and (iv) the Landau parameter $G_0^{'}$, crucial for the spin properties of the finite nuclei and the nuclear matter, should be positive at $\rho = \rho_o$.

Using these experimental data along with the additional constrains, we have carried out [5] three fits which differ from each other in the way the contribution due to the Coulomb interaction is treated. These fits are named as (i) DE; the direct as well as exchange Coulomb terms are included, (ii) DE0; only the direct Coulomb term switched on and (iii) XDE; just like DE but with overall enhancement factor x_{cn}. The corrections to the binding energy and rms charge radii due to the centre of mass motion are performed using a simple but consistent scheme. We find that all the interactions presented in this work have similar features except for the binding energy of the proton rich nucleus ^{48}Ni. The DE0 interaction gives the best value for the binding energy for ^{48}Ni. As a result the binding energy difference B(^{48}Ca) - B(^{48}Ni) is quite reasonable in this case. Whereas, for the DE and XDE interactions the value of B(^{48}Ca) - B(^{48}Ni) are lower by ~ 4 - 5 MeV. Further, the second constraint (i.e., $L > 0$ for $\rho \leq 3\rho_o$) ensures that the DE, DE0 and XDE interactions can be used to study the properties of the neutron star. Thus, the DE0 interaction encompasses the merits of the recently proposed SKX and SLy7 interactions. In other words, the DE0 interaction can be used to evaluate the Coulomb energy differences in mirror nuclei as well as to study the properties of the neutron star.

[1] D. Vautherin and D. M. Brink, Phys. Rev. C **5**, 626 (1972).

[2] B. A. Brown, Phys. Rev. C **58**, 220 (1998).

[3] J. R. Stone *et al.,* Phys. Rev. C **68**, 034324 (2003).

[4] E. Chabanat *et al.*, Nucl. Phys. **A627**, 710 (1997).

[5] B. K. Agrawal, S. Shlomo and V. Kim Au, to be published.

Isoscalar Giant Dipole Resonance in Nuclei

S. Shlomo, O. G. Pochivalov, and B. K. Agrawal

We report here on our research of the strength function for isoscalar giant monopole resonance (ISGMR) and isoscalar giant dipole resonance (ISGDR) within the formalism of the Hartree-Fock (HF) based random phase approximation (RPA). In our HF-RPA calculation we have adopted the modern Skyrme-like effective interaction SLY4 [1], which is considered to be one of the promising interactions for describing ground state and collective properties of many nuclei. Correction for the spurious state mixing (SSM) in the strength function of the ISGDR was taken into account using to the projection operator method described by Shlomo and Sanzhur [2].

Highly accurate data by M. Uchida *et al.* at RCNP, Osaka, Japan [3] and D.H. Youngblood *et al.* at the Cyclotron Institute, Texas A&M University [4,5] have been recently reported. Comparison of this experimental data (see Table1) with the theoretical calculations is shown.

Table 1: Data reported by M. Uchida *et al.* [a)][3] and D. H. Youngblood *et al.* [b)][4,5] compared with the results obtained by HF-RPA calculations [c)].

	E_{ISGMR} (MeV)	EWSR (%)	$E_{LE\ ISGDR}$ (MeV)	EWSR (%)	$E_{HE\ ISGDR}$ (MeV)	EWSR (%)
^{90}Zr a)	16.6±0.1	101±3	17.8±0.5	7.9±2.9	26.9±0.7	67±8
b)	$17.81^{+0.32}_{-0.20}$	100±12	17.1±0.4	13±3	26.7±0.5	70±10
c)	18.5	95.4	12.86	9.8	27.18	65.4
^{116}Sn a)	15.4±0.1	95±4	15.6±0.5	4.9±2.2	25.4±0.5	68±9
b)	15.85±0.20	112±15	14.38±0.25	25±15	25.50±0.60	61±15
c)	17.0	95.0	10.7	5.9	25.3	75.5
^{144}Sm a)	$15.3^{+0.11}_{-0.12}$	84^{+4}_{-25}	14.2±0.2	23^{+4}_{-10}	$25.0^{+1.7}_{-0.3}$	91^{+25}_{-17}
b)	15.40±0.30	92±12	14.00±0.30	32±15	24.51±0.40	64±12
c)	16.1	94.5	12.6	12.2	26.2	73.9
^{208}Pb a)	13.4±0.2	104±9	13.0±0.1	7.0±0.4	22.7±0.2	111±6
b)	13.96±0.20	99±15	13.26±0.30	24±15	22.20±0.30	88±15
c)	14.5	94.2	12.4	13.6	24.5	72.8

As we can see from the Table 1, there exists a noticeable discrepancy between the positions of the low-energy (LE) and high-energy (HE) components of the experimentally deduced and theoretically calculated strength functions. The discrepancy between the experimental data and microscopic calculation in the position of the LE-peak and the HE-peak remains to be investigated.

[1] E. Chabanat *et al.*, Nucl. Phys. **A635**, 231 (1998)

[2] S. Shlomo and A.I. Sanzhur, Phys. Rev. C **65**, 044310 (2002)
[3] M. Uchida *et al.*, Phys. Rev. C **69**, 051301(R) (2004)
[4] D.H. Youngblood *et al.*, Phys. Rev. C **69**, 034315 (2004)
[5] D.H. Youngblood *et al.*, Phys. Rev. C **69**, 054312 (2004)

Splitting of Isoscalar and Isovector Giant Multiple Resonances in Spherical Neutron-Rich Nuclei

V.M. Kolomietz,[1] A.G. Magner,[1] and S. Shlomo
[1]*Institute for Nuclear Research, Kiev 03680, Ukraine*

We suggest a new explanation of the splitting of both the isoscalar and the isovector modes in spherical neutron-rich nuclei within the Fermi liquid drop model (FLDM). The FLDM provides the existence of the isoscalar and isovector vibrations, related to the two different dimensionless zero-sound velocities s and s'. They are determined by the isoscalar and the isovector Landau interaction amplitudes, respectively. Due to the macroscopic self-consistency and the boundary condition on the free nuclear surface the FLDM shows a new satellite structure of the isovector and isoscalar giant multipole resonances in addition to the predictions of commonly used isospin splitting shell model (ISSM) and dynamical collective model (DCM).

We have performed the calculations of the characteristics of the isovector giant dipole resonance (IVGDR) and its satellite for several isotopes of *Ca* and *Sn* nuclei. We determined the energy $E_{\rm GDR}$ of the main IVGDR and its satellite, their relative strength $m^{(s)}/m^{(m)}$ and the depletion of the energy weighted sum rule (EWSR), $m_1/m_{\rm EWSR}$. The splitting magnitude in our FLDM almost does not depend on the neutron excess N-Z and there is an agreement with the experimental data. This is in contrast to another splitting effect predicted by the ISSM which shows an increase of the energy splitting of the IVGDR with the isospin quantum number $T_3=(N-Z)/2$. The satellite strength ratio $m^{(s)}/m^{(m)}$ is small and increases linearly with the asymmetry parameter $X=(N-Z)/A$ in contrast to both the opposite ISSM-splitting behavior like $1/T_3$ and the case of splitting due to deformation in the collective model, with approximately equivalent strengths of the peaks. The relative strengths and the depletion of the EWSR for all (Fermi-liquid) satellites turn into zero and they disappear in the symmetric limit X=0. The strength ratios of the two peaks and their depletion of the EWSR are also in agreement with the experimental results presented by squares or triangles.

Small Damping Approach in Fermi Liquid Theory

V.M. Kolomietz,[1] S.V. Lukyanov,[1] and S. Shlomo
[1]*Institute for Nuclear Research, Kiev 03680, Ukraine*

We investigated the validity of the small damping approximation (SDA) in the Fermi liquid theory for the description of collective motion in hot nuclei. In the SDA one assumes that the relaxation width is small compared to the energy of collective excitation. This approach is reasonable in cold Fermi systems where the excitation energy of strongly collectivized states is very high (due to distortion of a Fermi surface) and the relaxation damping is quite small. With the heating of the system the energy of excitation of collective vibrations is decreasing as the two-body relaxation rate is increasing. Thus, with an increase of the temperature, the ratio of the relaxation width to the corresponding eigenenergy increases rapidly and the use of the SDA can be invalid.

Using the collision kinetic theory, we have performed a comparison of the main characteristics of the isoscalar quadrupole vibrations in hot nuclei for two cases: (1) the exact solution of the equations of motion for the nuclear shape variables and (2) the solution of the same equations within the SDA. The calculations were carried out for the nucleus A=224. We find that the collision width does not show a tendency to decrease in the high temperature regime and the difference between the results of the SDA calculation and the exact one does not exceed ≈10% for the width Γ. For the eigenenergy E, we observed a significant difference between the results of the two types of calculations in the high temperature region. This difference strongly increases with temperature.

Nuclear Fermi-Liquid Drop Model

V. M. Kolomietz[1] and S. Shlomo
[1]*Institute for Nuclear Research, Prosp. Nauki 47, 252028 Kiev, Ukraine*

Starting from quantum considerations, we have [1] first reduced the many body Schrodinger equation to a semiclassical kinetic equation for the Wigner distribution function $f(\mathbf{r},\mathbf{p},t)$ and then to equations of motion for several local quantities, namely, particle density ρ, velocity field $\mathbf{u}$ and pressure tensor $P_{\nu\mu}$. The structure of these equations is critically dependent on the distortion of the Fermi surface in momentum space. In general, these equations are closed if the multipolarity l of the Fermi distortion is restricted by a certain l_{max}. The well-known time dependent Thomas-Fermi approximation is obtained with $l_{max}=1$. Many few aspects of nuclear dynamics appear at $l_{max}\geq 2$. The Fermi surface distortion with $l\geq 2$ bring about the tensor structure of the pressure and lead to a strong renormalization of the restoring force for the particle density fluctuations. In fact, the presence of Fermi surface distortions with $l\geq 2$ allows for a satisfactory description of phenomena such as the giant multipole resonances.

In the case of small amplitude eigenvibrations with eigenfrequency ω, we have shown that, even at $l_{max}=\infty$, it is possible to obtain a closed set of equations for the above mentioned local quantities, if the equations of motion are augmented by the corresponding Landau's dispersion equations for ω. In this case an additional phenomena like Landau damping can also be taken into consideration. We have adopt a simple Fermi liquid drop model (FLDM) with two essential ingredients: (i) For the interior region we assume that the dynamic part of the distribution function, $\delta f(\mathbf{r},\mathbf{p},t)$, is given by a superposition of plane waves, associated with a certain multipolarity L of the particle density vibrations, (ii) In the surface region we use the boundary conditions for the involved local quantities, the velocity field and the pressure tensor. This model provides a satisfactory description of the gross structure of both the isoscalar and the isovector giant multipole resonances.

The approach adopted here allows for simple generalizations to incorporate effects of temperature and of damping. The effect of damping was studied by taking into account the collision integral in the kinetic equation. An important consequence of the Fermi surface distortion is the fact that the interparticle collisions lead to contributions of the memory effect to the conservative and dissipative parts of the equations of motion for local quantities ρ, $\mathbf{u}$ and $P_{\nu\mu}$. The memory effects are especially important for a proper description of the transition from the zero-sound regime at low temperature to the first-sound regime at high temperatures. Moreover, the memory effects on the nuclear collective motion lead to peculiarities of the random-force correlation function, which are absent in a classical system. The spectral correlation function is independent of $\omega\tau$ (τ is the relaxation time) and corresponds to a white noise in the first-sound regime, at $\omega\tau \to 0$, whereas in the zero-sound regime, at $\omega\tau \to \infty$, it corresponds to a blue noise.

We have also applied the FLDM to the case of a large change in the nuclear shape, which is accompanied by a small distortion of the Fermi surface. We have thus extended the well-known liquid drop model (LDM) for large amplitude motion (for example, nuclear fission), taking into account the memory effects associated with the Fermi surface distortion. This provides an extension of the LDM to

the case of non-Markovian large amplitude dynamics. It was shown that the memory effects strongly influence the development of instability near the fission barrier for a large enough relaxation time τ. The memory integral brings about an additional elastic force, which acts against the adiabatic force, leading to a hindrance of the drift of the nucleus from the barrier to the scission point and inducing characteristic shape oscillations. Thus, the Fermi surface distortions lead to an important effect of hindrance of the collective motion. This hindrance is due to the time-reversible elastic force and it represents an additional effect, beside the hindrance due to the usual time-irreversible friction force.

[1] V.M. Kolomietz and S. Shlomo, Phys. Rep. **390**, 133 (2004).

Flow Effects on Multifragmentation in the Canonical Model

S. K. Samaddar,[1] J. N. De,[1] and S. Shlomo
[1]*Saha Institute of Nuclear Physics, 1/AF Bidhannagar, Kolkata 700064, India*

In intermediate energy heavy ion reactions the colliding nuclei get compressed in the initial phase with subsequent decompression thereby generating collective flow energy. At energies around 100 MeV per nucleon or above, large radial collective flow has been observed in many experiments. In a hydro dynamical model with site-bond percolation, it has been shown that compression is very effective in multifragmentation. Such a conclusion is further reached in microscopic BUU-type formulations as well as in a grand canonical thermodynamic calculation. It's crucial importance on the extracted value of the freeze-out density from yield ratios of fragment isotopes differing by one neutron in a statistical fragmentation model was also pointed out [1].

We have performed calculations [2] for multifragmentation of a heated nucleus in a canonical model with incorporation of flow both at constant volume as well as at constant flow pressure. It may be pointed out that under the experimental conditions none of these constraints may exist. In the absence of any definite knowledge of the actual scenario, the calculations were done with these constraints imposed. It is found that the average multiplicity increases with flow; the average intermediate mass fragments (IMF) multiplicity shows a rise and fall with excitations commensurate with the experimental data. The calculated caloric curves also follow the experimental trend very closely. The plateau in the caloric curve and the peaked structure of the corresponding heat capacity at temperature around 5-6 MeV signal a liquid-gas phase transition in the finite nuclear systems. At constant flow pressure, the caloric curve shows a negative slope in a small domain of temperature and gives rise to negative heat capacity. Negative heat capacity at constant thermal pressure has been observed in the same model without flow; it is interpreted as arising in regions of mechanical instability where the isobaric volume expansion coefficient is negative. The same effect is seen to persist with incorporation of flow. A sudden jump in entropy is also seen, both at constant volume and at constant pressure. It is interesting to note that the maximum in the average number of IMF $<N_{IMF}>$, the peak in the heat capacity at constant volume C_v, the discontinuity in the heat capacity at constant pressure C_p and the sudden jump in entropy are all around the same temperature signaling a liquid-gas phase transition.

[1] S. Shlomo, J.N. De and A. Kolomiets, Phys. Rev. C **55**, R2155 (1997).
[2] S.K. Samaddar, J.N. De, and S. Shlomo, Phys. Rev. C (in press).

Liquid-Gas Phase Transition in Infinite and Finite Nuclear Systems

Tapas Sil,[1] S. K. Samaddar,[1] J. N. De,[2] and S. Shlomo
[1]*Saha Institute of Nuclear Physics, 1/AF Bidhannagar, Kolkata 700064, India*
[2]*Variable Energy Cyclotron Center, 1/AF Bidhannagar, Kolkata 700064, India*

The study of liquid-gas phase transition in finite nuclear systems is of considerable contemporary interest. Experimental analyses of the accumulated data on multifragmentation and caloric curves show compelling evidence of such a transition. Phase transitions are normally signaled by peaks in the heat capacity with rise in temperature. Theoretical models of different genres, such as the micro canonical or the canonical description of multifragmentation, the lattice–gas model or even the microscopic treatment in a relativistic or a non-relativistic Thomas-Fermi framework support such a structure in the heat capacity. A clear idea about the subtle details of the liquid-gas phase transition in finite nuclei, however, has not emerged yet. Confusion remains about whether the system has evolved dynamically through the critical point; a coherent picture about the order of the phase transition is also missing. Analyses of the experimental data by the EOS group and the ISiS group give strong circumstantial evidence for a continuous (second order) phase transition. Calculations performed in the mean-field model also lead to a similar conclusion. Predictions from the lattice-gas model calculations are, however, compatible with a first order transition. Anomalous negative heat capacities as obtained from fluctuation analysis in energetic heavy-ion collisions have been claimed as indicators of first order phase transition. However, questions have been raised on the origin of the negative heat capacity for nuclear systems with mass number A>60.

The liquid-gas phase transition in infinite asymmetric nuclear matter with explicit conservation of baryon number and total isospin has been investigated [1] in a mean field framework employing the Skyrme-like SKM^* interaction. The calculations have been extended for finite nuclei in a heated liquid-drop model where the drop is assumed to be in thermodynamic equilibrium with its emanated vapor. As observed earlier for infinite asymmetric nuclear matter in a relativistic mean field model, we observe in this non-relativistic calculation that the pressure changes continuously along the liquid vapor coexistence line for infinite asymmetric system as well for finite nuclei, symmetric or asymmetric. The neutron and proton concentration in the liquid and the vapor phase are found to be very different resulting in the so-called isospin fractionation. For systems with $N > Z$ that we have investigated, both infinite and finite, the gas phase is always found to be neutron-rich. For symmetric finite system, however the gas phase is mostly proton-rich. This is likely to be signaled from the predominant production of proton-rich isotopes in collisions between medium-heavy symmetric nuclei. The peaked structure in the heat capacity indicates further the occurrence of liquid-gas phase transition. From the evolution of entropy at constant pressure, it is seen that the transition occurs over range of temperatures contrary to fixed temperature in the first order transition; this suggests that the liquid-gas phase transition in a finite nuclear system is continuous in the mean field model we adopt. However, the said temperature interval is comparable, if not less, to the present day accuracy in the temperature measurement. Thus the continuous nature of the transition found in our calculation would be hard to disentangle from the first order transition. The thermodynamic

concepts we use may not be very meaningful when the number of particles in one of the phases is very small, still this model serves as a window to understand the basic features of liquid-gas phase transition in finite system.

[1] Tapas Sil, S.K. Samaddar, J.N. De, and S. Shlomo, Phys. Rev. C **69**, 014602 (2004).

Liquid Gas Phase Transition and Negative Heat Capacity

S. K. Samaddar,[1] J. N. De,[1] S. Shlomo, and J. B. Natowitz
[1]*Saha Institute of Nuclear Physics, 1/AF Bidhannagar, Kolkata 700064, India*

The equation of state of relativistic finite nuclei was investigated in a heated liquid-drop model where the drop is assumed to be in thermodynamic equilibrium with its own vapor. Explicit conservation of baryon number and total isospin is just maintained. The calculations were done in a mean-field framework employing the *SKM** interaction. From the peaked structure of the heat capacity at constant pressure, it was inferred that the finite systems also undergo a liquid-gas phase transition, however, the finite nuclear drop changes over in a continuous transition to a fully gaseous phase. The neutron and proton concentration in the liquid and vapor phase were found to be very different resulting in the so-called isospin distillation.

Closer examination of the isotherms in this heated liquid-drop model revealed that even in the completely physical region (obtained from the thermodynamic equilibrium conditions), the isotherms display a Van der Waals type looping which is never admitted for infinite systems. Compared to the ones calculated with both Coulomb and surface effects, the loops become more pronounced with the Coulomb interaction switched off. At constant pressure, in a narrow temperature domain, such loops allow higher specific volumes at lower temperature. The system may then have higher excitations at lower temperature resulting in negative specific heat.

The negative specific heat obtained earlier in microcanonical or canonical formulations has been taken as tacit evidence that the liquid-vapor phase transition in finite nuclei is first order. Our calculations in a grand canonical framework, however, show that it is not incompatible with a continuous phase transition.

Hot Nuclei

S. Shlomo and V. M. Kolomietz[1, 2]
[1]*Physik-Department TU Munchen, 85747 Garching, Germany*
[2]*Institute for Nuclear Research, Prosp. Nauki 47, 03028 Kiev, Ukraine*

The study of properties of hot nuclei and the search for the liquid-gas phase transition in nuclei have been the subjects of many investigations in recent decades. Recent experiments indicate that hot nuclei exhibit the phenomena of multifragmentation and the saturation of the caloric curve. It should be pointed out that the main difficulty in the interpretation of experimental data is the separation between the dynamic and the statistical effects. In this work [1] we limit the consideration to the description of the properties of hot nuclei, assuming the existence of thermal equilibrium in a certain freeze out volume.

The equation of state (EOS) was analyzed within the thermal Thomas-Fermi approximation (TTFA), using the effective Skyrme-like interaction. The EOS was derived from the free energy as dependence of the pressure P on the particle density ρ for certain values of the temperature T and the isotopic asymmetry parameter X. We obtained the shape of (P,T,X)-surface of equilibrium for nuclear matter, using the Gibbs equilibrium conditions for the pressure P and the chemical potential μ_q ($q=n$ for neutron and $q=p$ for proton), and discussed its important features. We also discussed the conditions for the first-order phase transition in an asymmetric nuclear matter. We deduced the isobaric (T,X) phase diagram for the boiling and condensation and noted the two different regimes for the boiling in an asymmetric nuclear matter. One of them is the usual boiling of a two-component system where the boiling process is accompanied by a preferable evaporation of neutrons. In another regime, the (T,X) phase diagram contains the critical point and the boiling leads to a very specific effect of retrograde condensation. The Maxwell construction allowed us to derive the caloric curve for the case of isobaric heating and demonstrate the existence of a plateau (saturation) region in the caloric curve. The derivation of the EOS for a hot finite nucleus is still an open question, since an accurate method for accounting for the effects of the finite size and of the Coulomb interaction is needed. However, we carried out calculations of the EOS for a hot finite nucleus which is in equilibrium with an external nucleon gas, i.e. by imposing an external pressure.

Using the finite temperature Thomas-Fermi approximation, we have also determined the temperature dependence of bulk properties of nuclei, such as nuclear density, radius, incompressibility, surface tension, binding energy, etc., for temperature below the phase separation temperature (5 MeV). These results, which are very important for astrophysical problems, were used later in the calculations of the level density.

We considered the conditions for the generation of the embryonic vapor phase (cavitations) and the dependence of the critical radius of the embryonic vapor bubbles on the temperature and the asymmetry parameter in an overheated nuclear matter. Using the collision kinetic equation, we provided a detailed analysis of the time evolution of the bubble radius R beyond the barrier, i.e. at R larger than critical radius R^*. We showed that if the relaxation time τ is large enough, the development of instability of the bubble radius near the barrier point $R=R^*$ is strongly influenced by the memory effects. The growth of the bubble radius R is accompanied by characteristic shape oscillations of the bubble. These oscillations are caused by the elastic

force, which is induced by the memory effects. This elastic force acts against the usual adiabatic force and hinders the growth of the bubble radius. The characteristic oscillations disappear in short relaxation time limit $\tau \to 0$.

The behavior of nuclear dynamic in a heated nucleus is one of the most interesting open problems in nuclear physics. Staring from the collision kinetic equation we investigated the propagation of sound waves in hot nuclear matter and demonstrated the importance of the memory effects and the effects of the Fermi surface distortion (FSD). We pointed out that in low temperature limit, the FSD effect leads to a significant increase in the isoscalar sound velocity, whereas the effect on the isovector mode is relatively small. We discussed the conditions for the transition from the zero sound regime to the first sound regime and defined the transition temperature T_r to be the position of the maximum of the attenuation coefficient.

Experimental investigations of the isovector giant dipole resonance (*IVGDR*) built on excited states indicate that the centroid energy vary slowly with the temperature *T*. In contrast, the *IVGDR* width increases significantly with *T* and then saturate at high excitation energy. Starting from the linearized collisionless Landau-Vlasov equation, we first presented the peculiarities of Landau's damping in hot nuclear matter. Then, taking into account the effect of two-body collisions, one body dissipation and particle decay, we presented results of calculations, obtained within the Steinwedel-Jensen model, for the energy and width of the *IVGDR* in hot nuclei, which reproduce the trend of experimental data.

We presented the main approaches for the calculations of the single particle level density $g(\varepsilon)$ in a finite depth potential well and pointed out that $g(\varepsilon)$ decrease with ε in the continuum region. Therefore, a proper accounting for the continuum is important for determining nuclear properties, especially of an excited nucleus. We have also considered the level density parameter (LDP) $a=E/T^2$, which relate the excitation energy *E* to the temperature *T* and presented a simple and realistic model for calculating *a* as a function of *T*, taking into account the finite size of the nucleus, the effects of the continuum, the shell effects and the nucleon effective mass, and the variation of these effects with *T*. It is pointed out that the LDP *a* decreases with increasing excitation energy *E* due to the decrease of the frequency dependent effective mass and the above mentioned peculiarities of the contribution of the continuum states to the single particle level density $g(\varepsilon)$ in a Fermi system. The need for a proper treatment of the single particle level density $g(\varepsilon)$ in the continuum was also demonstrated in the description of the hard energy particle spectra, obtained within the exciton model of preequilibrium decay of highly excited nuclei. It was shown that a proper treatment of the continuum led to an enhancement in the emission of high-energy particle.

The problem of the liquid gas phase transition in nuclei and its relation to the multifragmentation process was investigated. We have concentrated on the determination of the temperature using the method proposed by Albergo et al (ACCR method) [2]. The method is based on the evaluation of the double ratios R_2 of the yields of the emitted fragments and depends essentially on the existence of both thermal equilibrium and chemical equilibrium in the decaying system. We discussed this method and derived a relation between the temperature *T* and R_2 of fragment yields, which is similar to the ACCR method, but only impose the condition of thermal equilibrium. We have extended the ACCR method in order to account for the Coulomb interaction and the effect radial flow. We have also modified this method to include the population of excited states that γ-decay to ground state and compare the calculated caloric curve with experimental data. It was shown that with these modifications of the method one obtains a reasonable value

for the freezing volume and extracts the same transition temperature using different thermometers (double yields ratios).

[1] S. Shlomo and V.M. Kolomietz, Invited Review Article, Rep. Prog. Phys. (in press).
[2] S. Albergo *et al.*, Nouvo Cimento **89A**, 1 (1985).

SECTION IV

ATOMIC, MOLECULAR AND MATERIALS SCIENCE

Target K Vacancy Production by 2.5 to 25 MeV/u Ar, Kr, and Xe Ions

Y. Peng, R. L. Watson, V. Horvat, and A. N. Perumal

The theoretical description of inner-shell vacancy production in fast heavy ion-atom collisions is an extremely challenging problem due of its many-body nature and because excitation, ionization, and electron transfer to the projectile all contribute to the process. So far, rigorous treatments that account only for the interactions between a single active target electron and a bare projectile nucleus have been attempted. While methods based upon the Born approximation (such as the SCA and the ECPSSR) have been reasonably successful at predicting ionization cross sections for projectiles of low atomic number (e.g., $Z_1 \leqslant 10$), they have been found to greatly overestimate the cross sections for heavy ions [1,2]. Therefore, a detailed experimental examination of the dependence of inner-shell vacancy production cross sections on projectile energy and atomic number, and on target atomic number is warranted to stimulate further theoretical progress and to develop semiempirical methods of prediction.

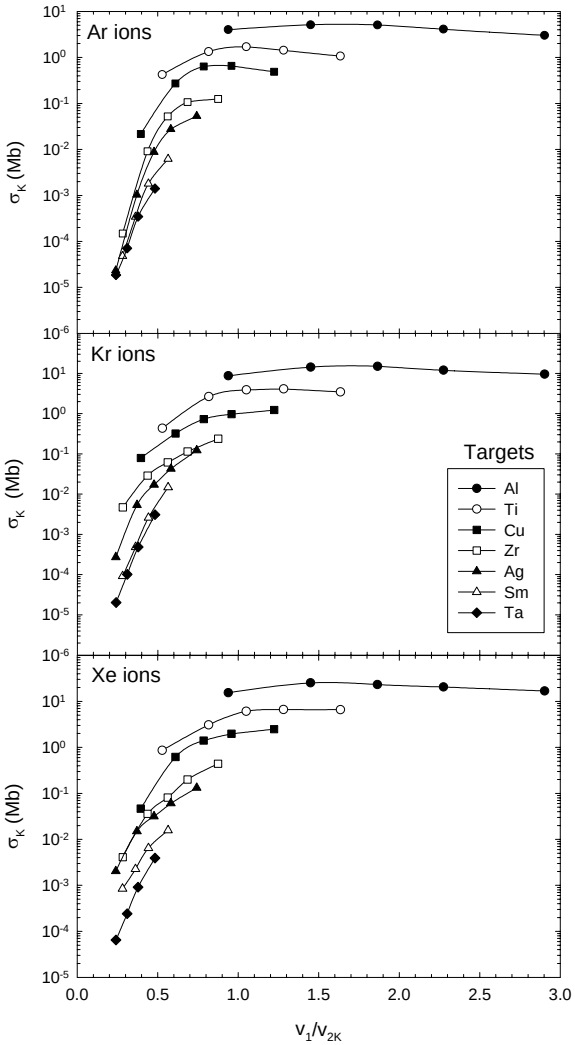

Figure 1. Target K vacancy production cross sections for Ar, Kr, And Xe ions as a function of the average projectile to target K-electron velocity ratio.

Work on this topic during the past year has focused on K-vacancy production in targets of Al, Ti, Cu, Zr, Ag, Sm, and Ta by 2.5 to 25 MeV/u Ar, Kr, and Xe projectiles in order to supplement the limited amount of data presently available in this collision regime. Determination of the x-ray production cross sections was accomplished using an Si(Li) detector to measure the intensities of K x-rays emitted from the targets and a plastic scintillator to directly count the number of projectiles passing through the targets. The data for the Al through Ag targets were recorded in both singles and coincidence modes to insure that all projectiles were counted. However, the cross sections for K x-ray production in Sm and Ta were too small to measure using the coincidence method. Instead, they were determined by measuring

the intensities of Sm and Ta K x rays relative to those of Ag. The Ag targets were positioned immediately behind the primary targets in the same target mounts. All targets were self supporting metallic foils ranging in thickness from 0.8 to 5.9 mg/cm^2.

The approximate K vacancy production cross sections, obtained by dividing the measured x-ray production cross sections by the normal (single-vacancy) fluorescence yields, are shown in Fig. 1. They are plotted as a function of the ratio of the projectile velocity (v_1) to the target average K-electron velocity (v_{2K}) and span a range of five to six orders of magnitude. In general, the cross sections vary in a systematic manner as functions of target atomic number and velocity ratio, but evidence for cross section enhancement due to electron promotion in quasi-molecular orbital level crossings may be seen in the data for Xe ions on Ag and Sm at velocity ratios less than 0.5.

The K vacancy production cross sections multiplied by the scaling factor B_K^2/Z_{eff}^2 , where B_K is the K binding energy of the target and Z_{eff} is an effective projectile atomic number, are shown in Fig. 2. The values of Z_{eff} were chosen to equalize the scaled Al cross sections for the three projectiles and are close to their average equilibrium charges. Except for the sizable offset of the Al data below the data for the rest of the targets, this scaling (which is based on the binary encounter approximation) appears to work rather well. Also shown in Fig. 2 are scaled ECPSSR cross sections for protons on Al and Ta.

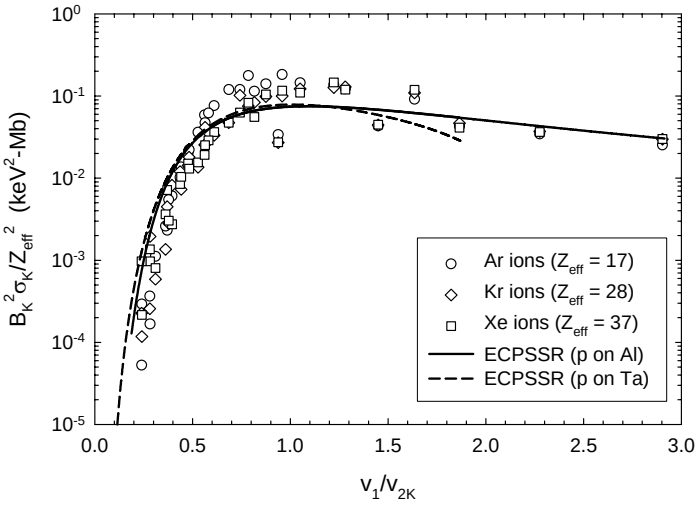

Figure 2. Scaled target K vacancy production cross sections. See text for details.

High resolution measurements employing a curved crystal spectrometer are currently being carried out for the purpose of providing data required to correct the K x-ray production cross sections for contributions from ionization by secondary electrons and photon fluorescence. In addition, these measurements will reveal the systematics of spectator L and M vacancy production, thereby providing the information needed to correct the fluorescence yields for the effects of multiple ionization and vacancy rearrangement.

[1] R.L. Watson, V. Horvat, J.M. Blackadar, and K.E. Zaharakis, Phys. Rev. A **62**, 052709 (2000).
[2] R.L. Watson, J.M. Blackadar, and V. Horvat, Phys. Rev. A **60**, 2959 (1999).

L X Rays Emitted from Multiply Ionized Holmium Atoms

V. Horvat, R. L. Watson, A. N. Perumal, and Yong Peng

Spectra of L x rays emitted from Ho targets bombarded by 6 MeV/u C, Ne, Ar, and Kr ions were measured in high resolution using a curved crystal spectrometer. A simplified preliminary analysis of the $L\alpha$ x-ray satellite structure was performed earlier and the results were described in a previous report [1]. Meanwhile, analysis of the spectra was extended to higher energies, up to the L_3 absorption edge (8000 eV), and a more elaborate approach was used in order to determine the average M-electron ionization probabilities in L-shell ionizing collisions (p_M).

A total of nine most prominent transitions were considered. Those transitions (in order of increasing energy) are $L\alpha_2$ (L_3M_4), $L\alpha_1$ (L_3M_5), $L\eta$ (L_2M_1), $L\beta_4$ (L_1M_2), $L\beta_1$ (L_2M_4), $L\beta_6$ (L_3N_1), $L\beta_3$ (L_1M_3), $L\beta_{15}$ (L_3N_4), and $L\beta_2$ (L_3N_5). Each transition may take place in a single-vacancy atom, which results in the emission of a diagram x ray, or in the presence of additional (spectator) vacancies, which results in the emission of a satellite x ray. The energy of a satellite x ray depends on the total number of vacancies, their location, and the way their angular momenta are coupled in the initial and the final state of the atom. In collisions with heavy ions at small impact parameters, a large variety of target-atom vacancy configurations can be produced. Consequently, their decay results in a complex distribution of satellite lines. This distribution may or may not be structured, depending on relative contributions from the most prominent spectator vacancy configurations at the time of x-ray emission and associated energies and widths of the emitted x rays.

Least squares fitting of the measured spectra was performed using Voigt functions to describe the peaks and straight lines to describe the background, as illustrated in Fig. 1. The peaks included those due to the diagram x rays as well as those due to distributions of satellite x rays emitted in the presence of a given number of L and M spectator vacancies. The number of M spectator vacancies (n_M) considered in the analysis ranged from 0 to 18 in all cases, while the number of L spectator vacancies (n_L) was kept to a minimum required to obtain a good fit. In each spectrum the Lorenzian width of all peaks was assumed to be the same. Its value was fixed at that obtained in the analysis of Ho L x rays excited by 10 keV electrons (measured previously).

Gaussian widths (standard deviations) of the satellite peaks reflected the inherent energy distribution of contributing satellite x rays due to multiplet splitting as well as the distribution of outer-shell spectator vacancies present at the time of x-ray emission. For each transition j ($j = L\alpha_2, L\alpha_1, L\eta, L\beta_4, L\beta_1, L\beta_6, L\beta_3, L\beta_{15}, L\beta_2$) it was assumed that they depend smoothly on n_M as

$$(\sigma^j_{nM})^2 = (\sigma^j_o)^2 + n_M\,(\Delta\sigma^j)^2 \quad , \qquad (1)$$

where σ^j_o and $\Delta\sigma^j$ are variable parameters of the fit. Equal values of σ^j_o and $\Delta\sigma^j$ were assumed for $L\alpha_2$, $L\alpha_1$, and $L\eta$, for $L\beta_4$, $L\beta_1$, $L\beta_6$, and $L\beta_3$, and for $L\beta_{15}$ and $L\beta_2$ transitions.

Positions of the satellite peaks in the spectra were determined based on a set of reference values obtained for each transition using the multiconfigurational Dirac-Fock program of Desclaux [2]. The

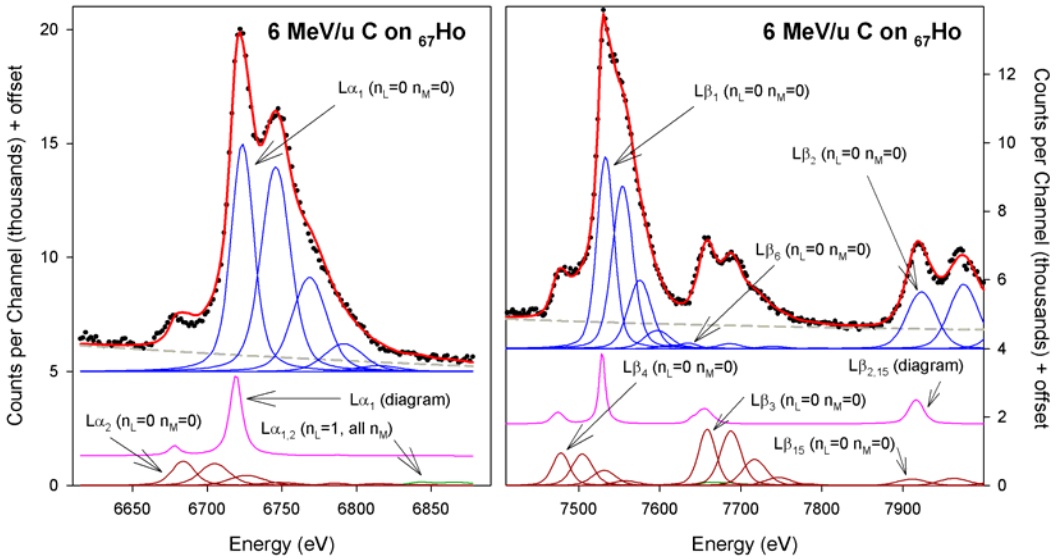

Figure 1. Spectrum of Ho *L* x rays emitted under bombardment by 6 MeV/u C ions. Experimental data points, fitted curve, background component curve, four satellite peak groups and combined diagram peaks are offset in the vertical direction to avoid excessive overlapping. Only one representative peak in each group is labeled in order to avoid overcrowding. Two spectral regions are shown separately in order to enhance the details, although the entire spectrum was fit simultaneously.

calculations were done in the average-of-configuration mode for initial state vacancy configurations L^1M^0, L^1M^1, L^1M^{16} (*LM* transitions only), L^1M^{17}, and L^1M^{18} (*LN* transitions only). Spectator vacancies and electrons, if present, were distributed statistically over *M* subshells and the calculations were performed for all contributing configurations simultaneously. Reference values of transition energies for other degrees of *M*-shell ionization were obtained from the calculated values by interpolation using a cubic polynomial. In all the calculations, ground state configurations were assumed for the outer shells in the initial state. Therefore, in a simple description, the obtained reference values represent the lowest possible satellite energies, which would have to be corrected only for outer-shell ionization effects. However, due to the uncertainties in the MCDF calculations and the outer-shell vacancy configuration distributions, it was simply assumed that the satellite peak centroids could be parametrized as linear functions of the calculated reference energies, so that for each transition j and given n_M,

$$(E^j_{nM})_{\text{observed}} = (E^j_{nM})_{\text{calculated}} + \Delta E^j + n_M \times b^j \,. \qquad (2)$$

The values of ΔE^j and b^j were optimized in the fitting procedure. To simplify the fit even further, it was assumed that the constants ΔE^j and b^j are the same for $L\alpha_2$, $L\alpha_1$, and $L\beta_6$, for $L\beta_{15}$ and $L\beta_2$, for $L\beta_1$ and $L\eta$, and for $L\beta_4$ and $L\beta_3$ transitions.

For each transition, the relative numbers of counts in the satellite peaks as a function of n_M were assumed to follow a binomial distribution. This is a simplifying, yet reasonably good, approximation derived from the independent electron approximation model [3]. Assuming that (a) the corrections due to *M*-vacancy rearrangement between the time of collision and the time of *L* x-ray emission are negligible and (b) the effective fluorescence yield does not depend significantly on n_M, the probability parameter of the binomial distribution can be interpreted as the average *M*-electron ionization probability in *L*-shell

ionizing collisions (p_M). To simplify the analysis, the value of p_M was assumed to be the same for all transitions involving the same L subshell, but otherwise different. It should be noted that the binomial distributions are relatively narrow, so that only a few adjacent satellite peaks account for a large majority of counts in the distribution.

Relative intensities of the peaks due to transitions to the same L subshell were kept fixed at their theoretical values [4]. This was done for the diagram x rays as well as for the satellites. Contributions to the spectra due to multiple L ionization were found to be small in all cases studied here (see Fig. 2). Consequently, they were described with much less sophistication. Namely, it was assumed that the satellites corresponding to $n_L > 0$ could be described in the same way as those corresponding to $n_L = 0$, only scaled down in intensity. The same scaling factor was applied to all peaks corresponding to the same value of n_L. The best value of the scaling factor was determined from the fit. Associated energy shifts for $n_L = 1$ were estimated by first determining the corresponding reference energies using the MCDF program [2] and a method similar to that described above for $n_L = 0$, and then calculating the corresponding differences. These shifts were assumed to be exactly twice as large for the satellites corresponding to $n_L =$

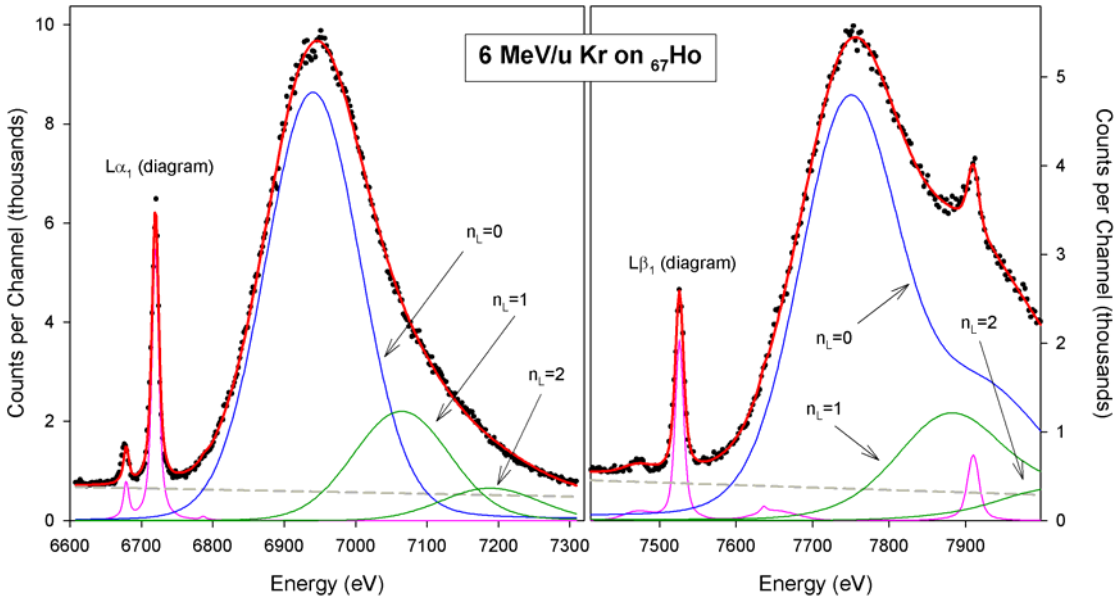

Figure 2. Spectrum of Ho L x rays emitted under bombardment by 6 MeV/u Kr ions. Solid circles represent the measured data points, while solid lines represent the overall fit, combined contributions from the satellites for all values of n_M (shown separately for different values of n_L, as indicated) and combined contribution from the peaks due to diagram x rays.

2.

[1] A. N. Perumal, V. Horvat, R. L. Watson, and Y. Peng, *Progress in Research*, Cyclotron Institute, Texas A&M University (2002-2003) , p.IV-11.

[2] J. P. Desclaux, Comp. Phys. Commun. **9**, 31 (1975).

[3] J. H. McGuire and P. Richard, Phys. Rev. A **9**, 1374 (1973).

[4] J. H. Scofield, At. Data Nucl. Data Tables **14**, 122 (1974).

Scaling Properties of Target Electron Ionization Probability in Near-Central Collisions with Fast Heavy Ions

V. Horvat, R. L. Watson, A. N. Perumal, and Yong Peng

Spectra of *L* x rays emitted from Ho targets and *K* x rays emitted from Co, Ni, and Cu targets under bombardment by 6 MeV/u C, Ne, Ar, and Kr ions were measured in high resolution using a curved crystal spectrometer. The goal of the experiment was to study the effects of multiple ionization on Ho *L* x-ray spectra as a function of the projectile atomic number (Z_1) and to compare them with the effects of multiple ionization on the spectra of *K* x rays having comparable transition energies. Specifically, the *L* x-ray spectra of Ho were analyzed in order to determine the *M*-shell ionization probability per electron in *L*-shell ionizing collisions (p_M), while the *K* x-ray spectra of Co, Ni, and Cu were analyzed in order to determine the *L*-shell ionization probability per electron in *K*-shell ionizing collisions (p_L). Details of the analysis are presented in the preceding report [1]. The results are presented in Table 1.

Table 1. *M*-shell ionization probability per electron in *L*-shell ionizing collisions (p_M) for Ho and *L*-shell ionization probability per electron in *K*-shell ionizing collisions (p_L) for Co, Ni, and Cu at 6 MeV/u.

Target	Projectile			
	C	Ne	Ar	Kr
Ho	0.063 ± 0.002	0.125 ± 0.005	0.269 ± 0.010	0.435 ± 0.069
Co	0.105 ± 0.002	0.245 ± 0.006	0.359 ± 0.002	0.474 ± 0.005
Ni	0.092 ± 0.002	0.205 ± 0.002	0.351 ± 0.003	0.480 ± 0.006
Cu	0.084 ± 0.003	0.216 ± 0.003	0.346 ± 0.003	0.483 ± 0.006

The same results are also shown in Figure 1, in which the ionization probabilities per electron obtained in the analysis (p_M for Ho and p_L for Co, Ni, and Cu) are plotted as a function of Z_1/n, where n is the principal quantum number of the ionized electron (n = 3 for the p_M data points and n = 2 for the p_L data points). The solid line is the best-fit logistic curve for all the points in the plot. This curve appears to represent a universal function for *L*- and *M*-shell ionization probabilities per electron in near-central collisions.

The above observations are consistent with the geometrical model [2], which predicts that ionization probabilities can be described rather accurately by a function of the universal variable X, where

$$X = (1 / n)\,(Z_1 / v_1)\,V\,[G(V)]^{1/2}\,, \qquad (1)$$

and

$$V = v_1 / v_2\,. \qquad (2)$$

In the expressions above, Z_1 and v_1 are the (effective) atomic number and the speed of the projectile, while v_2 and n are the (effective) average orbital speed and the principal quantum number of the ionized target electron. Function G is the universal inner-shell ionization function in the binary encounter approximation (BEA) [3].

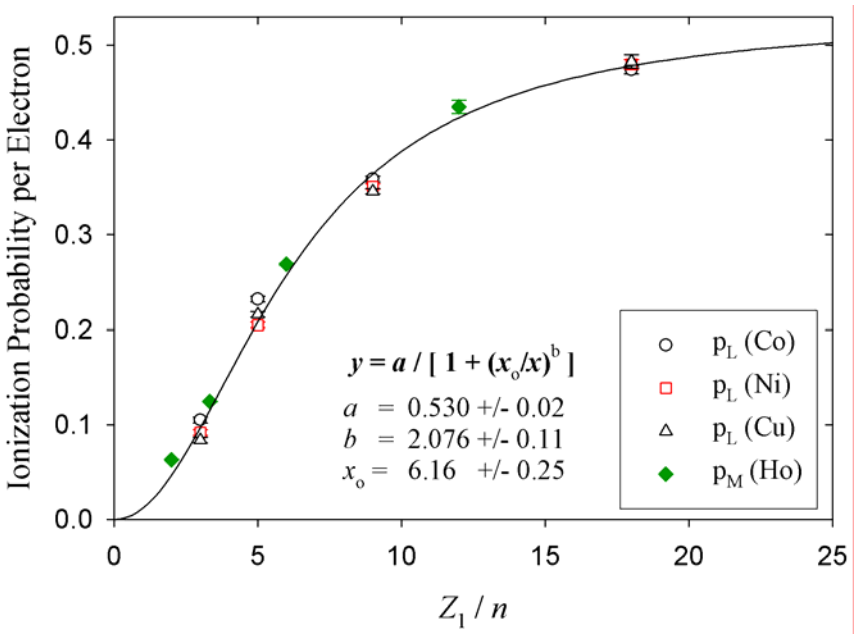

Figure 1. Ionization probability per electron in near-central collisions at 6 MeV/u as a function of the projectile atomic number (Z_1) divided by the principal quantum number of the ionized electron (n).

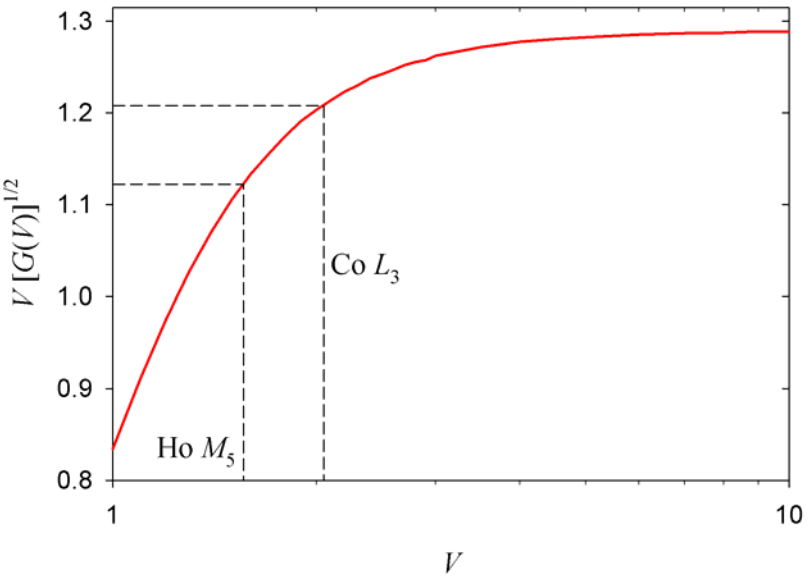

Figure 2. Plot of V $[G(V)]^{1/2}$ as a function of V, where V is the (effective) speed of the projectile divided by the (effective) average orbital speed of the ionized target electron. Function G is the universal inner-shell ionization function in the binary encounter approximation, as tabulated in Ref. 4.

It should be noted that within the geometrical model there is a variety of options for calculating the various parameters. Consequently, results of the calculations may vary based on the chosen approach and the assumptions made. In this work X was calculated using the unscreened projectile nuclear charge for Z_1 and the incident projectile speed for v_1. Furthermore, v_2 was determined from experimental values of the electron binding energies in neutral atoms, while G was calculated using the analytical formula of Gerjuoy, Vriens, and Garcia, as tabulated in Ref. 4. In this approach, v_1 has the same value in all four cases studied here (15.5 au), while v_2 ranges effectively from 7.56 au (for Co L_3 electrons) to 9.95 au (for Ho M_5 electrons). In the corresponding range of V (1.56 to 2.05), the function $V\,[G(V)]^{1/2}$ varies by only 8%, as shown in Figure 2. This is why in Figure 1 there is no noticeable dependence of the ionization probability per electron on v_2.

[1] V. Horvat, R.L. Watson, A.N. Perumal, and Y. Peng, *Progress in Research*, Cyclotron Institute, Texas A&M University (2003-2004), p. IV-3.

[2] B. Sulik, I. Kádár, S. Ricz, D. Varga, J. Végh, G. Hock, and D. Berényi, Nucl. Instrum. Methods Phys. Res. B **28**, 509 (1987).

[3] J. S. Hansen, Phys. Rev. A **8**, 822 (1973).

[4] J. H. McGuire and P. Richard, Phys. Rev. A **9**, 1374 (1973).

Projectile Charge Dependence of Electron Capture and Loss Cross Sections for Uranium Ions in Collisions with Ar

A. N. Perumal, K. S. Fruchey, R. L. Watson, V. Horvat, and Y. Peng

Cross sections for electron capture and loss are the fundamental parameters needed to describe how the charge distributions of energetic ions evolve as they travel in matter. In the present work, single and multiple electron loss and capture cross sections were measured for 3.5 MeV/u U^{q+} (q = 28, 31, 33, 39, 42, and 51) in collisions with argon target atoms. The cross sections were determined using the well-known growth rate method [1]. Charge fractions were measured for each contributing charge state and plotted against target thickness, which is the product of atom density and the effective length of the gas cell. The cross sections were then extracted from the linear terms of second order polynomials that were fit to the measured growth curves.

The measured cross sections are plotted in Fig. 1 as a function of charge change (Δq) for up to 13 electrons. Positive Δq is for loss and negative Δq is for capture. The loss cross sections show an overall decline with increase of Δq as well as with the incident projectile charge (q). It also appears that the loss cross sections decline rather steeply when the projectile charge state is larger than 37, which is the corresponding average equilibrium charge for uranium ions in argon. On the other hand, the capture cross-sections generally increase with projectile initial charge but decrease sharply with Δq. In addition, the multiple capture cross sections increase as a function of q faster than those for single electron capture.

Multiple electron loss is a highly probable outcome of heavy ion - heavy atom collisions when the

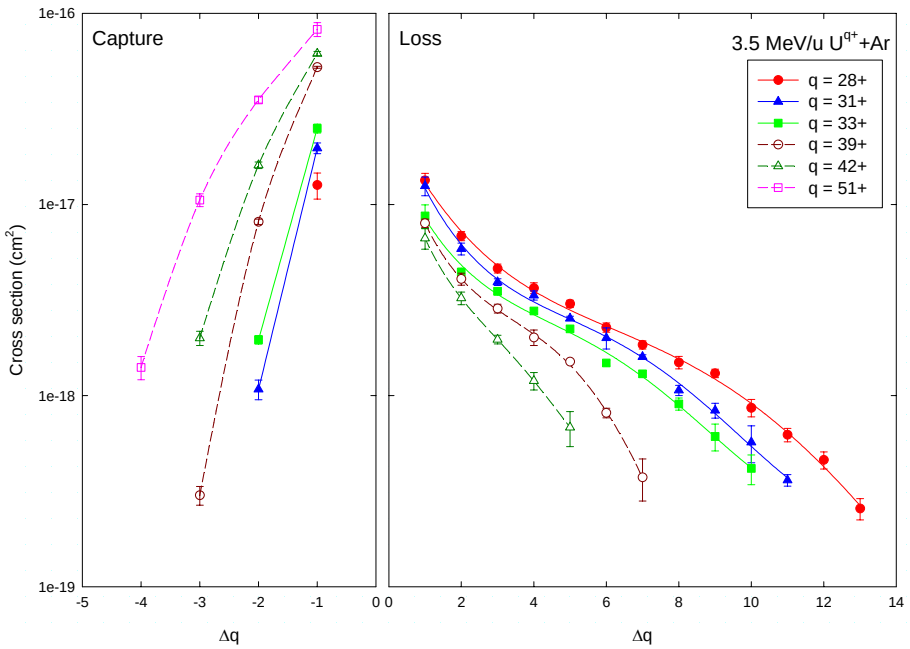

Figure 1. Projectile incident charge dependence of single and multiple electron capture and loss cross-sections for 3.5 MeV/u uranium ions in collision with argon gas. The cross sections are plotted as a function of charge change (Δq). The error bars are due to the statistical uncertainties only.

incident charge of the projectile is below its average equilibrium value. This feature is very well supported by the present results. The cross sections for double electron loss are only ~50% smaller than those for single electron loss, while the total cross section for the loss of more than one electron is ~2 times the single loss cross section. This high probability of multiple electron loss has a profound influence on the charge state evolution of the projectile since higher stages of ionization can be readily achieved in a single collision rather than proceeding through a sequence of single electron removal steps.

Another interesting feature, a change of slope in the electron loss cross section as a function of Δq, has been reported earlier and convincingly explained to be due to the sequential removal of the most weakly bound outermost electrons (shell effect). The onset of the change in slope appears to correlate with the removal of electrons from the next innermost subshell of the projectile [2,3]. In the present case, the outermost orbitals are $4f^8$, $4f^5$, $4f^3$, $5p^5$, $5p^2$, and $4d^7$ for the corresponding uranium projectile charge states 28+, 31+, 33+, 39+, 42+, and 51+, respectively. Slope changes are therefore anticipated in the electron loss cross sections at Δq = 8, 5, 3, 5, 2, and 7 for the corresponding incident charge states. However, the observed effect in the present case is rather small. The absence of strong outer shell effects may be due to contributions from inner shell ionization, which is expected to increase as the projectile energy increases. Besides, the electron binding energies of the outermost orbitals differ very little and therefore the shell effects are not expected to be very large.

[1] H. Tawara and A. Russek, Rev. Mod. Phys. **45**, 178 (1973).

[2] H. Knudsen, C.D. Moak, C.M. Jones, P.D. Miller, R.O. Sayer, G.D. Alton, and L.B. Bridwell, Phys. Rev. A **19** , 1029 (1979).

[3] R.D. Dubois, A.C.F. Santos, R.E. Olson, Th. Stöhlker, F. Bosch, A. Bräuning-Demian, A. Gumberidze, S. Hagmann, C. Kozhuharov, R. Mann, A. Oršić Muthig, U. Spillmann, S. Tachenov, W. Barth, L. Dahl, B. Franzke, J. Glatz, L. Gröning, S. Richter, D. Wilms, A. Krämer, K. Ullmann, and O. Jagutzki, Phys. Rev. A **68**, 042701 (2003).

Average Charge of 3.5 MeV/u Uranium Ions in Ar Gas

V. Horvat, R. L. Watson, A. N. Perumal, and Yong Peng

The charge distribution of an ion traveling in matter depends on its incident energy and charge, as well as the distance it travels inside the medium. It can be described in terms of the rate equations

$$\frac{dF_k}{d\pi} = \sum_{j=0}^{Z_1} (F_j \sigma_{jk} - F_k \sigma_{kj}) \qquad (j, k = 0, 1, \ldots, Z_1), \qquad (1)$$

where F_k is the fraction of ions with charge k, σ_{jk} is the cross section for charge change from j to k in a single collision, and π is the target thickness expressed in atoms/cm^2. Here the indices j and k assume all integer values from zero to Z_1, the projectile atomic number. If all the cross sections σ_{jk} are known, the charge fractions F_k can be determined from Eq.(1) in a straightforward way. However, in a typical situation, only a limited number of the cross sections can be measured directly. The remaining cross sections need to be estimated.

As a rule of thumb, cross sections for charge change should be measured for projectile incident charge q ranging from q_{min} to q_{max}, where q_{min} is the projectile incident charge at which electron capture cross sections ($j < k$) are too small to be measured and q_{max} is the projectile incident charge at which electron loss cross sections ($j > k$) are too small to be measured. In that case, Eq.(1) is expected to accurately describe all charge fractions F_q for q between q_{min} and q_{max} and the cross sections σ_{jk} for j or k greater than q_{max} or less than q_{min} are irrelevant.

Typically, the cross sections for charge change depend smoothly on the number of electrons captured or lost. In that case, they do not need to be measured for every projectile incident charge q between q_{min} and q_{max}, since the missing cross section values can be estimated with good accuracy by interpolation. Furthermore, if the range of available projectile incident charges does not extend all the way to q_{min} or q_{max}, the values of corresponding cross sections for charge change can be estimated by extrapolation. The accuracy of this extrapolation is not critical for determination of the projectile average charge if the corresponding charge fractions remain small.

Cross sections σ_{jk} were measured for uranium ions in argon gas [1] in order to determine the target thickness dependence of the projectile average charge. Projectile incident charges 28+, 31+, 33+, 39+, 42+, and 51+ were used in these experiments. It was found that q_{max} ~ 51+, while q_{min} was estimated to be 22+. The missing cross sections were determined using linear

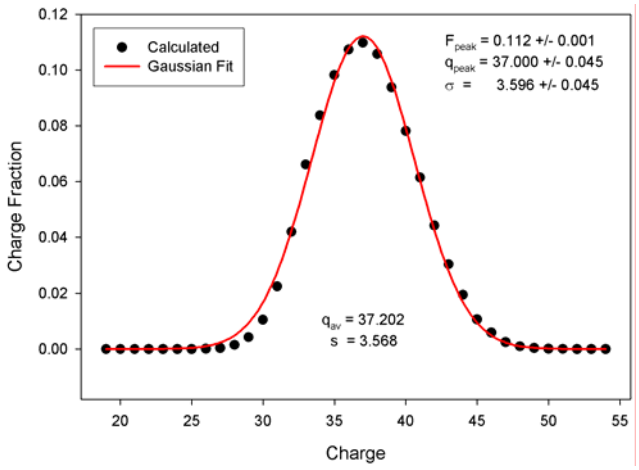

Figure 1. Calculated equilibrium charge distribution of 3.5 MeV/u U ions in Ar gas.

interpolation and extrapolation. This simple procedure proved to be adequate for this purpose as an alternative to the more elaborate method described previously [2].

Using the method described above, the average equilibrium charge q_{eq} of 3.5 MeV/u U ions in Ar gas was found to be 37.2. This result is in agreement with the results obtained using other methods, such as those described in Ref. 2. Shown in Figure 1 is the predicted equilibrium charge distribution. The data points were fitted with a Gaussian curve in order to emphasize a small asymmetry in the charge distribution manifested as a tail on the high charge-state side. The best-fit Gaussian curve was found to have a centroid 0.2 charge units below the average equilibrium charge q_{eq} determined by the data points. The distribution width (variance) was found to be 3.6 charge units in both cases.

The average charge q_{av} of 3.5 MeV/u U ions in Ar gas was also determined as a function of target thickness and projectile incident charge q using the method described above. Results for q = 22+ (q_{min}), 32+, 36+, 37+, 38+, 43+, and 51+ (q_{max}) are shown in Figure 2. A striking feature is that q_{av} approaches its equilibrium value q_{eq} along an almost pure exponential curve (i.e. almost a straight line in the semi-log plot). Furthermore, its "decay constant" λ (i.e. absolute value of the slope in the semi-log plot) does not depend significantly on the projectile incident charge. As may be seen in Figure 2, the thickness at which $|q_{av} - q_{eq}| = 0.1$, designated as $d_{0.1}$, does depend on the projectile incident charge q. Figure 3 shows how $d_{0.1}$ varies with q. The value of $d_{0.1}$ ranges roughly from 3 μg/cm^2 for q = 37+ (incident charge closest to q_{eq}) to 23 μg/cm^2 for q = 51+ (q_{max}) and q = 22+ (q_{min}). It can be estimated using the formula $d_{0.1}$ = 10.6 μg/cm^2 × (log $|q-q_{eq}|$ +1).

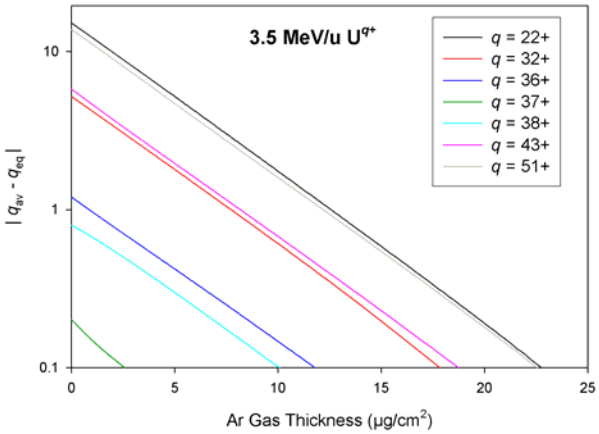

Figure **2.** Absolute difference between the average charge and its equilibrium value as a function of target thickness for 3.5 MeV/u U ions in Ar gas.

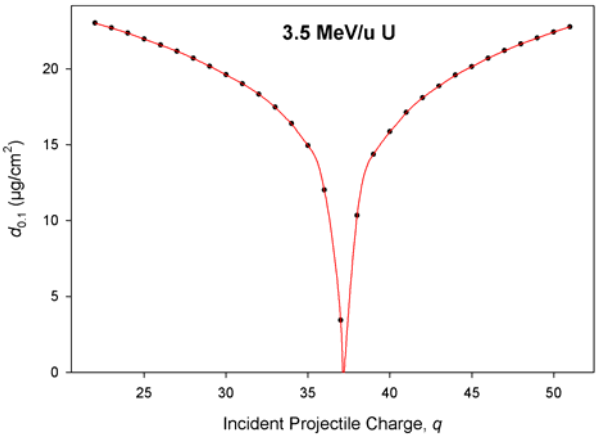

Figure 3. Target thickness at which the average charge approaches its equilibrium value within 0.1 charge units as a function of projectile incident charge for 3.5 MeV/u U ions in Ar gas.

[1] A.N. Perumal, R.L. Watson, V. Horvat, and Y. Peng, *Progress in Research*, Cyclotron Institute, Texas A&M University (2003-2004), p. IV-9.

[2] V. Horvat, R.L. Watson, K.E. Zaharakis, and Y. Peng, Nucl. Instrum. Methods Phys. Res. B **211**, 495 (2003).

Density Effect of Swift Heavy Ions Passing Through Gaseous and Solid Targets

A. N. Perumal, K. S. Fruchey, R. L. Watson, V. Horvat, and Y. Peng

It is well known that the density of the target medium influences the distribution of charge states of the emerging projectile ions. This, so called density effect, stems from the collision frequencies. As the target density increases, the time between collisions becomes shorter than the lifetimes of the projectile excited states and therefore some of the projectile ions enter subsequent collisions with their electrons still in excited states. As a consequence, the evolution of the various charge states within the target will differ from that in a dilute gas since the cross sections that describe this evolution are changed. The objective of the present work is to extend the investigation of the density effect on the average equilibrium charge of uranium and xenon ions in gaseous and solid targets to higher energies in order to further delineate the projectile energy dependence of the gas-solid effect.

Charge distributions have been measured for 3.5 MeV/u uranium ions passing through an argon gas target as a function of pressure and incident charge state. Charge changing cross sections were then determined by the growth rate method [1]. The average equilibrium charge in Ar gas was estimated using a newly proposed method [2] which relies only on the charge changing cross sections for a few projectile charge states. Further, to compare the equilibrium charge in a gas with that produced by a solid target, the charge distributions of uranium ions emerging from solid carbon targets were also measured. The average equilibrium charge for solid carbon was then determined by plotting the average charge as a function of target thickness.

The measured average equilibrium charges for 3.5 MeV/u uranium ions in argon and carbon are 37.4 and 52.5, respectively. The difference between these two targets is ~15.1 charge units, an increase of 40% from gas to solid, which may be attributed to the density effect. In Fig. 1(a), the average equilibrium charges of uranium ions from the present measurements and those obtained by other investigators [3-6] are plotted as a function of incident energy. The average equilibrium charges calculated using the semiempirical formulas of Schiwietz and Grande (SG) [7] also are shown for comparison. The energy dependence of the density effect is clearly observed from the vertical separation between the two data groups. The average equilibrium charges estimated using the SG formulas agree reasonably well with the experimental values for argon and carbon targets with the largest discrepancy being approximately 20% at the lowest energy of 0.01 MeV/u.

The average equilibrium charge of 2 MeV/u Xe ions in collisions with nitrogen gas was also estimated [2] and plotted in Fig. 1(b) along with other available results as a function of projectile energy. Since there are no experimental results for xenon ions, iodine data [6] have been used for comparison. A substantial density effect is in evidence for xenon/iodine ions similar to that observed in the case of uranium. The SG formula reproduces the results well for nitrogen with the maximum discrepancy of 6% at 2 MeV/u. However, for carbon it underestimates the experimental results throughout the energy range.

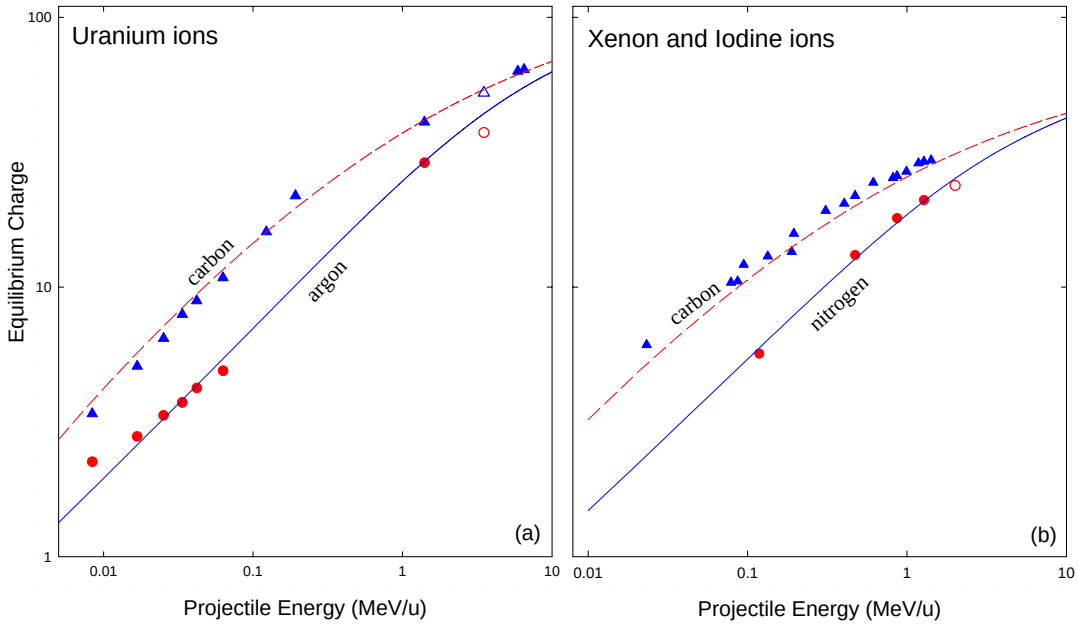

Figure 1. Average equilibrium charges plotted as a function of projectile energy. (a) Uranium ions in C and Ar (b) Xenon and iodine ions in C and N_2. The open and closed symbols represent the present and available experimental results [3-6], respectively. The solid and dashed lines are the average equilibrium charges, calculated using Schiwietz and Grande's semiempirical formulas [7] for gaseous and solid targets.

[1] R.E. Olson, R.L. Watson, V. Horvat, and K.E. Zaharakis, J. Phys. B **35** (2002) 1893.

[2] V. Horvat, R.L. Watson, K.E. Zaharakis, and Y. Peng, Nucl. Instrum. Methods Phys. Res. B **211** (2003) 495.

[3] M.D. Brown, Phys. Rev. A **6**, 229 (1972).

[4] B. Wittkower and H. Betz, Phys. Rev. A **7**, 159 (1973).

[5] H. Geissel, Y. Laichter, W.C.F. Schneider, and P. Armbruster, Phys. Lett. A **99**, 77 (1983).

[6] H.D. Betz, Rev. Mod. Phys. **44**, 465 (1972).

[7] G. Schiwietz and P.L. Grande, Nucl. Instrum. Methods Phys. Res. B **175**, 125 (2001).

Electron Capture Cross Sections from Ar Atoms to Inner Shells of Ar^{q+} Ions at 10 MeV/u

A. N. Perumal, V. Horvat, R. L. Watson, and Y. Peng

Electron capture, excitation, and ionization are among the most important inelastic processes in ion-atom collisions. At intermediate velocities, where the projectile velocity (v_p) is approximately equal to the orbital velocity of the active electron (v_e), the strengths of these processes are of the same order of magnitude and coupling among these different channels makes the problem very cumbersome to describe theoretically. However, depending on the symmetry parameter (Z_1/Z_2) of the collision system, where Z_1 and Z_2 are the projectile and target atomic numbers, respectively, the electron transfer channel can be much larger than the others. Of current interest are the state selective electron transfer cross sections involving deeply bound initial and final states in strong perturbative collisions.

In the present work, single electron capture cross sections have been measured for 10 MeV/u Ar ions colliding with Ar gas as a function of the projectile incident charge (q). The projectile charge fractions were measured by the method of beam deflection after passing through a gas cell containing Ar gas at different pressures ranging from 0 to 64 mTorr. The single capture cross section for each of the charge state was then determined by the growth curve method [1].

The measured single electron capture cross-sections are plotted in Fig. 1 as a function of projectile charge (q). They increase with increasing projectile charge. A sudden change in slope however,

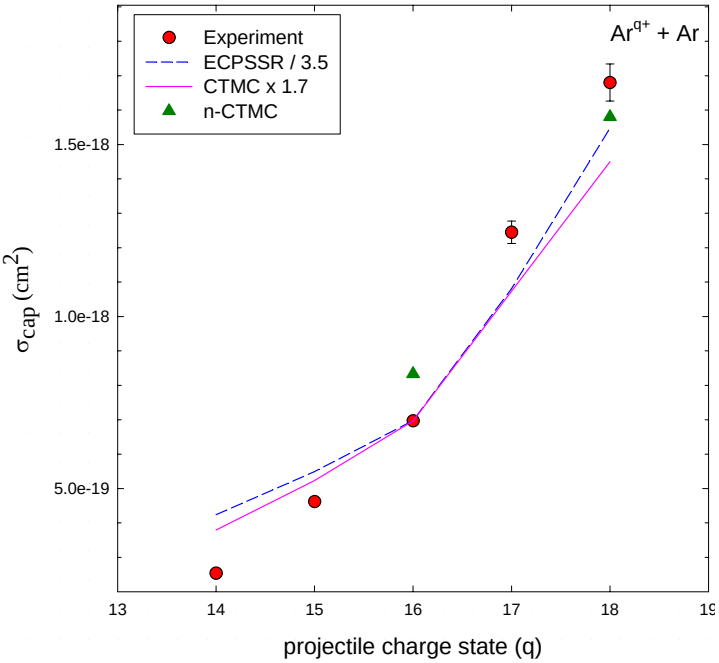

Figure 1. Single electron capture cross sections for 10 MeV/u Ar ions colliding with Ar gas as a function of incident projectile charge. Note that the ECPSSR and CTMC cross sections are scaled by a factor of 3.5 and 1.7 respectively. The error bars are due to statistical uncertainties only.

is noticed for H- like or bare projectiles. This distinct feature is caused by the opening of the projectile K-shell to electron capture from the target.

The single electron capture cross sections are compared with the ECPSSR theory [2] and with classical trajectory Monte Carlo (CTMC) calculations [3] in Fig. 1. The trend of the charge dependence is very well reproduced both by ECPSSR and CTMC calculations. However, the absolute values differ by a factor of 3.5 and 1.7, respectively. It is to be noted that, the ECPSSR theory is normally suitable for asymmetric systems and the CTMC method employed here does not take all the interactions between the collision partners into consideration. Preliminary calculations based on the more sophisticated n-body CTMC method [1], which takes into account all the interactions between the interacting bodies, including the electron-electron interaction, are also shown in Fig. 1. The n-CTMC results are in good agreement with the measured data on an absolute scale.

Capture to different inner shells of the projectile has also been estimated from the charge dependence of single electron capture cross sections. For instance, capture to the K-shell was determined from the difference of cross sections for projectiles with and without a K-vacancy. This cross section was found to be $\sim 4.9 \cdot 10^{-19}$ cm^2. In the same way, the cross section for capture to the L-shell was estimated from the difference of cross sections with and without an L-vacancy in the projectile and it was $\sim 2.2 \cdot 10^{-19}$ cm^2.

It is important to note here that capture to the projectile K-shell stems not only from the K-shell of the target but also from the outer L and M shells. In the present case, however, the direct K-K (i.e., from the K shell of the target to the K shell of the projectile) capture channel is the dominant one since the projectile energy of the argon ion matches approximately with the target K-shell binding energy.

Similar measurements for different target-projectile species, and projectile energies are presently underway in order to obtain a detailed description of the problem.

[1] R.E. Olson, R.L. Watson, V. Horvat, and K.E. Zaharakis, J. Phys. B **35**, 1893 (2002).
[2] W. Brandt and G. Lapicki, Phys. Rev. A **23**, 1717 (1981).
[3] R.E. Olson, A. Salop, Phys. Rev. A **16**, 531 (1977).

SECTION V

SUPERCONDUCTING CYCLOTRON AND INSTRUMENTATION

K500 Operations and Development

D. P. May, G. J. Kim, H. L. Clark, F. P. Abegglen, G. J. Derrig, and W. H. Peeler

Introduction

During the 2003-2004 reporting period a total of 63 different beams, including 27 newly developed beams, were used for experiments. There were a total of 118 beam tunings not counting multiple tunes of beams for the SEE program. The SEE program will be treated separately.

Ion Sources

Two years ago a gradual degradation in the performance of ECR1 was correlated with a damaged area near the middle of one of the hexapole bars. First noticed in January of 2002 as a melting in the aluminum wall of the plasma chamber, the area corresponded to a dip in the nominal 5 kilogauss hexapole wall-field to 3.9 kilogauss. The original measurements on the hexapole, made in 1995, show a dip to 4.3 kilogauss at this position.

This area was measured again in January of 2003 and was found to have not gotten worse, probably because higher microwave powers were no longer being used. In January of 2004 the bar was replaced with the new one that had been assembled several months before. To do this the plasma chamber had to be pulled from the yoke and mounted on the hexapole-assembly device that had been used for ECR2. The bar was pulled from the chamber radially using the force of attraction between the NdFeB bar and a steel bar attached to the assembly. The field strength in the middle of the bar had declined to just below the ECR resonance at 2.3 kilogauss as measured on the face of the magnets.

Cyclotron Beams

Of the newly developed beams, those of platinum and ytterbium are of note. These elements were sputtered into the ECR1 ion source.

Operations

For the period April 1, 2003 through March 31, 2004, the operational time is summarized in Table I, while Table II lists how the scheduled time was divided. There were no major repairs except an unsuccessful one to ECR2 to try to repair the small water leak in its plasma chamber.

Table 1. 2003-2004 Operational Time.

Time	Hrs.	%Time
Beam on target	4967.50	**65.6**
Tuning, optics, set-up	994.0	**13.1**
Beam development	698.25	**9.2**
Scheduled maint.	163.75	**2.2**
Unscheduled maint.	468.0	**6.2**
Idle time	281.5	**3.7**
Cool down	0.00	**0.0**
Total	**7573.00**	**100.0**

Table 2. Scheduled Beam Time.

Time	Hrs.	%Time
Nuclear physics	1223.75	**17.2**
Nuclear chemistry	2669.75	**37.4**
Atomic physics	586.00	**8.2**
Outside collaboration	0.0	**0.0**
Outside users	1992.25	**27.1**
Beam development	722.25	**10.1**
Total	**7131.00**	**100.0**

Radiation Effects Facility

H. L. Clark, V. Horvat, B. Hyman, and D. Utley

The activity of the Radiation Effects Facility (REF) decreased over the previous reporting year. In this reporting period, the facility was used for 1474 hours, which is a ~20% decrease over the 1851 hours used in the 2002-2003 reporting period. Users of the facility (and hours used) over the past year were: NASA GSFC (278), NASA JPL (203.5), Boeing Satellite Systems (120.25), Harris (80.25), International Rectifier (74), BAE Systems (73), Innovative Concepts (68), Xilinx (65.75), Maxwell Technology (61.5), General Dynamics (48.5), United Space Alliance (48), NAVSEA (46.75), Raytheon (45.5), Mission Research Corp. (40), Prairie View A&M University (38), Mitsubishi (33.5), Radiation Assured Devices (29.25), Northrop Grumman (24.25), Sandia National Lab (23.50), Ball Aerospace (20.25), Lockheed Martin (15), Aeroflex UTMC (14.50), SEAKR (13) and Honeywell (9.5). Northrop Grumman and Radiation Assured Devices were new customers of the facility.

Table 1. Radiation Effects Facility usage by commercial and government customers for this and previous reporting years.

Reporting Year	Total Hours	Commercial Hours (%)	Government Hours (%)
2003-2004	1474	785 (53%)	689 (47%)
2002-2003	1851	1242 (67%)	609 (33%)
2001-2002	1327	757 (57%)	570 (43%)
2000-2001	1500	941 (63%)	559 (37%)
1999-2000	548	418 (76%)	131 (24%)
1998-1999	389	171 (44%)	218 (56%)
1997-1998	434	210 (48%)	224 (52%)
1996-1997	560	276 (49%)	284 (51%)
1995-1996	141	58 (41%)	83 (59%)

Table I compares the facility usage by commercial and government customers. The ratio from this reporting year (53% to 47%) is similar to the trend seen in the 2001-2002 reporting period. The number of commercial hours decreased by ~450 while the number of government hours increased by ~100. Much of the testing conducted at the facility has been for defense systems by both government and commercial agencies. It is expected that the facility will continue to be as active in future years.

Table 2. Beams used and the number of times requested for this reporting year and previous years. 324 beams were run this year.

Particle Type	A MeV	Requests 2000-01	Requests 2001-02	Requests 2002-03	Requests 2003-04
^{20}Ne	15	1	13	19	15
^{40}Ar	"	4	24	43	46
^{63}Cu	"	N/A	N/A	5	14
^{84}Kr	"	6	26	55	47
^{109}Ag	"	N/A	N/A	6	18
^{129}Xe	"	5	18	43	51
^{141}Pr	"	N/A	N/A	2	2
^{165}Ho	"	3	11	17	7
^{181}Ta	"	4	5	4	3
^{197}Au	"	12	9	23	34
^{22}Ne	25	27	13	19	6
^{40}Ar	"	31	20	32	16
^{84}Kr	"	32	20	35	26
^{129}Xe	"	25	18	24	15
H-D	40	1	8	10	4
^{20}Ne	"	5	3	5	6
^{40}Ar	"	12	8	10	7
^{78}Kr	"	13	9	6	5
Total		192	207	360	324

Table II lists the beams used this year and the number of times each was requested. In total, 342 beams were run this year, which is almost 10% less than the previous year. 40A MeV ^{12}C and 25A MeV ^{16}O were developed for detector tests. No new beams were added to SEELine users list.

Cyclotron Computing

R. Burch, K. Hagel, and M. Vasilyev

In continuing to strive to supply the Institute with the necessary computational power it requires, we installed two new computational servers and reallocated two old computational servers to non computational intensive administrative tasks. Currently there are three high performance machines available for general lab computational usage. We are building a dedicated file server which will house all home, data, and scratch drives that we manage. The file server will utilize Fermi-Linux since Red Hat Linux is no longer available. The file server will utilize the journaling file-system JFS to improve reliability and recovery speed and house a tape-less backup system. The file server is being developed in parallel with it's DRP (Disaster Recovery Plan). In addition, we upgraded all servers under our management to Red Hat Linux 7.3 or higher and switched to NFS v3, yielding a performance increases for users who use the computational servers with remotely mounted disks.

An important aspect of the Institutes computational infrastructure is our LAN (local area network.) We enhanced our networking capabilities by adding a Gigabit backbone switch capable of feeding 12 Gigabit switches. We currently have 6 switches feeding the backbone switch at Gibabit speed. To aid in continued operation and accessibility, all computational and administrative (AAA, DNS/DHCP, Backup) computers and all network switches are on UPS's (Uninterpretable Power Supplies).

Security has become a pressing requirement for our safe coexistence within the University and the Internet in general. In order to straighten our security posture, we continue to add servers to our Kerberos /LDAP strong encryption password based AAA (Authentication, Authorization, and Accounting) system. The AAA system is running in full production mode with Primary and Fail-over servers that supply the lab with continuous AAA services. We added "Research Group Server Cluster" capability to our AAA system. Any research group may request that we manage their AAA. This service allows group user access to these managed servers using their email password and access is restricted to users in their research group, or additional users at their request. We implemented automatic password expiration, password expiration notification via email, and a password policy in accordance to TAC 202 (Texas Administrative Code 202), as well as other TAC 202 requirements, such as DRP's for servers. We have a DRP for the AAA computers, one for the computational servers and others are in progress.

We now have in production an Amanda based backup and recovery system for our computational servers and for any Linux machine that research groups may wish to add. The current policy for backup is: Research Groups may request backup of their home directories, but no data or system files systems. The computational and administrative machines are backup up in their entirety. The backup cycle is one Full backup per week, every second week is archived, and every third month is archived offsite at CIS.

We have implemented, a Trouble Ticket system where by any user may email helpdesk@comp.tamu.edu for any computer/LAN related issue. The trouble ticket system will generate an automated response and log the ticket in a database for us to act on.

[1] R.Burch *et al.*, *Progress in Research*, Cyclotron Institute, Texas A&M University (2000-2001), p.V-11.

SECTION VI

PUBLICATIONS

PAPERS PUBLISHED
April 1, 2003 – March 31, 2004

Isoscalar Multipole Strength in ^{110}cd and ^{116}Cd, Y.-W. Lui, D.H. Youngblood, Y. Tokimoto, H.L. Clark, and B. John, Phys. Rev. C **69**, 034611 (2004).

Isoscalar E0-E3 Strength in ^{116}Sn, ^{144}Sm, ^{154}Sm, and ^{208}Pb, D.H. Youngblood, Y.-W. Lui, H.L. Clark, B. John, Y. Tokimoto and X. Chen, Phys. Rev. C **69**, 034315 (2004).

Isoscalar Giant Dipole Resonance for Several Nuclei with A $\geqslant$ 90, Y.-W. Lui, X. Chen, H.L. Clark, B. John, Y. Tokimoto, and D.H. Youngblood, Nucl. Phys. **A731**, 28c (2004).

Isoscalar E0 Strength Between 6 and 11 MeV in ^{40}Ca, D.H. Youngblood, Y.-W. Lui, H.L. Clark,, Y. Tokimoto and B. John, Phys. Rev. C **68**, 057303 (2003).

Isoscalar Electric Multipole Strength in ^{12}C, Bency John, Y. Tokimoto, Y.-W. Lui, H.L. Clark, X. Chen, and D.H. Youngblood, Phys. Rev. C **68**, 014305 (2003).

Determination of the Astrophysical S Factor for ^{11}C(p,γ)^{12}N from the ^{12}N$\rightarrow^{11}$C+p Asymptotic Normalization Coefficient, X. Tang, A. Azhari, C.A. Gagliardi, A.M. Mukhamedzhanov, F. Pirlepesov, L. Trache, R.E. Tribble, V. Burjan, V. Kroha, F. Carstoiu, Phys. Rev. C **67**, 015804 (2003).

Capture Gamma Reaction Rates at Stellar Energies by the Asymptotic Normalization Coefficient Method, R.E. Tribble, A. Azhari, C.A. Gagliardi, A.M. Mukhamedzhanov, F. Pirlepesov, A. Sattarov, X. Tang, L. Trache, P. Bem, V. Burjan, V. Kroha, J. Novak, S. Piskor, E. Simeckova, J. Vincour and R. Carstoiu, Proceedings of Capture Gamma Spectroscopy 11, Pruhonice, Czech Republic, September, 2002, (World Scientific, Singapore, 2003) p. 298.

Asymptotic Normalization Coefficients in Nuclear Astrophysics, V. Kroha, A. Azhari, P. Bem, V. Burjan, C.A. Gagliardi, A.M. Mukhamedzhanov, J. Novak, S. Piskor, E. Simeckova, X. Tang, L. Trache, R.E. Tribble, and J. Vincour, Nucl. Phys. **A719**, 119c (2003).

Asymptotic Normalization Coefficients for ^{8}B$\rightarrow^{7}$Be+p from a Study of ^{8}Li$\rightarrow^{7}$Li+n, L. Trache, A. Azhari, F. Carstoiu, H.L. Clark, C.A. Gagliardi, Y.-W. Lui, A.M. Mukhamedzhanov, X. Tang, N. Timofeyuk, R.E. Tribble, Phys. Rev. C **67**, 062801 (2003).

Breakup of ^{8}B and the S_{17} Astrophysical Factor Reexamined, L. Trache, F. Carstoiu, C.A. Gagliardi and R.E. Tribble, Phys. Rev. C **69**, 032802(R) (2004).

New Results for $^{8}B(p,\gamma)^{9}C$, $^{11}C(p,g\ \gamma)^{12}N$, $^{13}C(p,\ \gamma)^{14}N$ and $^{14}N(p,\ \gamma)^{15}O$ at Stellar Energies, R.E. Tribble, A. Azhari, P. Bern, V. Burjan, F. Carstoiu, C.A. Gagliardi, V. Kroha, A.M. Mukhamedzhanov, J. Novak, F. Pirlepesov, S. Piskor, A. Sattarov, E. Simeckova, X. Tang, L. Trache, J. Vincour, Nucl. Phys. **A718**, 147c (2003).

Determination of the S_{17} and S_{18} Astrophysical Factors from the Breakup of ^{8}B and ^{9}C at Intermediate Energies, L. Trache, F. Carstoiu, C.A. Gagliardi, A.M. Mukhamedzhanov, R.E. Tribble, Nucl. Phys. **A718**, 493c (2003).

The $^{17}F(p,\ \gamma)^{18}Ne$ Direct Capture Cross Section, J.C. Blackmon, D.W. Bardayan, C.R. Brune, A.E. Champagne, R. Crespo, T. Davinson, J.C. Fernandes, C.A. Gagliardi, U. Greife, C.J. Gross, P.A. Hausladen, C. Iliadis, C.C. Jewett, R.L. Kozub, T.A. Lewis, F. Liang, B.H. Moazen, A.M. Mukhamedzhanov, C.D. Nesaraja, F.M. Nunes, P.D. Parker, D.C. Radford, L. Sahin, J.P. Scott, D. Shapira, M.S. Smith, J.S. Thomas, L. Trache, R.E. Tribble, P.J. Woods, C.H. Yu, Nucl. Phys. **A718**, 587c (2004).

High Precision Branching Ratio Measurement for the Superallowed β-Decay of ^{74}Rb: A Prerequisite for Exacting Tests of the Standard Mode, A. Piechaczek, E.F. Zganjar, G.C. Ball, P. Bricault, J.M. D'Auria, J.C. Hardy, D.F. Hodgson, V. Iacob, P. Klages, W.D. Kulp, J.R. Leslie, M. Lipoglavsek, J.A. Macdonald, H.-B. Mak, D.M. Moltz, G. Savard, J. von Schwarzenberg, C.E. Svensson, I.S. Towner and J.L.Wood, Phys. Rev. C **67**, 051305(R) (2003).

Beta Decay of ^{62}Ga, B.C. Hyman, V.E. Iacob, A. Azhari, C.A. Gagliardi, J.C. Hardy, V.E. Mayes, R.G. Neilson, M. Sanchez-Vega, X. Tang, L. Trache and R.E. Tribble, Phys. Rev C **68**, 015501 (2003).

High Precision Measurement of the Superallowed $0^{+} \rightarrow 0^{+}$ Decay of ^{22}Mg, J.C. Hardy, V.E. Iacob, M. Sanchez-Vega, R.G. Neilson, A. Azhari, C.A. Gagliardi,, V.E. Mayes, X. Tang, L. Trache and R.E. Tribble, Phys. Rev. Lett. **91**, 082501 (2003).

Beta Particles, J.C. Hardy, McGraw-Hill Encyclopedia of Science and Technology, ninth edition (2003).

The Use of Monte Carlo Calculations in the Determination of a Ge detector efficiency Curve, R.G. Helmer, J.C. Hardy, V.E. Iacob, M. Sanchez-Vega, R.G. Neilson and J. Nelson, Nucl. Instrum. Methods Phys. Res. A **511**, 360 (2003).

Superallowed 0^{+} To 0^{+} Beta Decay: Current Status and future Prospects, J.C. Hardy and I.S. Towner in Quark-Mixing, CKM-Unitarity, eds: H. Abele and D. Mund (Mattes Verlag, Heidelberg, 2003) p. 11.

Precise Efficiency Calibration of an HPGe detector Up To 3.5 MeV, with Measurements and Monte Carlo Calculations, R.G. Helmer, N. Nica, J.C. Hardy and V.E. Iacob, Int. J. Appl. Radiat. Isot. **60**, 173 (2004).

New Results in Superallowed Nuclear Beta Decay, J.C. Hardy, In Intersections of Particle and Nuclear Physics; 8th Conference CIPANP2003, ed: Zohreh Parsa, AIP Conference Proceedings **698** (2003) pg. 184.

A New Astrophysical γ Probe and Its Applications, H. Utsunomiya, H. Akimune, S. Goko, T. Hayakawa, Y.-W. Lui, H. Ohgaki, M. Ohta, T. Shizuma, H. Toyokawa, and T. Yamagata, Nucl. Phys. **A718**, 199 (2003).

Photodisintegration of Deuterium and Big Bang Nucleosynthesis, K.Y. Hara, H. Utsunomiya, S. Goko, H. Akimune, T. Yamagata, H. Toyokawa, K. Kubo, A. Uritani, Y. Shibata, Y.-W.Lui, and H. Ohgaki, Phys. Rev. D **68**, 072001 (2003).

Identified Particle Distributions in pp and Au+Au Collisions at $\sqrt{s_{NN}}$ = 200 GeV, J. Adams *et al.* (STAR Collaboration), Phys. Rev. Lett. **92**, 112301 (2004).

Azimuthal Anisotropy at RHIC: the First and Fourth Harmonics, J. Adams *et al.* (STAR Collaboration), Phys. Rev. Lett. **92**, 062301 (2004).

Δ^0 Production and Possible Modification in Au+Au and p+p Collisions at $\sqrt{s_{NN}}$ = 200 GeV, J. Adams *et al.* (STAR Collaboration), Phys. Rev. Lett. **92**, 092301 (2004).

Particle-Type Dependence of Azimuthal Anisotropy and Nuclear Modification of Particle Production in Au+Au Collisions at $\sqrt{s_{NN}}$ = 200 GeV, J. Adams *et al.* (STAR Collaboration), Phys. Rev. Lett. **92**, 052302 (2004).

***J/Ψ* Polarization in 800 -GeV p-Cu Interactions**, T.H. Chang, M.E. Beddo, C.N. Brown, T.A. Carey, W.E. Cooper, C.A. Gagliardi, G.T. Garvey, D.F. Geesaman, E.A. Hawker, X.C. He, L.D. Isenhower, D.M. Kaplan, S.B. Kaufman, D.D. Koetke, P.L. McGaughey, W.M. Lee, M.J. Leitch, J.M. Moss, B.A. Mueller, V. Papavassiliou, J.C. Peng, P.E. Reimer, M.E. Sadler, W.E. Sondheim, P.W. Stankus, R.S. Towell, R.E. Tribble, M.A. Vasiliev, J.C. Webb, J.L. Willis, and G.R. Young (FNAL E866/NuSea Collaboration), Phys. Rev. Lett. **91**, 211801 (2003).

Pion-Kaon Correlations in Central Au+Au Collisions at $\sqrt{s_{NN}}$ = 130 GeV, J. Adams *et al.* (STAR Collaboration), Phys. Rev. Lett. **91**, 262302 (2003).

Net Charge Fluctuations in Au+Au Collisions at $\sqrt{s_{NN}}$ = 130 GeV, J. Adams *et al.* (STAR Collaboration), Phys. Rev. C **68**, 044905 (2003).

Evidence from d+Au Measurements for Final-State Suppression of High-pT Hadrons in Au+Au Collisions at RHIC, J. Adams *et al.* (STAR Collaboration), Phys. Rev. Lett. **91**, 072304 (2003).

Three-Pion Hanbury Brown-Twiss Correlations in Relativistic Heavy-Ion Collisions from the STAR Experiment, J. Adams *et al.* (STAR Collaboration), Phys. Rev. Lett. **91**, 262301 (2003).

Transverse-Momentum and Collision-Energy Dependence of High-pT Hadron Suppression in Au+Au Collisions at Ultrarelativistic Energies, J. Adams et al. (STAR Collaboration), Phys. Rev. Lett. **91**, 172302 (2003).

Narrowing of the Balance Function with Centrality in Au+Au Collisions at $\sqrt{s_{NN}}$ = 130 GeV, J. Adams *et al.* (STAR Collaboration), Phys. Rev. Lett. **90**, 172301 (2003).

Measurement of the Absolute Drell-Yan Dimuon Cross Sections in 800 GeV/c pp and pd Collisions, C.A. Gagliardi, T.C. Awes, M.E. Beddo, M.L. Brooks, C.N. Brown, J.D. Bush, T.A. Carey, T.H. Chang, W.E. Cooper, G.T. Garvey, D.F. Geesaman, E.A. Hawker, X.C. He, L.D. Isenhower, D.M. Kaplan, S.B. Kaufman, P.N. Kirk, D.D. Koetke, G. Kyle, D.M. Lee, W.M. Lee, M.J. Leitch, N. Makins, P.L. McGaughey, J.M. Moss, B.A. Mueller, P.M. Nord, V. Papavassiliou, B.K. Park, J.C. Peng, G. Petitt, P.E. Reimer, M.E. Sadler, W.E. Sondheim, P.W. Stankus, T.N. Thompson, R.S. Towell, R.E. Tribble, M.A. Vasiliev, Y.C. Wang, Z.F. Wang, J.C. Webb, J.L. Willis, D.K. Wise, and G.R. Young (FNAL E866/NuSea Collaboration), Nucl. Phys. **A721**, 344c (2003).

Strange Anti-Particle to Particle Ratios at Mid-Rapidity in $\sqrt{s_{NN}}$ = 130 GeV Au+Au Collisions, J. Adams *et al.* (STAR Collaboration), Phys. Lett. B **567**, 167 (2003).

Intermediate Mass Fragments and Isospin Dependence in ^{124}Sn, ^{124}Xe + ^{124}Sn, ^{112}Sn Reactions at 28 MeV/nucleon, D.V. Shetty, A. Keksis, E. Martin, A. Ruangma, G.A. Souliotis, M. Veselsky, E. Winchester, S.J. Yennello, K. Hagel, Y.G. Ma, A. Makeev, N. Marie, M. Murray, J.B. Natowitz, L. Qin, P. Smith, R. Wada, J. Wang, M. Cinausero, E. Fioretto, G. Prete, D. Fabris, M. Lunardon, G. Nebbia, V. Rizzi, G. Viesti, J. Cibor, Z. Majka, P. Staszel, R. Alfaro, A. Martinez-Davalos, A. Menchaca-Rocha, Y. El Masri, T. Keutgen, Phys. Rev. C **68**, 054605 (2003).

Relationships Between Caloric Curves and the Critical Point of Nucleonic Matter, J.B. Natowitz, K. Hagel, Y. Ma, M. Murray, L. Qin, S. Shlomo, R. Wada, J. Wang, Int. J. Mod. Phys. E **13**, 269 (2004).

Fusion-Fission and Fusion-Evaporation Processes in 20Ne+159Tb and 20Ne+169Tm Interactions Between E/A=8 and 16 MeV, J. Cabrera, T. Keutgen, Y. El Masri C. Dufauquez, V. Roberfroid, I. Tilquin, J. Van Mol, R. Regimbart, R.J. Charity, J.B. Natowitz, K. Hagel, R. Wada, D.J. Hinde, Phys. Rev. C **68**, 034613 (2003).

Search for Temperature and N/Z Dependent Effects in the Decay of A = 98 Compound Nuclei, S. Moretto, D. Fabris, M. Lunardon, S. Pesente, V. Rizzi, G. Viesti, M. Barbui, M. Cinausero, E. Fioretto, G. Prete, A. Brondi, E.Vardaci, F. Lucarelli, A. Azhari, X. D. Tang, K. Hagel, Y. Ma, A. Makeev, M. Murray, J.B. Natowitz, L. Qin, P. Smith, L. Trache, R.E. Tribble, and R. Wada, Phys. Rev. C **69**, 044604 (2004)

Evidence of Critical Behavior in the Disassembly of Nuclei with A~36, Y.G. Ma, R. Wada, K. Hagel, J. Wang, T. Keutgen, Z. Majka, M. Murray, L. Qin, P. Smith, J.B. Natowitz, R. Alfaro, J. Cibor, M. Cinausero, Y. El Masri, D. Fabris, E. Fioretto, A. Keksis, M. Lunardon, A. Makeev, N. Marie, E. Martin, A. Martinez-Davalos, A. Menchaca-Rocha, G. Nebbia, G. Prete, V. Rizzi, A. Ruangma, D. V. Shetty, G. Souliotis, P. Staszel, M. Veselsky, G. Viesti, E.M. Winchester, and S.J. Yennello, Phys. Rev. C **69**, 031604(R) (2004).

Transverse Momentum Spectra in Au+Au and d+Au Collisions at $\sqrt{s_{NN}}$ = 200 GeV and the Pseudorapidity Dependence of High pt Suppression, I. Arsene *et al.* (BRAHMS Collaboration), Phys. Rev. Lett. **91**, 072305 (2003).

Plastic Scintillator Centrality Detector for BRAHMS, Y.K. Lee *et al.* (BRAHMS Collaboration), Nucl. Instrum. Methods. Phys. Res. A **516**, 281 (2004).

The BRAHMS Experiment at RHIC, M. Adamczyk *et al.* (BRAHMS Collaboration), Nucl. Instrum. Methods Phys. Res. A **499**, 437 (2003).

Rapidity Dependence of Charged Anti-particle-to-Particle Ratios in Au+Au Collisions at $\sqrt{s_{NN}}$ = 200 GeV, I.G. Bearden *et al.* (BRAHMS Collaboration), Phys. Rev. Lett. **90**, 102301 (2003).

The BRAHMS Experiment at the Relativistic Heavy ion Collider, Y.K. Lee, I.G. Bearden, D. Beavis, C. Besliu, Y. Blyakhman, J. Brzychczyk, B. Budick, H. Boggild, C. Chasman, C.H. Christensen, P. Christiansen, J. Cibor, R. Debbee, E. Enger, J.J. Gaardhoje, K. Grotowski, K. Hagel, O. Hansen, A. Holm, A.K. Holme, H. Ito, E. Jakobsen, A. Jipa, J.I. Jorde, F. Jundt, C.E. Jorgensen, T. Keutgen, E.J. Kim, T. Kozik, T.M. Larsen, J.H. Lee, Y.K. Lee, G. Lovhoiden, Z. Majka, A. Makeev, B. McBreen, M. Mikelsen, M. Murray, J.B. Natowitz, B.S. Nielsen, J. Norris, K. Olchanski, J. Olness, D. Ouerdane, R. Planeta, F. Rami, D. Rohrich, B.H. Samset, D. Sandberg, S.J. Sanders, R.A. Sheetz, Z. Sosin, P. Staszel, T.F. Thorsteinsen, T.S. Tveter, F. Videbaek, R. Wada, A. Wieloch, I.S. Zgura, J. Korean Phys. Soc. **43**, s27 (2003).

Formation of Excited Systems with a Wide Range in N/Z, D.J. Rowland, R. Laforest, E. Ramakrishnan, M. Veselsky, E.M. Winchester, A. Ruangma, E. Martin and S.J. Yennello, Phys. Rev. C **67**, 064602 (2003).

Production and Separation of Neutron-Rich Rare Isotopes Around and Below the Fermi Energy, G.A. Souliotis, M. Veselsky, G. Chubarian, S.J. Yennello, Nucl. Instrum. Methods Phys. Res. B **204**, 166 (2003).

Heavy Residues with A<90 in the Asymmetric Reaction of 20 A MeV ^{124}Sn + ^{27}Al as a Sensitive Probe of the Onset of Multifragmentation, M. Veselsky, G.A. Souliotis, G. Chubarian, L. Trache, A. Keksis, E. Martin, A. Ruangma, E. Winchester, S.J. Yennello, Nucl. Phys. **A724**, 431 (2003).

Energy Dependence of the Isotopic Composition in Nuclear Multifragmentation, D.V. Shetty, S.J. Yennello, E. Martin, A. Keksis, and G.A. Souliotis Phys. Rev. C **68**, 021602(R) (2003).

Isotopic Scaling of Heavy Projectile Residues from the Collisions of 25 MeV/nucleon ^{86}Kr with ^{124}Sn, ^{112}Sn and ^{64}Ni, ^{58}Ni, G.A. Souliotis, D.V. Shetty, M. Veselsky, G. Chubarian, L. Trache, A. Keksis, E. Martin, and S.J. Yennello Phys. Rev. C **68**, 024605 (2003).

Enhanced Production of Neutron-Rich Rare Isotopes in Peripheral Collisions at Fermi Energies, G.A. Souliotis, M. Veselsky, G. Chubarian, L. Trache, A. Keksis, E. Martin, D.V. Shetty, and S.J. Yennello Phys. Rev. Lett. **91**, 022701 (2003).

Investigation of the α-Cluster Structure of ^{22}Ne and ^{22}Mg, V.Z. Goldberg, G.V. Rogachev, W.H. Trzaska, J.J. Kolata, A. Andreyev, C. Angulo, M.J.G. Borge, S. Cherubini, G. Chubarian, G. Crowley, P. Van Duppen, M. Gorska, M. Gulino, M. Huyse, P. Jesinger, K.-M. Källman, M. Lattuada, T. Lönnroth, M. Mutterer, R. Raabe, S. Romano, M.V. Rozhkov, B.B. Skorodumov, C. Spitaleri, O. Tengblad, and A. Tumino, Phys. Rev. C **69**, 024602 (2004)

T=5/2 States in ^{9}Li: Isobaric Analog States of ^{9}He, G.V. Rogachev, V.Z. Goldberg, J.J. Kolata, G. Chubarian, D. Aleksandrov, A. Fomichev, M.S. Golovkov, Yu.Ts. Oganessian, A. Rodin, B. Skorodumov, R.S. Slepnev, G. Ter-Akopian, W.H. Trzaska, and R. Wolski, Phys. Rev. C **67**, 041603(R) (2003).

Probing Fission Time Scales with Neutrons and GDR Gamma Rays, R.P. Schmitt, T. Botting, G.G. Chubarian, K.L. Wolf, B.J. Hurst, H. Jabs, M. Hamelin, A. Bacak, Yu. Ts. Oganessian, M.G. Itkis, E.M. Kozulin, N.A. Kondratiev, V.S. Salamatin, I.V. Pokrovsky, F. Hanappe, E. de Goes Brennand, A. Huck, L. Stuttge, E. Liatard, J. Been, R. Varner, M. Halbert, and N. Gun, Phys. of Atomic Nuclei **66**, 1163 (2003).

Target and Projectile K-vacancy Production by Fast Heavy Ions in the Molecular Orbital Regime, V. Horvat, R.L. Watson, A.N. Perumal, and Y. Peng, , Application of Accelerators in Research and Industry, AIP Conference Proceedings **680**, AIP Press, Melville, New York, 2003.

Projectile Ionization in Collisions of U^{28+} and Xe^{18+} with Gases, R.E. Olson, R.L. Watson, V. Horvat, K.E. Zaharakis, and T. Stöhlker, Application of Accelerators in Research and Industry, AIP Conference Proceedings **680**, (AIP Press, Melville, New York, 2003).

Target Z Dependence and Additivity of Cross Sections for Electron Loss by 6 MeV/amu Xe^{18+} Projectiles, R.L. Watson, Y. Peng, V. Horvat, G.J. Kim, and R.E. Olson, Phys. Rev. A **67**, 022706 (2003).

Projectile Charge Dependence of Cross Sections for Multiple Electron Capture and Loss by 2 Mev/u Xe Ions in Nitrogen, V. Horvat, R.L. Watson, K.E. Zaharakis, and Y. Peng, Nucl. Instrum. Methods Phys. Res. B **211**, 495 (2003)

Effects of Symmetry Energy on Two-Nucleon Correlation Functions in Heavy Ion Collisions Induced by Neutron-Rich Nuclei, L.W. Chen, V. Greco, C.M. Ko, and B.A. Li, Phys. Rev. Lett. **90**, 162701 (2003).

Parton Coalescence and the Antiproton/Pion Anomaly at RHIC, V. Greco, C.M. Ko, and P. Levai, Phys. Rev. Lett. 90, 202302 (2003).

Charm Production from Photon-Proton Reactions in a Hadronic Model, W. Liu, S. H. Lee, and C. M. Ko Nucl. Phys. **A724**, 375 (2003).

Light Clusters Production as a Probe to Nuclear Symmetry Energy, L.W. Chen, C.M. Ko, and B.A. Li, Phys. Rev. C **68**, 017601 (2003).

Isospin Effects on Two-Nucleon Correlation Functions in Heavy Ion Collisions at Intermediate Energies, L.W. Chen, V. Greco, C.M. Ko, and B.A. Li,, Phys. Rev. C **68**, 014605 (2003).

Partonic Coalescence in Relativistic Heavy Ion Collsions, V. Greco, C.M. Ko, and P. Levai, Phys. Rev. C **68**, 034904 (2003).

Deuteron-Nucleus Collisions in a MultiPhase Transport Model, Z.W. Lin and C.M. Ko , Phys. Rev. C **68**, 054904 (2003).

Cross Sections for Pentaquark Baryon Production from Protons in Reactions Induced by Hadrons and Photons, W. Liu and C.M. Ko, Phys. Rev. C **68**, 045203 (2003).

Charm Production from Proton-Proton Collisions, W. Liu, C.M. Ko, and S.H. Lee, Nucl. Phys. **A728**, 457 (2003).

Light Cluster Production in Intermediate Energy Heavy-Ion Collisions Induced by Neutron-Rich Nuclei, L.W. Chen, C.M. Ko, and B.A. Li , Nucl. Phys. **A729**, 809 (2003).

Kaon Interferometry at RHIC from the AMPT model, Z.W. Lin and C.M. Ko, J. Phys. G **30**, S263 (2004).

Multistrange Baryon Production in Relativistic Heavy Ion Collision, S. Pal, C.M. Ko, Z.W. Lin, Nucl. Phys**. A730**, 143 (2004).

Pentaquark Θ^+ Production from the Reaction $\gamma p \to \pi^+ K^- \Theta^+$, W. Liu, C.M. Ko, V. Kubarovsky , Phys. Rev. C **69**, 025202 (2004).

Cascade Production in Heavy-Ion Collisions at SIS Energies, L.W. Chen, C.M. Ko, and Y.H. Zheng, Phys. Lett. B **584**, 269 (2004).

Partonic Effects on Higher-Order Anisotropic Flows in Relativistic Heavy-Ion Collisions, L. W. Chen, C. M. Ko, and Z.W. Lin, Phys. Rev. C **69**, 031901(R) (2004).

Relativistic Effects in the search for High Density Symmetry Energy, V. Greco, V. Baran, M. colonna, M. Di Toro, T. Gaitanos, H.H. Wolter, Phys. Lett. B **562**, 215 (2003).

On the Lorentz Structure of the symmetry Energy, T. Gaitanos, M. Di Toro, S. Typel, V. Baran, C. Fuchs, V. Greco, H.H. Wolter, Nucl. Phys. **A732**, 24 (2004).

Transport Properties of Isospin Effective Mass Splitting, J. Rizzo,M. Colonna, M. Di Toro, V. Greco, Nucl. Phys. **A732**, 202 (2004).

Relation Between Proton and Neutron Asymptotic Normalization Coefficients for Light Mirror Nuclei and Its Relevance for Astrophysics, N.E. Timofeyuk, R. Jonson, A.M. Mukhamedzhanov, Phys. Rev. Lett. **91**, 232501 (2003).

Resolution of Long-Standing Problems in the Theory of Ionization, A.S. Kadyrov, A.M. Mukhamedzhanov, A.T. Stelbovics, and I. Bray, Phys. Rev. Lett. **91**, 253202 (2003).

Asymptotic Behavior of the Coulomb Three-Body Scattered Wave, A.S. Kadyrov, A.M. Mukhamedzhanov, A.T. Stelbovics, I. Bray, F. Pirlepesov, Phys. Rev. A **68**, 022703 (2003).

Asymptotic Normalization Coefficients from Proton Transfer Reactions and Astrophysical S Factors for the CNO $^{13}C(p, \gamma)^{14}N$ Radiative Capture Process, A.M. Mukhamedzhanov, A. Azhari, V. Burjan, C.A. Gagliardi, V. Kroha, A. Sattarov, X. Tang, L. Trache, R.E. Tribble, Nucl. Phys. **A725**, 279 (2003).

Post-Decay Acceleration in the Coulomb Breakup of Light Nuclei, E.O. Alt, B.F. Irgaziev, A.M. Mukhamedzhanov, Selected Topics in Theoretical Physics and Astrophysics, Joint Institute of Nuclear research, Dubna, (2003) p. 78.

Asymptotic Normalization Coefficients for $^{14}N+p\rightarrow^{15}O$ and the Astrophysical S Factor for $^{14}N(p,\gamma)^{15}O$, A.M. Mukhamedzhanov, P. Bem, B.A. Brown, V. Burjan, C.A. Gagliardi, V. Kroha, J. Novak, F.M. Nunes, S. Paskor, F. Pirlepesov, E. Simeckova, R.E. Tribble, J. Vincour, Phys. Rev. C **67**, 065804 (2003).

Asymptotic Normalization Coefficients in Nuclear Astrophysics, V. Kroha, A. Azhari, P. Bem, V. Burjan, C.A. Gagliardi, A.M. Mukhamedzhanov, J. Novak, S. Piskor, E. Simeckova, X. Tang, L. Trache, R.E. Tribble, J. Vincour, Nucl Phys. **A719**, 119c (2003).

Coulomb Breakup of Light Nuclei in the Field of a Heavy Ion at Relativistic Collision Energies, B.F. Irgaziev, Sh. Kalandarov and A.M. Mukhamedzhanov, Phys. Atomic Nuclei **66**, 684 (2003).

Low-Lying Levels in ^{15}F and the Shell Model Potential for Drip-Line Nuclei, V.Z. Goldberg, G.G. Chubarian, G. Tabacaru, L. Trache, R.E. Tribble, A. Aprahamian, G.V. Rogachev, B.B. Skorodumov, X. Tang, Phys. Rev. C **69**, 031302(R) (2004).

$\pi^+\pi^-$ Emission in High-energy Nuclear Collisions, R. Rapp, Nucl. Phys. **A725**, 254 (2003).

Theoretical Overview on (Hidden) Charm in High-Energy Heavy-Ion Collisions, R. Rapp and L. Grandchamp, J. Phys. G **30**, s305 (2004).

Hadronic Production of Thermal Photons, S. Turbide, R. Rapp, and C. Gale, Phys. Rev. C **69**, 014903 (2004).

Isoscalar Giant Monopole and Dipole Resonances and the Nuclear Matter Incompressibility Coefficient, S. Shlomo, A.I. Sanzhur, and B.K. Agrawal, Nucl. Phys. **A719**, 225c (2003).

Current Status of the Nuclear Matter Incompressibility Coefficient as Deduced from Data on Compression Models, S. Shlomo, and B.K. Agrawal, Nucl. Phys. **A722**, 98c (2003).

Nuclear matter Incompressibility Coefficient in Relativistic and Nonrelativistic Microscopic Models, B.K. Agrawal, S. Shlomo, and V. Kim Au, Phys. Rev. C **68**, 031304(R) (2003).

Isoscalar Giant Monopole Resonance and Its Overtone in Microscopic and Macroscopic Models, S. Shlomo, V.M. Kolomietz, and B.K. Agrawal, Phys. Rev. C **68**, 064301 (2003).

Self-Consistent Hartree-Fock Based Random Phase Approximation and the Spurious State Mixing, B.K. Agrawal, S. Shlomo, and A.I. Sanzhur, Phys. Rev. C **67**, 034314 (2003).

Non-Markovian Effects on the Dynamics of Bubble Growth in Asymmetric Nuclear Matter, V.M. Kolomietz, A.I. Sanzhur, and S. Shlomo, Phys. Rev. C **68**, 014614 (2003).

Liquid-Gas Phase Transition in Finite and Infinite Nuclear Systems, Tapas Sil, S.K. Samaddar, J. De and, S. Shlomo, Phys. Rev. C **69**, 014602 (2004).

Nuclear Fermi Liquid Drop Model, V.M. Kolomietz, and S. Shlomo, Phys. Rep. **390**, 133 (2004).
Shape Fluctuations in a Fermi System With Nonlinear Dissipativity, V.M. Kolomietz, S.V. Lukyanov, and S. Shlomo, Phys. Rev. C **69**, 024314 (2004).

HF-RPA Theory for Giant Resonances and the Nuclear Matter Incompressibility Coefficient: Is There a Problem?, S. Shlomo, and B.K. Agrawal, , Eds: H. Sagawa and H. Iwasaki, (World Scientific, Singapore, 2003) p. 327.

SECTION VII

APPENDIX

TALKS PRESENTED
April 1, 2003 – March 31, 2004

Isoscalar Giant Dipole Resonance for Several Nuclei with A ⩾ 90, **Y.-W. Lui**, X. Chen, H.L. Clark, B. John, Y. Tokimoto and D.H. Youngblood, International Conference on Collective Motion in Nuclei Under Extreme Conditions (COMEX1), La Sorbonne, Paris, France, (June 2003).

Compression Mode Giant Resonances and Nuclear Matter Compressibility, **Y.-W. Lui**, **Invited Talk**, National Technical University in Athens, Athens, Greece, (June 2003).

Radioactive Beams at Texas A&M University, Recent Results and Future Plans, **R.E. Tribble**, RNB6, Argonne, Illinois, (September 2003).

Recent Results for Astrophysical S Factors from Measurements of Asymptotic Normalization Coefficients, **R.E. Tribble**, **Invited Talk**, OMEG03, Tokyo, Japan, (November 2003).

Measurements of Asymptotic Normalization Coefficients – An Indirect Technique for Determining Capture Reaction Rates at Stellar Energies, **R.E. Tribble**, Workshop on Nuclear Reactions on Unstable Nuclei and the Surrogate Reaction Technique, Asilomar, California, (January 2004).

Jet Quenching at RHIC, **C.A. Gagliardi**, **Invited Talk**, Wayne State University, Detroit, Michigan, (March 2004).

Modern Particle Accelerators and Detectors: A Household Survey, **C.A. Gagliardi**, **Invited Talk**, Nuclei and the Cosmos – Quark Matter 2004 Workshop for Science Teachers, Oakland, California, (January 2004).

Jet Quenching at RHIC, **C.A. Gagliardi**, **Invited Talk**, DNP Annual Meeting 2003, Tucson, Arizona, (November 2003).

Jet Quenching at RHIC, **C.A. Gagliardi**, **Invited Talk**, XXXI SLAC Summer Institute, Stanford, California, (August 2003).

Jet Quenching at RHIC, **C.A. Gagliardi**, **Invited Talk**, TRIUMF, Vancouver, British Columbia, Canada, (June 2003).

Dimuon Production in Fermilab E866, **C.A. Gagliardi**, **Invited Talk**, Nuclear Science Division, Lawrence Berkeley National Laboratory, Berkeley, Calfornia, (June 2003).

TWIST: Measuring the Space-Time Structure of Muon Decay, **C.A. Gagliardi** (for the TWIST Collaboration), **Invited Talk**, 8th Conf. Intersections Part. Nucl. Phys., New York, New York, (May 2003).

Determination of Astrophysical S-Factors from the Breakup of Loosely Bound Nuclei at Intermediate Energies, **L. Trache**, **Invited Talk**, Workshop on Nuclear Structure Physics Near the Coulomb Barrier: Into the 21st Century, Yale University, New Haven, Connecticut, (June 2003).

Separation of Neutron-Rich DIR Products with MARS, **L Trache**, **Invited Talk**, Decay Spectroscopy Workshop, Oak Ridge National Laboratory, Oak Ridge, Tennessee, (August 2003).

Indirect Methods in Nuclear Astrophysics, **L Trache**, **Invited Talk**, Institute for Physics and Nuclear Engineering, H. Hulubei, Bucharest, Romania, (October 2003).

From Breakup to Nuclear Astrophysics: ^{8}B and the S_{17} Astrophysical Factor, **L Trache**, DNP Annual Meeting 2003, Tucson, Arizona, (November 2003).

Spectroscopic Factors vs Asymptotic Normalization Coefficients from Breakup and Transfer Reactions with Loosely Bound Nuclei, **L. Trache**, **Invited Talk**, Workshop on Spectroscopic Factors, ECT, Trento, Italy, (March 2004).

New Results in Superallowed Nuclear Beta Decay, **J.C. Hardy**, **Invited Talk**, Conference on the Intersections of Particle and Nuclear Physics, CIPANP03, New York, (May 2003).

New Results in Superallowed Nuclear Beta Decay, **J.C. Hardy**, **Invited Talk**, Michigan State University, East Lansing, Michigan, (May 2003).

High Precision Efficiency Calibration of an HPGe Detector from 50 keV to 4.8 MeV, with Measurements and Monte Carlo Calculations, **J.C. Hardy**, **Invited Talk**, International Conference on Radiation Metrology, Dublin, Ireland, (June 2003).

Delimiting the Standard Model with Superallowed Nuclear Beta Decay, **J.C. Hardy**, **Invited Talk**, Oak Ridge National Laboratory, Oak Ridge, Tennessee, (September 2003).

Delimiting the Standard Model with Superallowed Nuclear Beta Decay, **J.C. Hardy**, **Invited Talk**, Arizona State University, Arizona, (October 2003).

How Idiosyncratic Is the Weak Force?, **J.C. Hardy**, **Invited Talk**, Inaugural R.E. Bell lecture, McGill University, Montreal, Quebec, Canada, (November 2003).

Precise Half-life Measurement of the Decays of ^{34}Cl and ^{34}Ar, **V.E. Iacob**, E. Mayes, J.C. Hardy, R.G. Neilson, M. Sanchez-Vega, A. Azhari, C.A. Gagliardi, L. Trache and R.E. Tribble, APS Meeting, Philadelphia, Pennsylvania, (April 2003).

Precise Ft-value Measurement for the Superallowed 0^{+}-to- 0^{+} -Decay of ^{22}Mg, J.C. Hardy, **V.E. Iacob**, M. Sanchez-Vega, R.G. Neilson, A Azhari, C.A. Gagliardi, V.E. Mayes, X. Tang, L. Trache and R.E. Tribble, International Conference on the Labyrinth in Nuclear Structure, Crete, Greece, (July 2003).

Accurate Ft-value Measurements for ^{22}Mg and ^{34}Ar, **V.E. Iacob**, J.C. Hardy, A. Azhari, C.A. Gagliardi, E. Mayes, R.G. Neilson, N. Nica, M. Sanchez-Vega, L. Trache and R.E. Tribble, APS meeting, Tucson, Arizona, (October 2003).

Precise Efficiency Calibration of an HPGe Detector up to 3.5 MeV, with Measurements and Monte Carlo Calculations, **N. Nica**, J.C. Hardy, V.E. Iacob and R.G. Helmer, APS meeting, Tucson, Arizona, (October 2003).

Dynamics and Thermodynamics in Nuclear Collisions Near the Fermi Energy, **J.B. Natowitz**, **Invited talk**, Arkansas State University, Jonesboro, Arkansas, (January 2003).

Coalescence, Caloric Curves, Critical (?) Comportment, **J.B. Natowitz**, **Invited talk**, Heavy Ion Conference 03, Montreal, Canada, (June 2003).

Coalescence, Caloric Curves, Critical Behavior, **J.B. Natowitz**, **Invited talk**, 10th Nuclear Physics Workshop in Kazimierz Dolny, Poland, (September 2003).

Caloric Curves, Phase Diagrams and Limiting Temperature, **J.B. Natowitz**, **Invited talk**, International Workshop on Multifragmentation 2003, Caen, France, (November 2003).

Resonance Scattering $^{8}He+p$ and T=5/2 states in ^{9}Li, **V.Z. Goldberg**, **Invited Talk**, VIII International Conference on Nucleus-Nucleus Collisions, Moscow, Russia, (June 2003).

A New Approach to Spectroscopy of Neutron Rich Nuclei, **V.Z. Goldberg**, **Invited Talk**, Halo 2003,St. Petersburg, Russia, (July 2003).

Resonances in Drip Line Nuclei, **V.Z. Goldberg**, **Invited Talk**, CFIF Workshop on Time Asymmetric Quantum Theory: The Theory of Resonances, Lisbon, Portugal, (July 2003).

Nuclear Structure of ^{15}F and ^{9}He, **V.Z. Goldberg**, **Invited Talk**, National Superconducting Cyclotron Laboratory, East Lansing, Michigan, (October 2003).

Resonance Scattering Studies at the Borders of Nuclear Stability, **V.Z. Goldberg**, **Invited Talk**, BNL, Berkeley, California, (March 2004).

Energy Dependence of the Isotopic Composition in Nuclear Fragmentation, **S.J. Yennello**, APS Meeting, Philadelphia, Pennsylvania, (April 2003).

Isospin Dependence of Intermediate Mass Fragments in ^{124}Sn, ^{124}Xe + ^{124}Sn, ^{112}Sn, **D.V. Shetty**, APS Meeting, Philadelphia, Pennsylvania, (April 2003).

Neutron-Rich Rare Isotope Production around the Fermi Energy, **G.A. Souliotis**, M. Veselsky, G. Chubarian, L. Trache and S.J. Yennello, VIII International Conference on Nucleus-Nucleus Collisions (NN03), Moscow, Russia, (June 2003).

Rare Isotope Production and Nuclear Dynamics Studies at Fermi Energies, **G.A. Souliotis**, **Invited Talk**, Institute of Nuclear Physics of NCSR 'Demokritos', Athens, Greece, (June 2003).

Novel Routes to Produce Extremely Neutron-Rich Rare Isotopes, **G.A. Souliotis**, **Invited Talk**, Physics Division, Argonne National Laboratory, Argonne, Illinois, (February 2004).

Gamma-Ray Multiplicities From the Heavy Ion Induced Fission Reactions, **G. Chubarian**, **Invited Talk**, VIII International Conference on Nucleus-Nucleus Collisions, Moscow, Russia, (June 2003).

A Multiphase Transport Model, **C.M. Ko**, **Invited Talk**, International Workshop on Transport Model for Heavy Ion Collisions, Trento, Italy, (May 2003).

Symmetry Energy Effects in Heavy Ion Collisions, **C.M. Ko**, **Invited Talk** ,International Conference on Topics in Heavy Ion Collisions, Montreal, Canada, (June 2003).

Transport Model for Heavy Ion Collisions, **C.M. Ko**, **Invited Talk**, International School on Nuclear Physics, Erice, Italy, (September 2003).

Cross Sections for Pentaquark Baryon Production in Photonucleon Reactions, **C.M. Ko**, **Invited Talk**, Penta-Quark 2003 Workshop, Jefferson Lab, Newport News, Virginia, (November 2003).

Transport Model Description of Flows at RHIC, **C.M. Ko**, **Invited Talk,** RIKEN BNL Workshop on Collective Flow and QGP Properties, Brookhaven National Laboratory, Upton, New York, (November 2003).

Quark Coalescence Model, **C. M. Ko**, **Invited Talk,** Mini-workshop on Quark Recombination, Institute for Nuclear Theory, Seattle, Washington, (December 2003).

Asymptotic Three-Body Coulomb Scattering Wave Function and the $^{208}Pb(^{8}B, ^{7}Be\ p)^{208}Pb$ *Coulomb Breakup*, **A.M. Mukhamedzhanov**, Few-Body 17. TUNL, Duke University, Durham, North Carolina, (June 2003).

Asymptotic Three-Body Coulomb Scattering Wave Function and Coulomb Breakup Processes, **A.M. Mukhamedzhanov**, DREB 2003 (Direct reactions with the exotic beams), University of Surrey, Guilford, United Kingdom, (July 2003).

Asymptotic Normalization Coefficients in Nuclear Astrophysics, **A.M. Mukhamedzhanov**, **Invited talk**, Oak Ridge National Lab., Oak Ridge, Tennessee, (September 2003).

Direct capture astrophysical factors, NSCL, **A.M. Mukhamedzhanov**, **Invited talk**, Michigan State University, East Lansing, Michigan, (September 2003).

Asymptotic Normalization Coefficients in Nuclear Astrophysics, **A.M. Mukhamedzhanov**, **Invited talk**, Argonne National Lab., Illinois, (September 2003).

Direct capture astrophysical factors, **A.M. Mukhamedzhanov**, **Invited talk**, Notre Dame University, South Bend, Indiana, (October 2003).

Charmonium and Open Charm in Heavy-Ion Collisions, **R. Rapp**, **Invited Talk**, International Conference on Topics in Heavy-Ion Collisions, McGill University, Montreal, Canada, (June 2003).

Charmonium and Open Charm in Heavy-Ion Collisions, **R. Rapp**, Workshop on Aspects of Nonperturbative QCD – Hadrons and Thermodynamics, Rostock University, Rostock, Germany, (July 2003).

Charmonium and Open Charm in Heavy-Ion Collisions, **R. Rapp**, **Invited Talk**, Darmstadt University, Germany, (July 2003).

Charmonium Suppression and Regeneration in Ultrarelativistic Heavy-Ion Collisions, **R. Rapp**, **Invited Talk,** Workshop on Heavy Quarkonium, Fermi Lab., Batavia, Illinois, (September 2003).

Theory of Electromagnetic and Charm Probes, **R. Rapp**, **Invited Talk**, DNP 2003 Workshop on QCD, Confinement and Heavy-Ion Collisions, Tucson, Arizona, (October 2003).

$\pi^{+}\pi^{-}$ *Emission at RHIC*, **R. Rapp**, DNP Annual Meeting 2003, Tucson, Arizona, (November 2003),

Theory Highlights of Quark Matter 2004, **R. Rapp**, **Invited Talk**, XVII International Conference on Ultrarelativistic Nucleus-Nucleus Collisions (Quark Matter '04), Oakland, California, (January 2004).

Status of of The Nuclear Matter Equation of States Determined From Compression Modes, **S. Shlomo** and B.K. Agrawal, **Invited Talk**, VIII International Conference on Nucleus-Nucleus Collisions, Moscow, Russia, (June 2003).

Microscopic Determination of Incompressibility Coefficient of Symmetric Nuclear Matter from Experimental Data on Compression Modes, **S. Shlomo**, and B.K. Agrawal, **Invited Talk**, International Symposium on Exotic Nuclei (HALO03), St. Petersburg, Russia, (June 2003).

Current Status of the Nuclear Matter Incompressibility Coefficient, **S. Shlomo**, and B.K. Agrawal, **Invited Talk**, Workshop on Data Base Development for Nuclear Astrophysics and Nuclear Fusion, Almaty, Kazakhstan, (September 2003).

Current Status of the Nuclear Matter Incompressibility Coefficient, **S. Shlomo**, **Invited Talk**, International Workshop on Nuclear Response Under Extreme Conditions, The European Center for Theoretical Studies in Nuclear Physics and Related Areas (ECT), Trento, Italy, (October 2003).

Nuclear Matter Incompressibility Coefficient, **S. Shlomo**, **Invited Talk**, The 49th Meeting of The Israeli Physical Society, Bar-Ilan University, Ramat-Gan, Israel, (December 2003).

Comments on Hartree-Fock and Random Phase Approximation Calculations and Self-Consistency, **S. Shlomo**, **Invited Talk**, International Workshop on Spectroscopic Factors, The European Center for Theoretical Studies in Nuclear Physics and Related Areas (ECT), Trento, Italy, (March 2004).

Consequences of Violation of Self-Consistency in Hartree-Fock Based Random Phase Approximation Calculations of the Nuclear Response Function, **S. Shlomo**, **Invited Talk**, Munich Technical University, Munich, Germany, (March 2004).

Quark Coalescence in the Parton Transport Model, **L.W. Chen**, **Invited Talk**, Mini-workshop on Quark Recombination, Institute for Nuclear Theory, Seattle, Washington, (December 2003).

Two-Nucleon Correlation Functions and $t/^3$He Ratio As Probes of the Nuclear Symmetry Energy, **L.W. Chen**, **Invited Talk**, National Superconducting Cyclotron Laboratory, Michigan State University, East Lansing, Michigan, (February 2004).

Equation of State and Nuclear Dynamics of Asymmetric Nuclear Matter, **V. Greco**, Conference on Relativistic Structure Models of the Physics of Radioactive Nuclear Beams, Bad Honnef, Germany, (May 2003).

Parton Coalescence at RHIC, **V. Greco**, International Conference on Topics in Heavy Ion Collisions, Montreal, Canada, (June 2003).

Coalescence and Fragmentation at RHIC, **V. Greco**, Meeting of the INFN working group on the Phenomenology of Quark-Gluon Plasma, University of Catania, Italy, (December 2003).

Hadronization via Coalescence, **V. Greco**, Winter workshop on Nuclear Dynamics, Trelawny Beach, Jamaica, (March 2004).

RESEARCH PERSONNEL AND ENGINEERING STAFF

April 1, 2003 - March 31, 2004

Faculty and Research Group Leaders

Carl A. Gagliardi, Professor of Physics
John C. Hardy, Professor of Physics
Che Ming Ko, Professor of Physics
Akram M. Zhanov, Senior Scientist –From 2/1/04
J. B. Natowitz, Professor of Chemistry, Bright Chair
Ralf Rapp Assist. Prof. of Physics – From 8/29/03
Richard P. Schmitt, Professor of Chemistry – To 2/28/04
Shalom Shlomo, Senior Scientist
Robert E. Tribble, Professor of Physics, Director
Rand L. Watson, Professor of Chemistry
Sherry J. Yennello, Prof. of Chemistry
Dave H. Youngblood, Professor of Physics

Research Staff

Henry Clark, Accelerator Physicist (50%)
Grigor Chubaryan, Research Scientist
John C. Hagel, Research Scientist (50%)
Vladimir Horvat, Research Scientist (50%)
Victor Iacob, Associate Research Scientist
Yiu-Wing Lui, Research Scientist
George Souliotis, Assistant Research Scientist
Livius Trache, Research Scientist
Maxim Vasilyev, Assistant Research Scientist (80%)
Ryoichi Wada, Research Scientist

Visiting Scientists

Erwin Alt – From 5/503 To 6/5/03
Juha Arje – From 3/10/04
Leonid Blokhintsev – From 5/19/03 To 6/18/03
Alexander Botvina - From 7/29/03 To 3/31/04
Judunath De – From 9/15/03 To 12/19/03
Vladilen Goldberg
Bakhadir Irgaziev – From 10/13/03 To 12/12/03
Alisher Kadirov - From 5/23/03 To 7/21/03
Zbigniew Majka – From 2/23/04
V. Kolomietz – To 6/27/03
Su Hong Lee – To 8/8/03
Peter J. Levai - From 11/4/02 to 11/30/02
Ian Towner – From 6/19/03 To 8/20/03

Accelerator Physics And Radiation Line Staff

Henry Clark, Accelerator Physicist (50%)
Vladimir Horvat, Assoc. Res. Scientist (50%)
Bruce Hyman, Research Associate
George Kim, Accelerator Physicist
Don May, Accelerator Physicist
Dennis Utley, Research Associate (25%)

Computer Systems Staff

Robert Burch, Jr., Systems Analyst II
John C. Hagel, Assoc. Research Scientist (50%)
Maxim Vasilyev, Asst. Research Scientist (20%)

Engineering Staff

Walter Chapman, Mech. Engineer – To 9/30/02
Greg Derrig, Senior Mechanical Engineer
Robert Olsen, Mechanical Engineer

Postdoctoral Research Associates

Bijay Agrawal
Narayana P. Appathurai
Afshin Azhari – To 5/7/03
Lie-Wen Chen
Vicenzo Greco
Marian Jandel – From 1/1/04
Seweryn Kowalski – From 10/8/03
Yu-Gang Ma – To 7/11/03
Thomas Materna – From 10/6/03
Ninel Nica
Vladimir Salamatin – To 6/25/03
Dinesh Shetty
Gabriel Tabacaru
Xiaodong Tang – To 5/2/03
Yoshiaki Tokimoto
Martin Veselsky – From 4/7/03 To 7/3/03
Hendrik van Hees – From 1/8/04

STUDENTS

April 1, 2002 - March 31, 2003

Graduate Students

Tariq Al-Abdullah
Joseph Brinkley – From 6/1/03
Xinfeng Chen
Bogdan Dobrescu – To 1/15/04
Changbo Fu
Thomas Henry
August Keksis
Wei Liu
Elizabeth Martin
James Musser
Luciano Pappalardo – From 8/29/03
Yong Peng
Fakhriddin Pirlepesov
Oleksiy Pochivalov
Li Jun Qin
Sarah Soisson – From 8/29/03
Brian Stein – From 8/29/03
Au Kim Vuong
Yongjun Zhai – From 9/1/02
Feng Zhang –From 6/1/03 To 12/15/03

Undergraduates and Student Technicians

Christopher J. Bemben – To 8/31/03
Jaime L. Estes – From 4/17/03
Erin Eurek – To 8/29/03
Christina M. Freeborn – To 8/31/03
Travis Gardner – To 8/27/03
Joshua Garey – From 5/1/03
Stephen Hanssen – From 6/3/02
Chelsey Jones – From 9/2/02
Chelsi Kaltwasser – From 8/25/03
Sarah Parketon
Barrett C. Parker – From 5/30/02
Landon Reneau – From 5/13/03 To 6/11/03
Casseday Richers – From 5/1/03
Ryan Romero – From 5/8/03 To 8/29/03
David Rosenfeld – To 9/6/03
Michael Sarahan – From 3/1/04
Patrick Smith – To 9/6/03
Nicole Steiner – To 5/5/03
Patrick Tamain – From 6/24/02 To 8/2/02
Kazuki Wada - To 9/6/03
William D. Wright – From 9/9/02

ORGANIZATIONAL CHART - CYCLOTRON INSTITUTE

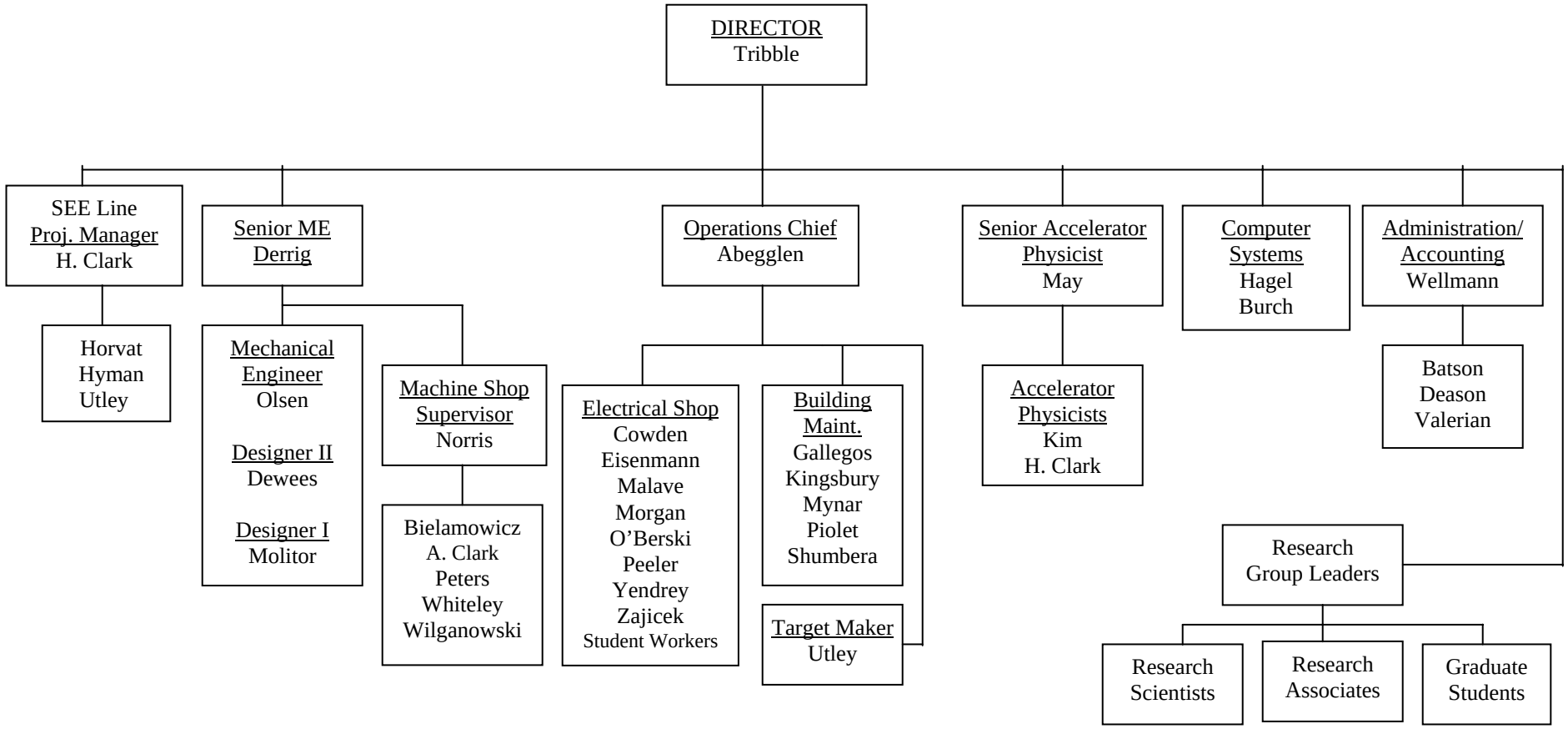

INSTITUTE COLLOQUIA AND SEMINARS
April 1, 2003-March 31, 2004

2003

April 1	Dr. Hans A. Schuessler, Department of Physics, Texas A&M University, College Station, Texas	*On- and Off-Line Laser Spectroscopy*
April 8	Dr. M.H. Urin, Moscow Engineering Physics Institute, Moscow, Russia	*Giant Resonance Overtones: Structure and Decay Properties*
April 15	Professor Witold Nazarewicz, Department of Physics, University of Tennessee, Knoxville, Tennessee	*Gamow Shell Model Description of Weakly Bound Nuclei and Unbound Nuclear States*
April 23	Dr. Jennifer Church, Michigan State University, E. Lansing, Michigan	*Coulomb Excitation with Fast Exotic Beams: The Neutron-rich Nucleus ^{34}Mg*
April 29	Professor V. M. Kolomietz, Institute for Nuclear Research, Kiev, Ukraine	*Non-Markovian Effects on Nuclear Large Amplitude Motion*
May 6	Dr. George Souliotis, Cyclotron Institute, Texas A&M University, College Station, Texas	*Heavy Residue Isotopic Scaling and N/Z Equilibration*
May 12	Dr. Carl R. Brune, Ohio University, Athens, Ohio	*New Approaches to the Analysis of Resonant Reactions*
May 20	Professor V. M. Kolomietz, Institute for Nuclear Research, Kiev, Ukraine	*Cavitation in Hot Nuclear Matter*
May 27	Professor Dr. Erwin O. Alt, Institut für Physik, Mainz Universität, Mainz, Germany	*Scattering of Charged Particles*
June 3	Professor Dr. Erwin O. Alt, Institut für Physik, Mainz Universität, Mainz, Germany	*Scattering Wave Function for Three Charged Particles in the Continuum: Theory and Applications*
June 10	Dr. M. Veselsky, Cyclotron Institute, Texas A&M University, College Station, Texas and Institute of Physics, Slovak Academy of Sciences, Bratislava, Slovakia	*Complete and Incomplete Fusion in Heavy-ion Collisions at Low and Intermediate Energies (Two Extreme Cases)*

June 17	Dr. Leonid Blokhintsev, Skobeltsyn Institute of Nuclear Physics, Lomonosov Moscow State University, Moscow, Russia	*Asymptotic Properties of Bound-state Wave Functions in Two-fragment Channels*
July 8	Dr. Yu-Gang Ma (for the NIMROD Collaboration), Cyclotron Institute, Texas A&M University, College Station, Texas and Shanghai Institute of Nuclear Research, Chinese Academy of Sciences, China	*Evidence of the Critical Behavior in Light Nuclear Systems*
July 18	Professor Romualdo de Souza, Indiana University, Bloomington, Indiana	*What Can We Learn from the Decay of Excited Projectile-like Fragments Resulting from Peripheral Heavy-ion Collisions?*
August 5	Dr. Aurora Tumino, Laboratori Nazionali del Sud - INFN and Universita' di Catania, Italy	*The Trojan-Horse Method Applied to Nuclear Astrophysics*
August 11	Dr. Rajdeep Chatterjee, Saha Institute of Nuclear Physics, Calcutta, India	*Coulomb and Nuclear Breakup of Halo Nuclei*
August 12	Professor Arturo Menchaca Rocha, National Autonomous University of Mexico (UNAM), Mexico City, Mexico	*Search for Hidden Chambers in the Mexican Sun Pyramid at Teotihuacan Using a Muon Detector*
August 19	Dr. A. S. Botvina, INR, Moscow, Russia and Cyclotron Institute, Texas A&M University, College Station, Texas	*Fragment Production in Supernova Explosions: What Can We Learn from Nuclear Multifragmentation?*
August 19	Dr. Wayne D. Cornelius, Cyclotron Institute, Texas A&M University, College Station, Texas	*S Solutions/JPAW Ion Source and Accelerator Projects*
September 2	Professor R. P. Scharenberg, Purdue University, West Lafayette, Indiana	*Evidence for Hadronic Deconfinement in* $\bar{p}$ *-* p *collisions at 1.8 TeV*
September 9	Dr. Michael Kreisler, National Nuclear Security Administration, Washington DC	*Nucleaar Physics and the DOE National Security Mission: a Bi-Coastal Perspective*
October 14	Professor J. N. De, Variable Energy Cyclotron Center, Kolkata, India	*Neutron Star Matter and Isospin-rich Nuclei*
October 21	Dr. Aldo Bonasera, INFN, Laboratorio Nazionale del sud, Catania, Italy	*Formation and Decay of Super-heavy Systems*

October 24	Dr. Ralf Rapp, cyclotron Institute, Texas A&M University, College Station, Texas	*Theory of Charm(onium)and Electromagnetic Probes in URHICs*
November 4	Dr. Saskia Mioduszewski, Brookhaven National Laboratory, Upton, New York	*The Search for the Quark Gluon Plasma at RHIC*
November 7	Dr. Vincenzo Greco, Cyclotron Institute, Texas A&M University, College Station, Texas	*Partonic Coalescence in Heavy-Ion Collisions*
November 10	Mr. Fakhridden Pirlepesov, cyclotron Institute, Texas A&M University, College Station, Texas	*Asymptotic Scattering Wave Function for Three Charged Particles and Astrophysical Radiative Capture Processes*
November 10	Mr. Changbo Fu, Cyclotron Institute, Texas A&M University, College Station, Texas	*Determine S_{34} Factor from Breakup Reaction (^{7}Be, ^{3,4}He)*
November 14	Dr. Peter Kolb, Department of Physcis and Astronomy, SUNY, Stony Brook, New York	*Anisotropies in Non-Central Heavy Ion Collisions*
November 17	Professor Chhanda Samanta, Saha Institute of Nuclear Physics, Bidhannagar, Kolkata, India and Physics Department, Virginia Commonwealth University, Richmond Virginia	*Does Z=82 Shell Gap Quench Near Proton Drip Line?*
November 19	Mr. August Keksis, Cyclotron Institute, Texas A&M University, College Station, Texas	*Qusaiprojectile Fragmentation Using 32, 45 MeV/u ^{40}Ca, ^{40}Ar, ^{48}Ca on ^{112}Sn, ^{124}Sn*
November 19	Ms. Elizabeth Martin, Cyclotron Institute, Texas A&M University, College Station, Texas	*Progress in Research of Isospin Equilibration*
November 19	Mr. Wei Liu, Cyclotron Institute, Texas A&M University, College Station, Texas	*Exotic Baryon Production within a Hadronic Model*
November 21	Professor Thomas Cohen, University of Maryland, college Park, Maryland	*Large N_c QCD and the Exotic θ^+ Baryon*
December 1	Mr. Au Kim Vuong, Cyclotron Institute, Texas A&M University, College Station, Texas	*New Effective Nucleon-Nucleon Interaction*

December 1	Mr. Oleksiy Pochivalov, Cyclotron Institute, Texas A&M University, College Station, Texas	*Properties of Isoscalar Giant Dipole Resonance in Nuclei*
December 1	Mr. Bogdan Dobrescu, Cyclotron Institute, Texas A&M University, College Station, Texas	*Skyme-Force Tine-Dependent Hartree-Fock Description of Isoscalar Giant Monopole Resonsnce in Nuclei*
December 5	Professor Jochen Wambach, TU Darmstadt and GSI, Germany	*Hadrons in Hot and Dense Matter-Part I*
December 9	Professor Jochen Wambach, TU Darmstadt and GSI, Germany	*The GSI Future Facility Accelerator for Heavy-Ion beams of High Intensity*
December 11	Professor Jochen Wambach, TU Darmstadt and GSI, Germany	*Hadrons in Hot and Dense Matter-Part II*
December 11	Mr. Xinfeng Chen, Cyclotron Institute, Texas A&M University, College Station, Texas	*Giant Resonance Study by ^{6}Li scattering*
December 11	Mr. Yong Peng, Cyclotron Institute, Texas A&M University, College Station, Texas	*Target K Vacancy Production in Heavy Ion Collisions*
December 11	Mr. Lijun Qin, Cyclotron Institute, Texas A&M University, College Station, Texas	*p-A, A-A Collisions with NIMROD*
December 12	Dr. A Mukhamedzhanov, Cyclotron Institute, Texas A&M University, College Station, Texas	*Asymptotic Normalization Coefficients and Nuclear Astrophysics-Part I*

2004

January 23	Dr. A Mukhamedzhanov, Cyclotron Institute, Texas A&M University, College Station, Texas	*Asymptotic Normalization Coefficients and Nuclear Astrophysics-Part II*
January 30	Dr. Hendrik van Hees, Cyclotron Institute, Texas A&M University, College Station, Texas,	*Self-consistent Renormalization Schemes for Thermodynamic Potentials*
February 6	Dr. Lie-Wen chen, Cyclotron Institute, Texas A&M University, College Station, Texas	*High–p_T hadron Production in Relativistic Heavy-Ion Collisions from the AMPT Model*
February 10	Dr. Joydip Kundu, Massachusetts Institute of Technology, Cambridge, Massachusetts	*Mass-Induced Crystalline Color Superconductivity*

February 20	Dr. Harry Lee, Argonne National Laboratory, Argonne, Illinois	*Study of Nucleon Resonances with GeV Electromagnetic Meson Production Reactions*
March 2	Mr. Wei Liu, Cyclotron Institute, Texas A&M University, College Station, Texas	*Pentaquark Production in Elementary Reactions*
March 25	Dr. Berndt Muleller, Duke University, Durham, North Carolina	*Messages from a Different World: Probing Quark Deconfinement with RHIC*
March 26	Dr. Giuseppe Viesti, Dipartimento di Fisica "Galileo Galilei" dell' Universita di Padova and INFN, Padova, Italy	*The Silicon Pixel Detector of the ALICE Experiment at LHC*
March 30	Dr. Silvia Pesente, Dipartimento di Fisica "Galileo Galilei" dell' Universita di Padova and INFN, Padova, Italy	*Development of Inspection Systems Using 14 MeV Tagged Neutron Beams*
March 31	Professor Michal Praszalowicz, Jagellonian University, Krakow, Poland	*Pentaquarks in the Chiral Models*